SEISMIC WAVE PROPAGATION IN ANISOTROPIC WAVEGUIDES

by

Min   Lou

(B.Sc. University of Petroleum, East China)

Thesis submitted for the degree of Doctor of Philosophy

Department of Geology and Geophysics

University of Edinburgh

January   1992

There is no speech or language

   where their voice is not heard.

Their voice goes out into all the earth.

Psalm 19, 3-4.

I hereby declare that this thesis has been completed by myself and that the work described is entirely my own unless otherwise explicitly stated in the text.

Min Lou

ABSTRACT

The thesis studies the propagation of guided-waves in crack-induced anisotropic media, and exploits the potential applications of guided-waves in production seismology by crosshole seismic surveys.

Firstly, by extending Crampin's technique for calculating surface-wave dispersion, we present a procedure for determining the dispersion and amplitude/depth distribution of guided-waves in multilayered anisotropic media. We also exploit the method to calculate synthetic seismograms of guided-waves in layered anisotropic structures in ANISEIS package.

By using the developed techniques, we study the propagation behaviour of guided-waves in crack-induced anisotropic waveguides. Our studies have shown that: (a) almost any interface, or combination of interfaces, will support the propagation of guided-waves in crosshole seismic surveys, if signals at appropriate frequencies, amplitudes, and polarizations can be generated in one well and recorded at appropriate levels in neighbouring wells; (b) in crack-induced anisotropic waveguides, the distinct families of Rayleigh and Love modes of guided-waves in isotropic waveguides combine into a single family of *Generalized* modes with 3-D elliptical particle motions; (c) guided-waves are very sensitive to the internal properties and geometry of waveguide, and such guided-wave characteristics vary substantially for different crack orientations, crack densities, crack saturations, and crack aspect ratios.

Guided-waves have been clearly identified from a shallow crosshole survey at the Conoco Borehole Test Facility (CBTF) and, in many circumstances, have dominant energy in the seismograms. We have demonstrated that guided-waves in crosshole surveys have two potential applications: continuity tests of plane-layered reservoirs; and monitoring Enhanced Oil Recovery (EOR) operations for thin-layered sedimentary reservoirs.

Finally, we have modelled the propagation of guided-waves in two particular waveguides: a crack-controlled channel which may be formed in hydraulic fracturing in geothermal reservoirs; and an active fault zone. The study of such guided-waves is useful in understanding the fracture structure and distribution in geothermal reservoirs, and delimitating fault zone or monitoring the stress and fracture development inside an active fault zone.

ACKNOWLEGEMENTS

CONTENTS

CHAPTER 1

INTRODUCTION

In this thesis, we call guided-waves   any form of seismic wave
that propagates energy parallel to an interface, or combination of
interfaces. A variety of guided-waves are possible, and in
particular circumstances they may be more appropriately called
channel-waves, Stoneley waves, interface-waves, or head-waves.

1.1 PURPOSE AND ORGANIZATION OF THIS THESIS

The Love modes of channel-waves (or guided-waves) in isotropic
waveguides have been extensively studied, and they have been widely
used in coal mining to detect faults or discontinuities within
coal-seams, where coal-seams usually provide suitable low-velocity
waveguides. It has now been recognized that the dominant energy in
crosshole seismic surveys in some reservoir configurations may also
be guided-waves, rather than body-waves as are frequently assumed.
Such guided-waves are usually observed as *Generalized* modes with
elliptical particle-motions in three-dimensions as a result of
inclusion-induced anisotropy in the most crustal rock.

In this thesis, we shall attempt to study the behaviour of
guided-waves in anisotropic media, and investigate the potential
applications of guided-waves in exploration and production seismics
by crosshole surveys. The thesis is organized as follows:

Firstly, this chapter will give a brief review of the general seismic anisotropy, surface-waves, interface-waves and Stoneley waves in isotropic media, and channel-waves in in-seam seismics. They form the basis of the work in this thesis.

Chapter 2 will present the theory of propagation of normal-mode guided-waves in multilayered anisotropic media. The theoretical development is based on the technique of Crampin and Taylor (1971) for computing seismic surface-wave dispersion in a plane-layered anisotropic half-space. We will give a matrix procedure for determining the theoretical dispersion, and three-dimensional amplitude/depth distribution of guided-waves in multilayered anisotropic waveguides.

Chapter 3 will investigate the propagation of seismic waves in both isotropic and anisotropic waveguides. Our particular interest is the waveguides displaying effective anisotropy of stress-aligned fluid-filled cracks or inclusions *(extensive-dilatancy anisotropy,* or EDA, Crampin *et al.* 1984b, Crampin 1987, Crampin and Lovell 1991), which is belived to pervade most rocks in the crust. Following the theory developed in Chapter 2, we will calculate velocity/frequency dispersion curves, amplitude/depth distributions, and synthetic seismograms for different isotropic and anisotropic waveguides. The synthetic seismograms will be calculated using the ANISEIS modelling package (Taylor 1990).

Chapter 4 will analyse a dataset from a shallow crosshole seismic survey at the Conoco Borehole Test Facility (CBTF), Oklahoma. Liu, Crampin and Queen (1991) have observed that the dominant energy in

the crosshole survey at the CBTF site is carried by guided-waves not body-waves. We will attempt to identify those guided-waves associated with some particular velocity structures from their dispersion and polarization characteristics, and model them with synthetic seismograms.

Chapter 5 is a study of two potential applications of guided-waves in production seismology by crosshole seismic surveys: the use of guided-waves for continuity tests between boreholes; and the use of guided-waves for monitoring Enhanced Oil Recovery (EOR) processes.

Chapter 6 will briefly describe the propagation of seismic waves in two special waveguides: a crack-controlled channel, which may be found in geothermal reservoir engineering; and an active fault zone.

Some conclusion remarks, and some suggestions for future work will be presented in Chapter 7.

1.2 SEISMIC ANISOTROPY

1.2.1 CAUSES OF SEISMIC ANISOTROPY

Any homogeneous uniform elastic material whose physical properties vary with direction is anisotropic, and seismic anisotropy refers to the variation of some characteristics (usually velocities, polarization patterns) of seismic wave-motion with direction. The general theory of wave motion in a uniform anisotropic elastic solid is well-documented (Love 1944, Musgrave 1954, Duff 1960, Lighthill 1960, Kraut 1963, Dieulesaint and Royer 1980). Comprehensive reviews for wave motions in layered anisotropic solids have been given by

Crampin (1977, 1981) and Crampin and Lovell (1991).

The rapid development in seismic wave recording and interpretation technology has made us realize that much of the Earth's crust displays effective anisotropy to seismic waves, and neglect of anisotropy is no longer appropriate to most geophysicists working in both earthquake and exploration seismology. Until recently, five possible sources of seismic anisotropy in the crust have been suggested (Crampin *et al.* 1984a, Crampin and Lovell 1991):

(a) Aligned crystals

Crystalline anisotropy occurs when the individual crystals in a crystalline solid have preferred orientations over a volume sufficiently large to affect the transmission of seismic waves (Babuska 1984). Such anisotropy (caused by minerals such as olivine or orthopyroxene) has been widely used to explain the observations in the upper mantle (Hess 1964, Francis 1969, Avé Lallemant and Carter 1970, Peselinick and Nicolas 1978, Christensen and Salisbury 1979, Fuchs 1983, Silver and Chan 1988).

(b) Direct stress-induced anisotropy

Direct stress-induced anisotropy occurs only when the stress becomes a large proportion of the eventual fracture strength (Dahlen 1972, Nikitin and Chesnokov 1984). It is suggested that direct stress-induced anisotropy is seldom likely to be a dominant source of anisotropy in the crust(Crampin *et al.* 1984b).

(c) Lithologic anisotropy

A sedimentary solid may have lithological anisotropy when the individual grains, which may or may not be elastically anisotropic, are elongated or flattened and those shapes are aligned by gravity or fluid flow when the material is first deposited, or by plastic deformation thereafter (Crampin *et al.* 1984b). Lithological anisotropy has been observed in shales by Kaarsberg (1960), Robertson and Corrigan (1983), White *et al* (1983), and Banik (1984), and in submarine turbidit*es* by Davis and Clowes (1986).

(d) Structural anisotropy

Periodic thin-layers (PTL) or finely layered media display this kind of anisotropy. PTL-anisotropy is often found in sedimentary basins (Bush and Crampin 1991). It has also been observed in marine sediments and in calcareous sediments (Johnson *et al.* 1977). This kind of anisotropy is sometimes refered to as transverse isotropy with a vertical symmetry axis (Levin 1978, Helbig 1984, Crampin 1986).

(e) Stress-aligned crack-induced anisotropy

It has now been recognized that stress-aligned fluid-filled cracks, microcracks and preferentially orientated pore-space exist in most rocks in the uppermost 10km to 20km of the crust, where it is known as *extensive-dilatancy anisotropy* or EDA (Crampin *et al.* 1984b, Crampin 1987). It is considered that EDA is the most important source of crustal anisotropy (Crampin and Lovell 1991), and will be reviewed in some details in the following section.

1.2.2 SHEAR-WAVE SPLITTING AND THE EDA HYPOTHESIS

Anisotropy in the crust will usually have two major effects on seismic body-wave propagation. Firstly, the velocities of both P-waves and shear-waves vary with the direction of propagation. Secondly, on entering a region of effective anisotropy, shear-waves split into two (or more) phases with fixed velocities and fixed polarization that propagate in that particular direction through the anisotropy. It is often difficult to recognize smooth variations of P-wave or shear-wave velocities unless arrival times can be observed over a wide range of directions in a single homogeneous layer. Shear-wave splitting is likely to be diagnostic of some form of seismic anisotropy in the crust. Shear-waves splitting was first positively identified above small earthquakes by Crampin *et al.* (1980, 1985), and Buchbinder (1985). As three-component digital recording has been become increasingly more available, shear-wave splitting in the crust has been widespreadly recognized in both earthquake recordings and controlled-source seismic data over the last decade. (For example, in earthquake recording data: Crampin *et al.* 1985, Booth *et al.* 1985, Buchbinder 1985, Evans *et al.* 1987, Peacock *et al.* 1988, Kaneshima 1990, Crampin *et al.* 1990, and in exploration seismic data: Crampin 1984a, Alford 1986, Lynn and Thomsen 1986, Willis *et al.* 1986, Johnston 1986, Crampin *et al.* 1986a, Martin and Davis 1987, Lewis 1989, Squires *et al.* 1989, Bush 1990, Liu *et al.* 1991.)

It is now believed that comparatively uniform shear-wave splitting is mainly caused by *extensive-dilatancy anisotropy* or EDA. Crampin and Lovell (1991) give six principal arguments to support the EDA

hypothsis: (1) Shear-wave splitting is seen along ray paths in almost all geological materials from poorly consolidated sediments (Crampin *et al*. 1986b) and sedimentary basins (Willis *et al*. 1986) to granite batholiths (Roberts and Crampin 1986, Kaneshima, Ando and Crampin 1987). Stress-aligned fluid-filled inclusions are the only source of anisotropy that has been suggested that is common to all rocks (Crampin *et al*. 1984b, Kaneshima 1990); (2) The polarization of the leading (faster) split shear-wave, within the shear-wave window at the surface, is usually observed to be parallel or sub-parallel to the direction of maximum horizontal compressional stress (see Figure 1.1); (3) The successful match of synthetic with observed polarization diagrams in the Paris Basin dataset (Bush and Crampin 1991); (4) The identification of fractures and fracture alignments in the Austin Chalk in Texas by the use of shear-wave splitting, which was later comfirmed by horizontal drilling (Mueller 1991); (5) Correlation of the amount of hydrocarbon production with the percentage of differential shear-wave velocity anisotropy in oil fields with variable production in Wyoming (Lewis 1989, Davis and Lewis 1990) and Russia (Brodov *et al*. 1991, Cliet *et al*. 1991). (6) The changes of shear-wave splitting with time would be a confirmation of fluid-filled cracks as the cause of shear-wave splitting (Crampin 1978), as none of the other possible causes are likely to vary with time. Temporal changes are believed to have been observed before and after earthquakes (Crampin *et al*. 1990, Booth *et al*. 1990), and before and after hydraulic fracturing (Crampin and Booth 1989).

The propagation of guided-waves is controlled by the shear-waves reflected or refracted on interface(s) with different frequencies. Therefore, we expect the propagation of guided-waves will also be significantly modified by the stress-aligned fluid-filled inclusions.
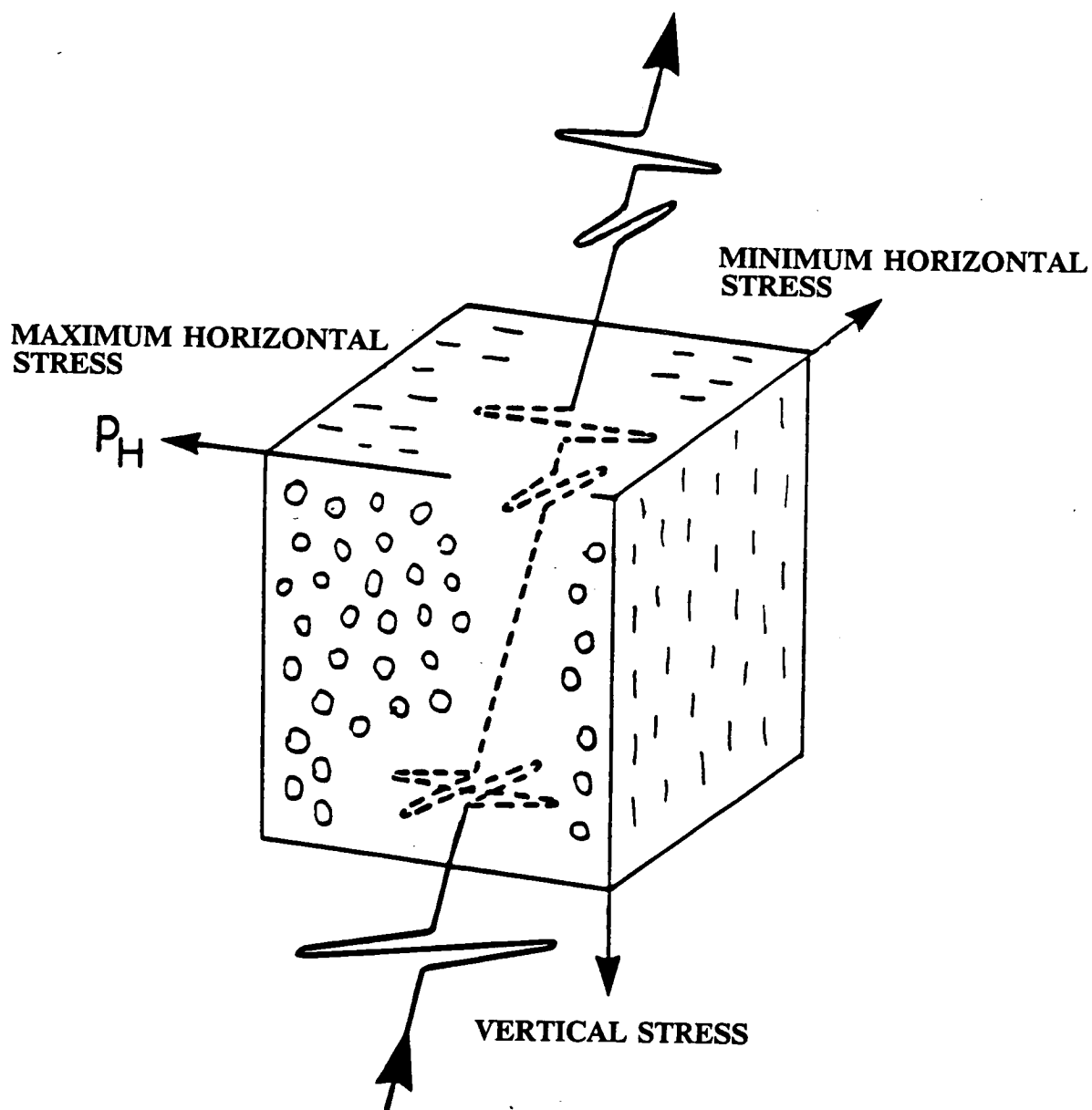
Figure 1.1 Schematic illustration of shear-wave splitting in aligned EDA cracks. The cracks are aligned by the typical stress relationships in the subsurface crust. The leading split shear-wave is polarized parallel to the strike of the cracks (after Crampin 1987).

1.2.3 THEORY AND FORMULATIONS FOR ALIGNED CRACKS

One of the most important developments in wave propagation studies in cracked solid is the use of effective elastic constants for the cracked material so that wave propagation can be calculated by a range of computer programs. A number of theories for this simulation have been developed under a wide range of conditions. Theoretical formulations for the elastic constants of a homogeneous and multiphase medium with randomly distributed, dry, and liguid-filled inclusions, have been studied by a number of investigators: Eshelby (1957), Hashin (1962), Walsh (1965), Wu(1966), Korringa (1973), O'Connel and Budiansky (1974, 1977), Kuster and Toksöz (1974).

Crampin (1978) obtained effective elastic constants by modelling the variation of velocity through a cracked solid derived in a first-order approximation theory by Garbin and Knopoff (1973, 1975a, b). Hudson (1980, 1981) then developed a more general theoretical approach for calculating the elastic constants of cracked solids that includes first-order (Hudson 1981) and second-order (Hudson 1982) interactions between the scattering inclusions. They all assume that material contains a uniform weak condition of aligned cracks, and the dimensions of cracks are small with respect to the seismic wavelength. Hudson (1981) also developed techniques for modelling attenuation in cracked solids. The most straightforward formulation for anisotropic attenuation is to express the attenuation parameter $1/Q$ as the eigenvalue of a matrix of the imaginary parts of complex elastic constants (Crampin 1981), where the real parts model the purely elastic behaviour. This allows attenuative wave propagation to be calculated by the same range of anisotropy programs as the purely elastic behaviour (Crampin 1981). Hudson's expression for the

elastic constants of medium containing aligned cracks is:

$$c_{ijkl} = c^0_{ijkl} + \varepsilon c^1_{ijkl} + \varepsilon^2 c^2_{ijkl}$$

where crack density (CD) ε is defined as the number of cracks in a unit volume, $\varepsilon = N a^3/v$, where N is the number of cracks of radius a in volume v (Budiansky and O'Connell 1976); c^0_{ijkl} are elastic constants of uncracked rock; c^1_{ijkl} and c^2_{ijkl} are first and second order perturbation due to cracks, respectively, which are given by Crampin (1984b). The result may be formulated so that real parts model the velocity variation of body-waves and imaginary parts model attenuation (Crampin 1981). This allows wave propagation through a two-phase cracked solid to be modelled by wave propagation through a homogeneous anisotropic material with complex elastic constants.

Hudson's formulations are currently restricted to crack density less than about 0.1 (Crampin 1984b), and aspect ratio, $AR = d/a$, less than about 0.1, where d is half-thickness of cracks (Douma 1988). Nishizawa (1982) used the Eshelby's (1957) technique to calculate elastic response for cracks with arbitrary aspect ratios, but with similar limitations of crack density. Nishizawa's formulation has no restriction on the value of the aspect ratio. Douma (1988) compared the formulations of Nishizawa (1982) and Hudson (1980,1981) for a large range of aspect ratios. The two techniques give identical results up to an aspect ratio $AR = 0.1$ and have similar angular patterns of velocity variations up to $AR = 0.3$ although the absolute value of the velocities begins to differ for $AR > 0.1$.

Hudson (1986, 1990) has extended his formulations to include

distributions of cracks with more than one crack orientation and distibutions of cracks in anisotropic matrix rocks. His latest formulations include the second order interactions of the perturbations from cracks (the effective crack-to-crack interactions).

[In this thesis, all effective elastic constants for material containing aligned fluid-filled cracks will be calculated by using Hudson's (1980, 1981) formulations for small aspect ratios(< 0.05), and by Nishizawa's formulations for large aspect ratios (> 0.05).]

1.2.4 SYNTHETIC SEISMOGRAMS AND THE ANISEIS PACKAGE

The calculation of synthetic seismograms is one of major techniques for the study of wave propagation, and for the interpretation of seismic data. In particular, synthetic seismograms and numerical experimentation have been a major aid to understanding wave propagation in anisotropic media. There are, at present, two principal techniques for computing synthetic seismograms in anisotropic media. These are the ray tracing (Cerveny and Psencik 1972, Petrashen and Kashtan 1984, Gajewski and Psencik 1987), and the reflectivity method or propagator-matrix method (Keith and Crampin 1977a,b,c, Taylor and Crampin 1978, Booth and Crampin 1983a,b). The ray tracing method may be applied to the study of propagation of seismic waves in laterally inhomogeneous anisotropic media and complex geological structures where other methods may not be appropriate. One of the problems with the anisotropic ray tracing method is how to specify and attach meaning to varying anisotropic media, where a number of elastic constants vary in three-dimensions (Crampin 1981). Another disadvantage of the ray method is that it is

invalid near caustics, such as the singularities on the shear-wave velocity sheets (Crampin 1991), which in many circumstances may be very common phenomenon (Wild and Crampin 1991). Up to now, the most successful and effective modelling technique in plane-layered anisotropic media is the reflectivity method or propagator matrix method which has been used in the ANISEIS package (Taylor 1990).

ANISEIS is a flexible interactive computer modelling system for calculating synthetic seismograms from a point source in horizontal plane-layered anisotropic and cracked media. Variable source-geophone geometries such as surface-surface reflections, VSPs, crosshole surveys can be accommodated. Based on plane-wave analysis, synthetic seismograms are calculated in ANISEIS with an intergration of plane-waves along summation paths over frequency, slowness (vertical plane) and azimuth (horizontal plane). There is a variety of choices of source types and source signature shapes: Point sources can be explosive, vertical force or horizontal force; source signals can be chosen among six pulses offered by ANISEIS, or defined by users. However, the source signals need not be given until the impulse response of the model has been calculated. This allows a number of different source signals to be tested, each being convolved with the impulse response.

The reflectivity technique used in the ANISEIS package is a fullwave modelling technique. Almost all kinds of seismic waves including body-waves, surface-waves, guided-waves and other non-geometrical inhomogeneous waves can be included. However, there are some restrictions in uses of ANISEIS: All models must be horizontal plane-layered structures; the material containing point

source should be isotropic; for certain types of summation path in the slowness plane, any halfspace used must also be isotropic. The restriction on source layer is not serious since the layer can be made very thin and internal reflections within it can be suppressed.

All synthetic seismograms in this thesis will be calculated in ANISEIS package.

1.3 SURFACE-WAVES

Seismic surface-waves travel along the free surface of the earth, which are also called surface waveguides. Rayleigh (1887) first found surface-waves which propagate along the free surface with elliptical particle motion in a vertical plane, where they are known as Rayleigh waves. Richter (1941) derived the mathematical formulations of Rayleigh waves over an isotropic halfspace. The amplitude of Rayleigh wave motion decreases exponentially with depth below the surface. The velocity of Rayleigh waves is slower than any body-wave, being about nine-tenths that of shear wave in the same medium. If a low-velocity surface layer overlies the halfspace, Rayleigh waves are dispersive, that is, the velocities vary with frequency. On the surface of the low-velocity layer, another kind of dispersive surface-waves with horizontal transverse wave motion can exist, where it is called Love waves (Love 1892).

The calculation of surface-wave dispersion in plane-layered structures has played a major part in analysing the isotropic earth structure for over several decades (Crampin 1981). The effects on surface-waves of anisotropy in the crust and upper-mantle have been observed both for continental (Crampin and King 1977) and oceanic

paths (Forsyth 1975, Kirkwood and Crampin 1981). Crampin (1970) first extended the Thompson-Haskell matrix formulation (Haskell 1953) to calculate the dispersion of surface-waves in anisotropic multilayered halfspaces. Surface-waves in anisotropic media have some distinctive differences from the propagation in isotropic media. The two independent families of isotropic Rayleigh-modes and Love-modes coalesce in anisotropic media into one family of *Generalized* modes propagating with elliptical particle-motion in three-dimensions (Crampin 1970, 1975). In structures with weak anisotropy, alternate modes usually correspond to isotropic Rayleigh- and Love-mode particle-motion, and in directions of sagittal symmetry the *Generalized* waves have strictly Rayleigh- or Love-type particle-motion. The polarization anomalies in three-dimensional particle-motions are the most distinctively recognizable feature of surface-wave propagation in anisotropic media. Crampin (1975) showed that particle-motion of higher-mode surface waves is particularly sensitive to the presence of anisotropy in the crust or upper-mantle. Crampin and King (1977) have observed coupled transverse and sagittal particle-motion of higher-mode waves for a number of paths across Eurasia. They identified them as third *Generalized* mode (corresponding to second Rayleigh-type mode), with aligned anisotropy in the upper-mantle throughout North Eurasia.

The propagation of surface-waves in laterally inhomogeneous structures also have been recently studied (Levshin 1984, 1985, Snieder and Romanowicz 1988). The heterogeneity may also result in the interconversion between Love and Rayleigh wave motions in isotropic media.

We demonstrate in this thesis that the theory and concepts

developed for propagation of surface-waves will still be applicable to the generalized guided-waves. By extending the technique of Crampin (1970) and Crampin and Taylor (1971) for calculating the dispersion of surface-waves in halfspaces of anisotropic layers, we will establish the theory of propagation of guided-waves in multilayered anisotropic structures in this thesis.

1.4 INTERFACE-WAVES AND STONELEY WAVES

On an interface between two elastic halfspaces, there is an inhomogeneous guided-wave with an elliptical particle-motion and energy propagating parallel to, and decaying exponentially away from, the interface, where it is usually known as interface-wave. Theroretically, interface-waves propagating along the interface between two elastic halfspaces are independant of frequency and are not dispersive.

Although inhomogeneous attenuating interface-wave propagation is possible along almost any interface, for a specific narrow range of elastic constants, there may also exist a normal mode non-attenuating non-dispersive Stoneley wave travelling at a velocity less than any of the body-wave velocities in two halfspaces (Stoneley 1924). The Stoneley equation which controls the phase velocity of Stoneley waves for an isotropic solid/solid interface is given by Pilant (1972), and for an isotropic liquid/solid interface by Strick and Ginzbarg (1956). The Stoneley waves can exist at a solid/solid interface only under the stringent condition that shear-wave velocities in the two halfspaces are nearly equal. However, Stoneley waves are always possible at a liquid/solid interface (Aki and Richards 1980). For a given interface, if the Stoneley equation is not satisfied, or
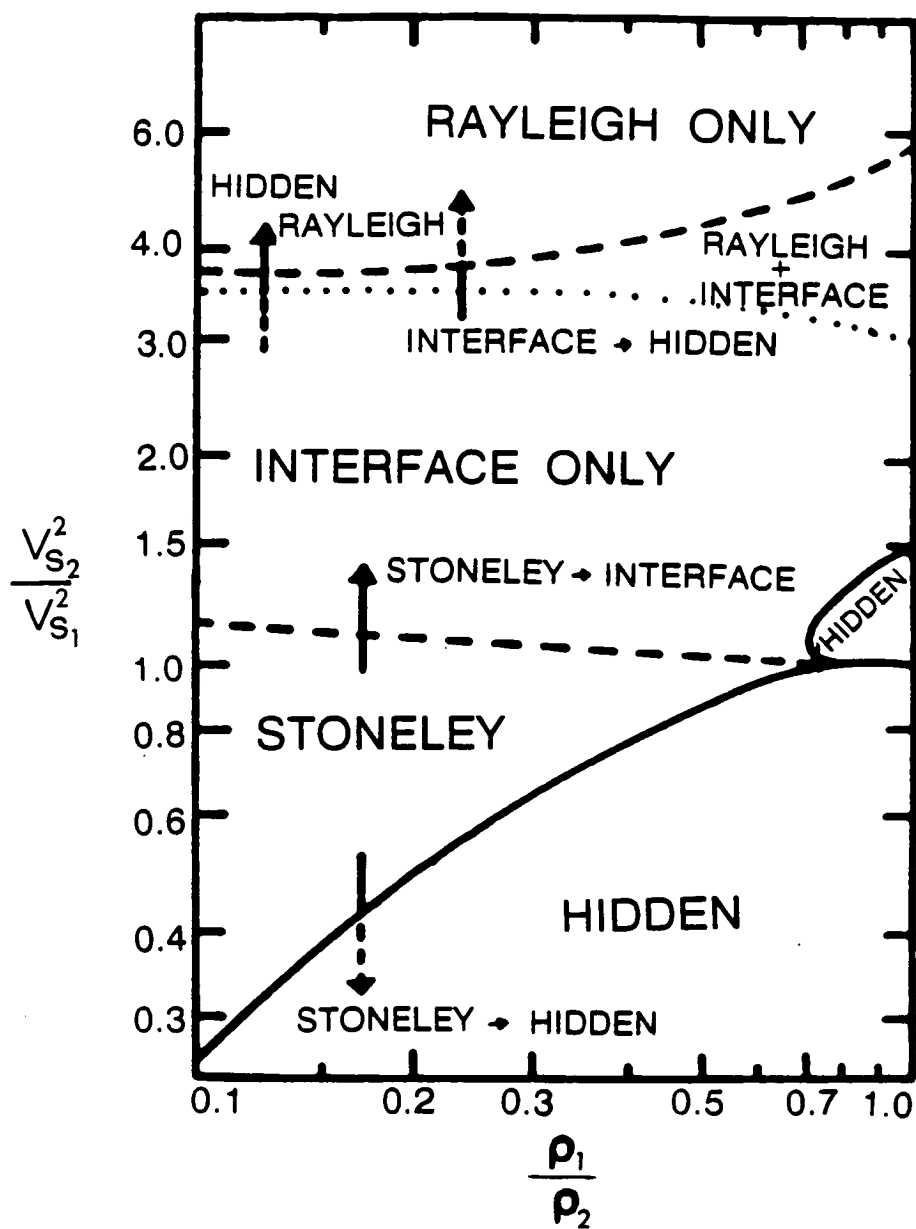
Figure 1.2 Stoneley, Interface, Rayleigh waves regimes and associated transitions for different shear-wave velocity ratios and density ration between two isotropic halfspaces (after Pilant 1972).

phase-velocity roots from the equation are complex, the Stoneley waves are degraded into inhomogeneous interface-waves. Pilant (1972) calculated Stoneley, Interface, Rayleigh waves regimes and associated transitions for different shear-wave velocity ratios and density ratios, between two isotropic halfpaces having Poisson's ratio 0.25 (See Figure 1.2).

In borehole seismics or acoustic logging , the Stoneley wave which propagates along the borehole or tube, is often found, where it is usually called tube-wave. Tang *et al.* (1991) have recently studied the propagation of Stoneley waves in a fluid-filled borehole with a vertical fracture. They presented a quantitative relationship between the Stoneley wave propagation and fracture character in conjunction with formation and fluid properties. Their study provided a method for estimating the charecteristics of a vertical fracture by means of Stoneley wave measurements.

1.5 CHANNEL-WAVES IN COAL-SEAM SEISMICS

Guided-waves in in-seam seismics are often called channel-waves. Coal-seams usually act as low-velocity waveguides, and trap much of the seismic energy when a source is shot within coal-seams. The wave-guiding phenomenon of coal-seams was first observed by Evison (1955) in a coal mine in New Zealand. Since then, channel-waves have been accepted as a routine tool in coal mining geophysics to map coal-seams and to detect faults inside coal-seams (Krey 1963, Mason *et al.* 1980, Buchanan *et al.* 1981, Krey *et al.* 1982, Mason *et al.* 1985, Greenhalgh *et al.* 1986, Krajewski *et al.* 1987). Buchanan (1983), Jackson (1985) and Regueiro (1990) have given comprehensive reviews of the theory and practice of channel-waves in coal-seam

seismics.

The propagation of channel-waves in isotropic coal-seams has been extensively studied (For example, Krey 1963, Buchanan 1978, 1987, Buchanan *et al*. 1981, Franssens *et al*. 1985). However, anisotropy in coal-seams has been reported. One form of anisotropy present in coal-seams is due to aligned cleats (Jackson 1985). To achieve a better resolving power for estimating/imaging in-seam faulting, anisotropy of coal-seams should be considered (Buchanan *et al*. 1983). Liu *et al* (1992) successfully modelled the observed channel-waves in a British coal mine, where cleat-induced anisotropy has been taken into account.

In this thesis, we will study the propagation of guided-waves in crack-induced anisotropic media in crosshole surveys. We believe that, as in in-seams seismics, guided-waves will play an important role in sedimentary reservoir production seismics in the future.

CHAPTER 2

THEORY OF NORMAL-MODE GUIDED-WAVE PROPAGATION IN MULTILAYERED ANISOTROPIC STRUCTURES

2.1 INTRODUCTION

The propagation of guided-waves (or channel-waves) in multilayered isotropic solids has been extensively studied, and the mathematical formulations for calculating dispersion of guided-waves and the amplitude/depth distribution of Love type guided-waves have been available by Räder et al. (1985) and Buchanan (1987).

Here we will present a procedure for determining the dispersion and amplitude/depth distribution of guided-waves in multilayered anisotropic structures. The procedure is an extension of the technique of Crampin (1970) and Crampin and Taylor (1971) for calculating the dispersion of surface-waves in a halfspace of multilayered anisotropic layers. We consider a model made of n parallel anisotropic layers embedded between two halfspaces (Figure 2.1). The halfspaces are assumed to be isotropic. This simplifies mathematical treatment without loss of generality: since anisotropic halfspaces may be treated by increasing the thickness of first and nth layers to a large enough value.

The coordinate system is shown in Figure 2.1. The interference of body-waves, which are multiply reflected or refracted within the
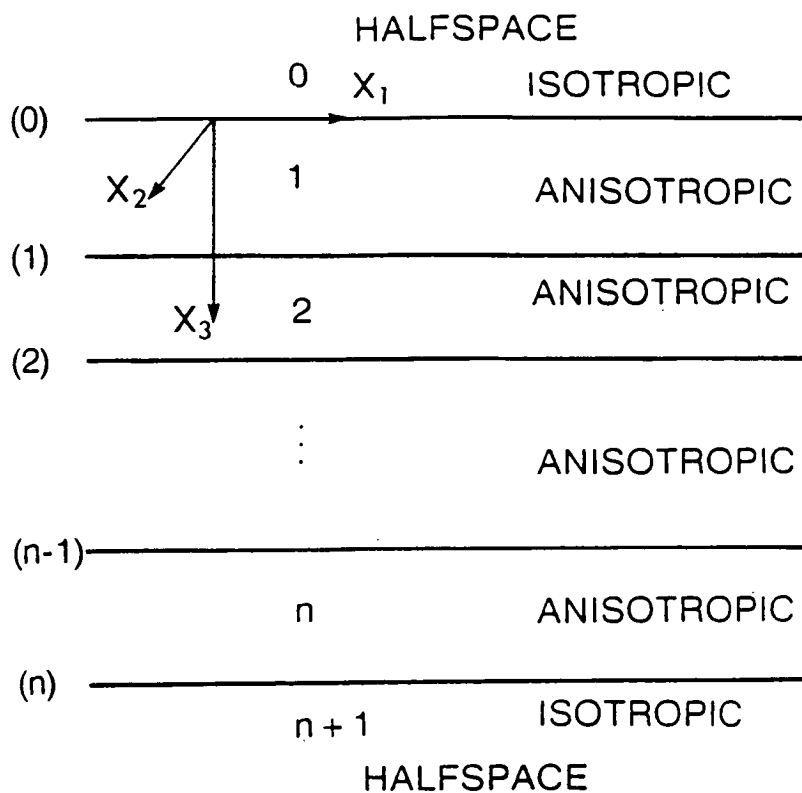
Figure 2.1 Multilayered anisotropic waveguide model and the coordinate system for guided-wave dispersion calculations.

internal layers, forms guided-waves propagating in the x_1 direction with phase-velocity c. The conditions for forming the propagator matrix formulations are the continuity of three displacement components (u_1, u_2, u_3) and the three stresses $(\sigma_{13}, \sigma_{23}, \sigma_{33})$ of a plane body-wave at an interface, where there are no sources at infinity in the halfspaces.

2.2 WAVE EQUATIONS IN ANISOTROPIC LAYERS

We choose the following notations:

x_1, x_2, x_3 = orthogonal coordinates;

u_1, u_2, u_3 = components of displacement;

σ_{13}, σ_{23}, σ_{33} = vertical, and horizontal radial and transverse stress components;

d_i = thickness of ith layer; and

ρ = density.

In each anisotropic layer, the equations of motion for elastic waves propagating with infinitesimal displacements may be written:

$$\rho \ddot{u}_i = C_{ijkm} u_{k,jm}; \quad (i,j,k,m=1,2,3) \tag{1}$$

where C_{ijkm} are the fourth order tensor of elastic constants with the following symmetries:

$$C_{ijkm} = C_{kmij} = C_{mkij}. \quad (i,j,k,m=1,2,3) \tag{2}$$

We suppose the periodic solution of a plane wave with displacements:

$$u_j = a_j \exp[i\omega(t - q_k x_k)]; \qquad (j, k = 1, 2, 3) \tag{3}$$

where a_j is the amplitude coefficient of the jth displacement; and q_k is the kth component of slowness vector. In the sagittal plane (x_1, x_3), there is no variation of motion normal to the plane, so we assume $q_2 = 0$ and write $q_1 = 1/c$, where c is phase velocity along x_1 direction.

Substitution of (3) into (1) gives three simultaneous equations in a_k:

$$F_{ik} a_k = 0; \tag{4}$$

where $F_{ik} = -\rho\delta_{ik} + C_{ijkm}q_j q_m \qquad (i, j, k, m = 1, 2, 3)$.

The condition for a non-trivial solution of (4) is:

$$\det(\mathbf{F}) = 0, \tag{5}$$

yielding a polynomial of degree six in q.

Following Taylor and Crampin (1978), equation (4) can be written in the matrix form:

$$\mathbf{Fa} = (\mathbf{R}p^2 + \mathbf{S}p + \mathbf{T} - \rho c^2 \mathbf{I})\mathbf{a} = 0; \tag{6}$$

where $\mathbf{a}$ is the vector of amplitude coefficients; $q_1 = 1/c$; $q_2 = 0$; $q_3 = p/c$; $\mathbf{I}$ is the unit matrix; $\mathbf{R} = \{C_{i3j3}\}$; $\mathbf{S} = \mathbf{V} + \mathbf{V}^T$; $\mathbf{V} = \{C_{i3j1}\}$; and $\mathbf{T} = \{C_{i1j1}\}$ for $(i, j = 1, 2, 3)$.

Furthermore, since the matrix **R** is non-singular, the equation (6) can be written in the form:

$$\left\{ \begin{bmatrix} -\mathbf{R}^{-1}\mathbf{S} & -\mathbf{R}^{-1}\mathbf{T}' \\ \mathbf{I} & \mathbf{0} \end{bmatrix} - p \begin{bmatrix} \mathbf{I} & \mathbf{0} \\ \mathbf{0} & \mathbf{I} \end{bmatrix} \right\} \begin{bmatrix} p\mathbf{a} \\ \mathbf{a} \end{bmatrix} = 0; \qquad (7)$$

where $\mathbf{T}' = \mathbf{T} - \mathbf{I}\rho c^2$.

This ia a 6X6 linear eigenvalue problem for p, and forms the basis of numerical computation in the procedure.

Each eigenvalue p contributes to the displacements, and the solution **u** may be constructed by:

$$\mathbf{u} = \mathbf{A}\,\mathbf{B}\,\mathbf{f}\,e(x_1, t); \qquad (8)$$

where $\mathbf{u} = (u_1, u_2, u_3)^T$; $\mathbf{A} = (\mathbf{a}_1, \mathbf{a}_2, \mathbf{a}_3, \mathbf{a}_4, \mathbf{a}_5, \mathbf{a}_6)$;

$\mathbf{B} = \mathrm{diag}(b_1, b_2, b_3, b_4, b_5, b_6)$;

$b_i = \exp[-i\omega p_i x_3/c]$; **f** is a vector of excitation factor; and $e(x_1, t) = \exp[i\omega(t - x_1/c)]$.

The relation between displacements and stresses is given by:

$$\tau_{jk} = C_{jkm}\, u_{m,n}. \qquad (j, k = 1, 2, 3) \qquad (9)$$

Combining (8) and (9), we have:

$$\begin{bmatrix} \mathbf{u} \\ \tau \end{bmatrix} = \begin{bmatrix} \mathbf{0} & \mathbf{I} \\ \mathbf{R} & \mathbf{V} \end{bmatrix} \begin{bmatrix} \mathbf{A}P \\ \mathbf{A} \end{bmatrix} \mathbf{B}\,\mathbf{f}\,e(x_1, t); \qquad (10)$$

where $\mathbf{u}^T = (u_1, u_2, u_3)$; $\tau^T = (ic/\omega)(\sigma_{13}, \sigma_{23}, \sigma_{33})$; and

$$\mathbf{P} = \text{diag}(p_1, p_2, p_3, p_4, p_5, p_6).$$

Let $\begin{bmatrix} \mathbf{0} & \mathbf{I} \\ \mathbf{R} & \mathbf{V} \end{bmatrix} \begin{bmatrix} \mathbf{AP} \\ \mathbf{A} \end{bmatrix} = \mathbf{E},$ then

$$(\mathbf{u} \quad \tau)^T = \mathbf{E}\,\mathbf{B}\,\mathbf{f}\,e(x_1, t). \tag{11}$$

The boundary conditions at an interface between two layers are the continuity of the three displacements and three stresses. Applying (11) to all the interfaces of the model, we have the matrix recurrence relation:

$$[u_1, u_2, u_3, (ic/\omega)\sigma_{13}, (ic/\omega)\sigma_{23}, (ic/\omega)\sigma_{33})]_0^T$$
$$= \mathbf{G}\,[u_1, u_2, u_3, (ic/\omega)\sigma_{13}, (ic/\omega)\sigma_{23}, (ic/\omega)\sigma_{33})]_n^T; \tag{12}$$

where

$$\mathbf{G} = \mathbf{E}_1\,\text{diag}(\exp(i\omega q_3^{(1)}d_1))\,\mathbf{E}_1^{-1}.\mathbf{E}_2\text{diag}(\exp(i\omega q_3^{(2)}d_2))\mathbf{E}_2^{-1}\ldots\mathbf{E}_n;$$

and subscript 0 and n refer to at the top and bottom interfaces, respectively.

2.3 DISPLACEMENTS AND STRESSES IN ISOTROPIC HALFSPACES

In the isotropic halfspaces, *P-SV* components and *SH* component are decoupled and may be treated independently.

2.3.1 *P-SV* COMPONENTS

The displacements may be constructed by combining the dilatational and the rotational wave solutions:

$$u_1 = U_p + U_s; \text{ and } u_3 = W_p + W_s; \tag{13}$$

where superscript p and s refer to dilatational and rotational

components; U_p and W_p satisfy the dilatational wave equation; and

U_S and W_S satisfy the rotational wave equation.

The dilatational motion is irrotational, and the rotational motion

is divergence-less, that is:

$$\nabla \times \begin{bmatrix} U_p \\ 0 \\ W_p \end{bmatrix} = 0; \text{ and } \nabla \cdot \begin{bmatrix} U_S \\ 0 \\ W_S \end{bmatrix} = 0. \tag{14}$$

The U_p, U_S, W_p, W_S have the following general periodic solutions:

$$U_p = [A' \exp(-ik\gamma_\alpha x_3) + A'' \exp(ik\gamma_\alpha x_3)] \, e(x_1, t);$$

$$U_S = [B' \exp(-ik\gamma_\beta x_3) + B'' \exp(ik\gamma_\beta x_3)] \, e(x_1, t);$$

$$W_p = [C' \exp(-ik\gamma_\alpha x_3) + C'' \exp(ik\gamma_\alpha x_3)] \, e(x_1, t); \text{ and} \tag{15}$$

$$W_S = [D' \exp(-ik\gamma_\beta x_3) + D'' \exp(ik\gamma_\beta x_3)] \, e(x_1, t);$$

where $\{A', B', C', D'\}$ and $\{A'', B'', C'', D''\}$ are constants referring to

downward and upward travelling plane-waves, respectively, where

$$\gamma_\alpha = \begin{cases} [(c/\alpha)^2 - 1]^{\frac{1}{2}} & c > \alpha \\ -i[1-(c/\alpha)^2]^{\frac{1}{2}} & c < \alpha \end{cases}; \qquad \gamma_\beta = \begin{cases} [(c/\beta)^2 - 1]^{\frac{1}{2}} & c > \beta \\ -i[1-(c/\beta)^2]^{\frac{1}{2}} & c < \beta \end{cases}$$

$\alpha = [(\lambda + 2\mu)/\rho]$ = velocity of propagation of dilational waves in an

isotropic halfspace; $\beta = [\mu/\rho]$ = velocity of propagation of rotational

waves in an isotropic halfspace; and λ, μ = Lamé elastic constants in

an isotropic halfspace.

The curl and divergence conditions (14) give:

$$C' = \gamma_\alpha A';$$

$$C'' = -\gamma_\alpha A'';$$

$$D' = -B'/\gamma_\beta; \text{ and}$$

$$D'' = B''/\gamma_\beta. \tag{16}$$

The normal and tangential stress components are:

$$\sigma_{33} = \rho\alpha^2 \partial u_3/\partial x_3 + \lambda\, \partial u_1/\partial x_1; \text{ and}$$

$$\sigma_{13} = \mu(\partial u_1/\partial x_3 + \partial u_3/\partial x_1). \tag{17}$$

So, we have the general displacements and stresses expressions for *P-SV* components:

$$u_1 = [A' \exp(-ik\gamma_\alpha x_3) + A'' \exp(ik\gamma_\alpha x_3)$$
$$+ B' \exp(-ik\gamma_\beta x_3) + B'' \exp(ik\gamma_\beta x_3)]\, e(x_1,t);$$

$$u_3 = [\gamma_\alpha A' \exp(-ik\gamma_\alpha x_3) - \gamma_\alpha A'' \exp(ik\gamma_\alpha x_3)$$
$$- B'/\gamma_\beta \exp(-ik\gamma_\beta x_3) + B''/\gamma_\beta \exp(ik\gamma_\beta x_3)]\, e(x_3,t);$$

$$\sigma_{33} = [-ik(\rho\alpha^2\gamma_\alpha^2+\lambda)(A' \exp(-ik\gamma_\alpha x_3) + A'' \exp(ik\gamma_\alpha x_3))$$
$$+ik(\rho\alpha^2-\lambda)(B' \exp(-ik\gamma_\beta x_3) + B'' \exp(ik\gamma_\beta x_3))]\, e(x_1,t); \text{ and}$$

$$\sigma_{13} = [-ik2\mu\gamma_\alpha(A' \exp(-ik\gamma_\alpha x_3) - A'' \exp(ik\gamma_\alpha x_3))$$
$$-ik\mu(\gamma_\beta-1/\gamma_\beta)(B' \exp(-ik\gamma_\beta x_3) - B'' \exp(ik\gamma_\beta x_3))]\, e(x_1,t). \tag{18}$$

2.3.2 *SH* COMPONENT

Similarly, the *SH* displacement and transverse stress in the isotropic halfspaces can be expressed by:

$$u_2 = [T' \exp(-ik\gamma_\beta x_3) + T'' \exp(ik\gamma_\beta x_3)]\, e(x_1,t); \text{ and}$$

$$\sigma_{23} = \mu\partial u_2/\partial x_3$$
$$= -ik\mu\gamma_\beta[T'\exp(-ik\gamma_\beta x_3) - T''\exp(ik\gamma_\beta x_3)]\, e(x_1,t); \tag{19}$$

where T' and T'' are constants referring to downward and upward

travelling plane-waves, respectively.

2.3.3 DISPLACEMENTS AND STRESSES AT INTERFACES

Setting $x_3=0$ in (18) and (19) and omiting the term $e(x_1,t)$, we obtain the displacements and stresses at top interface(0) and bottom interface(n):

$$[u_1,\ u_2,\ u_3,\ (ic/\omega)\sigma_{13},\ (ic/\omega)\sigma_{23},\ (ic/\omega)\sigma_{33}]_0^T$$
$$= \mathbf{E}_0\ [A'_0, T'_0, B'_0, A''_0, T''_0, B''_0]^T; \qquad (20)$$

where $\mathbf{E}_0 =$

$$\begin{bmatrix} 1 & 0 & 1 & 1 & 0 & 1 \\ 0 & 1 & 0 & 0 & 1 & 0 \\ \gamma_\alpha & 0 & -1/\gamma_\beta & -\gamma_\alpha & 0 & 1/\gamma_\beta \\ 2\mu\gamma_\alpha & 0 & \mu(\gamma_\beta-1/\gamma_\beta) & -2\mu\gamma_\alpha & 0 & \mu(1/\gamma_\beta-\gamma_\beta) \\ 0 & \mu\gamma_\beta & 0 & 0 & -\mu\gamma_\beta & 0 \\ \lambda+\rho\alpha^2\gamma_\alpha^2 & 0 & \lambda-\rho\alpha^2 & \lambda+\rho\alpha^2\gamma_\alpha^2 & 0 & \lambda-\rho\alpha^2 \end{bmatrix}_0$$

$$[u_1,\ u_2,\ u_3,\ (ic/\omega)\sigma_{13},\ (ic/\omega)\sigma_{23},\ (ic/\omega)\sigma_{33}]_n^T$$
$$= \mathbf{E}_{n+1}\ [A'_{n+1}, T'_{n+1}, B'_{n+1}, A''_{n+1}, T''_{n+1}, B''_{n+1}]^T; \qquad (21)$$

where the subscript "0" refers to parameters in layer 0; and $\mathbf{E}_{n+1}$ has the same form as $\mathbf{E}_0$, except that the subscript '0' is replaced by '$n+1$'.

2.4 DISPERSION EQUATION

Substituting (20) and (21) into (12), and noting that there are no sources at infinity in the halfspaces, that is, the downward

components in the top halfspace:

$$A'_0 = T'_0 = B'_0 = 0,$$

and upward components in the bottom halfspace:

$$A''_{n+1} = T''_{n+1} = B''_{n+1} = 0.$$

Thus, we have

$$[0, 0, 0, A''_0, T''_0, B''_0]^T$$
$$= E_0^{-1} G E_{n+1} [A'_{n+1}, T'_{n+1}, B'_{n+1}, 0, 0, 0]^T. \qquad (22)$$

The condition for non-trival values of A'_{n+1}, T'_{n+1} and B'_{n+1} is the vanishing of the following sub-determinant, and we have the dispersion equation:

$$\det (H_{ij}) = 0. \qquad (i,j = 1,2,3) \qquad (23)$$

where $H = E_0^{-1} G E_{n+1}$.

2.5 PHASE-VELOCITY AND GROUP-VELOCITY DISPERSION

2.5.1 PHASE-VELOCITY DISPERSION

By solving equation (23), we obtain the relationship for the phase-velocity dispersion of guided-waves. However, (23) is a complex determinant equation, and can only be solved by numerical methods. If we assume that the frequency is always real, normal-mode roots are found along the real velocity axis for simultaneous zero crossing of

both real and imaginary parts of the determinant. The system of matrices giving the determinant must be completely re-calculated for every new trial velocity. While at a fixed velocity, new frequency trials alter each matrix by only a simple diagonal multiplier. It usually takes less computing time to find the frequencies at which several modes travel at one velocity than it does to find the velocities at one frequency. In addition, when two modes of guided-waves come very close (For example, near pinch or intercross positions), computing in the neighbourhood of these positions may become extremely tight. We need to decrease the search interval value to ensure that modes are not missed.

2.5.2 GROUP-VELOCITY DISPERSION

In anisotropic media, the propagation of energy of guided-waves is not usually parallel to the propagation vector (except in particular symmetric directions), and the group-velocity cannot be obtained by a simple differentiation of the phase-velocity as in isotropic case.

It may be shown by an extension of Sommerfield's method (Richter 1958) that the longitudinal and transverse components of the group-velocity of a normal-mode guided-wave are $\delta\omega/\delta k_1$, $\delta\omega/\delta k_2$, where ω is the angular frequency, and k_1 and k_2 are the wave numbers parallel to the propagation vector, and the wave front, respectively. In isotropic structures, where for a given frequency there is no variation of wave number with directions, the wave numbers k_1 and k_2 are inversely proportional to the direction cosines, the group-velocity can be written in the well-known form $\delta\omega/\delta k$, where k is the wave number in the direction of the propagation vector.

By partial differentiation of $\omega(k_1, k_2)$, we have

$$\Delta\omega = (\delta\omega/\delta k_1)\Delta k_2 + (\delta\omega/\delta k_2)\Delta k_2 \qquad (24)$$

where $\Delta\omega$, Δk_1, and Δk_2 are small increments in ω, k_1, and k_2, respectively. $\delta\omega/\delta k_1$ is the group-velocity resolved perpendicular to the wave front and can be determined by differentiation of the phase-velocity dispersion curve. $\Delta\omega$, Δk_1, and Δk_2 can be obtained by calculating the dispersion after having made an infinitesimal change in direction of propagation in the waveguide structure. Substituting these values into (24), we have $\delta\omega/\delta k_2$, component of the group-velocity parallel to the wave front. The values of $\delta\omega/\delta k_1$ and $\delta\omega/\delta k_2$ together determine the group-velocity magnitude and direction at any point on a wave front of a normal-mode of guided-waves travelling in a given direction. In general, the variation of the phase-velocity with material orientation in the waveguide structure is insufficient to make $\delta\omega/\delta k_2$ very large, and for surface-waves the inclinations of group- and phase- velocities will differ by only a few degrees and the absolute values by a few percent (Crampin and Taylor 1975). In this thesis, we will calculate only the projection of the group-velocity ($\delta\omega/\delta k_1$) in the direction of propagation by differentiation of the phase-velocity. This is a good first-order approximation, except in strong anisotropy greater than 10%, say. In any case, however, there is no simple technique for calculating the group-velocity of surface- or guided-waves in particular azimuthal directions.

2.6 AMPLITUDE/DEPTH DISTRIBUTION

Determining the relative amplitude (or eigenfunction) /depth

distribution of each mode of guided-waves for different frequencies is very important to study the propagation behaviour of guided-waves. In anisotropic media, each mode of guided-waves usually has three-dimensional wave motion as a result of energy cross-coupling. Therefore, we need to calculate three-component amplitude/depth distribution for each mode of guided-waves.

From the matrix equation (22), we have

$$[H_{ij}] \ [A'_{n+1}, T'_{n+1}, B'_{n+1}]^{T} = 0 \qquad (i, \ j = 1,2,3) \qquad (25)$$

where $H = E_{0}^{-1} \ G \ E_{n+1}$.

When dispersion equation (23) $[H_{ij}] = 0$ holds, only two of the three equations in (24) are independent, three down-going wave excitations A'_{n+1}, T'_{n+1}, B'_{n+1} in the bottom halfspace can be determined from the two of which are independent. [The extra degree of freedom may be removed by normalizing the excitations]

Once A'_{n+1}, T'_{n+1} and B'_{n+1} are determined, all six wave excitations $f_i(1)$, ... $f_i(6)$ in i th layer can be decided by the matrix equation

$$[f_i(1), \ f_i(2), \ f_i(3), \ f_i(4), \ f_i(5), \ f_i(6)]^{T}$$
$$= B_i^{-1} E_i^{-1} E_{i+1} [f_{i+1}(1), \ f_{i+1}(2), \ f_{i+1}(3),$$
$$f_{i+1}(4), \ f_{i+1}(5), \ f_{i+1}(6)]^{T} \qquad (26)$$

Finally, for each mode and its different frequency, we can calculate three components of displacement of the guided-wave u_1, u_2, u_3 in different depths of the waveguide by solving the equation (10).

CHAPTER 3

GUIDED-WAVES IN CRACKED AND UNCRACKED ROCKS

3.1 INTRODUCTION

The crack-induced anisotropy has been observed in most coal
seams, where cracks are usually known as 'cleats' (Jackson 1985),
and in most reservoir rocks (Willis *et al.* 1986). The presence of
these cracks, fractures or pores will significantly modify the
propagation of guided-waves in such anisotropic media. Based on
the theory and techniques developed in Chapter 2, we will study the
effects of these cracks or fractures on the propagation of guided-
waves in crack-induced anisotropic waveguides.

As the behaviour of guided-wave modes has received comparatively
little attention in the past, we first examine the propagation of
guided-waves in simple isotropic structures before introducing the
effective anisotropy of stress-aligned fluid-filled cracks. We
will calculate velocity/frequency dispersion curves,
amplitude/depth distributions, and synthetic seismograms for
different isotropic and anisotropic waveguides.

Dispersion is one of the main characteristics of guided-wave
propagation, and the inversion of the observed dispersion of a
guided-wave is an important technique for determing the structure
and property of the waveguide. A preliminary study of dispersion
for a given structure can also help us to choose the most suitable

recording frequency bands to excite guided-waves (Räder *et al* .
1985). Consequently, we have given a particular emphasis to
examining the dispersion behaviour of guided-waves in crack-induced
anisotropic media. Comparing the theoretical dispersion with the
observed dispersion, which could be calculated from seismograms by
multiple filter technique (Appendix A), may provide a dispersion
inversion method in anisotropic media.

The studies could be particularly significant in production
geophysics. Here, the thin layers that may be present in
sedimentary reservoirs may act as seismic waveguides in crosshole
seismic surveys, if approriate source modes and frequency bands,
together with appropriate source and geophone positions at two
boreholes, can be chosen (Lou and Crampin 1991a, 1992b). Such
guided-waves may propagate with much of their energy confined to a
comparatively narrow zone in and around the waveguide.
Consequently, the dispersion, amplitudes, and waveforms of
guided-waves are sensitive to the internal structure of reservoirs
confined between nearly parallel strata. These guided-waves may
provide a new tool in determining extents and properties of
sedimentary reservoir, or in monitoring EOR operations, provided we
have achieved enough knowledge of their propagation in reservoir
zones.

3.2 GUIDED-WAVES BETWEEN TWO ISOTROPIC HALFSPACES

Liu and Crampin (1990) examined theoretically the reflection of
S-waves at a range of angles of incidence on internal interfaces
separating isotropic/isotropic, and isotropic/anisotropic
halfspaces. [Note that we follow the notation of Crampin (1989) in

using S-waves to specify transverse waves in isotropic solids and shear-waves in anisotropic solids.] For angles of incidence beyond the three critical angles, the incident-waves are totally reflected, and there is an inhomogeneous guided-wave (interface-wave) with elliptical particle motion and energy propagating parallel to, and decaying exponentially away from, the interface. These critical angles are exactly defined for plane-waves, where they mark abrupt changes of particle motion. For curved wavefronts from a point source, the effects of a critical angle are spread over a narrow range of directions, where the exact behaviour for any particular geometry depends on the curvature of the wavefront and the frequency of the incident-wave. Theoretically, guided-waves propagating along the interface between two halfspaces, excited by incident plane-waves, are independent of frequency and are not dispersive. Guided-waves excited by point-forces and having curved wavefronts will behave differently at different frequencies, but will still not be dispersive. In crosshole seismic surveys, sources may be very near to interfaces so that many incident-waves are beyond the critical angles and it is expected that interface-waves exist in most crosshole datasets.

Here we model these inhomogeneous guided-waves along the interface between two isotropic halfspaces. Figure 3.1 shows the source and geophone geometry for an interface model between two halfspaces (Model 1). Table 3.1 lists the material properties of Model 1. Figure 3.2(a) shows synthetic seismograms for Model 1 for three different source positions. The source is a vertical point-force generating SV-waves in the radial direction with a dominant frequency of 200Hz. There are non-dispersive inhomogeneous guided-waves (marked IGW) along the interface

```
                                    ─┬─ ●G1
            (LOW-VELOCITY)           5 m

   S1●                              ─┼─ ●G2

              MATERIAL 1             5 m
   S2                                ▼  G3
   ●─────────────────⌇⌇──────────────▼──●────
              MATERIAL 2

   S3●◄───────── 100 m ──────────►● G4
        (HIGH-VELOCITY)

                                      ●G5
        MODEL 1
```
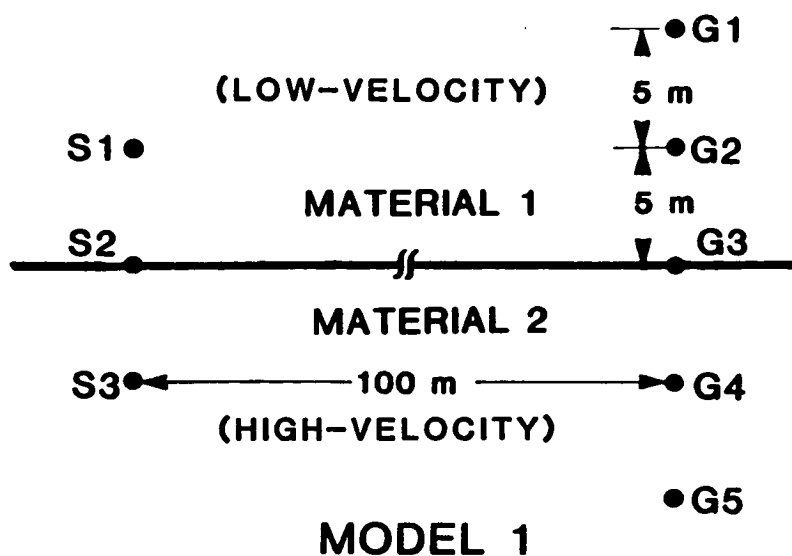
Figure 3.1 Source (S) and geophone (G) geometry of Model 1 for an interface between isotropic halfspaces (velocities in Table 3.1).

Tabel 3.1   Model 1   parameters.

layer	thickness	V_p m/s	V_s m/s	ρ g/cm^3
Shale	halfspace	3050	1760	2.34
Halite	halfspace	4500	2600	2.40
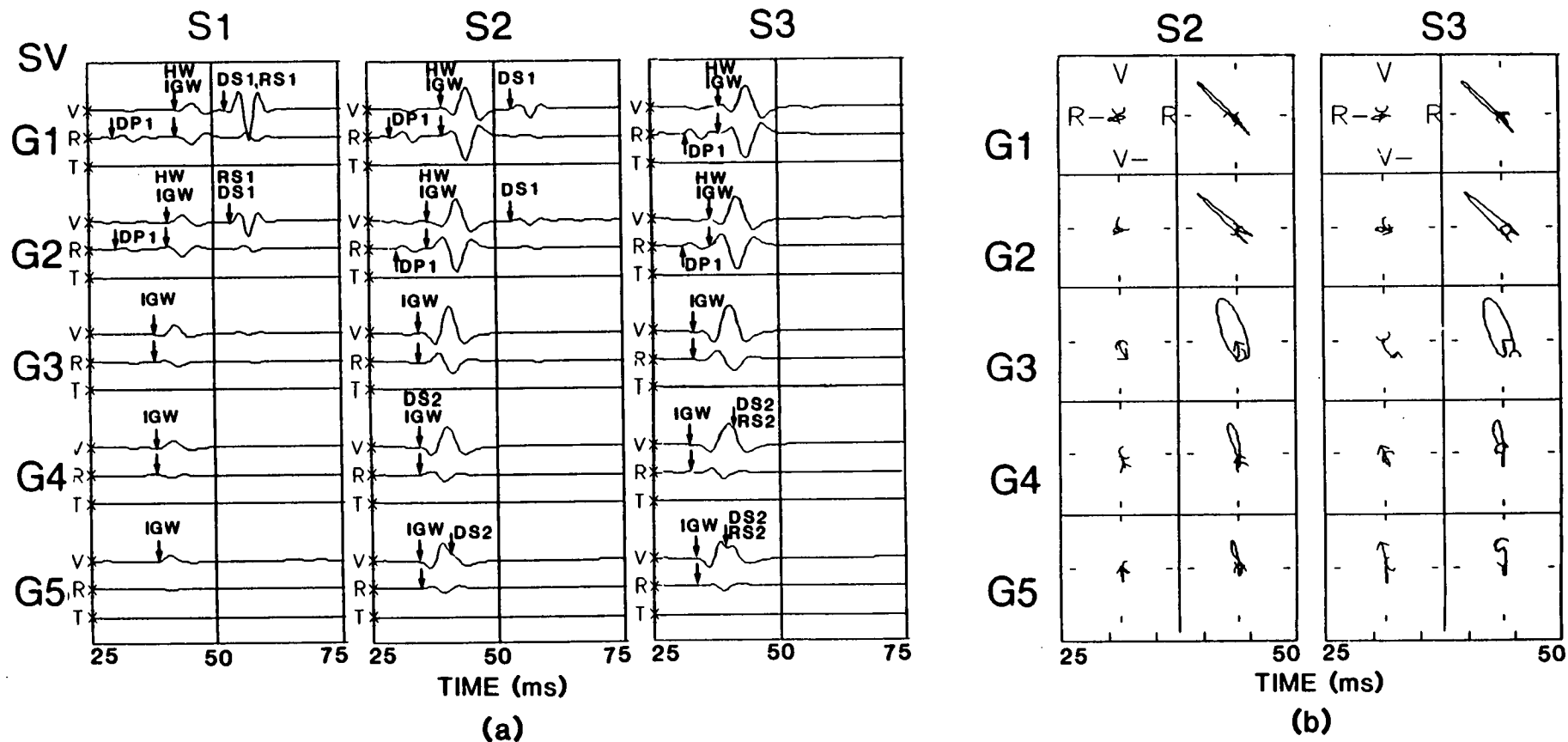
Figure 3.2 (a) Synthetic seismograms for a 200Hz vertical point-force in the three source positions and five geophone positions of Model 1. Different wave-types are marked: DP1 - Direct *P*-wave in shale; RS1 - Reflected *S*-wave in shale; IGW - Inhomogeneous Guided-Wave; HW - Head-Wave; DS1 - Direct *S*-wave in shale; DS2 - Direct *S*-wave in halite; and RS2 - Reflected *S*-wave in halite. (b) Polarization diagrams of selected synthetic seismograms of (a) in vertical/radial plane. The elliptical patterns in G3 show typical interface-wave motions.

recorded at all geophones. Other synthetic seismogram calculations show that the inhomogeneous guided-waves attenuate rapidly away from the interface. Figure 3.2(b) shows the polarization diagrams of inhomogeneous guided-waves, for two different source positions (S3 and S2). All inhomogeneous guided-waves along the interface have elliptical motion close to the interface (geophone G3), which becomes linear a short distance away from the interface. It also shows that the vertical components of other geophones from the interface basically receive body-waves like direct S-waves (marked DS) and reflected S-waves (marked RS), or head-waves (marked HW). There is also a direct P-wave (marked DP) on the radial component of G1 and G2.

Although inhomogeneous attenuating guided-wave propagation is possible along almost any interface, for a specific narrow range of elastic constants there may also exist a normal mode, non-attenuating, non-dispersive, Stoneley wave (Stoneley 1924) travelling at a velocity less than any of the four body-wave velocities in the two halfspaces (also see Chapter 1). The restrictive conditions for the existence of Stoneley waves (that the S-wave velocities in two halfspaces are near equal, but the density ratio between two halfspaces should be less than about 0.7) make their presence in crosshole surveys unlikely, except where there are liquid/solid interfaces. At the interface between liquid and solid halfspaces there is almost always a real solution of the Stoneley equation, giving the possibility of Stoneley waves. In borehole geophysics, the tube-wave travelling along the fluid-filled borehole may be considered as a type of Stoneley wave, which usually has the maximum amplitude in acoustical logging seismograms.

3.3 GUIDED-WAVES IN ISOTROPIC WAVEGUIDES

The Love modes of guided-waves in isotropic waveguides have been
studied extensively in coal mining (Krey 1963, Räder *et al* 1985,
Buchanan 1987), where coal seams provide suitable low-velocity
waveguides. It has now been observed that the dominant energy in
crosshole surveys in some reservoir configurations may also be
guided-waves (Krohn 1990, Liu *et al*. 1991), rather than body-waves
as are frequently assumed. Such guided-waves in reservoirs are not
necessarily Love modes, but may include Rayleigh modes, and
Generalized modes in the presence of anisotropy (Liu *et al*. 1991).
Krohn (1990), Worthington (1991), and Lou and Crampin (1991b) have
suggested that continuity in oil or gas reservoirs may be monitored
by using such guided-waves. It has also been suggested (Lou and
Crampin 1991a,b, 1992c) that guided-waves in crosshole surveys may
provide a new tool for monitoring hydrocarbon production processes
in thin-layered sedimentary reservoirs, which may be beyond the
resolution of seismic reflection profiles or VSPs.

Here we initially consider a model of a simple three-layer
isotropic waveguide between two halfspaces. We calculate
dispersion curves and amplitude/depth distributions for different
source frequencies, and synthetic seismograms for different model
parameters (velocity contrasts) and different source/geophone
parameters (source polarizations, frequencies, and source/geophone
positions).

Figure 3.3(a) shows source and geophone positions for two
symmetric waveguides, Model 2 and Model 3, with material parameters
listed in Table 3.2 and Table 3.3, respectively. Model 2 has a

channel with a small velocity-contrast, *Vs1/Vs2* = 1.2. Model 3 has a larger velocity-contrast of 1.5, which is still small in comparison with the velocity-contrast in in-seam seismics, which is often greater than 2. We also use an asymmetric waveguide (Model 4), where the lower halfspace has a higher velocity than the upper halfspace (Figure 3.3(b)). Table 3.4 lists the material parameters. In all models, the thickness of the low-velocity channel is 4 meters. Note that layer thickness and frequency are inversely proportional, so that the dispersion curves for 4m-thick channel also hold for an 8m-thick channel if the frequency values are halved.

Modelling of guided-waves through models 2 - 4 shows the following five features:

1) Figure 3.4 shows the dispersion of guided-waves in Model 2, with the smaller velocity-contrast. There are two families of guided-wave modes displaying different velocity/frequency dispersion and orthogonal particle motion: a family of Rayleigh modes with elliptical motion in the vertical/radial (sagittal) plane; and a family of Love modes with transverse horizontal motion. We use *FR* and *FL* to indicate the First or Fundamental Rayleigh and Love modes, respectively, and *2R* and *2L* to indicate the corresponding Second (or First Higher) modes. Figure 3.5 shows the amplitude/depth distribution of the Fundamental and Second modes of Rayleigh and Love modes. At 400Hz and higher frequencies, the energy of both Fundamental modes is increasingly trapped inside the low-velocity waveguide. The group-velocity (dashed lines in Figure 3.4) of the dispersion curves have minima at about 540Hz for *FR*, and 480Hz for *FL*, known as Airy phases, which are associated
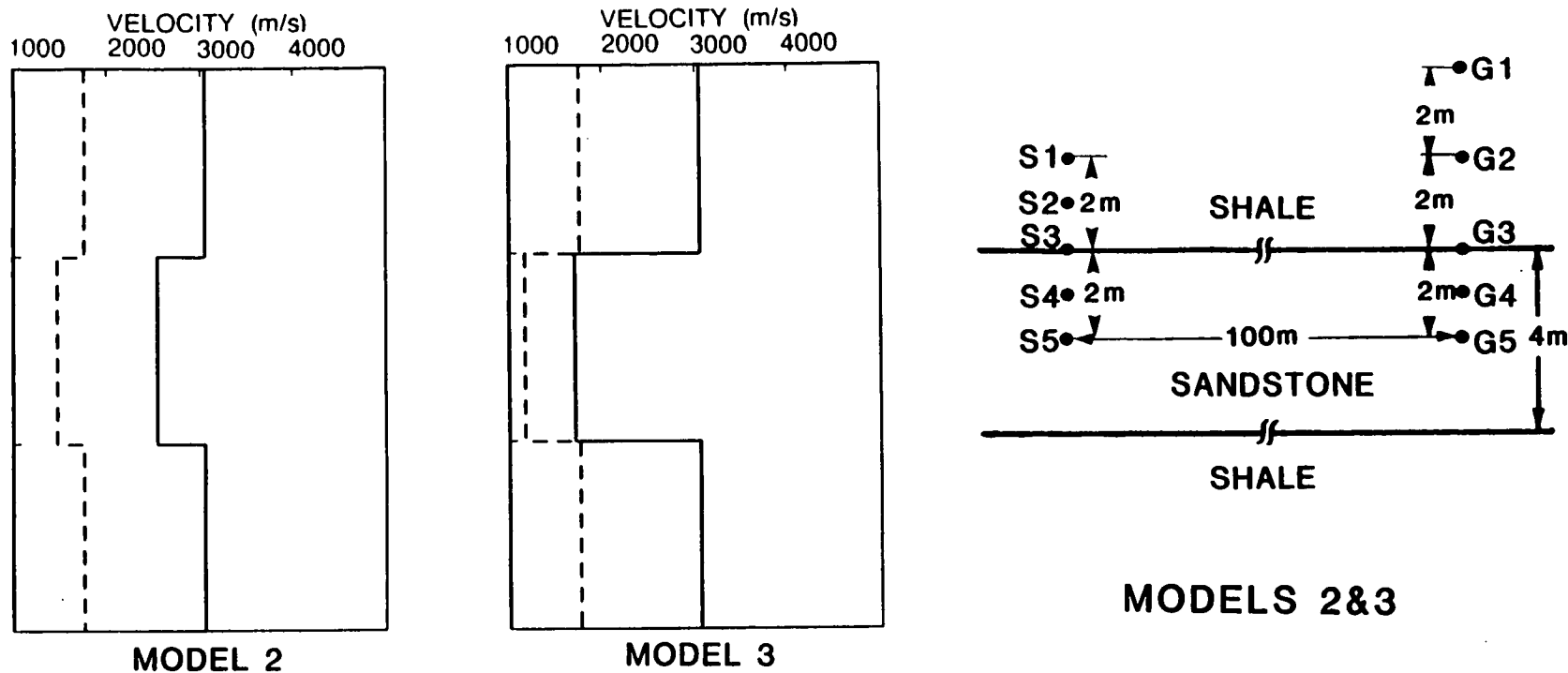
Figure 3.3(a)

Figure 3.3 (a) Source (S) and geophone (G) geometry of symmetric Model 2 and Model 3 for isotropic low-velocity channels with the material parameters listed in Table 3.2 and Table 3.2, respectively; **(b)** Source (S) and geophone (G) geometry of asymmetric Model 4 with the material parameters listed in Table 3.4.

VELOCITY (m/s)

1000 2000 3000 4000

MODEL 4

SHALE

HALITE

SANDSTONE

S ● ←———100m———→ ● G5 4m

G1
2m
G2
2m
G3
2m ● G4

● G6
G7

● G8

MODEL 4   ● G9
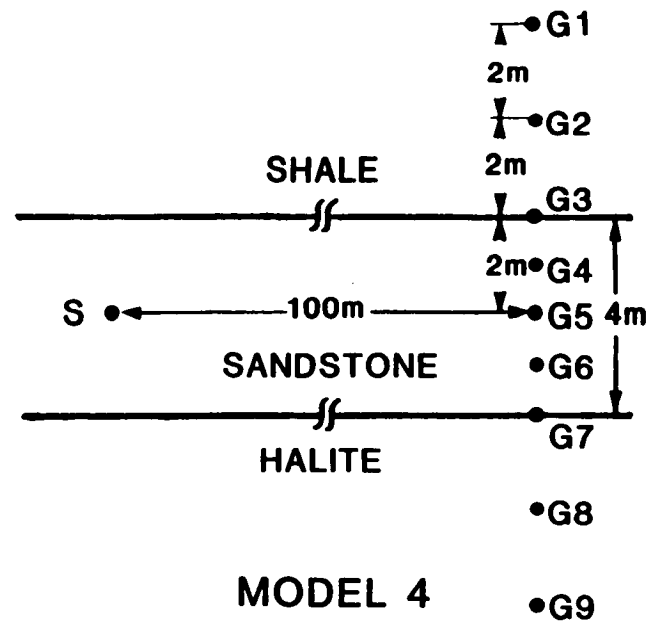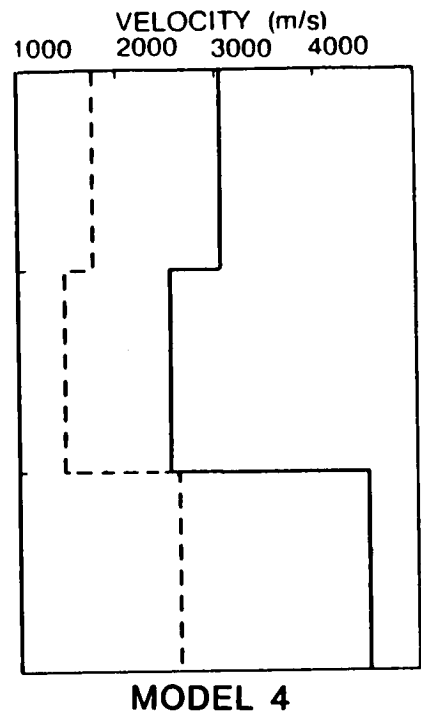
Figure 3.3(b)

34b

Table 3.2   Model 2   parameters.

layer	thickness	Vp m/s	Vs m/s	ρ g/cm^3
Shale	halfspace	3050	1760	2.34
Sandstone	4m	2540	1470	2.34
Shale	halfspace	3050	1760	2.34

Table 3.3   Model 3   parameters.

layer	thickness	Vp m/s	Vs m/s	ρ g/cm^3
Shale	halfspace	3050	1760	2.34
Sandstone	4m	1700	1170	2.10
Shale	halfspace	3050	1760	2.34

Tabel 3.4   Model 4   parameters.

layer	thickness	Vp m/s	Vs m/s	ρ g/cm^3
Shale	halfspace	3050	1760	2.34
Sandstone	4m	2540	1470	2.34
Halite	halfspace	4500	2600	2.40
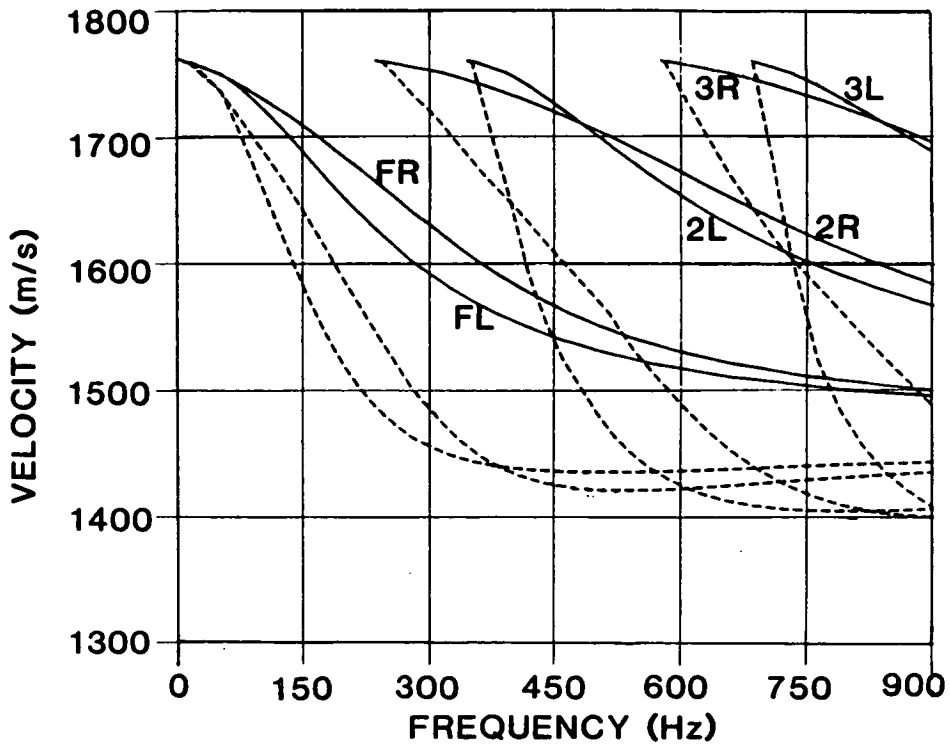
Figure 3.4 Dispersion curves for guided-waves in Model 2. Solid lines are phase-velocity, and dashed lines are group-velocity: *FR*, and *2R* - Fundamental and Second Rayleigh modes; *FL*, and *2L* - Fundamental and Second Love modes.

FUNDAMENTAL RAYLEIGH

VERTICAL

400Hz 400Hz 200Hz 100Hz

RADIAL

200Hz

400Hz

SECOND RAYLEIGH

VERTICAL

400Hz 400Hz 500Hz

RADIAL

500Hz 400Hz

FUNDAMENTAL LOVE

TRANSVERSE

400Hz 200Hz 100Hz

SECOND LOVE

TRANSVERSE

400Hz 500Hz
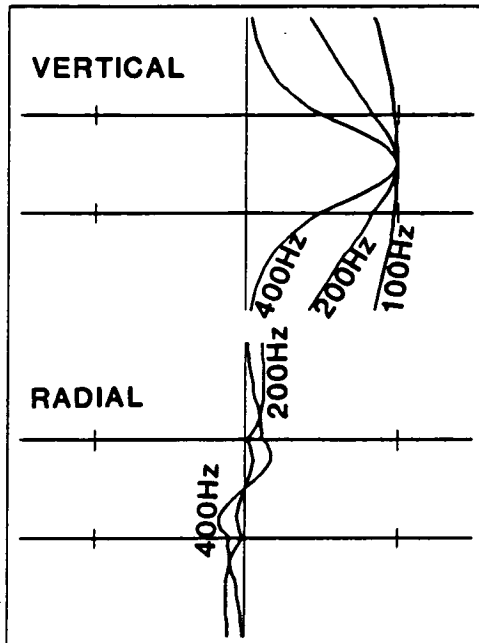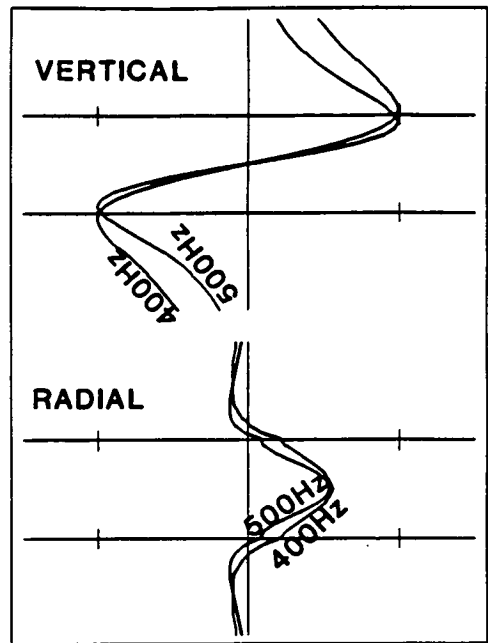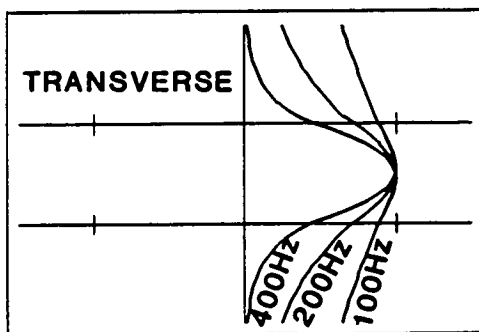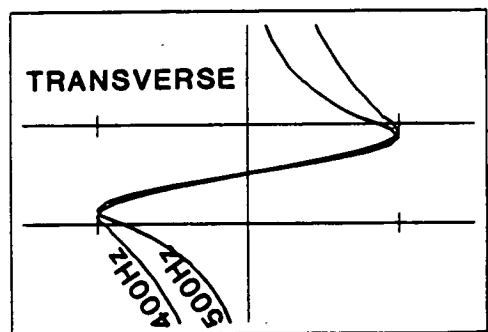
Figure 3.5   Amplitude/depth distributions of Fundamental and Second modes of both Rayleigh and Love guided-waves for Model 2 for several different frequencies.

with maxima in the seismograms, if the source excitation is appropriate. Many of the dispersion curves in Figure 3.4 overlap in frequency, indicating that multiple mode excitation must be expected.

Figure 3.6 shows synthetic seismograms of these guided-waves for two source orientations: a vertical point-force (marked SV) exciting Rayleigh modes, and a horizontal-transverse point-force (marked SH) exciting Love modes. The seismograms show that the significant dispersion for both FR and FL starts at frequencies of about 200Hz, and seismograms at geophones G3, G4, and G5 reach maxima associated with the Airy phase, at about 500Hz. Higher modes usually precede the Fundamental modes. These and other calculated synthetics suggest that almost any configuration of layers will support guided-wave propagation in seismic crosshole surveys, if the appropriate source parameters and source/geophone levels in appropriate wells can be chosen.

2) Channels with larger velocity-contrasts, as in Model 3, allow guided-waves to be excited at lower frequencies, so that more higher modes can be received in the same source/frequency band. Figure 3.7 shows dispersion curves for guided-waves in Model 3. In Model 3, the FR and FL reach Airy phases at about 320Hz and 250Hz, respectively, and there are several higher modes with Airy phases which do not appear within the same frequency band of 0 to 900Hz in Model 2.

3) Love guided-waves in in-seam seismics in isotropic channels in coal mines have been discussed extensively (see Chapter 1), but Rayleigh mode guided-waves are less frequently discussed. The

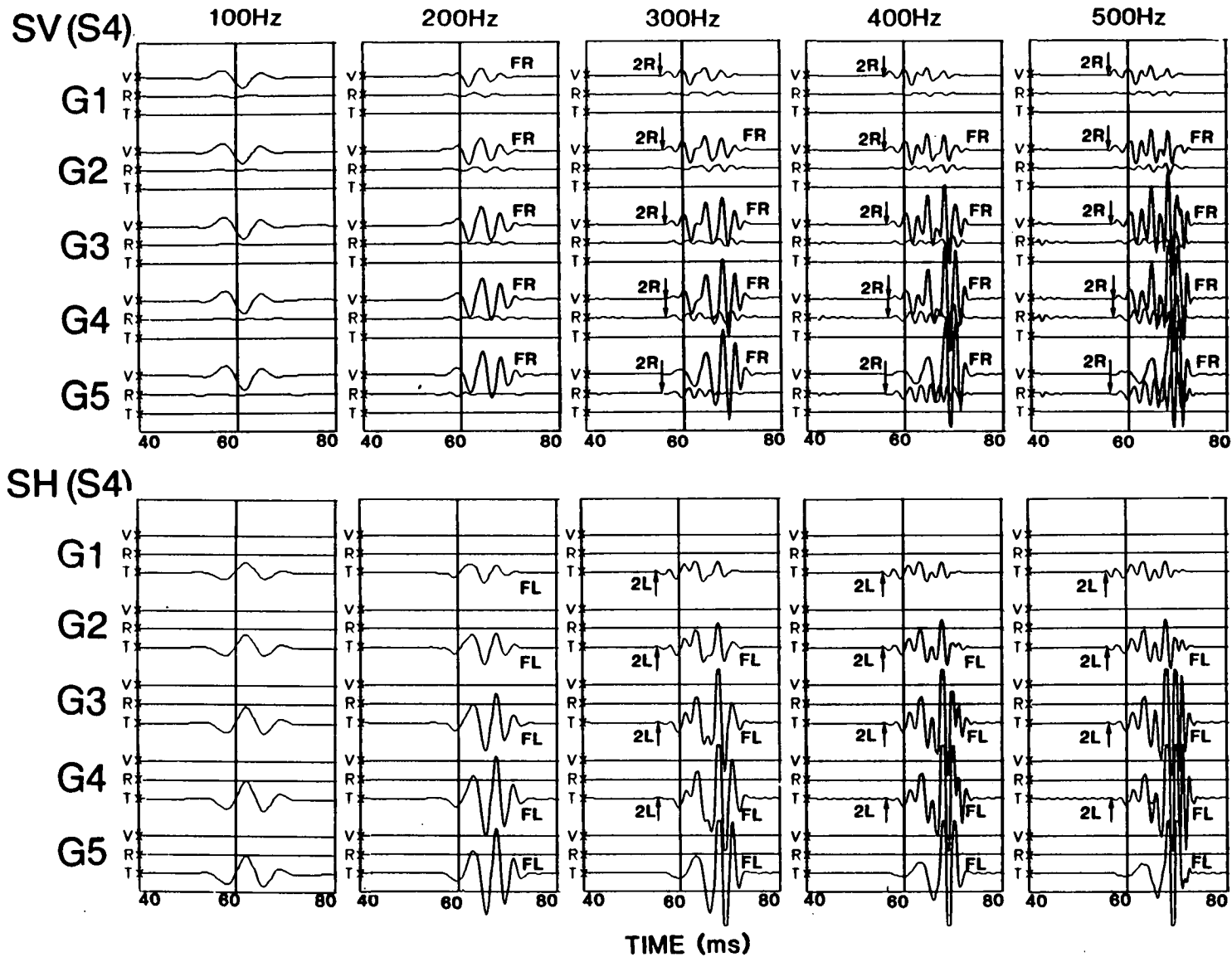**Figure 3.6** Synthetic three-component seismograms for a range of source dominant frequencies (indicated above seismograms) for Model 2. Source position is at S4, and seismograms are shown for a vertical point-force (marked *SV*) and a horizontal transverse point-force (marked *SH*).
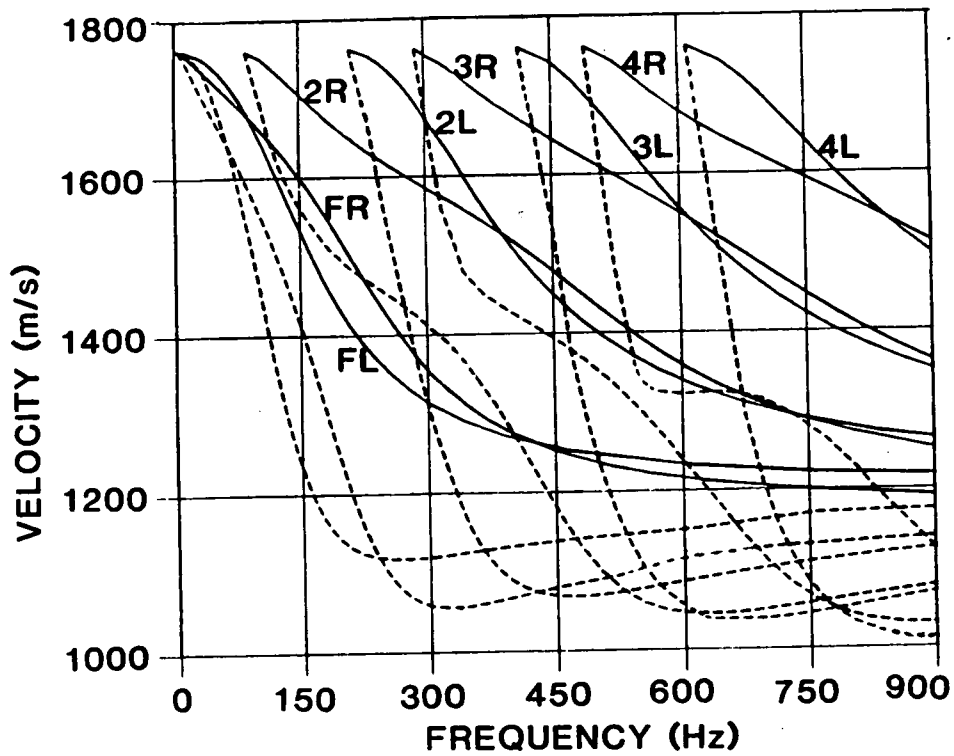
FIG. 4(a).

Figure 3.7 Dispersion curves for guided-waves in Model 3 with the same notation as Figure 3.4.

synthetic seismograms here demonstrate that with the smaller
velocity-constrasts expected in hydrocarbon reservoirs, Rayleigh
modes have many similar characteristics to Love modes, and may be
expected in similar situations, if the source excitations are
appropriate. Amplitude/depth distributions of Rayleigh
guided-waves in Figure 3.5 show that the amplitude of the
horizontal (radial) motion of the Fundamental mode *FR* is generally
about 1/5 or smaller than the vertical motion (see Model 2, Figure
3.5).

4) Source and geophone positions, together with source-type and
source-frequency, are crucial to the relative energy of
guided-waves that are excited and recorded. Figure 3.8 shows
synthetic seismograms of guided-waves in Model 2 for five different
source positions at a dominant source frequency of 400Hz. The
various modes are indicated. Source positions S1 and S2, outside
the low-velocity channel, excite weak, mostly higher mode,
guided-waves inside the channel. Sources S3, S4, and S5 all excite
strong guided-waves inside the channel, but modes are excited
preferentially: for example, S5 in the centre of the channel does
not excite the anti-symmetric *2R* and *2L* modes, which have small
amplitudes in the centre of the channel; and S1 - S4 provide
little excitation of *3R* and *3L* modes, again because these modes
have very small amplitude at the source positions.

Similarly, geophones at different levels record different modes
of guided-waves. For example, G5 only records low amplitude of *FR*
on the radial component for all source positions; and low
amplitude of *2R* on the vertical component (Figure 3.8). To excite
and receive selected modes, it is necessary to site source and

geophones at levels appropriate to the particular mode selected.

5) Figures 3.9-11 show the various characteristics of guided-waves in the asymmetrical Model 4. This is the same as Model 2 but with a high-velocity lower halfspace. The most marked difference between the seismograms in the symmetric model (Figure 3.6) and the asymmetric model (Figure 3.11) is the rapid fall off of amplitudes of all modes in the high-velocity halfspace. The seismograms in the asymmetric Model 4 show other characteristic differences from seismograms in Model 2:

a) The Fundamental modes now have non-zero cutoff frequencies, at the velocity of interface-waves in the absence of the channel (see Figure 3.9);

b) The cut-off frequencies of other guided-wave modes shift towards higher frequencies, whereas the frequencies of the Airy phases shift slightly towards the lower frequencies (now 450Hz for the Fundamental Love mode, and 520Hz for the Fundamental Rayleigh mode).

c) As indicated by the seismograms, all maxima in the amplitude/depth curves shift towards the halfspace with lower wave impedance (ρV_s) (see figure 3.10).
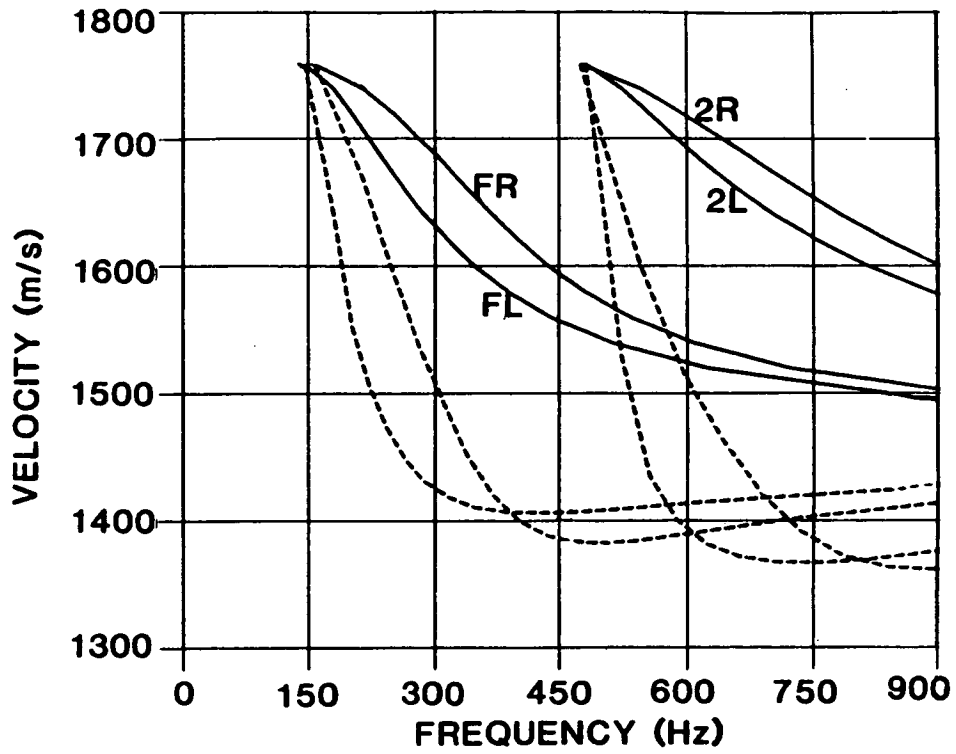
Figure 3.9 Dispersion curves for Model 4 with the same notation as Figure 3.4.

FUNDAMENTAL RAYLEIGH

SECOND RAYLEIGH

VERTICAL

VERTICAL

RADIAL

RADIAL

FUNDAMENTAL LOVE

SECOND LOVE

TRANSVERSE
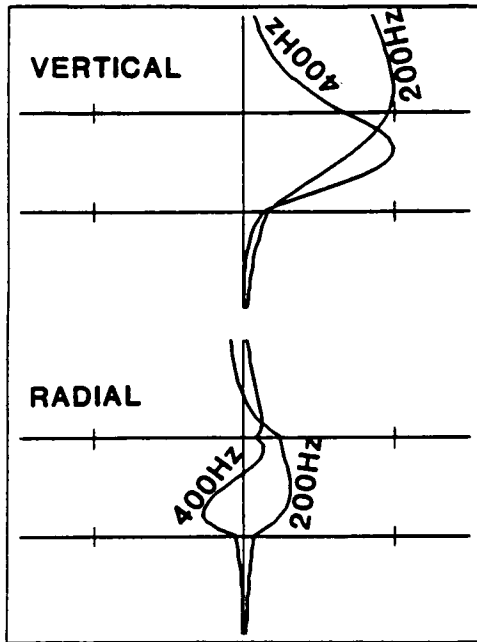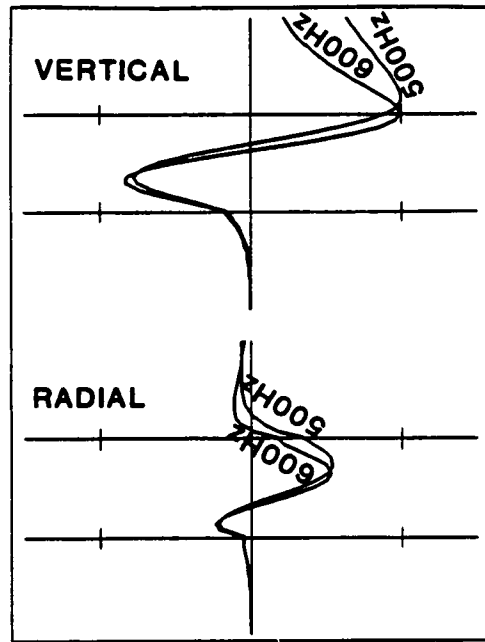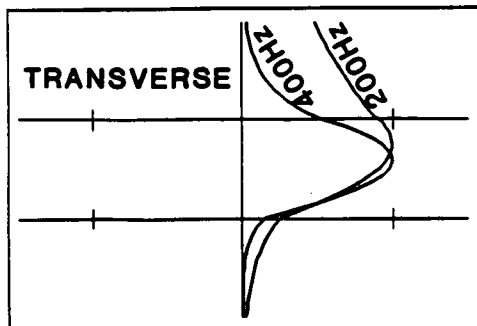
TRANSVERSE
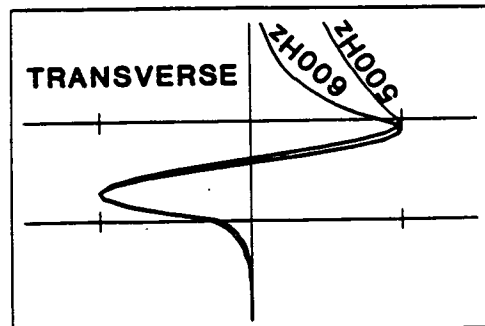
Figure 3.10 Amplitude/depth distribution of Fundamental and Second modes of Love and Rayleigh guided-waves for Model 4 for several different frequencies.
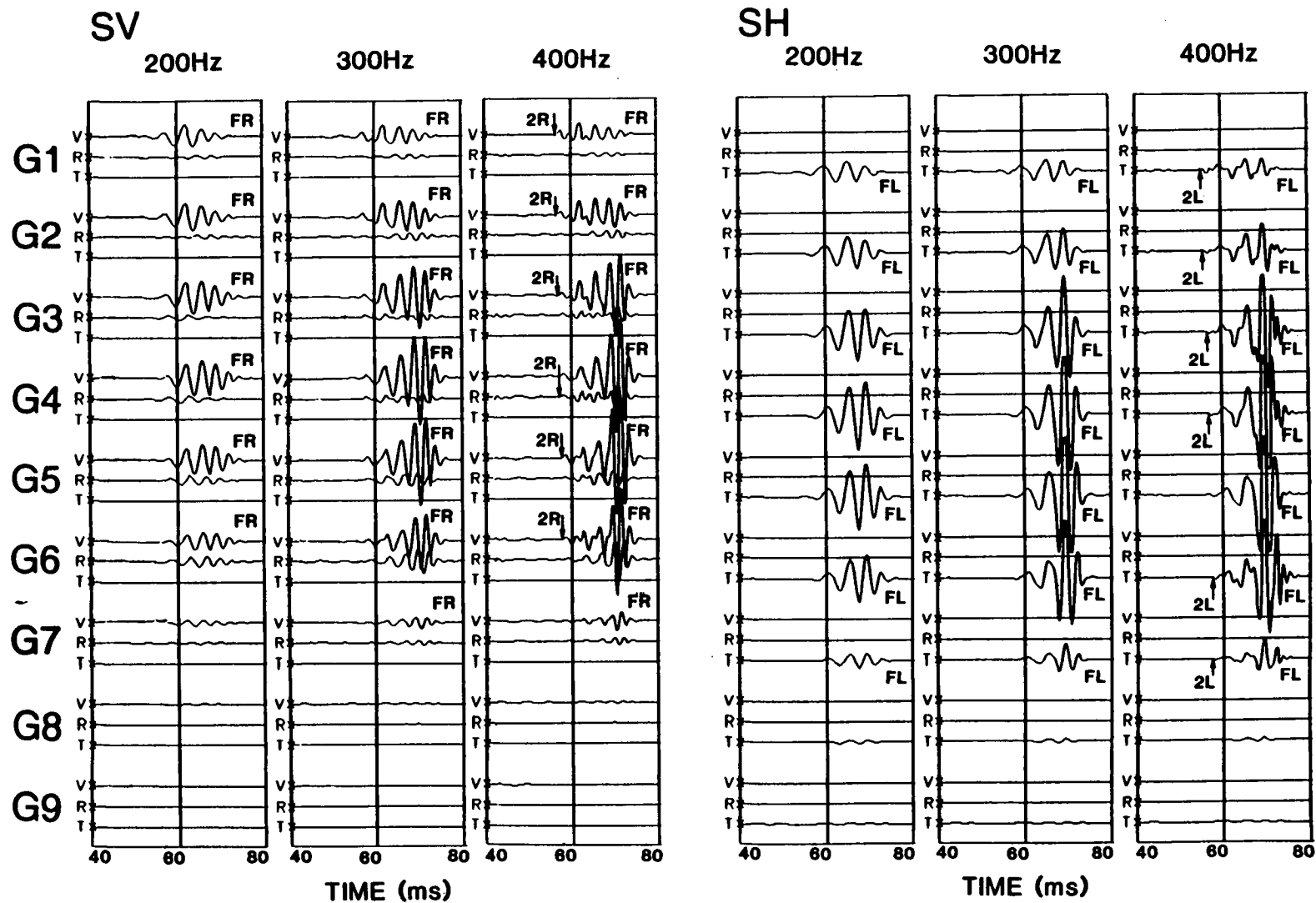
Figure 3.11 Synthetic three-component seismograms for three source frequencies (indicated above seismograms) for Model 4. Source position is in the central of sandstone layer, and seismograms are shown for transverse source (*SH*) and vertical source (*SV*).

3.4 GUIDED-WAVES IN CRACKED (ANISOTROPIC) WAVEGUIDES

3.4.1 GENERAL DESCRIPTION

Stress-aligned fluid-filled inclusions exist in most rocks in the uppermost 10km to 20km of the crust. The presence of such anisotropic inclusions in low-velocity channels will modify the detailed behaviour of guided-waves, so that if appropriate guided-waves can be excited in cracked reservoirs in crosshole seismic surveys, where most of their energy is trapped within the reservoir, the behaviour of the guided-waves will respond to the internal structure of the reservoir. Comparison of guided-wave seismograms taken at different times during production processes, which are expected to modify the internal structure in some way, would be particularly sensitive to changes in: pore-fluid velocity, viscosity, and attenuation; saturation levels (the gas/liquid ratio); and crack density and crack shape.

In anisotropic media, the separate families of Rayleigh and Love surface-wave or guided-wave modes in plane horizontally-layered isotropic media combine into one family of *Generalized* modes (labelled *FG*, *G1*, *G2*, etc.) with elliptical three-dimensional particle-motion (Crampin 1975). In positions where the phase-velocities of the equivalent Rayleigh and Love modes would cross each other, the phase-velocities of *Generalized* modes in off-symmetry directions pinch together. At such pinches, the guided-wave modes effectively exchange properties, in particular, the slopes of the dispersion curve and the characteristic particle displacement are interchanged. At these phase-velocity pinches,

the equivalent group-velocity/dispersion curves usually show large changes of slope. In directions of sagittal symmetry, the *Generalized* modes decompose into two families with strictly Rayleigh- and Love-type particle motions so that the isotropic *FR*, *FL*, *2R*, and *2L* notation is still appropriate.

To illustrate these pinches, Figure 3.12 shows the dispersion curves of the first four *Generalized* modes of guided-waves in a crack-induced anisotropic waveguide. This model has the same structure as Model 2 (Figure 3.3(a)), but the low-velocity sandstone contains aligned water-filled cracks with crack density $CD = 0.1$ and 67.5° strike to the direction of the guided-wave propagation. The pinch positions on dispersion curves are marked by solid arrows. At such positions, the corresponding group-velocity dispersion curves (dashed lines) show markedly changes to their slopes, with an interchange of their corresponding polarization properties. These pinches are sometimes very abrupt, with the two modes almost touching (see the first and second *Generalized* modes of Figure 3.12). In this example, the first mode is equivalent to the fundamental Love mode, and not the Rayleigh mode, as would usually be the case in surface-waves. This is because that there are three pinches near 30Hz, 150Hz and 280Hz in phase-velocity dispersion curves, which allow the Love type characteristics to be interchanged from the second mode to the first mode.

In the next section, we shall investigate the effects that a cracked channel has on the dispersion and amplitude/depth distribution of guided-waves. For this, we shall replace the isotropic channel of Model 2 with an anisotropic channel containing
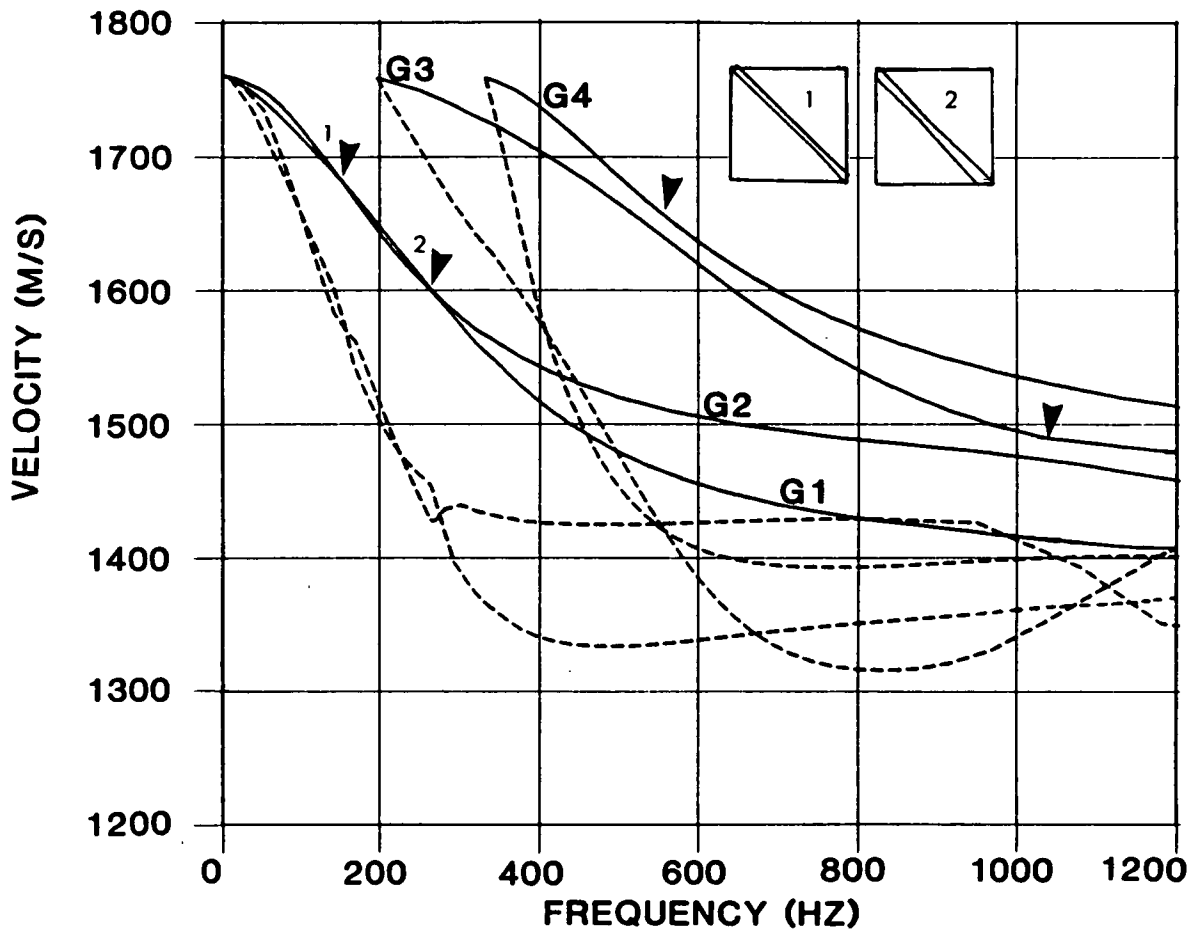
Figure 3.12 Dispersion curves of first four *Generalized* modes of guided-waves in a crack-induced anisotropic waveguide. Solid lines are phase-velocity, and dashed lines are group-velocity. The frequencies and phase-velocities at which different *Generalized* modes pinch together are approximately indicated by solid arrowheads.

Tabel 3.5 Parameters for parallel vertical cracks.

Crack density:	CD = 0.02 0.05, and 0.1;
Crack aspect ratio:	AR = 0.01 (Hudson 1980, 1981);
	AR = 0.05, 0.1, 0.3 (Nishizawa 1982);
Crack strike:	ϕ = 0°, 22.5°, 45°, 67.50°, and 90° to propagation direction of guided-waves;
Crack saturation:	gas-filled, and liquid-filled.

aligned cracks with the parameters listed in Table 3.5.

3.4.2 EFFECTS OF VARIATIONS OF CRACK DENSITY AND CRACK ORIENTATION

To observe the effects of variations in crack density and crack orientation on the propagation of guided-waves, we first assume that all cracks have the same aspect ratio (AR = 0.01), and that they are filled by water.

Figure 3.13 shows phase- and group-velocity dispersion curves for the three crack densities (CD = 0.02 (solid lines), 0.05 (dashed lines), and 0.1 (dash/dot lines) for five directions from parallel (0°) to perpendicular (90°) to the crack strike (see Table 3.5 for crack parameters). In the phase-velocity curves, arrows indicate the approximate positions of pinches where two modes exchange characteristics. The group-velocity curves have strong fluctuations in behaviour at frequencies near those of the corresponding phase-velocity pinch. In most directions, for crack densities between CD = 0.02 and CD = 0.1, the velocities can change by up to 15% for some frequencies, and the frequencies can change by at least 30% for some velocities. The sensitivity varies with direction of propagation: for directions of propagation between 0° and 22.5° to the crack strike, it is the *Generalized* modes with most nearly Rayleigh-type particle motion that show little differences in dispersion as the crack density is varied; whereas in directions near to 45° to the crack strike, it is the *Generalized* modes with most nearly Love-type motion show less sensitivity to crack density.

The three-component amplitude/depth distribution of guided-waves

Figure 3.13 Dispersion curves of first four *Generalized* mode guided-waves in Model 2 with low-velocity channel having the effective anisotropy of parallel vertical water-filled cracks. Curves are shown for five directions, 0°, 22.5°, 45°, 67.5°, and 90° to the crack strike, for three different crack densities: CD = 0.02 - solid line; 0.05 - dashed line; and 0.1 - dash/dot line. The frequencies and phase-velocities at which different *Generalized* modes phase-velocities pinch together in off-symmetry directions are indicated by arrowheads.

Figure 3.13

22.5°   **45°**   **67.5°**
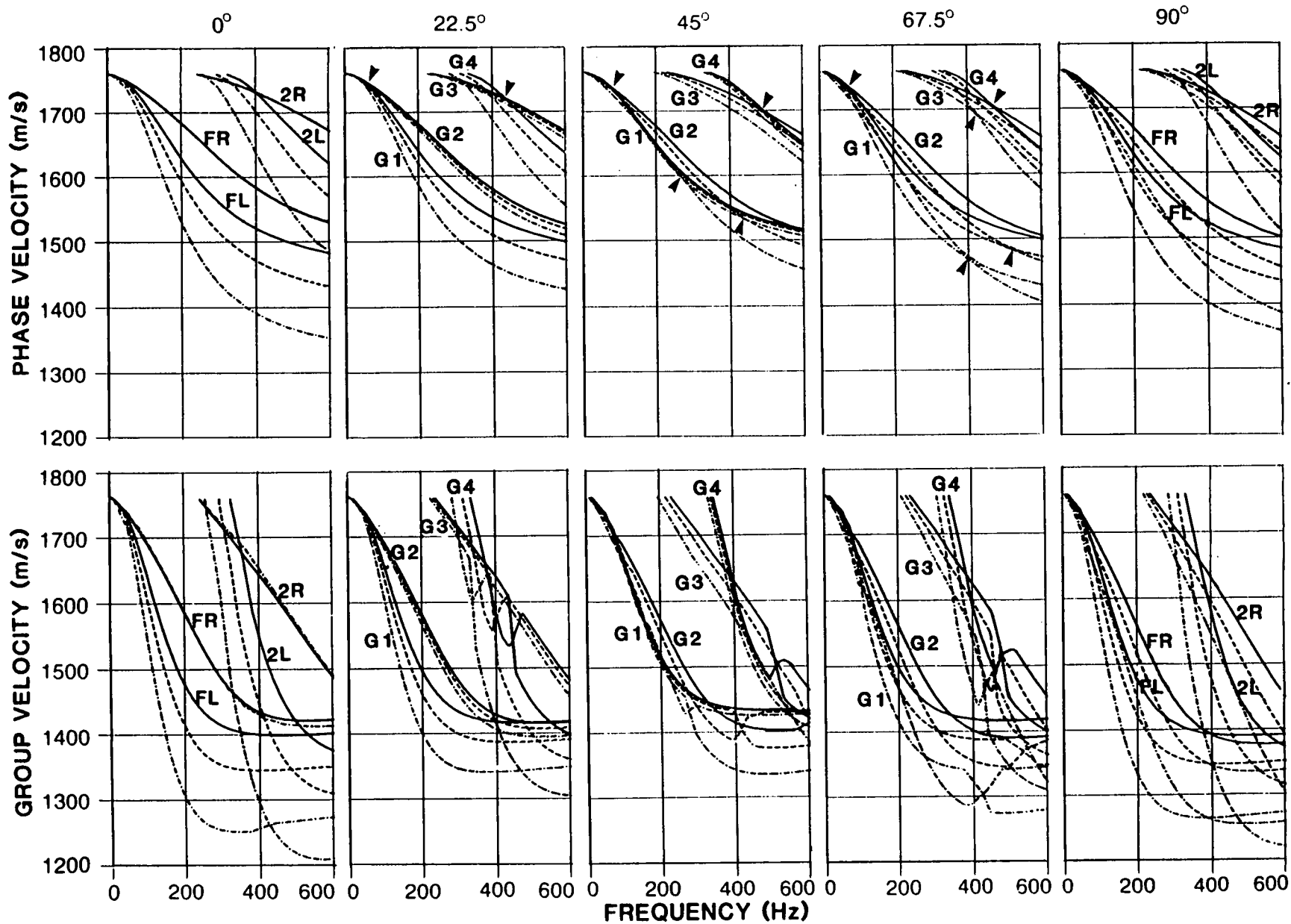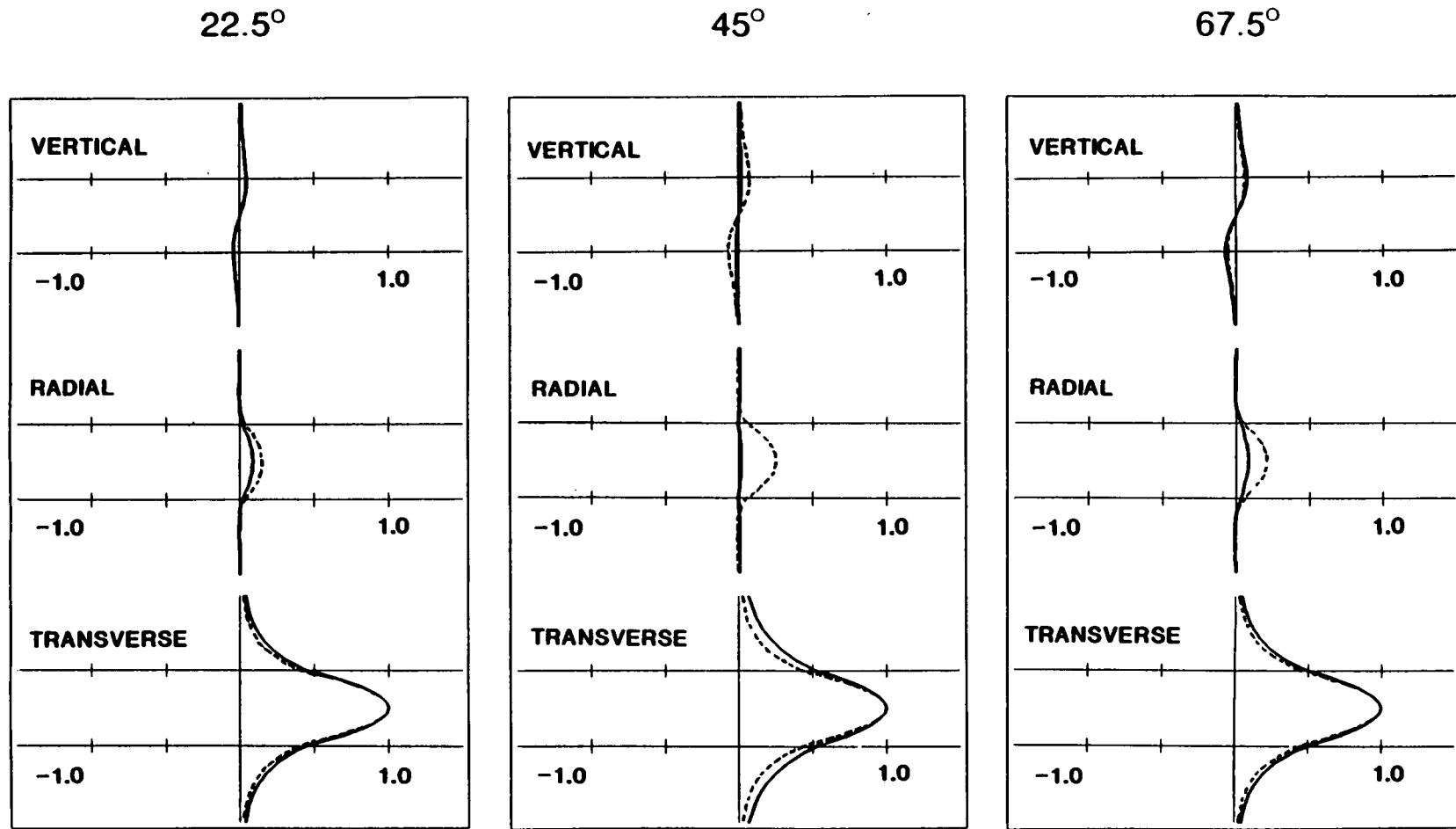
Figure 3.14(a)

Figure 3.14 Three-component amplitude/depth distribution curves of first four *Generalized* modes of guided-waves in the cracked Model 2 with $CD=0.1$, for water-filled cracks - solid lines, and gas-filled cracks - dashed lines, for three different directions of propagation relative to crack strike (22.5°, 45°, and 67.5°). Curves are shown for modes (a) $G1$, and (b) $G2$ at a frequency of 300Hz, and (c) $G3$, and (d) $G4$ at a frequency of 500Hz.
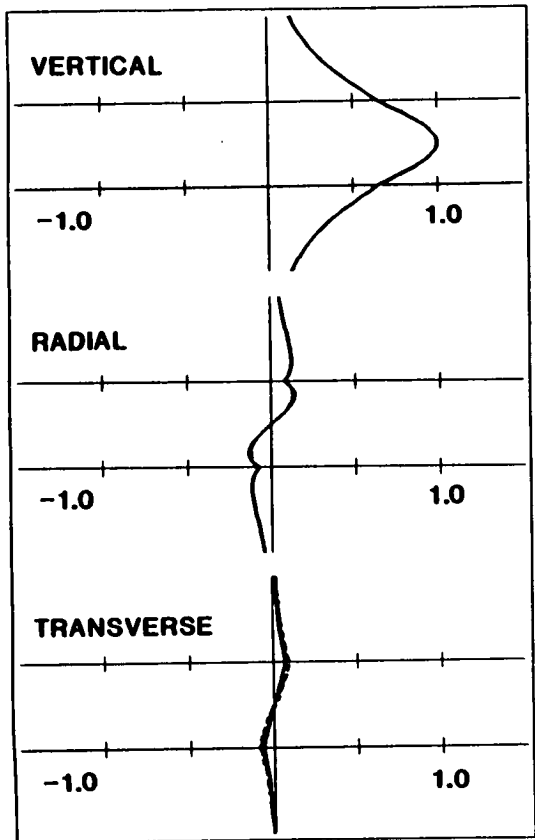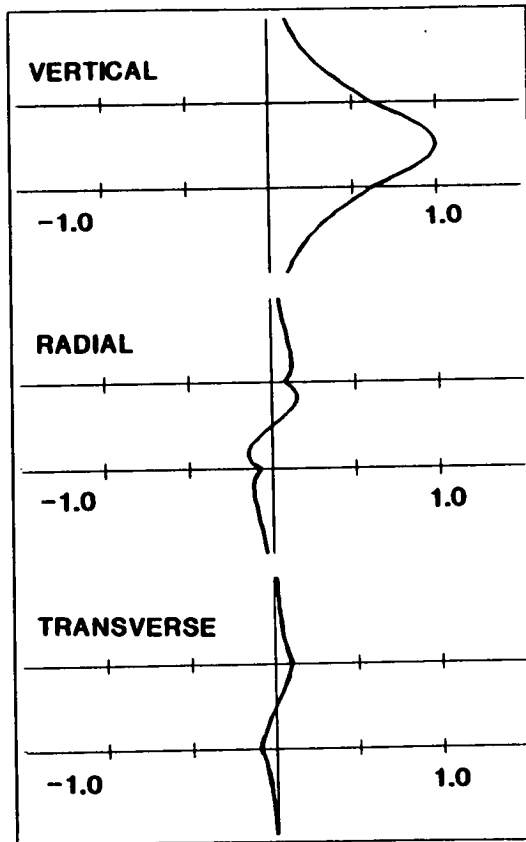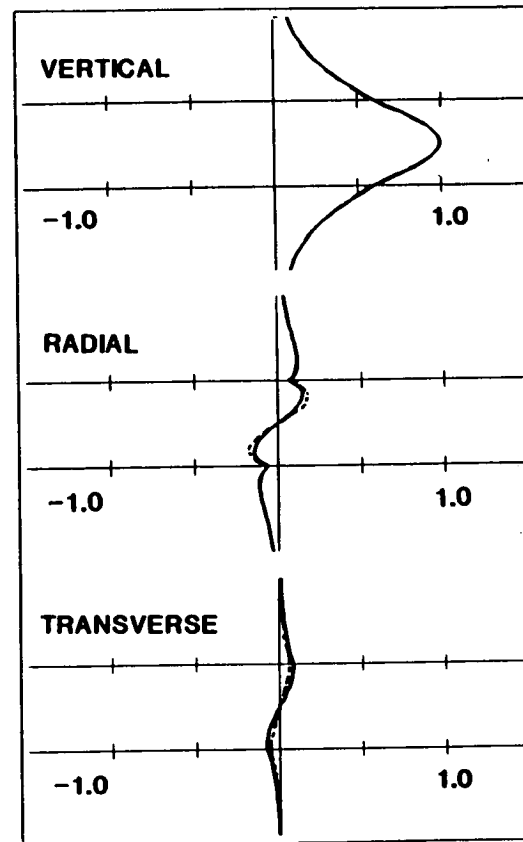
Figure 3.14(b)

22.5°   45°   67.5°

Figure 3.14(c)

22.5°

VERTICAL

−1.0   1.0

RADIAL

−1.0   1.0

TRANSVERSE

−1.0   1.0

45°

VERTICAL

−1.0   1.0

RADIAL

−1.0   1.0

TRANSVERSE

−1.0   1.0

67.5°

VERTICAL

−1.0   1.0

RADIAL

−1.0   1.0

TRANSVERSE

−1.0   1.0
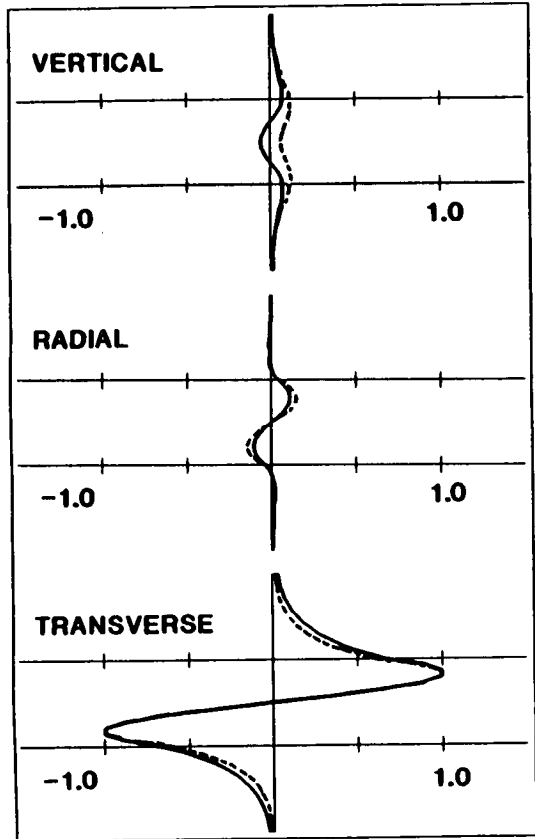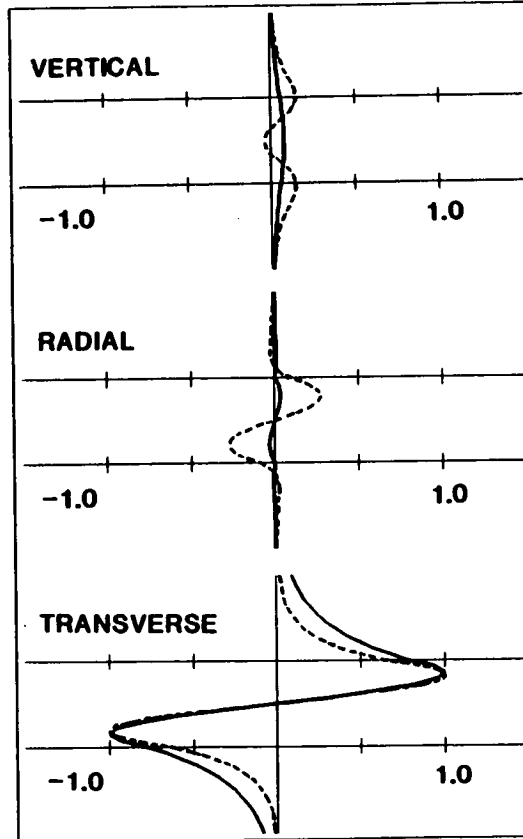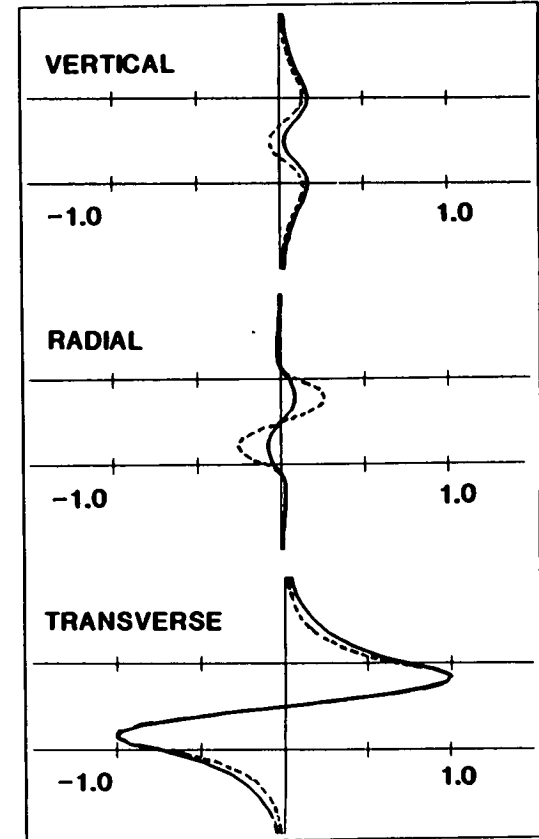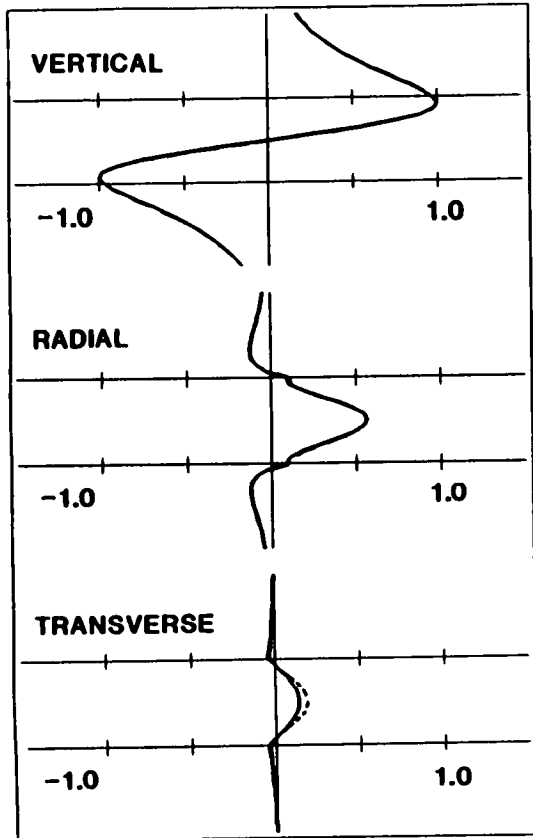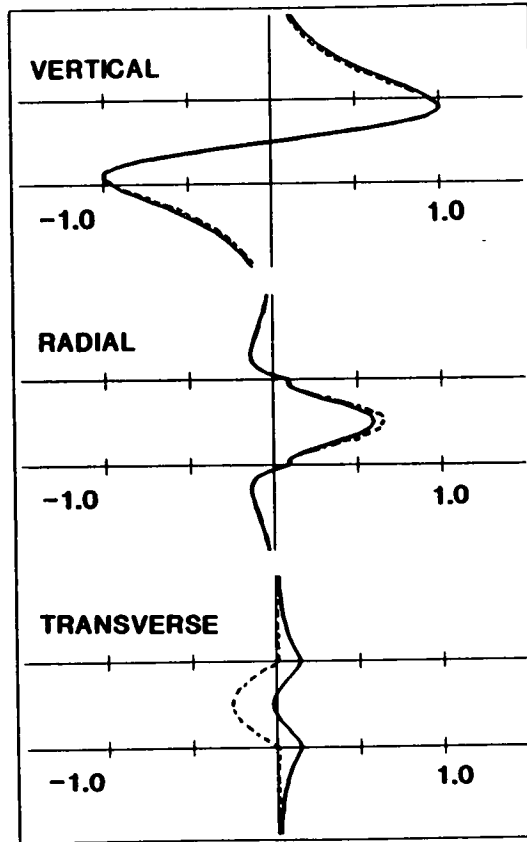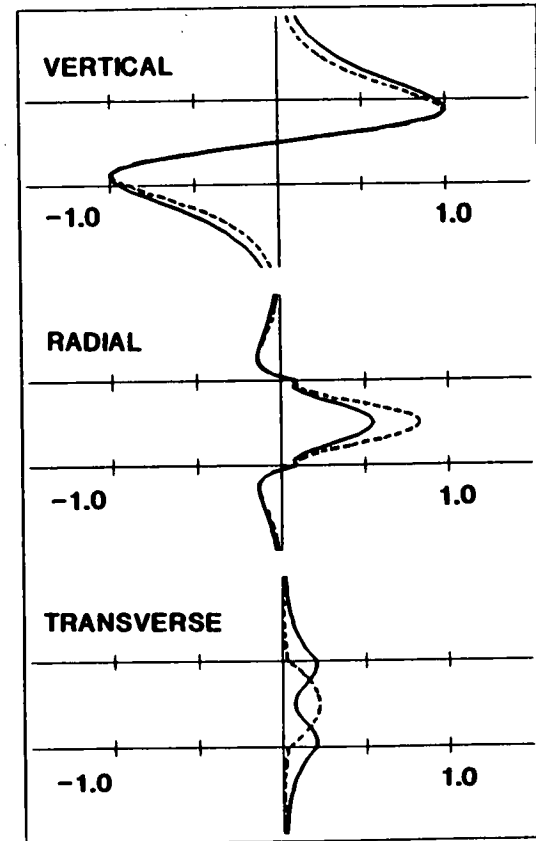
Figure 3.14(d)

provides some diagnostic information about crack-induced anisotropy in the low-velocity channel. Figures 3.14(a)-(d)(solid lines) show the amplitude/depth distributions of first four *Generalized* modes (at 300 Hz for first and second modes, and 500 Hz for third and fourth modes) for crack density CD = 0.1 directions of propagation of 22.5°, 45° and 67.5° to crack strike. The first and third modes approximate to fundamental and second Loves modes, respectively; the second and fourth modes approximate to fundamental and second Rayleigh modes, respectively. We will call the amplitudes in vertical and radial components of the seismograms excited by *SH* type source, and the amplitude in transverse component excited by *SV* type source, cross-coupling amplitudes. In general, except for propagation in directions of sagittal symmetry, an increase in crack density causes larger coupling amplitudes. The amplitude distribution of *Generalized* modes of guided-waves also varies with the direction of propagation. For liquid-saturated cracks, the Love like modes travelling at around 45° direction to the crack strike, and Rayleigh like modes travelling at around 22.5° direction to the crack strike show smaller coupling amplitudes than in other directions. From the distribution curves, it can be seen that the polarization patterns of guided-waves can also change with different source frequencies and receiver positions, as well as crack parameters.

Figure 3.15 shows synthetic seismograms for the dispersion curves of Figure 3.13 for a range of directions of propagation for three crack densities (CD = 0.02, 0.05, and 0.1) and two source types (*SV* and *SH*). The sources are at position S4 with dominant frequency 400Hz, and the geophone is at G4. The seismograms display the dispersion and amplitude characteristics discussed above. The
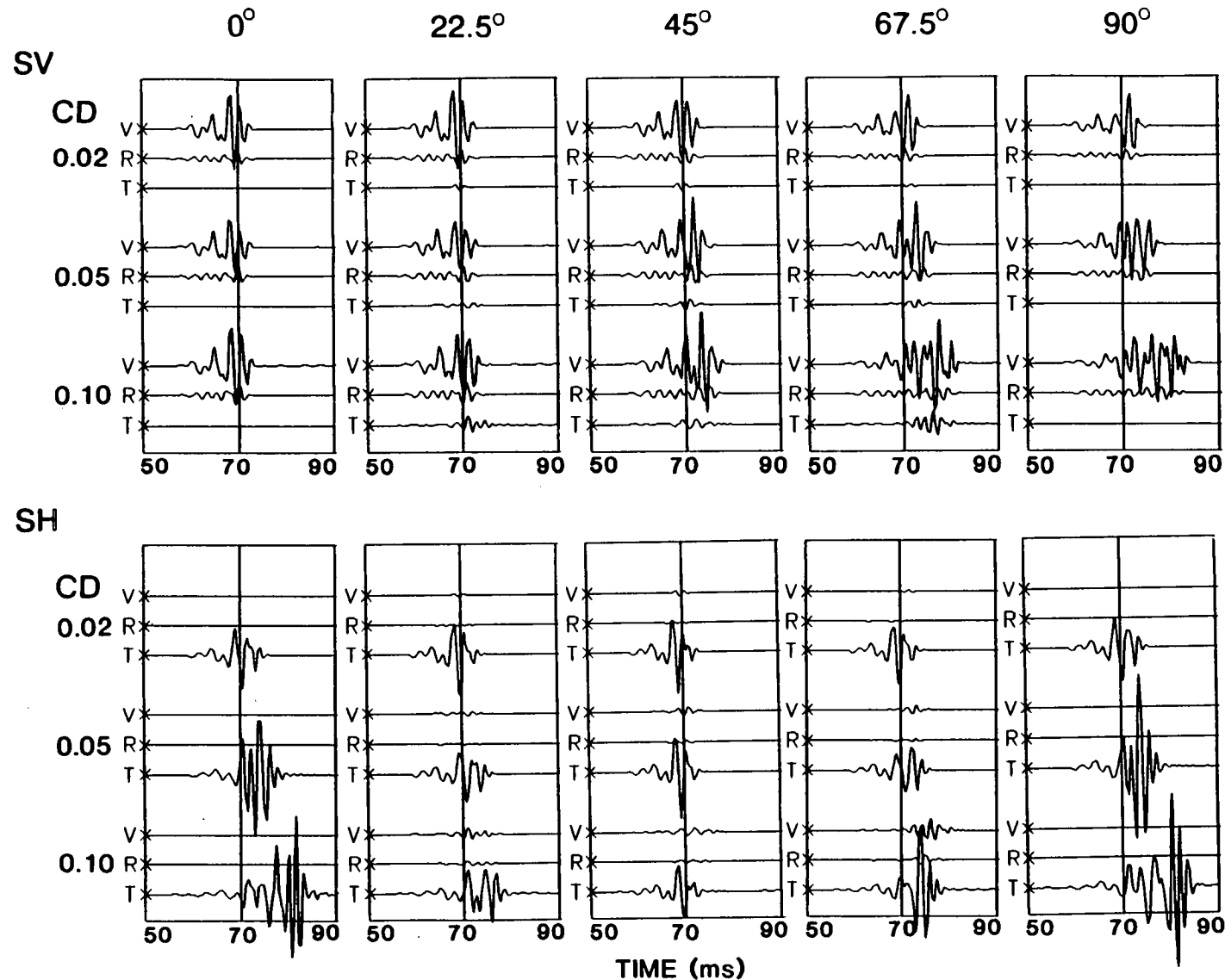
Figure 3.15 Synthetic seismograms in Model 2 with water-filled cracks, as in Figure 3.13 at three crack densities (*CD* = 0.02, 0.05, and 0.1), and for five directions of propagation with respect to the crack strike (0°, 22.5°, 45°, 67.5°, and 90°). *SV* is the vertical point-force, and *SH* is the transverse horizontal point-force at position S4 and with dominant frequency 400Hz.

cross-coupling between Rayleigh- and Love-motions is most
pronounced for directions at 22.5° and 67.5° to the crack strike.
Although the general appearance of the guided-waves may be similar
for each crack density, a closer inspection of the wavetrains shows
that there are siginicant differences. For example, the number of
cycles, and coupling amplitudes increase with increased crack
density.

To conclude, the behaviour of guided-waves is very sensitive to
the crack density and crack orientation (crack strike) in the
low-velocity channel. Although an interpretation of any single
three-component seismogram may be ambiguous, the comparison of
seismograms showing temporal changes would place more constraints
on any interpretation.

3.4.3 EFFECTS OF CRACK SATURATION

In this section, the effects of crack saturation on the
propagation of guided-waves, for crack density CD = 0.1 and aspect
ratio AR = 0.01, are observed.

Figure 3.16 shows the dispersion curves for both water-filled and
(dry) gas-filled cracks for the same model as in Figure 3.13 for
five directions of propagation (0°, 22.5°, 45°, 67.5°, and 90° to
crack strike). The solid line is for water-filled cracks, and
dashed line for gas-filled cracks. The dispersion of the $G2$-mode
(equivalent to FR for almost the whole frequency band) is almost
unchanged by the change of pore-fluid. In contrast, the $G1$-mode
(equivalent to FL) shows substantial differences between water- and
gas-filled cracks. In a direction of 45°, the $G2$-mode shows

Figure 3.16 Effects of differences in crack saturation. Dispersion curves of first four *Generalized* modes of guided-waves of Model 2 with crack density CD = 0.1 for five directions of propagation with respect to the crack strike (0°, 22.5°, 45°, 67.5°, and 90°), for different crack saturations: water-filled cracks - solid line; and gas-filled cracks - dashed line. Arrowheads indicate the positions of pinches in the phase-velocily curves.
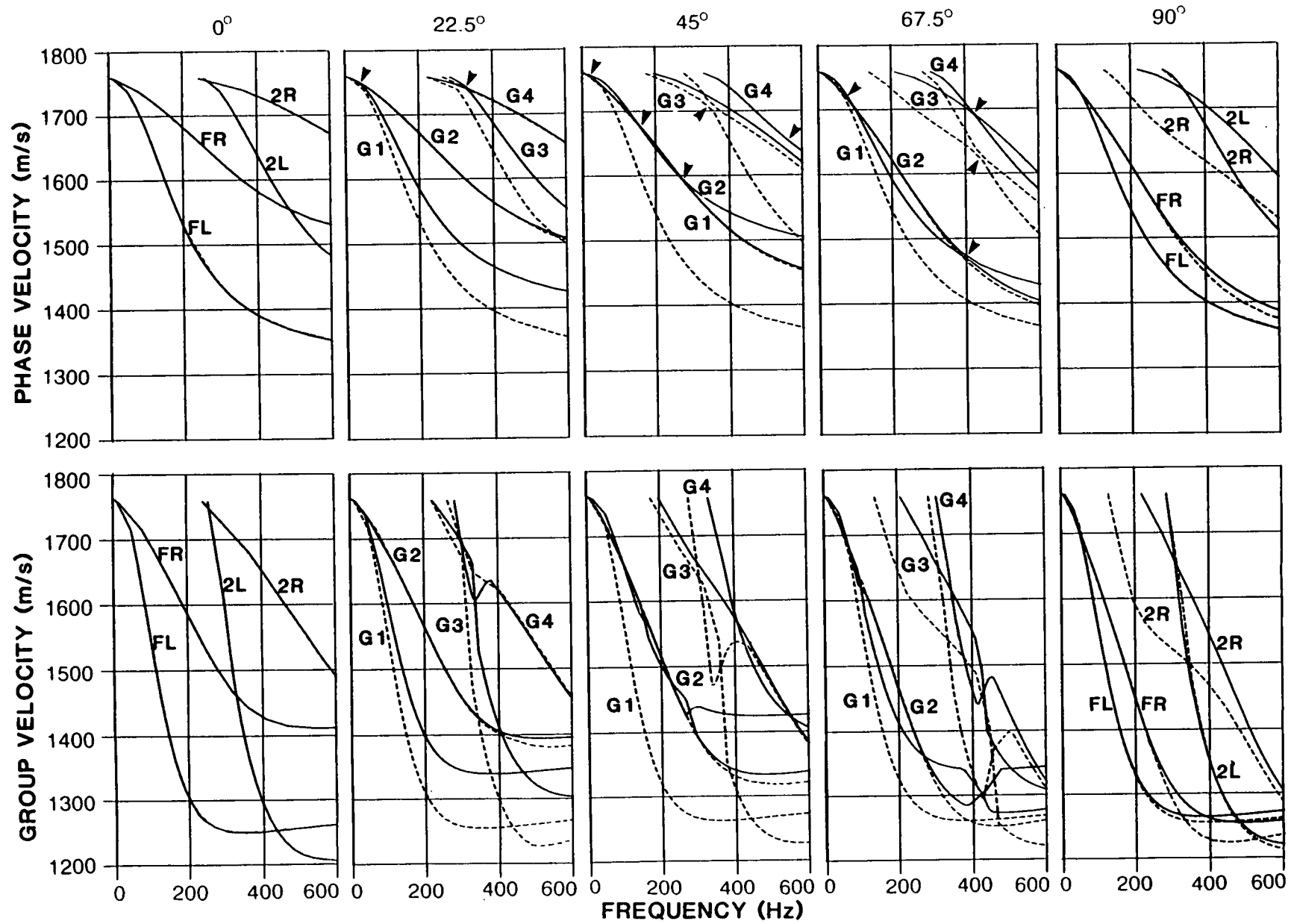
Figure 3.16

maximum difference in dispersion, with some frequencies showing a velocity change of over 10%, and some velocities showing a frequency change of over 40%. However, in directions 0° and 90°, the dispersion of the Love-type modes and the fundamental Rayleigh mode is largely independent of the crack saturation, whereas in directions 67.5° and 90° the dispersion behaviour of second Rayleigh like modes (G3 or 2R) shows a very significant difference for the two different crack saturations.

The amplitude/depth distribution of the first four *Generalized* modes for gas-saturated cracks are shown in Figure 3.14 (a-d) as dashed lines (crack density CD = 0.1, directions of propagation 22.5°, 45°, and 67.5°). Modes G1 and G2 are excited by a 300Hz source, and G3 and G4 by a 500Hz source. For most modes and in most directions of propagation, gas-filled cracks result in greater three-dimensional coupling than water-filled cracks. The difference in coupling between gas- and water-saturated cracks is particularly significant for G1 and G3 (Love-type modes) in directions away from sagittal symmetry, and causes large differences in the dispersion curves.

The differences between gas- and water-saturation in the dispersion and amplitude/depth distribution of *Generalized* modes of guided-waves are shown in the seismograms of Figure 3.17. Again, the sources are at position S4 with dominant frequency 400Hz, and the geophone is at G4. For the *SH*-source, except for directions of sagittal symmetry (0° and 90°) at which guided-waves have the same behaviour for both gas- and water-saturation, the guided-waves show substantial differences in arrival times, dispersion, and relative amplitudes on the different components. The guided-waves for

Figure 3.17 Synthetic seismograms for Model 2 of Figure 3.16 with crack density $CD = 0.1$ for five directions of propagation relative to the crack strike ($0°$, $22.5°$, $45°$, $67.5°$, and $90°$) for gas- and water-filled cracks. The seismograms are shown for SV and SH sources at position S4 and the geophone is at G4.

gas-saturated cracks have longer dispersive wavetrains with larger cross-coupling amplitudes than for water-saturated cracks. As expected from the dispersion, the waveforms of guided-waves for the *SV*-source have very similar behaviour between 0° and 45° directions, for both gas- and water-saturated cracks. However, at the directions between 67.5° and 90°, the guided-waves for *SV* source show significant differences in mode interference and three-dimensional coupling amplitude for the two different saturations.

In general, the gas-saturated cracks usually cause longer dispersive wavetrains, larger coupling amplitudes in three-components, and, therefore, more complicated waveforms of *Generalized* modes of guided-waves than the liquid-saturated cracks. The Love-like guided-waves seem to be more sensitive to the change of crack-saturations than Rayleigh-like guided-waves. But there are several exceptions: for propagation along the crack strike, guided-waves show no difference between gas- and fluid-saturations; for propagation in directions between 45° to 90°, the third *Generalized* mode of guided-waves (*G3* or *2R*, equavalent to second Rayleigh mode) is particular sensitive to changes of crack-saturation. These pronounced differences between the behaviour in gas- and water-filled cracks suggest that guided-waves may be useful for monitoring production processes.

3.4.4 EFFECTS OF CHANGING CRACK ASPECT RATIO

The Nishizawa (1982) crack formulation was used to model large aspect-ratio cracks. Figure 3.18 shows dispersion curves for Model 2, with crack density $CD = 0.05$ and aspect ratios of $AR = 0.05$

Figure 3.18 Effects of differences in aspect ratio. Dispersion curves of first four *Generalized* guided-wave modes of Model 2 with water-filled cracks with crack density CD = 0.05 for five directions of propagation relative to the crack strike (0°, 22.5°, 45°, 67.5°, and 90°) for three different aspect ratios: AR = 0.05 - solid line; 0.1 - dashed line; and 0.3 - dash/dot line. Arrowheads indicate the positions of pinches in the phase-velocity curves.
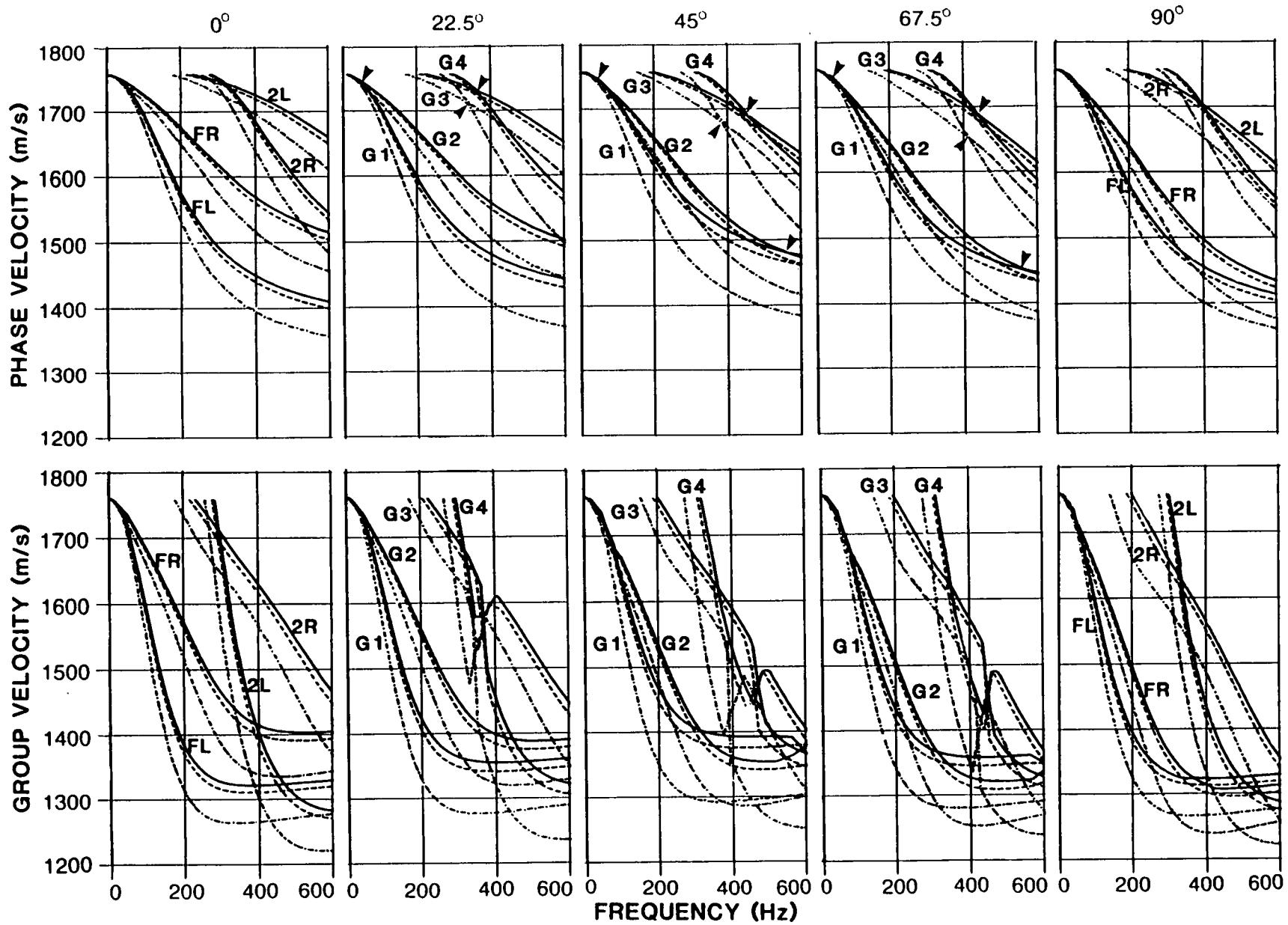
Figure 3.18

(solid line), 0.1 (dashed line), and 0.3 (dash/dot line). [If the porosity is entirely in aligned cracks, such aspect ratios would represent porosities of 1.57%, 3.14% and 9.42%, respectively.] For crack aspect ratios less than 0.1, dispersion curves show little difference for the different directions of propagation, but there is significant change in dispersion between aspect ratios of 0.05 and 0.3 for all directions of propagation. Larger aspect ratios usually result in lower velocities at any frequency. Unlike crack density and crack saturation, effects of crack aspect ratio on dispersion curves are less sensitive to the direction of guided-wave propagation relative to crack strike. Other calculations of synthetic seismograms (not shown) show that variations of crack aspect ratio have little effect on the amplitude/depth distribution of guided-waves. This suggests that the main effects of different aspect ratio on guided-wave propagation may be in the change of velocity/frequency dispersion. Figure 3.19 shows the difference of guided-waves on synthetic seismograms between $AR = 0.05$ and $AR = 0.30$, with the same source and geophone parameters as Figure 3.17.

3.5 COMPARISON OF THEORETICAL DISPERSION WITH SEISMOGRAMS

In this section, the theoretical dispersion curves are compared with the dispersion of the synthetic seismograms. From the synthetic seismograms of Model 2 (Figure 3.15), we have selected the three-component seismograms excited by SH type source, propagating in a direction of 67.5° to the strike of water-filled cracks ($CD = 0.1$). We have extracted their group-velocity dispersion by the multiple filter technique (see Appendix A). Figure 3.20(a) is the dispersion contoured map calculated from the
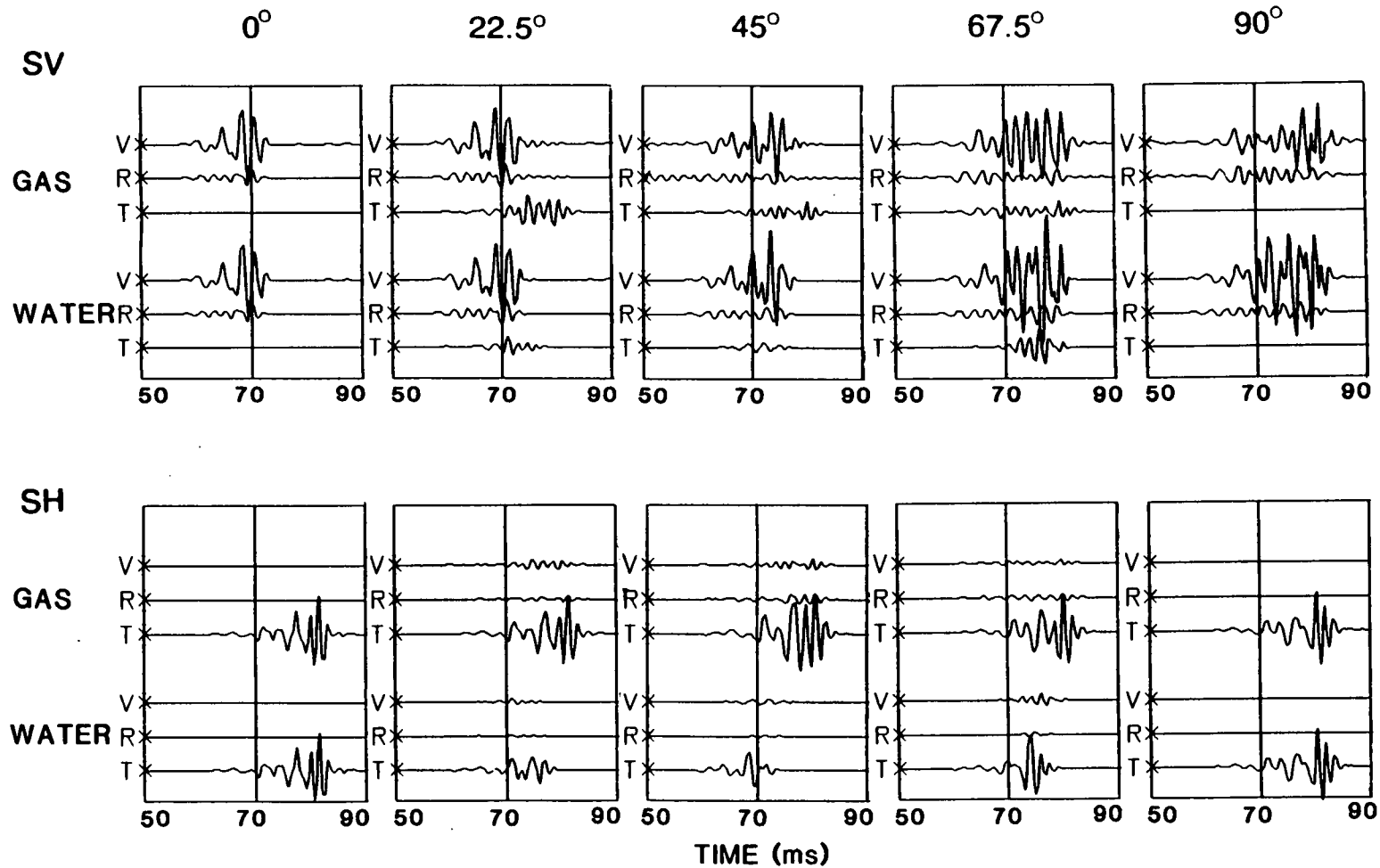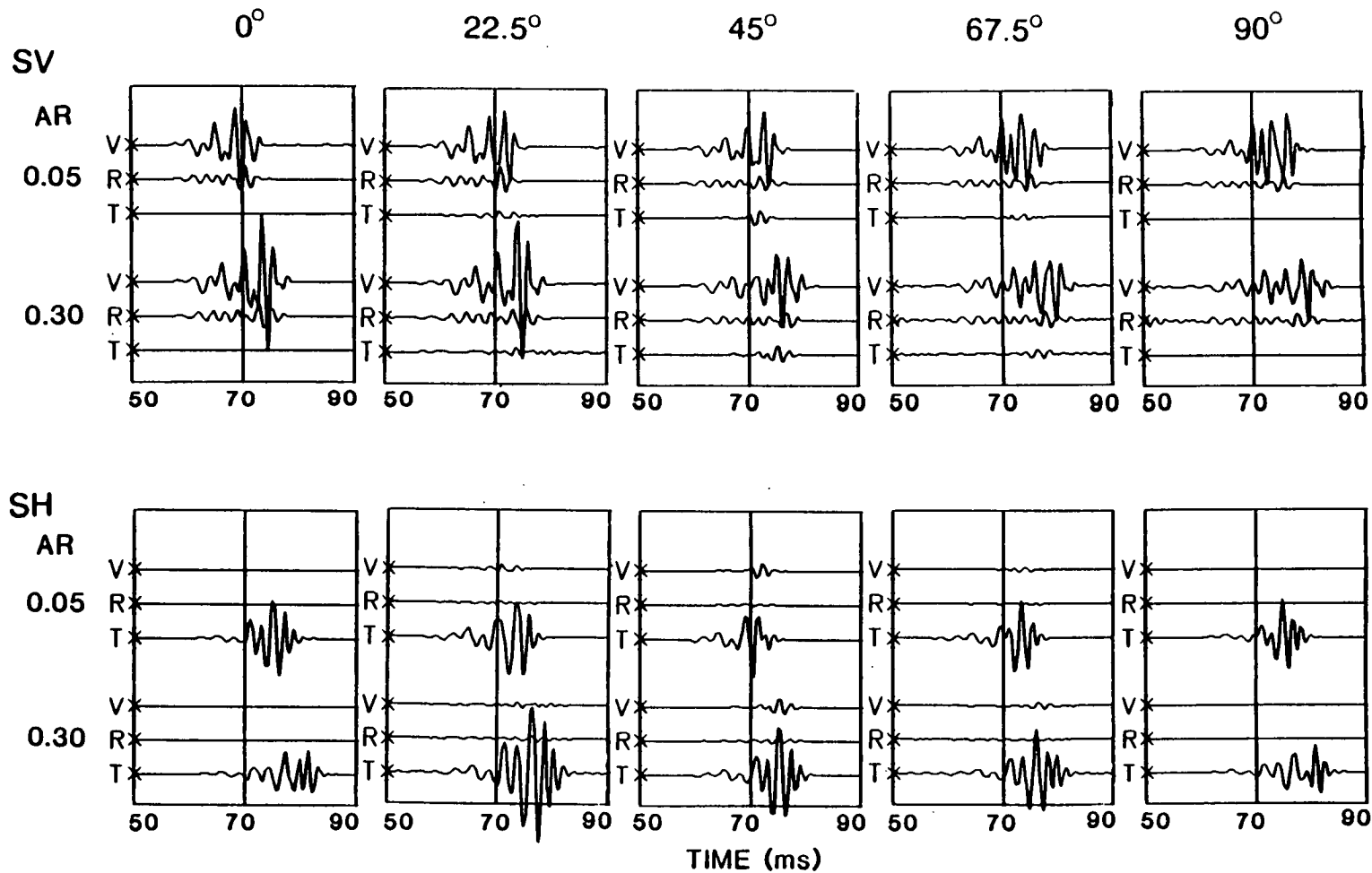
Figure 3.19 Synthetic seismograms for Model 2 of Figure 3.18 with crack density CD = 0.1 for five directions of propagation relative to the crack strike (0°, 22.5°, 45°, 67.5°, and 90°) for *AR* = 0.05 and *AR* = 0.30. The seismograms are shown for *SV* and *SH* sources at position S4 and the geophone is at G4.

horizontal transverse-component seismogram (see inset), and Figure 3.20(b) is calculated from vertical component seismogram (inset). Both contours and spectra (insets) suggest that there are basically two *Generalized* modes of guided-waves in the two seismograms, and the large amplitudes of the seismograms appear to be principally those of the higher modes. Two contoured maps display similar dispersion behaviours. The theoretical group-velocity dispersion curves of two Love-like modes are also ploted on the contours by solid lines, which agree reasonably well with the contoured multiple-filtering plots. The low values in the centre of the plots are probably due to the destructive interference of different *Generalized* modes at similar frequencies.

The fact that the horizontal transverse and vertical components both have almost identical dispersion features, implys that both components receive the same *Generalized* modes of guided-waves in three-dimensional motions in anisotropic media.

In summary, the group-velocity dispersion of guided-waves can be extracted by the multiple filter technique from observed seismograms. Comparing the theoretical dispersion curves from an anisotropic waveguide, with the observed results from seismograms may provide a method of inverting guided-wave dispersion to yield values of anisotropic parameters.

3.6 PARTICLE-MOTION OF GUIDED-WAVES IN ANISOTROPIC WAVEGUIDES

The above studies have shown that the dispersion of guided-waves can be significantly modified if they propagate through anisotropic region. In some cases, the anomalies in dispersion may not be so

marked that it could unequivocally be assigned to the presence of anisotropy, and not to some unknown inhomogeneity. However, guided-waves have distinctive particle motion when propagating through an anisotropic structure with certain symmetry relations, and those features can be used to diagnose the presence of effective anisotropy.

3.6.1 TYPES OF PARTICLE-MOTION OF GUIDED-WAVES

The particle-motion of a guided-wave in an anisotropic medium is characterized by polarization diagrams. Polarization diagrams display the cross-sections of the particle displacements and can show patterns of motion dominated by the anisotropic parameters along the wavepath. Crampin (1975) has theoretically established patterns of particle-motion of surface-waves propagating in a anisotropic halfspace for various symmetry conditions. We suggest that the particle-motion of guided-waves can also be characterized by these paterns. We summarize the possible types of particle-polarization of guided-waves in general anisotropic media as follows:

(a) Generalized motion - there is a constant phase difference between the components of displacement not to equal to zero or 90°.

(b) Tiltled Rayleigh motion - particle motion is elliptical in a plane rotated from the sagittal plane about the propagation vector.

(c) Inclined Rayleigh motion - motion is elliptical in a plane rotated from the sagittal plane about a vertical axis.

(d) Slopping Rayleigh motion - motion is elliptical in the sagittal plane with a non-vertical axis to the ellipse.

(e) Rayleigh motion - motion is elliptical in the sagittal plane with a vertical axis.

(f) Love motion - motion is linear with transverse horizontal polarization.

In the anisotropic structure with symmetry planes, there are generally three distinct particle-motions: *inclined Rayleigh*, *tiltled Rayleigh* and *sloping Rayleigh*, each of which is related to propagation direction with respect to the symmetry plane of anisotropy. Waves travelling parallel to any of the vertical symmetry planes have pure Rayleigh or pure Love motions as in purely homogeneous isotropic media. In general, if waves travel in any other direction, three distinct particle-motions are often observed. Figure 3.21 shows the three distinct particle-motion characteristics of symmetry orientations: (a) *inclined Rayleigh* motion - when there is a horizontal plane of symmetry, (b) *tiltled Rayleigh* motion - where the propagation is at right angle to vertical plane of symmetry, and (c) *sloping Rayleigh* motion - where the propagation is along sagittal plane of symmetry. From these particle-motion patterns of guided-waves, the symmetry of existing anisotropy may be determined.

3.6.2 PARTICLE-MOTION OF GUIDED-WAVES IN THE WAVEGUIDES WITH EDA CRACKS

In anisotropic waveguides with <u>vertical</u> parallel cracks, the

THREE DISTINCT PARTICLE-MOTIONS

OF GUIDED-WAVES IN ANISOTROPIC MEDIA
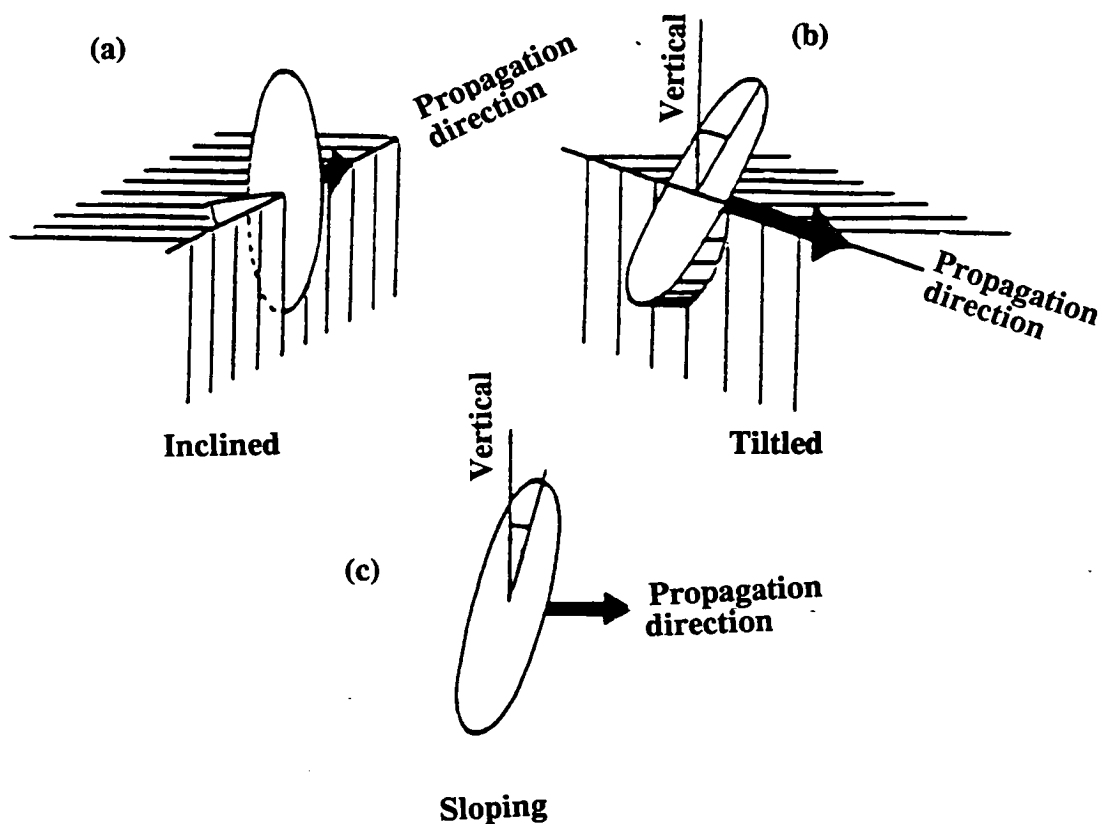
Figure 3.21 Three-types of *Generalized* guided-wave particle-motion characteristic of propagation in particular symmetry directions: (a) *inclined-Rayleigh* motion - propagation in a horizontal plane of symmetry, (b) *tiltled-Rayleigh* motion - propagation at right angle to a vertical plane of symmetry, and (c) *sloping-Rayleigh* motion - propagation in a sagittal plane of symmetry (after Crampin 1975).

particle-motion of guided-wave is *inclined Rayleigh* motion with elliptical motion in a plane inclined to the direction of propagation. Figure 3.22 shows polarization diagrams of selected synthetic seismogrames of Figure 3.17 at three off-symmetry directions 22.5°, 45° and 67.5° of propagation to crack strike. Elliptical particle-motion patterns inclined slightly from the transverse axis are clearly seen in the Radial-Transverse plane for both gas- and water-saturated cracks. On the Vertical-Transverse plane the elliptical particle motion also can be seen. Because of the interference of different modes, the particle-motion patterns of guided-waves at high frequency may be very complicated. The polarization diagrams of guided-waves may not be immediately interpreted in terms of crack alignments, but they may give the symmetry information of the anisotropic waveguide. However, the three-dimensional particle-motions of guided-waves are sensitive to the details of anisotropy and structure along the wavepath, and are worthy of further study.

3.7 DISCUSSION AND CONCLUSIONS

Modelling has suggested that a thin-layered sedimentary reservoir may act as a waveguide in crosshole seismic surveys, if approriate source polarization and frequency can be chosen. For a given velocity structure, the preliminary study of dispersion and amplitude/depth distribution of guided-waves can help us to choose the most appropriate source and geophone parameters to excite and receive appropriate modes of guided-waves in crosshole surveys. As most of the energy of such guided-waves may be confined to a comparatively narrow zone either side of the channel, guided-waves are very sensitive to the internal geometry of the reservoir.
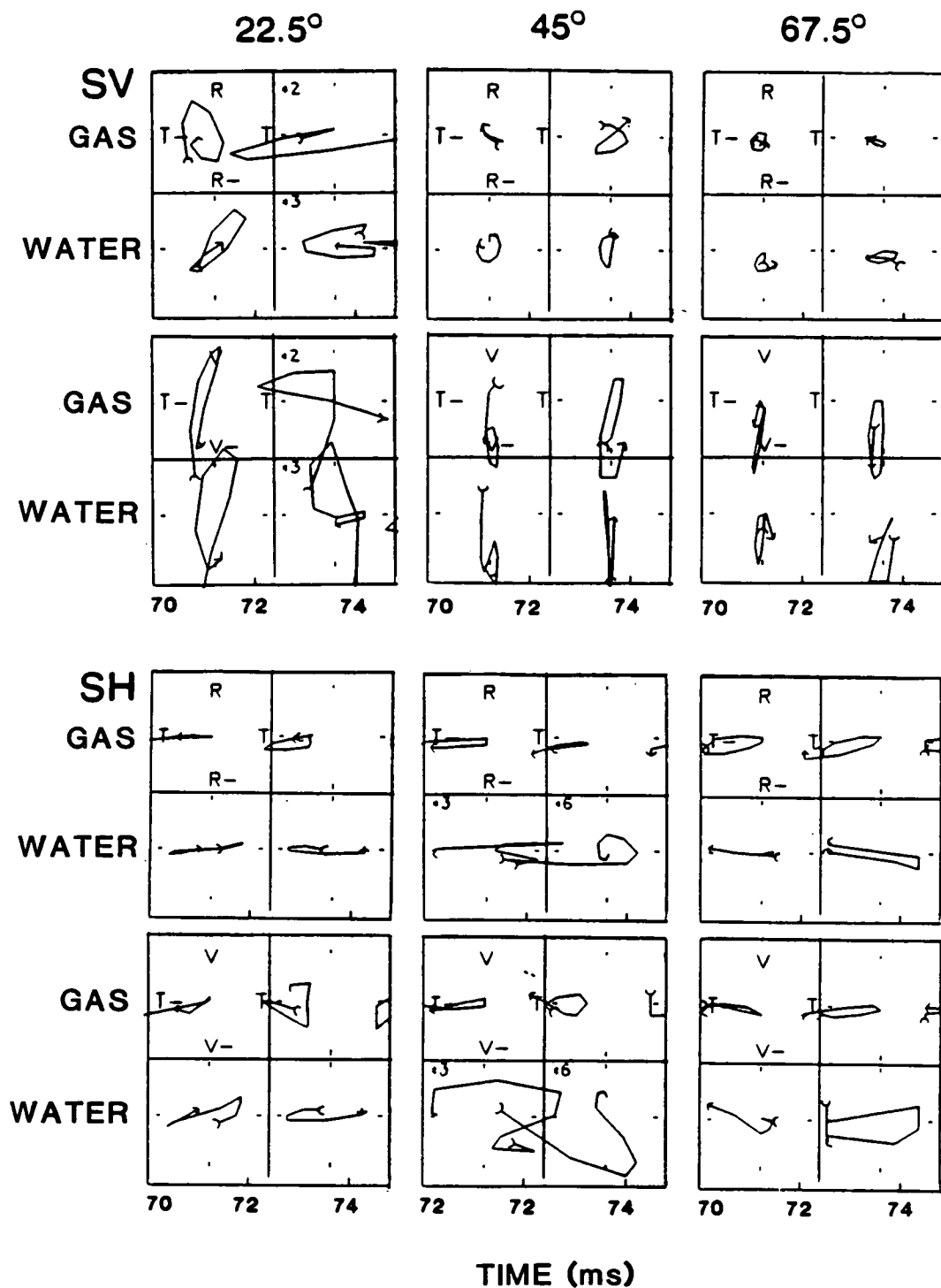
Figure 3.22 Polarization diagrams of selected synthetic seismograms of Figure 3.17 at three off-symmetry directions, 22.5°, 45° and 67.5° of propagation to the crack strike. The elliptical motion patterns are seen in radial(R)-transverse(T) and vertical(V)-transverse(T) planes.

By using the techniques developed in Chapter 2, we have studied the propagtion of guided-waves in sedimentary reservoir waveguide models displaying crack-induced anisotropy (EDA). We have calculated the dispersion, amplitude/distribution and synthetic seismograms of guided-waves in the model with different crack parameters. In crack-induced anisotropic media, the seperate families of Rayleigh and Love modes of guided-waves in plane isotropic layers, will be combined into one family of *Generalized* modes in three-dimensional particle motion.

The calculation results show that dispersion and other propagation behaviours of guided-waves are very sensitive to the changes of crack density, crack saturation, crack aspect ratio, and direction of propagation of guided-waves relative to crack strike. The increase of crack density usually result in the following: dispersion curves of guided-waves, especially the positions of Airy phase on the curves, shift towards the lower velocity at any frequency; and the cross-coupling amplitudes of guided-waves increase in most directions of propagation relative to crack strike. Gas-saturated cracks usually cause longer dispersive wavetrains, larger coupling amplitudes, and, therefore, more complicated waveforms of guided-waves than liquid-saturated cracks. Love like guided-waves are usually more sensitive to the change of crack-saturations than the corresponding Rayleigh like guided-waves. The change of aspect ratio of cracks will mainly modify the dispersion behaviour of guided-waves.

Comparing the theoretical dispersion curves with the observed results calculated from seismograms by multiple filter technique, may provide a method of anisotropic dispersion inversion of

guided-waves. However, like other inversion techniques, the results of this inversion are unlikely to be unique. Formal inversion of anisotropic dispersion to determine anisotropic structure and parameters has not been attempted, because of the large number of anisotropic parameters to be estimated, and the large amount of computer time required. In crack-induced anisotropic reservoir waveguides, if we could confine the changes of elastic constants to the crack parameter, say, crack-saturation, and if isotropic matrix parameters of the waveguides were determined, then the anisotropic dispersion inversion of guided-waves could be attempted without too severe computations.

Particle-motion of guided-waves provide some diagnostics for the presence of anisotropy. In the anisotropic structure with symmetry planes, there are generally three distinct particle-motions: *inclined Rayleigh*, *tiltled Rayleigh* and *sloping Rayleigh*, each of which is related to the propagation direction with respect to a certain symmetry plane of anisotropy. From these particle-motion patterns of guided-waves, we may determine the symmetry of existing anisotropy. In the waveguide model with vertical EDA cracks, the particle-motion of a guided-wave is *inclined Rayleigh* motion with elliptical motion in a plane inclined to the direction of propagation. The details of polarization diagrams of guided-waves are sensitive to the changes of crack parameters, and further studies are needed.

CHAPTER 4

GUIDED-WAVES IN CROSSHOLE SEISMIC SURVEYS

I. FIELD DATA ANALYSIS

4.1 INTRODUCTION

In oil production and Enhanced Oil Recovery (EOR) operations,
reservoir engineers usually require high geophysical imaging
resolution (of the order of 1m) of reservoirs to exploit the
resources by optimal techniques (Rutledge 1989). Because of
low-velocity and high-attenuation surface layers, large distances
from the target zones, and noisy surface environments, the
resolution power of surface seismic data is severely limited, and
crosshole surveying, where both source and geophone are at
subsurfaces, is playing an increasing role in production geophysics.
Crosshole seismic data may provide high-resolution images of the
structure and properties of producing formations as well as
measurements of changes in reservoirs brought about by production or
EOR operations.

Until recently, the seismic data from crosshole surveys have been
mainly employed from their first arrivals by P-wave tomography.
However, both theoretical study and field observations suggest that
the dominant energy in some crosshole surveys propagates as
guided-waves with the energy tied to an interface, or combination of
interfaces, when there are interfaces with significant

velocity-contrasts continuous between the wells (Krohn 1990, Worthington 1991, Liu *et al.* 1991, Lines *et al.* 1991, Lou and Crampin 1991a, b). It is necessary to identify and study these guided-waves from crosshole data, following the modelling study in Chapter 3, which has suggested that guided-waves contain useful information about interfaces and internal structures of waveguides.

In this chapter, we will analyse crosshole datasets recorded at the Conoco's Borehole Test Facility (CBTF) in Kay County, Oklahoma, to study the propagation of guided-waves in field crosshole surveys. Liu *et al* (1991) first identified the guided-waves in crosshole datasets at the CBTF site, and they have given a comprehensive modelling study from crosshole surveys and reverse vertical seismic profiles to detect natural fracture systems in the area. Here we will focus on the study of the guided-waves associated with certain interface structures at the CBTF site.

4.2 THE CONOCO CROSSHOLE DATA

4.2.1 GEOLOGY BACKGROUND

The crosshole data were collected at five shallow boreholes (down to 50m) at the Conoco Borehole Test Facility. The site geology is well-documented by Queen and Rizer (1990), and we summerize as follows:

The shallow structure at the CBTF site consists of low amplitude folds overlying an approximately 50km-wide zone of differentially uplifted blocks bordered by northeast and northwest trending faults active in the Paleozoic. Surface rocks consist primarily of

limestones and shales of the Lower Permian Chase Group. Surface structure in this area is subtle and uniform, characterized by a regional dip of less than 1.5° to the west-sourthwest with the velocity structure given in Figure 4.1 and Table 4.1. The CBTF area is highly fractured with two distinct fracture sets visible at surface outcrops. Figure 4.2 shows the surface and subsurface fracture patterns in a neighbouring outcrop of the Fort Riley Limestone, where the near-orthogonal sets of near-vertical fracture have been mapped by various techniques described by Queen and Rizer (1990). There is a systematic set striking about N75°E and a non-systematic set at N25°W (non-systematic fratures generally terminate against the systematic). The previous studies from three-component seismograms in VSPs and crosshole surveys (Queen and Rizer 1990, Liu *et al*. 1991) have suggested that crack density in this area is between $CD = 0.10$ and 0.15. Liu *et al* (1991) have shown that the fractures are also inclined at 15° to 30° to the vertical, dipping towards the south.

4.2.2 CROSSHOLE DATASETS

Figure 4.3 shows the plan view of five boreholes at the CBTF site. The five boreholes, GW1 to GW5 marked with circles, are shallow 50m-deep wells used for the crosshole seismic surveys. Sources are located at depths between 3m and 41m with about 0.6m spacing in borehole GW5. Three-component geophones were deployed in boreholes GW1 to GW4 at depths of approximately 5m to 42m with a spacing of about 3.7m. The detailed source-receiver parameters for CHSs are given in Tabel 4.2. All data were recorded with the Conoco rotary source, which is rotated in both clockwise and anticlockwise directions and radiating horizontally polarized shear-waves. These
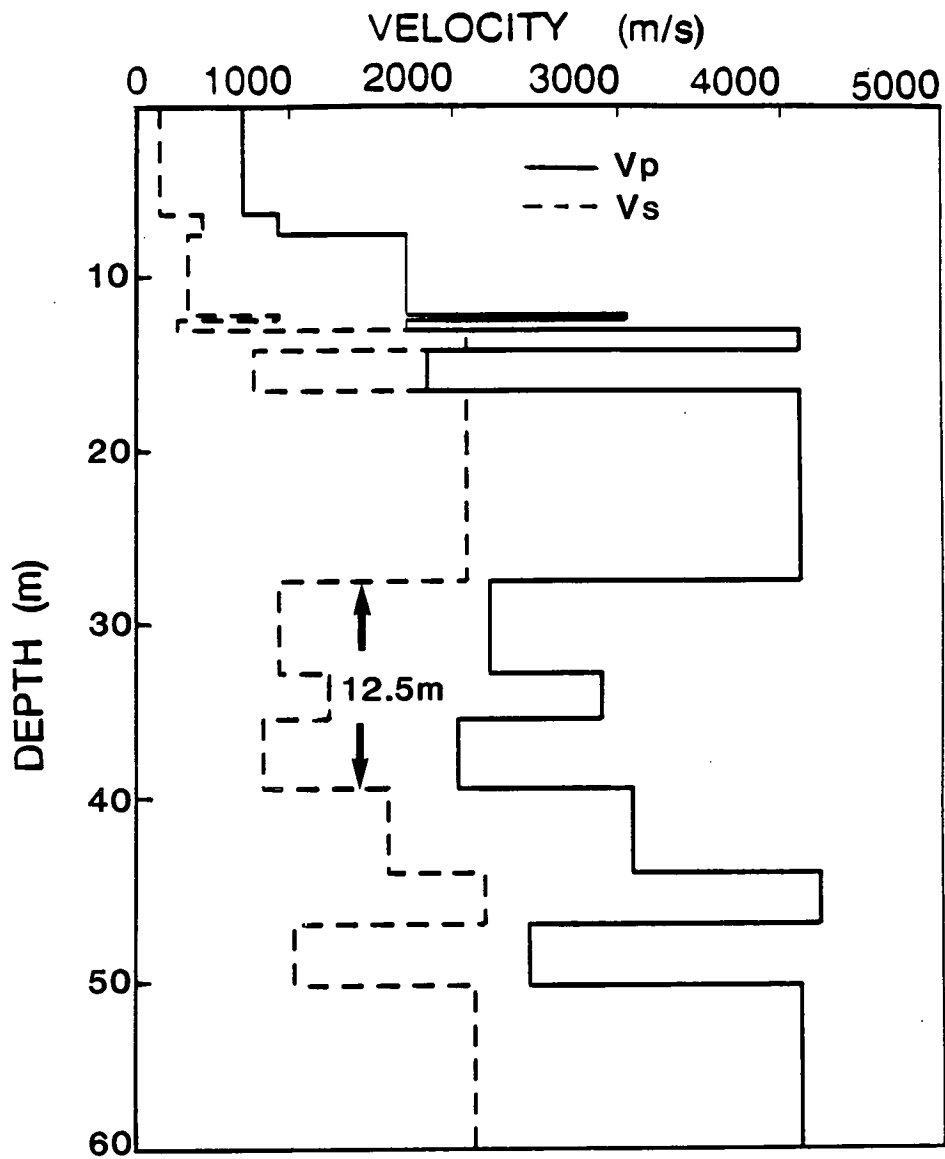
Figure 4.1 Shallow *P*-wave and shear-wave velocity structure from well-logs at the Conoco Borehole Test Facility, Oklahoma.

Tabel 4.1 Structure of the uncracked matrix at the
Conoco Borehole Test Facility (after Liu *et al* 1991).

Layer	Thickness (m)	Vp (m/s)	Vs (M/s)	ρ (g /cm^3)	Q
1	6.4	710	190	2.00	10
2	1.2	914	457	2.00	20
3	4.9	1706	356	2.00	20
4	0.03	3048	914	2.00	20
5	0.06	1706	305	2.00	20
6	1.2	4115	2072	2.42	50
7	2.4	1829	762	2.42	50
8	11.6	4115	2072	2.42	50
9	5.5	2212	914	2.42	20
10	2.7	2902	1219	2.50	20
11	4.3	2011	823	2.24	20
12	5.2	3078	1584	2.48	100
13	3.0	4236	2182	2.59	100
14	3.7	2453	1006	2.42	100
15	10.1	4115	2118	2.47	100
16	7.6	2194	902	2.43	100
17	∞	4115	2118	2.64	100
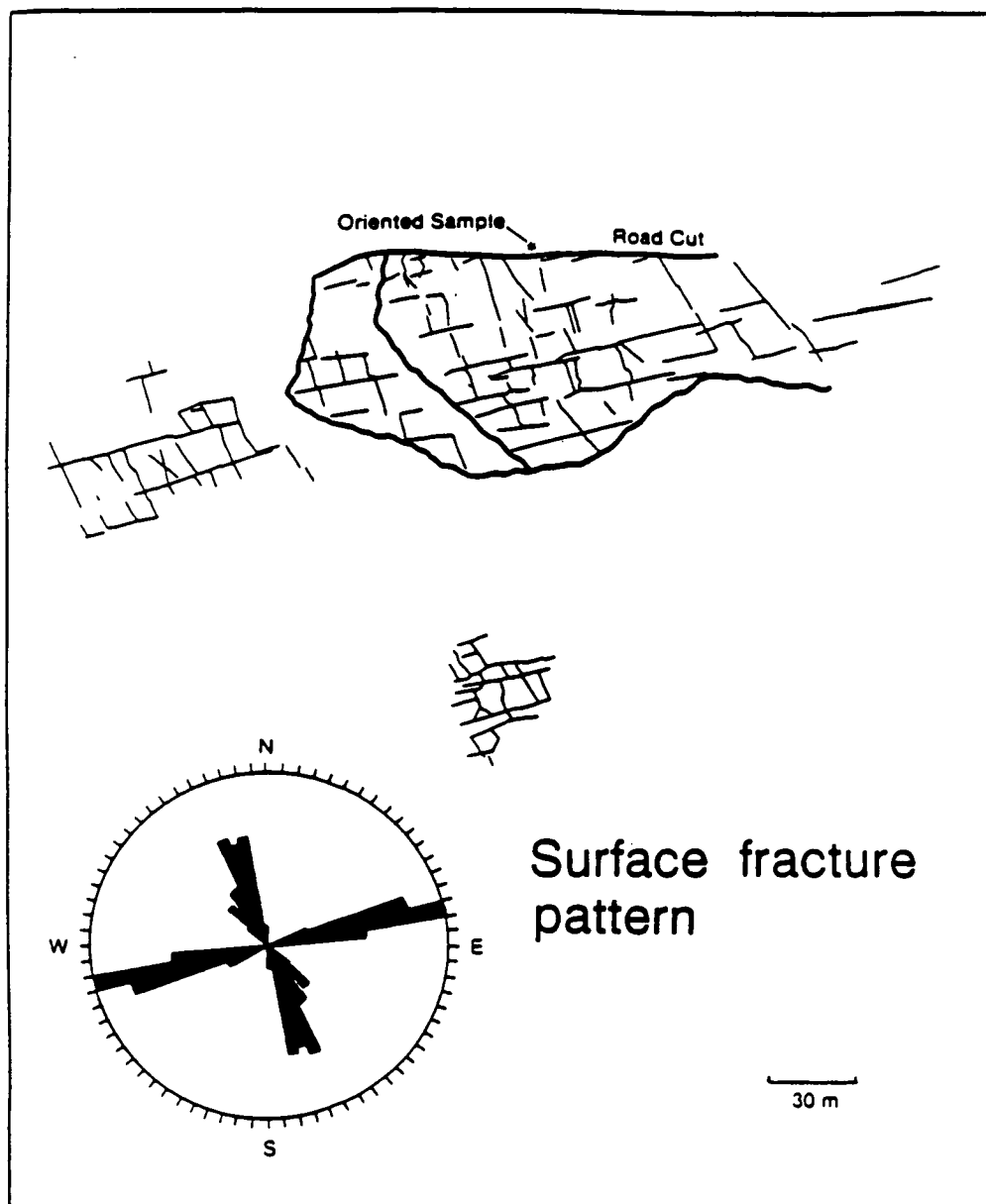
Figure 4.2 Map and rose diagrams of surface fracture pattern at a nearby outcrop of Fort Riley Limestone (after Queen & Rizer 1990).

Conoco Test Site
Kay County, Oklahoma

N

O GW-1

O GW-2

89m

O GW-3

GW-5

53m

O GW-4
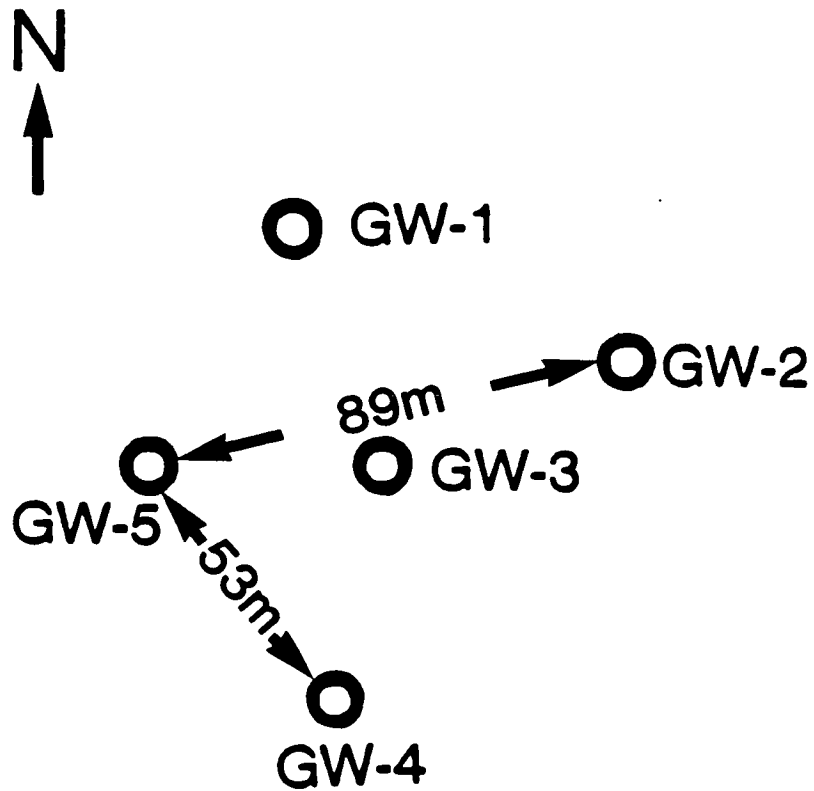
Figure 4.3 Plan of five shallow wells used for crosshole surveys at the Conoco Borehole Test Facility, Kay County, Oklahoma.

Table 4.2 Source and geophone positions for CHSs. All data were recorded with the source in well GW5, and depths are relative to top of GW5 (after Liu *et al* 1991).

Well	Distance from GW5 (m)	Top source depth (m)	Source incem. (m)	Top geophone depth (m)	Geophone incem. (m)
GW1	52.33	3	0.6	5.39	3.66
GW2	88.66	3	0.6	5.39	3.66
GW3	43.28	3	0.6	5.57	3.66
GW4	52.79	3	0.6	5.39	3.66

data are then demultiplexed and sweep correlated before decomposing into linear equivalents of radial and transverse components (in-line and X-line sources, respectively), where orientations were based on a gyro-compass attached to the source. The three-component traces have been re-orientated into vertical, radial (in-line), and transverse (X-line) components with rotations about the vertical axis. The source has a frequency band of 50Hz to 300Hz. The sampling rate is 1ms.

4.3 IDENTIFICATION OF GUIDED-WAVES

4.3.1 THE VELOCITY STRUCTURES AS POSSIBLE WAVEGUIDES

There is a series of low-velocity layers which appear alternatively with high-velocity layers at the CBTF site. All these continuous low-velocity layers with large wave-impedance contrast across horizontal interfaces may act as waveguides, if appropriate source frequencies and polarizations can be selected. For the source frequencies (50Hz to 300Hz) used at the CBTF site, the corresponding wavelength of seismic waves is between 5 and 30 meters. It is most likely that those layers having thicknesses equivalent to the wavelength act as seismic waveguides effectively. Therefore, we first consider the three layered low-velocity channel between about 28m and 40m depth, which are embedded between two high-velocity layers and have about 50 percent velocity-contrast, as the most effective waveguide structure (marked by arrows in Figure 4.1).

4.3.2 SELECTED SEISMOGRAMS

We have selected the seismograms excited by the sources in borehole GW5, and received by the geophones in two boreholes GW2 and GW4, respectively, to examine the propagation of guided-waves. The seismograms recorded in borehole GW1 show relatively poor quality, and borehole GW3 is almost on the same raypath with the line between GW5 and GW2. We have not displayed them here.

All seismograms are shown in true relative amplitudes so that amplitudes of radial, transverse, and vertical components may be directly compared. The seismograms are displayed in both commmon source gather and common geophone gather configurations. Figure 4.4(a) shows the source and geophones positions for a common source gather in the velocity/depth structure of Figure 4.1, and Figure 4.4(b) shows the sources and geophone positions for a common geophone gather. According to Liu *et al* (1991), the seismograms from the common geophone gather show more regular variation between different paths than from the common source gather. This is because that polarizations at any geophone are necessarily dominated by the anisotropic structure near the geophone site, and that records in common geophone gathers have all been filtered (or modified) by the same near-geophone structure.

Figure 4.5 shows the three-component seismograms of a common source gather recorded in borehole GW2 with source at 29.4m deep in borehole GW5 for (a) in-line source orientation, and (b) X-line source orientation.

Figure 4.6 shows the three-component seismograms of a common
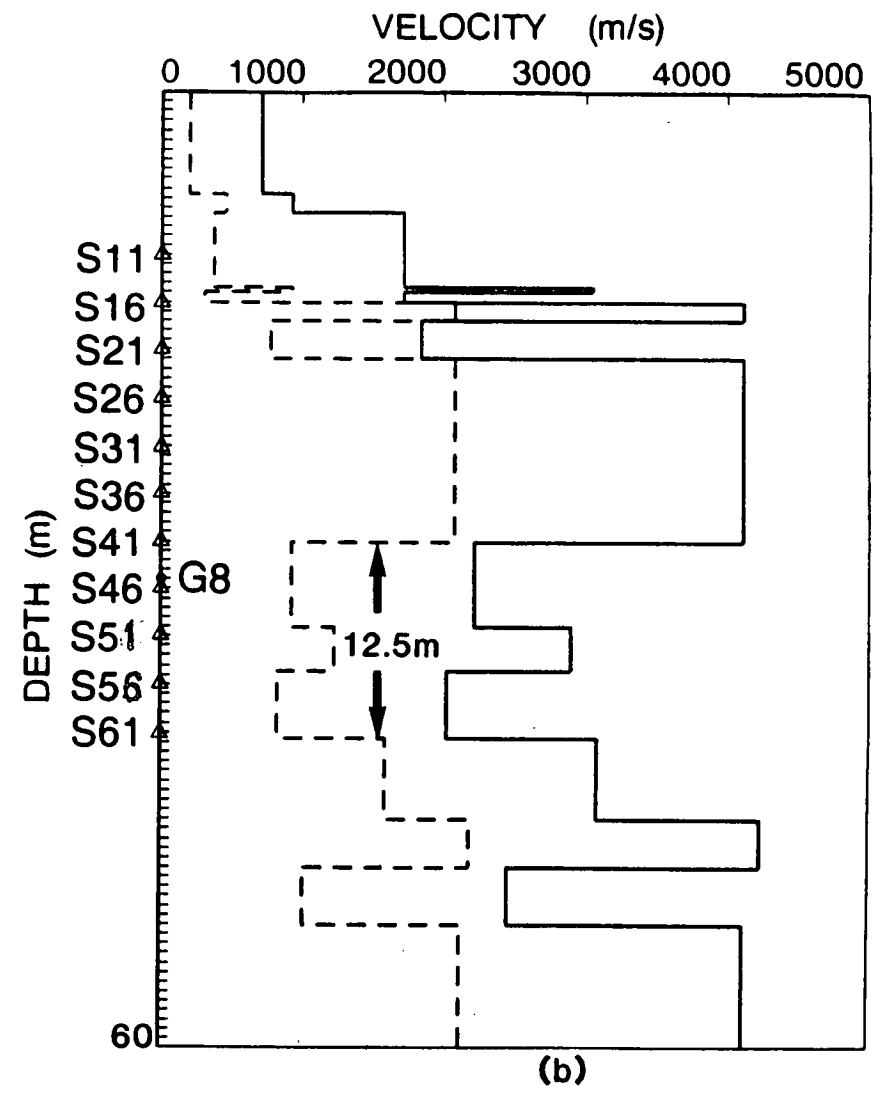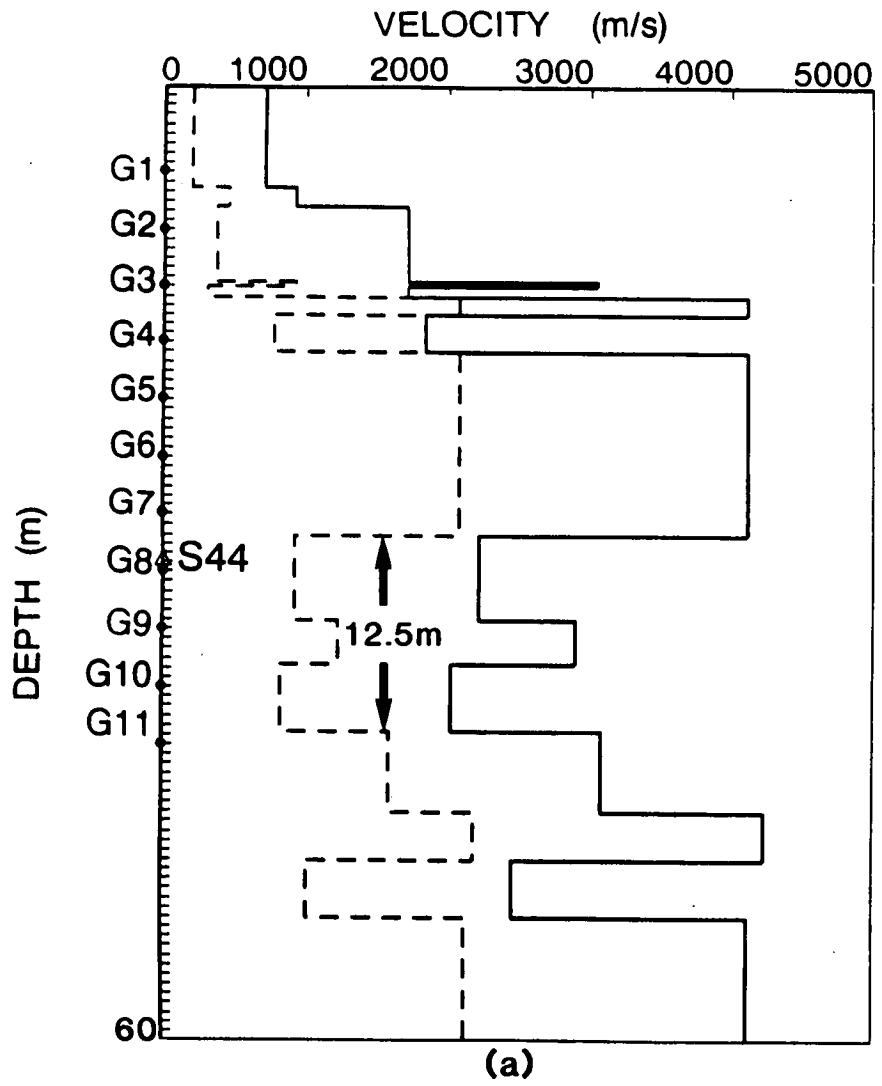
Figure 4.4 Source and geophone positions in the velocity/depth structure of Figure 4.1, for **(a)** a common source gather, and **(b)** a common geophone gather.

GW-2 (RADIAL)

Time (1/10 seconds)
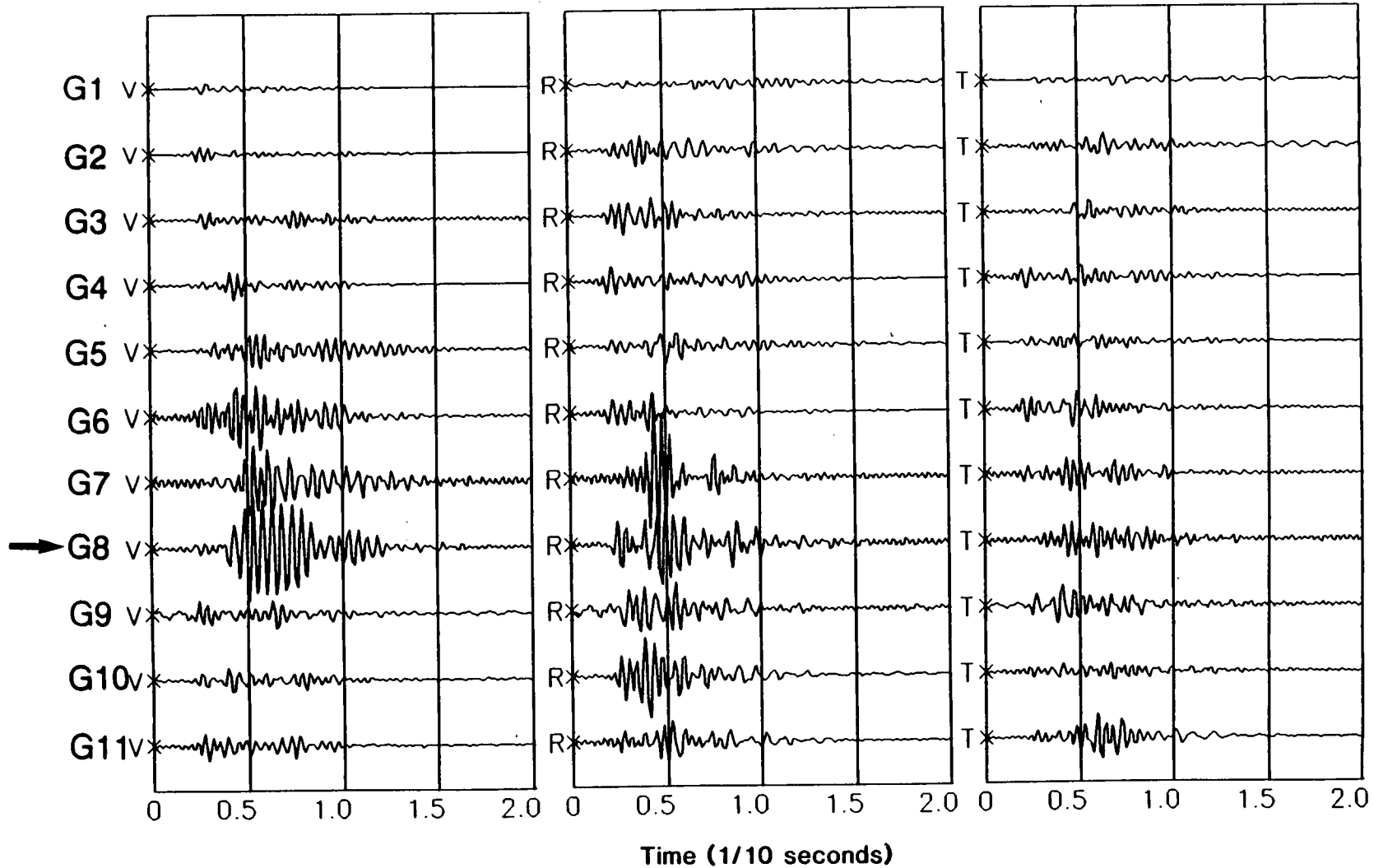
Figure 4.5(a)

Figure 4.5 Selected three-component seismograms of common source gather, recordeed in borehole GW2 with source at 29.4m deep in borehole GW5 for **(a)** in-line source orientation, and **(b)** X-line source orientation.

GW-2 (TRANSVERSE)

Time (1/10 seconds)
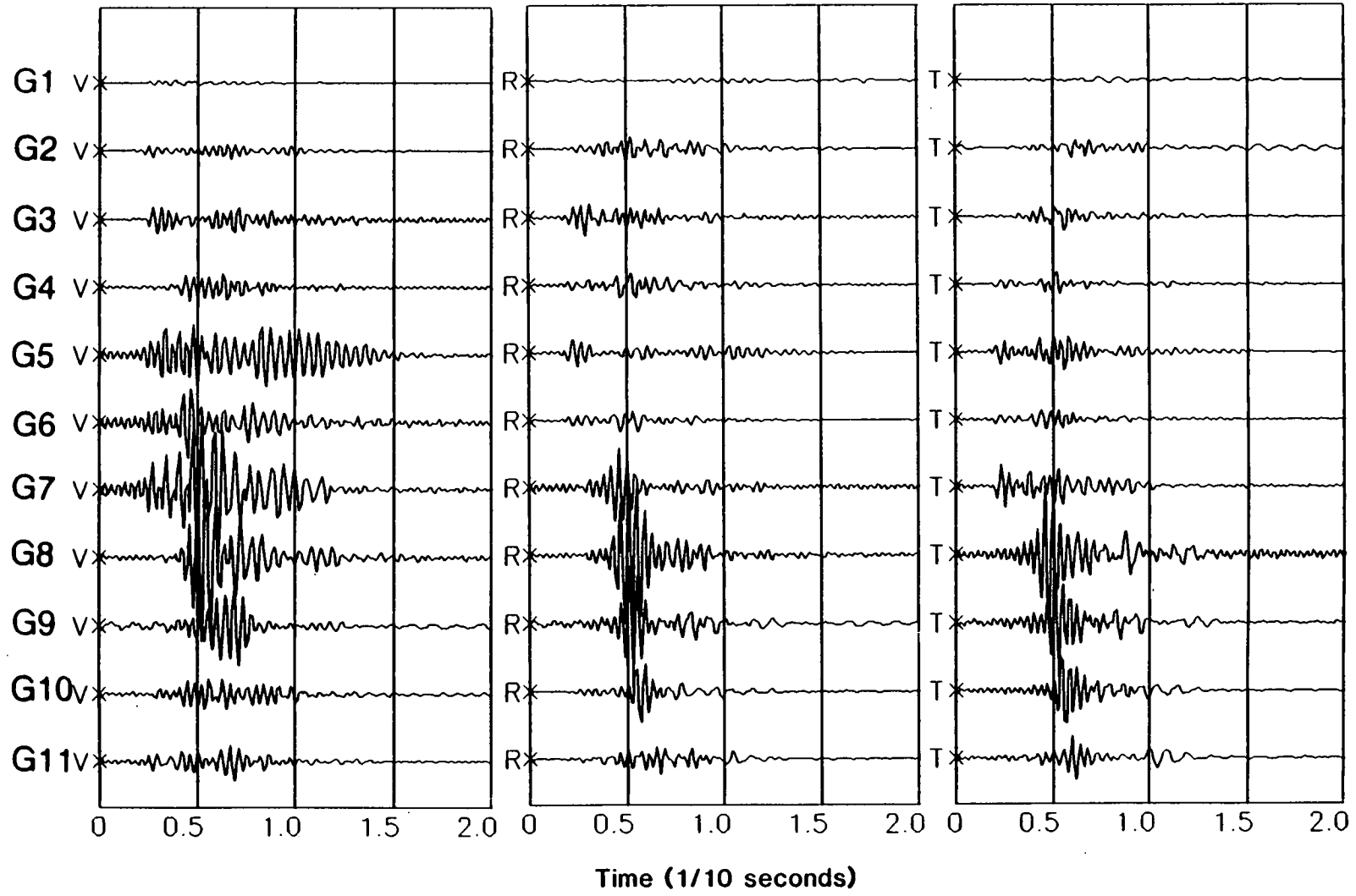
Figure 4.5(b)

GW-2 (RADIAL)
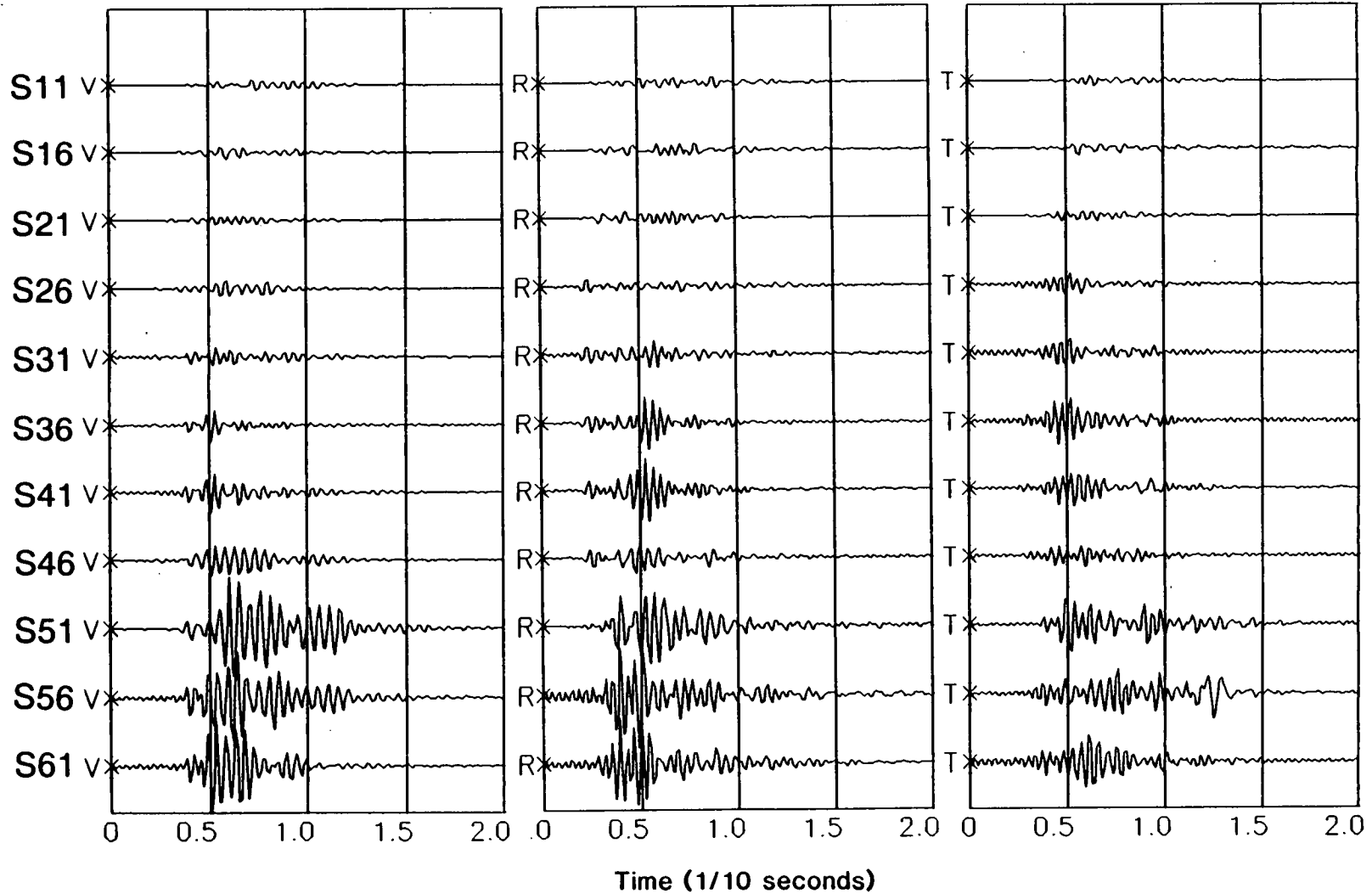
Figure 4.6(a)

Figure 4.6 Selected three-component seismograms of common geophone gather, recorded at a depth of 30.9m in borehole GW2 with eleven sources in borehole GW5 for **(a)** in-line source orientation, and **(b)** X-line source orientation.

GW-2 (TRANSVERSE)

Time (1/10 seconds)
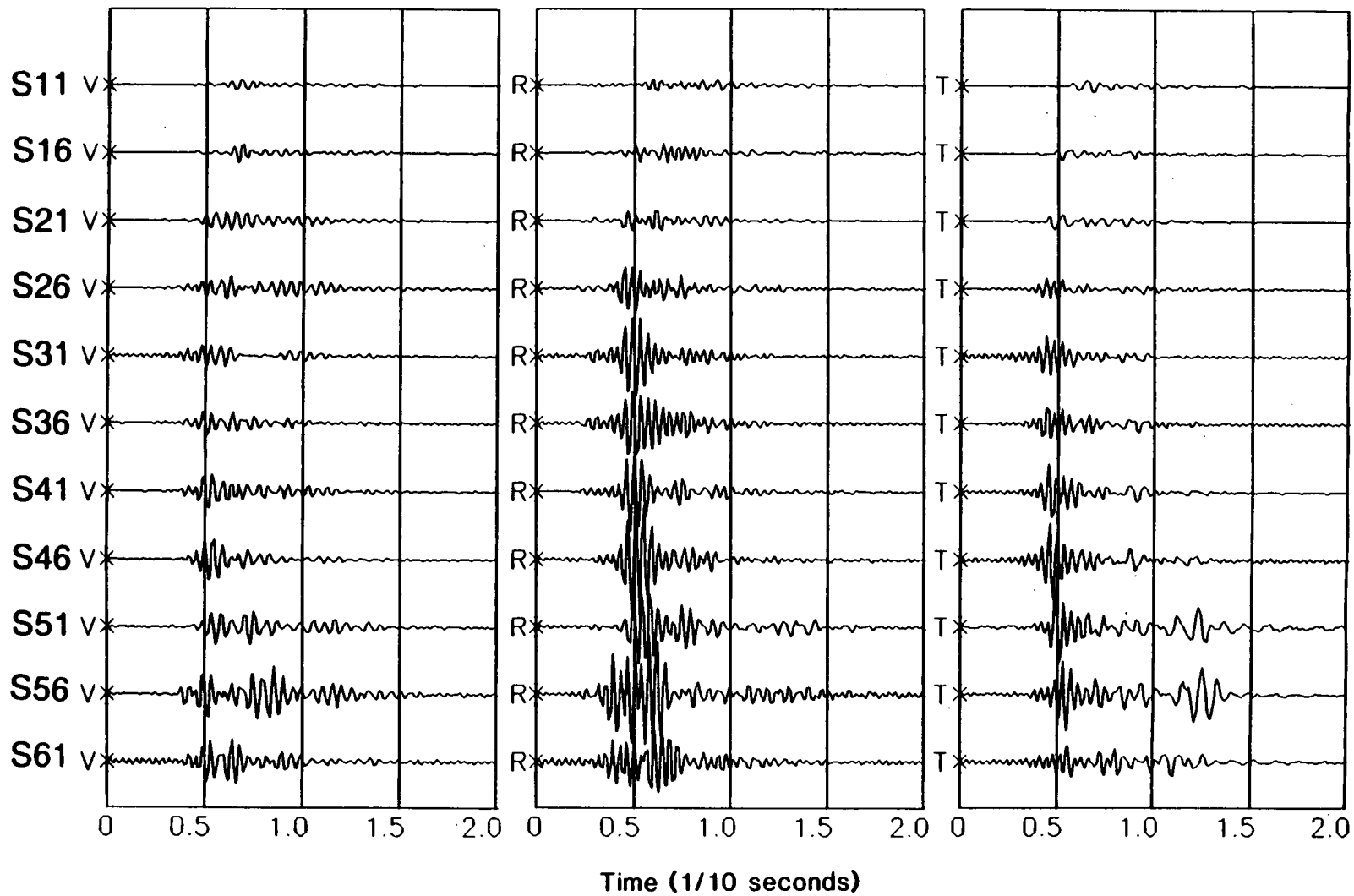
Figure 4.6(b)

geophone gather recorded at depth of 30.9m in borehole GW2 with eleven sources in borehole GW5 for (a) in-line source orientation, and (b) X-line source orientation. Figure 4.7 has the same sources and geophone configuration as Figure 4.6, but for the geophone in borehole GW4.

The selected seismograms show the following features:

(1) The dominant signals in seismograms are highly dispersive with large amplitudes tied to certain interface(s) having a big wave-impedance contrast. In particular, the vertical components from G8 in Figure 4.5(a), and from S51 in Figure 4.7(b), show the most distinguished dispersive signals with the maximum amplitude trapped within the low-velocity layers. These signals can be identified as the normal modes of guided-waves propagating along and inside the three low-velocity layers, which will be further analysed later.

(2) The strong coupling of three-component energy in seismograms for both in-line and X-line horizontal source orientations as a result of presence of strong fracture-induced anisotropy at the CBTF site. A remarkable feature in seismograms is anomalously pronounced vertical component amplitudes. For the X-line source in Figures 4.5(b) and 4.7(b), amplitudes of the vertical components are at least 1.5 to 2.0 times those of horizontal components. This is so even in Figures 4.5 and 4.6, where the raypaths between source borehole (GW5) and geophone borehole (GW2) are believed to be approximately in the plane parallel to the dominant fracture direction. As the CBTF site is relatively uniform with horizontal layering, it is unlikely that the local structure can produce such

GW-4 (RADIAL)

Time (1/10 seconds)
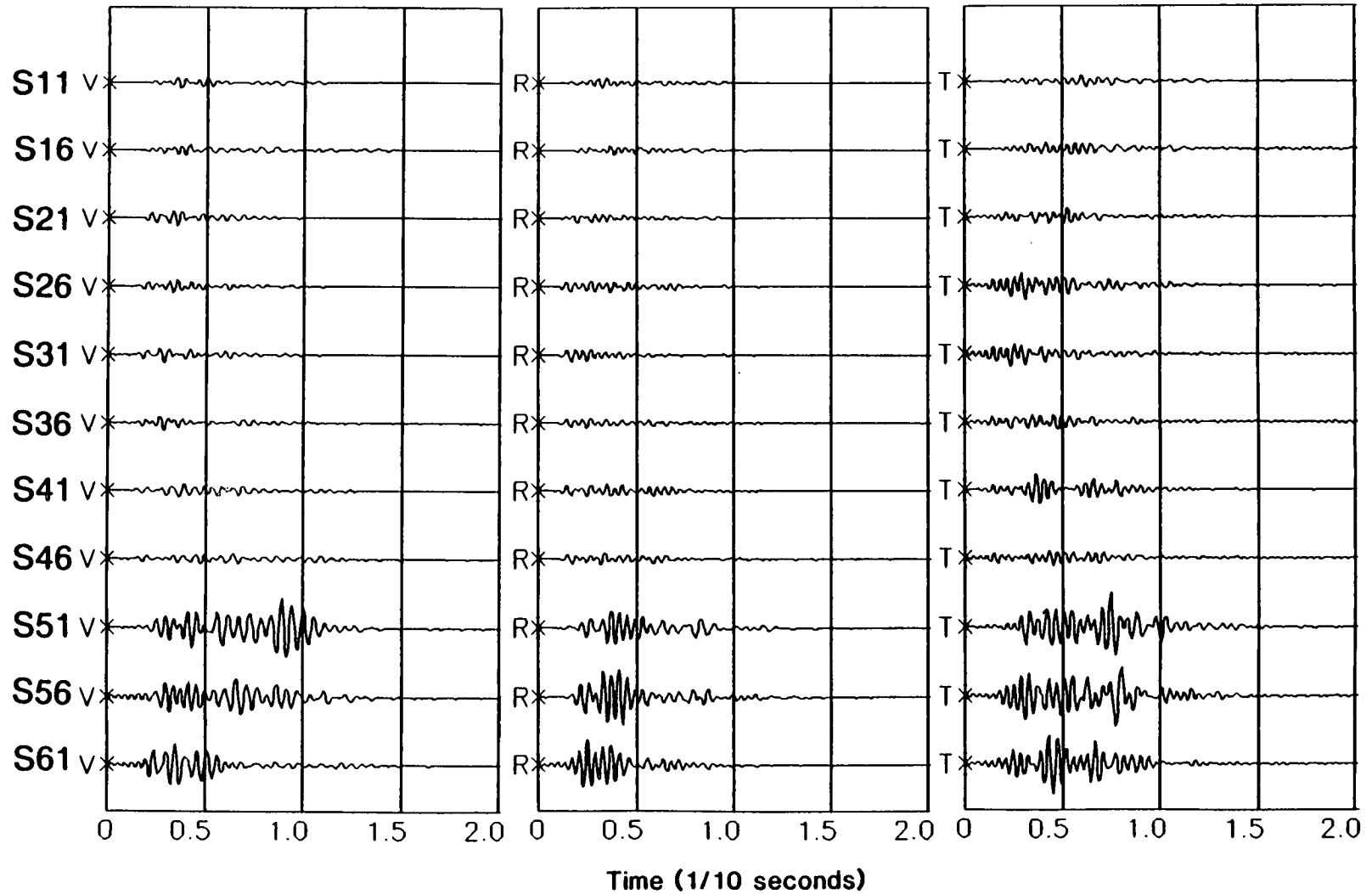
Figure 4.7(a)

Figure 4.7 Selected three-component seismograms of common geophone gather recorded at a depth of 30.9m in borehole GW4 with eleven sources in borehole GW5 for **(a)** in-line source orientation, and **(b)** X-line source orientation.

GW-4 (TRANSVERSE)

Time (1/10 seconds)
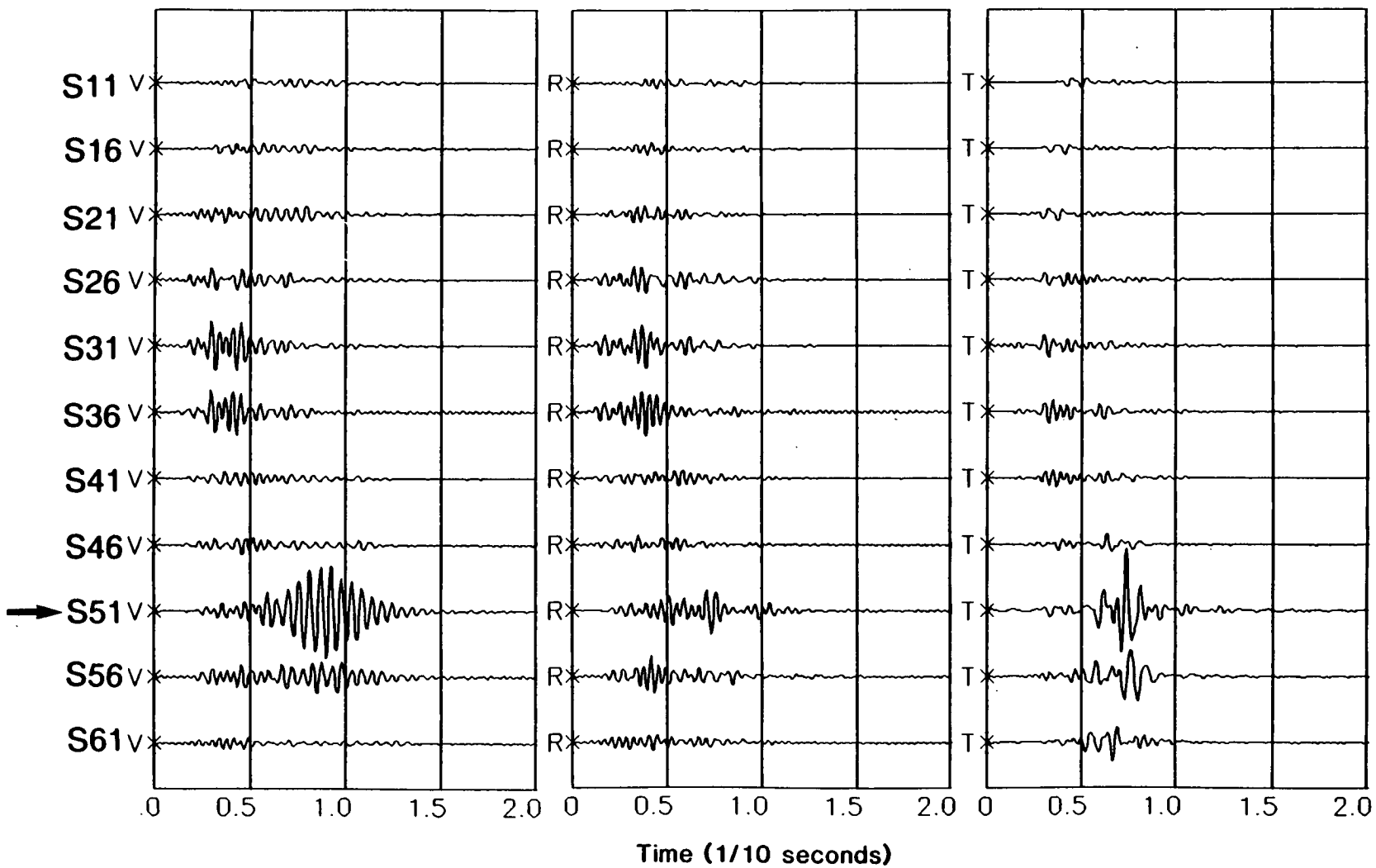
Figure 4.7(b)

strong vertical component wave motion. Liu *et al* (1991) have suggested that, by synthetic modelling, this dominant vertical energy is probably due to the presence of non-vertical cracks in the rockmass. It is also likely that the second fracture system at the site may be responsible for producing the strong energy coupling in the vertical component.

(3) The high-velocity layer   at the depth between 16.2m and 27.8m forms another high-velocity layer waveguide, and may excite some leaky modes of guided-waves (see Figure 4.5 and 4.7(b)). High-velocity waveguides will be discussed in Chapter 5.

(4) The waveform of guided-waves varies significantly with source polarization, source and geophone positions, and borehole site. This suggests that guided-waves are very sensitive to some changes of source and geophone parameters, local structures, and fracture properties.

4.3.3 DISPERSION CHARACTERISTICS

For the waveguide structure shown in Figure 4.1, we have used water-filled cracks with crack density $CD = 0.12$ to model large fracture distribution at the CBTF site (Liu *et al*. 1991). In the first instance, we only consider vertical cracks with their orientation being along the direction of propagation of guided-waves, *i.e.* the raypath between borehole GW5 and GW2, so that the *Generalized* modes of guided-waves are theoretically decoupled into pure Rayleigh- and Love- modes in this symmetric direction. Figure 4.8 shows the dispersion curves of the first eight possible modes of guided-waves, where the solid lines are phase-velocity, and dashed
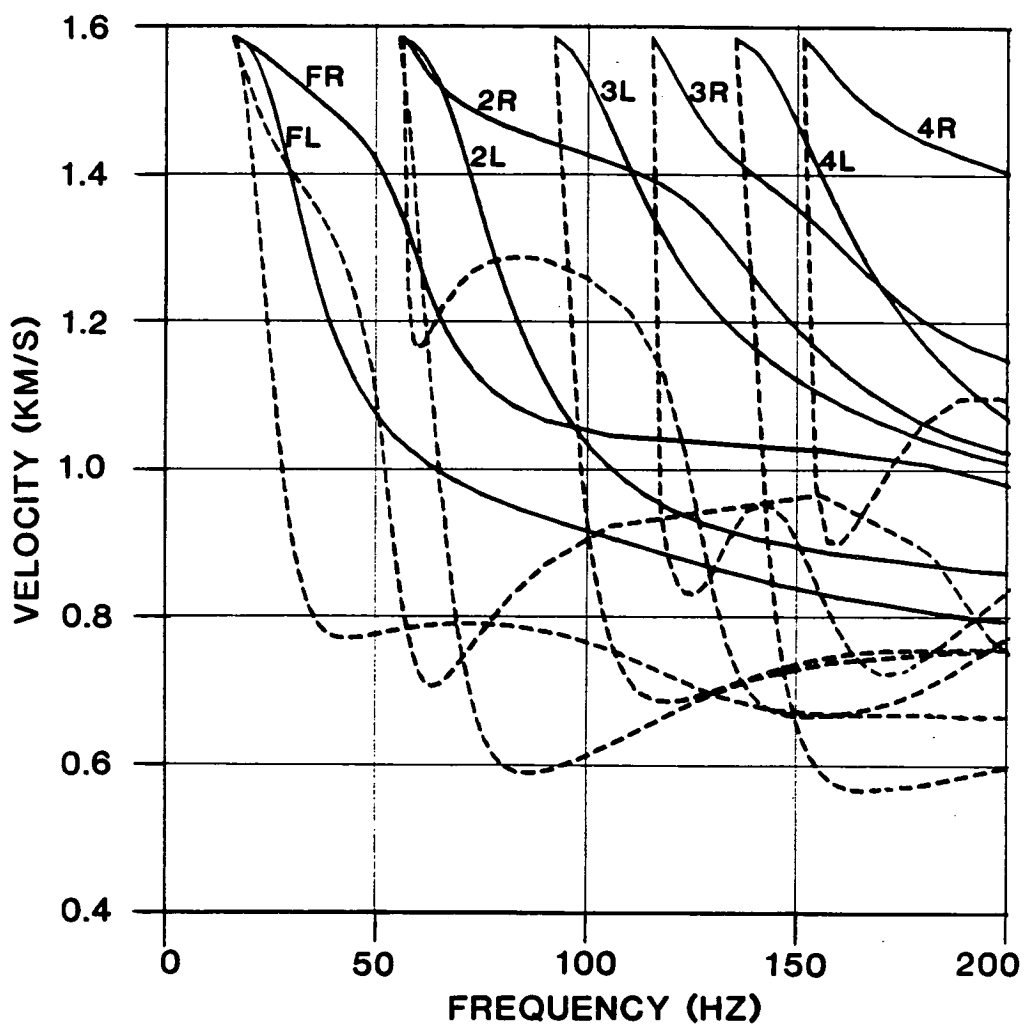
Figure 4.8 Dispersion curves of first eight modes of guided-waves in the velocity sturcture marked in Figure 4.1, containing vertical water-filled fractures with $CD = 0.12$. The direction of guided-wave propagation is along the strike of fractures (GW5 - GW2). Solid lines are phase-velocity, and dashed lines are group-velocity: *FR*, and *FL* - Fundamenatl Rayleigh and Love modes; *2R*, and *2L* - Second Rayleigh and Love modes, and so on.

lines are group-velocity dispersion curves. (*FR* marks Fundamental Rayleigh mode, *FL* for Fundamental Love mode, *2R* for Second Rayleigh mode, and so on.) The dispersion curves show that there are many possible modes of guided-waves propagating inside the three low-velocity layers even within 200Hz source frequecy. They may interfere with each other, and form very complicated waveforms. The theoretical results also show that the dispersive behaviour of Rayleigh or Rayleigh like modes change very irregularly with frequency, and they may have several minima and maxima on a single group-velocity dispersion curve. This perhaps is one of the reasons why the waveforms from in-line sources are more complicated than from X-line sources (Liu *et al* 1991).

From the seismograms shown on Figures 4.5 and 4.7, we select two typical wavetrains of guided-waves to calculate group-velocity dispersion by multiple filter technique. Figures 4.9 shows the contour map of group-velocity dispersion from the vertical component at G8 in Figure 4.5(a) (Insets show the seismogram and its amplitude spectrum). The theoretical group-velocity dispersion curves of several higher modes from Figure 4.8 have also been plotted on the contour map in stars. Following the ridges on the contour, we can see there are two possible modes of guided-waves in the seismograms. Since the dominant frequency of the signals is about 200Hz, we expect that the theoretical dispersion curves of higher modes *4L* and *4R* of guided-waves can fit the observed dispersion. As discussed in above section, the observed guided-waves usually propagate as *Generalized* modes with three-dimensional wave motion, as a result of the distribution of large dipping fractures at the CBTF site. Therefore, the theoretical dispersion curve of Love-like type mode (4L) of guided-waves can be matched with the observed dispersion
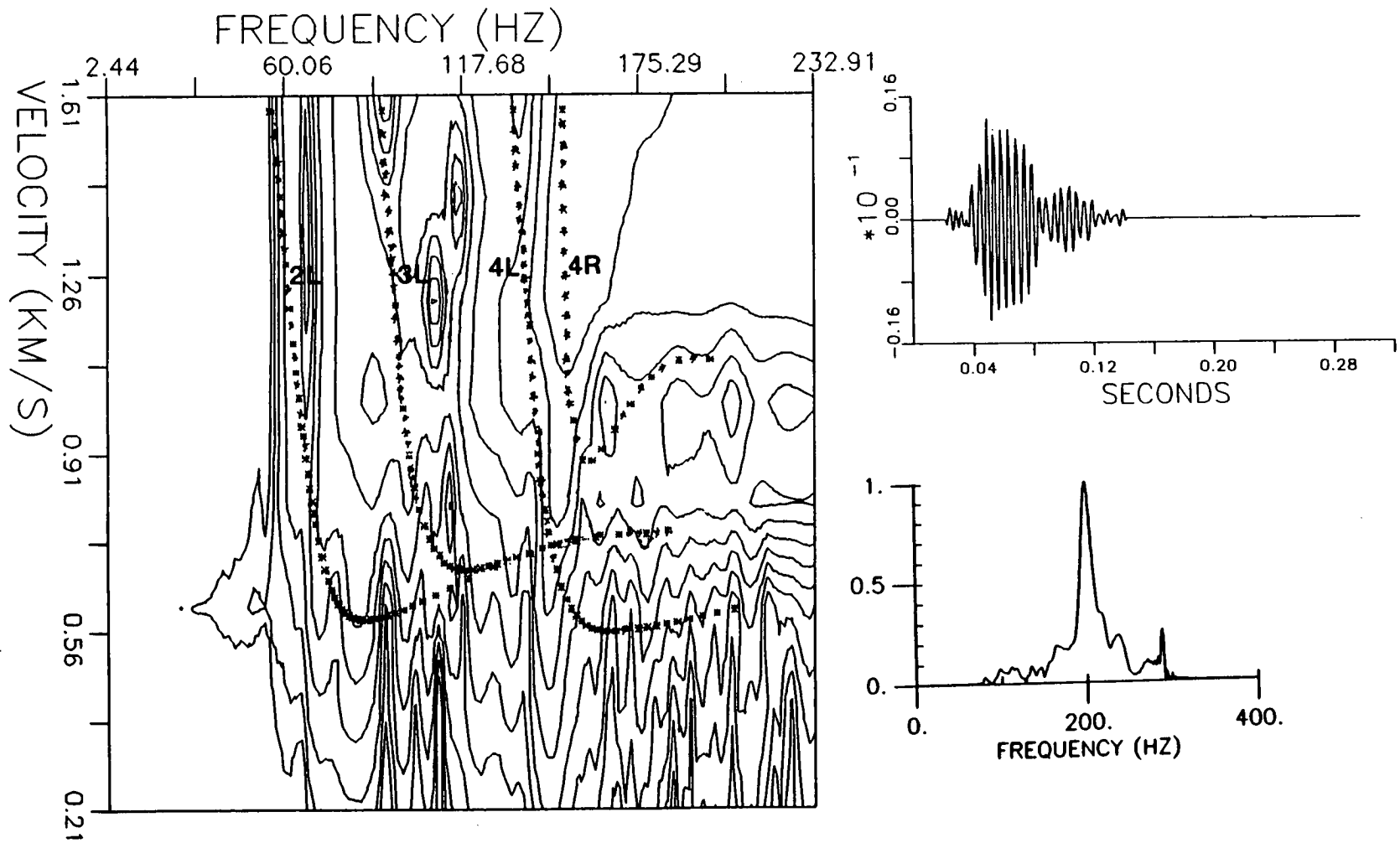
Figure 4.9 Contoured multiple-filter map of the dispersion of observed seismogram on vertical component of G8 in Figure 4.5(a). Insets show the seismogram and amplitude spectrum. Stars are the theoretical dispersion curves for several higher modes.

from the vertical components of seismograms. We have not attempted
to calculate the theoretical dispersion curves of *Generalized* modes
of guided-waves for different fracture orientations or other
parameters. Figure 4.9 only produces an approximate match between
theoretical and the observed dispersion. The low values in the
bottom of Figure 4.9 are probably due to the distructive
interference of different modes, and/or some unknown noises in the
data. Absence of the high-frequency energy in the contour map may
be due to the large seismic attenuation at the CBTF site.

Similarly, Figure 4.10 shows the group-velocity dispersion contour
of the vertical component record from S51 in Figure 4.7(b) (a common
geophone gather recorded in borehole GW4). It is noted that the
theoretical group-velocity dispersion curves of *4L* and *4R* well match
the observed dispersion in Figure 4.10, which have the dominant
energy in the seismograms (see amplitude spectrum of insets in
Figure 4.10).

4.3.4 POLARIZATION DIAGRAMS

Polarization diagram is an important tool to identify and study
guided-waves. Figure 4.11 shows the observed particle motions for
the selected traces recorded in the three low-velocity layers (S41 -
S61) of Figure 4.6 (a common geophone gather in borehole GW2, for
both in-line and X-line sources), and Figure 4.12 shows the observed
particle motions for the selected traces of Figure 4.7 (a common
geophone gather in borehole GW4, for both in-line and X-line
sources). Almost all the polarization diagrams of Figures 4.11 and
4.12 display elliptical particle motions with major axes inclined to
the vertical and radial directions, depending on the symmetry
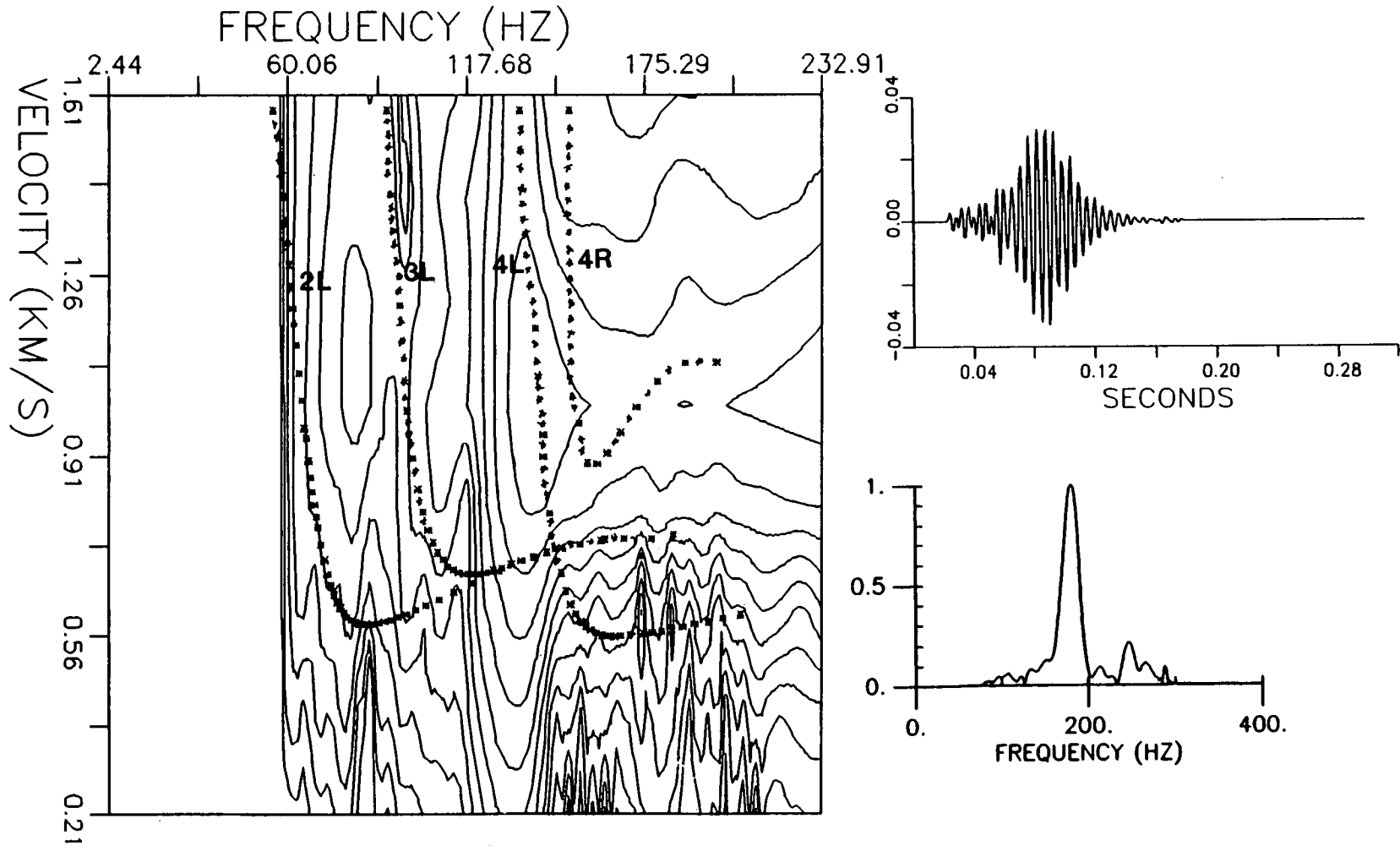
Figure 4.10 Contoured multiple-filter map of the dispersion of observed seismogram in vertical component for S51 in Figure 4.7(b), with the same notation as Figure 4.9.

GW-2 (RADIAL)

GW-2 (TRANSVERSE)

Time (mseconds)
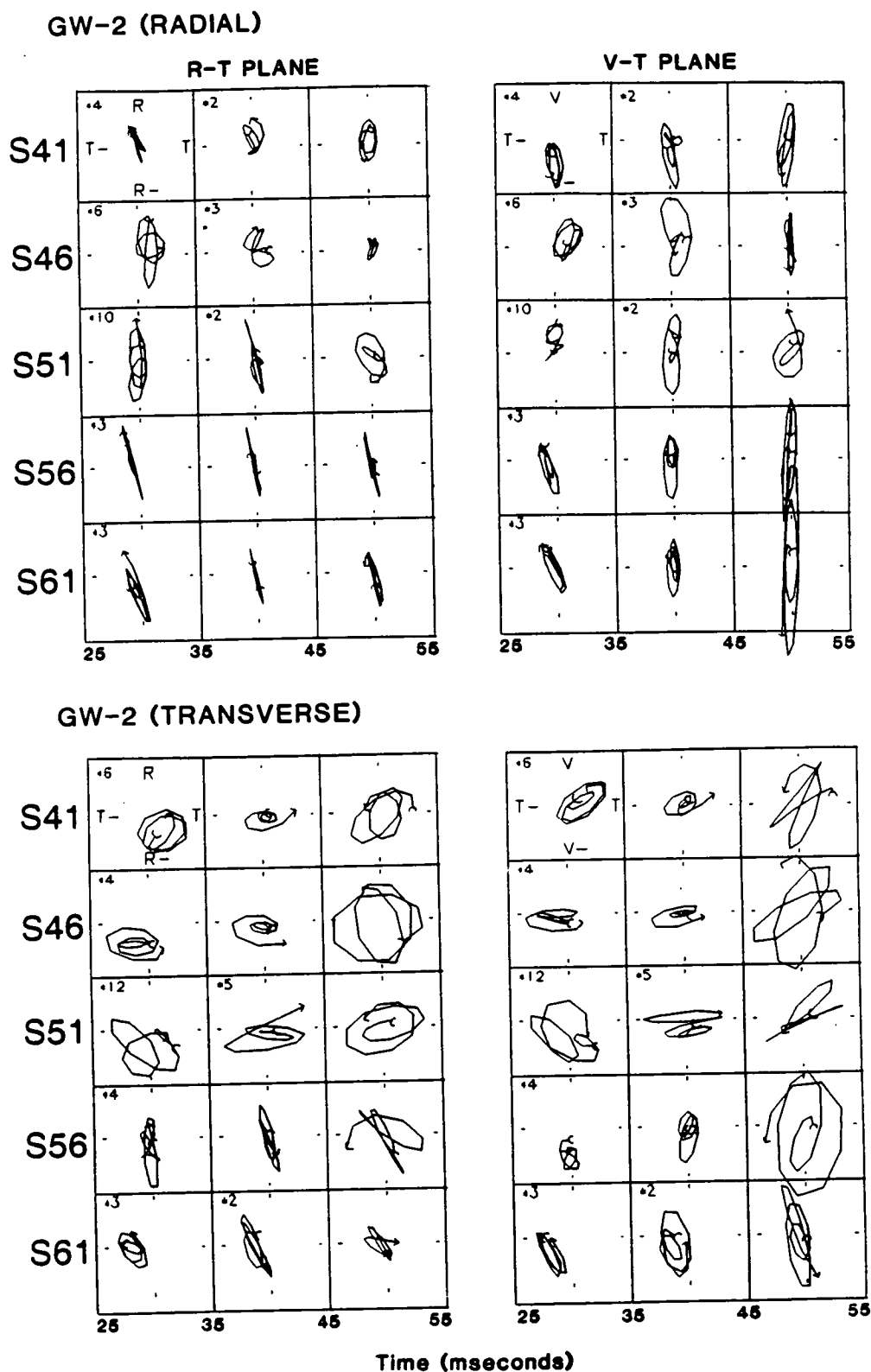
Figure 4.11 Selected polarization diagrams (PDs) for the observed seismograms (S41-S61) in Figure 4.6. The diagrams are displayed for horizontal R, T, and transverse vertical T, V planes for both in-line and X-line sources. The numbers in the top left corners of some of PDs indicate the gain applied to the original signals relative to the unnumbered PDs.

GW-4 (RADIAL)

GW-4 (TRANSVERSE)

Time (mseconds)
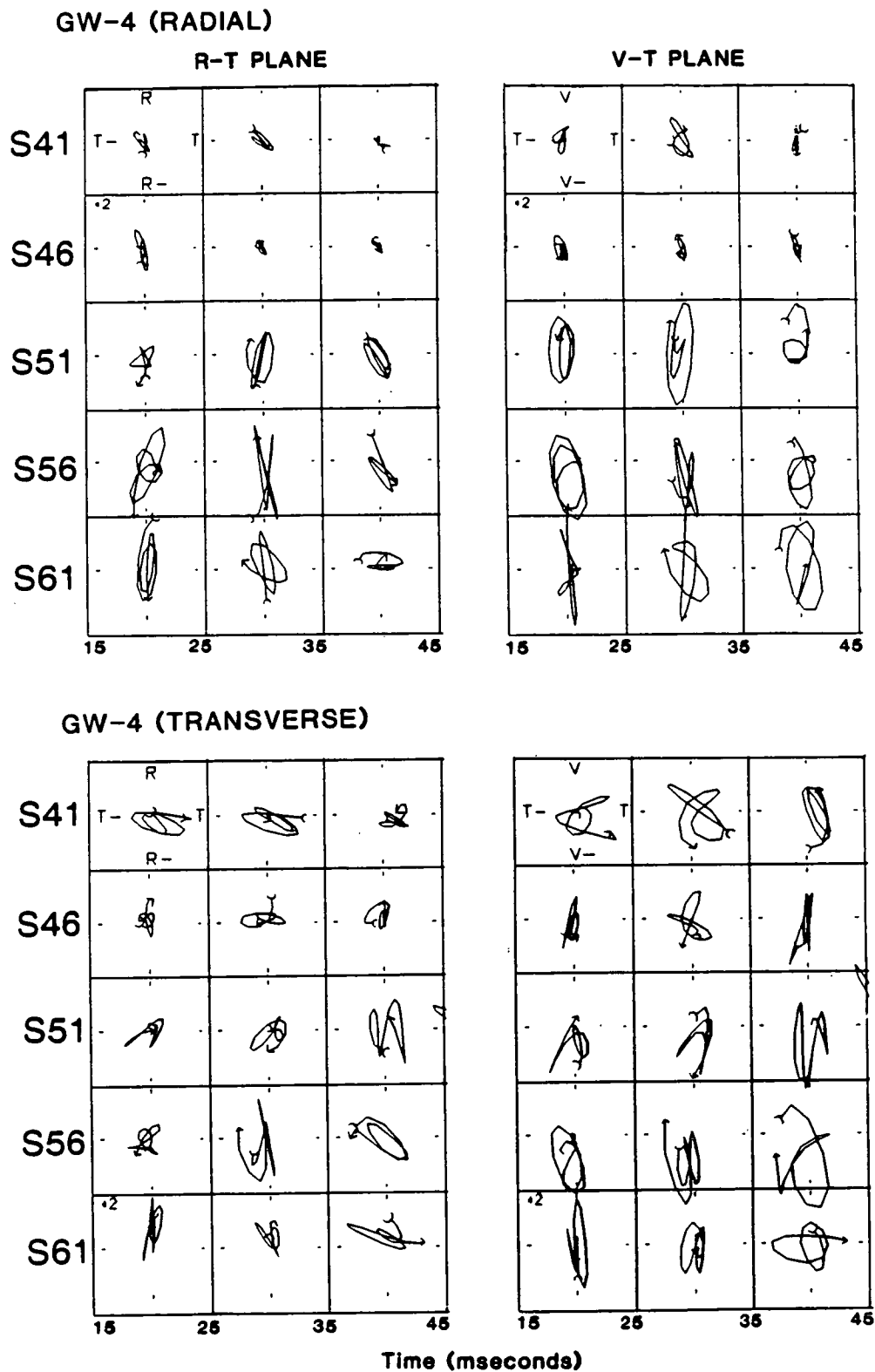
Figure 4.12 Selected polarization diagrams (PDs) for the observed seismograms (S41-S61) in Figure 4.7, with the same notation as Figure 4.11.

direction through the particular anisotropic structures. Such motion is typical of the single family of *Generalized* modes characteristic of modal propagation in structures containing azimuthal anisotropy. It is suggested that the seismograms received in and near the three low-velocity layers are dominated by normal *Generalized* modes of guided-waves. The variation with direction of propagation of these patterns of elliptical motions are characteristic of the orientation of the anisotropic structures.

4.3.5 THEORETICAL AMPLITUDE/DEPTH DISTRIBUTION

As section 4.3.2 has shown, a remarkable feature of the seismograms at the CBTF site is the strong three-component energy coupling for both in-line and X-line horizontal source orientations. It has been suggested that this strong energy coupling might be caused by the non-vertical large fractures in the rockmass. To examine the effects of these aligned fractures on amplitude distributions, we calculate theoretical three-component amplitude/depth distributions of different modes of guided-waves in and near the three low-velocity layers.

Considering the dominant frequency of seismograms is between 100Hz and 200Hz, we here present the amplitude/depth distribution curves of four higher modes (from fifth to eighth *Generalized* modes) with about 115 Hz, 135 Hz, 165 Hz and 195 Hz frequencies, respectively.

Figure 4.13 (a) shows the amplitude/depth distributions for vertical fractures (CD = 0.12) with the orientation being along the direction of propagation of guided-waves, which is approximately in the azimuth N75°E between GW5 and GW2. In this particular sagittal

5TH MODE (115HZ)   6TH MODE (135HZ)   7TH MODE (165HZ)   8TH MODE (195HZ)
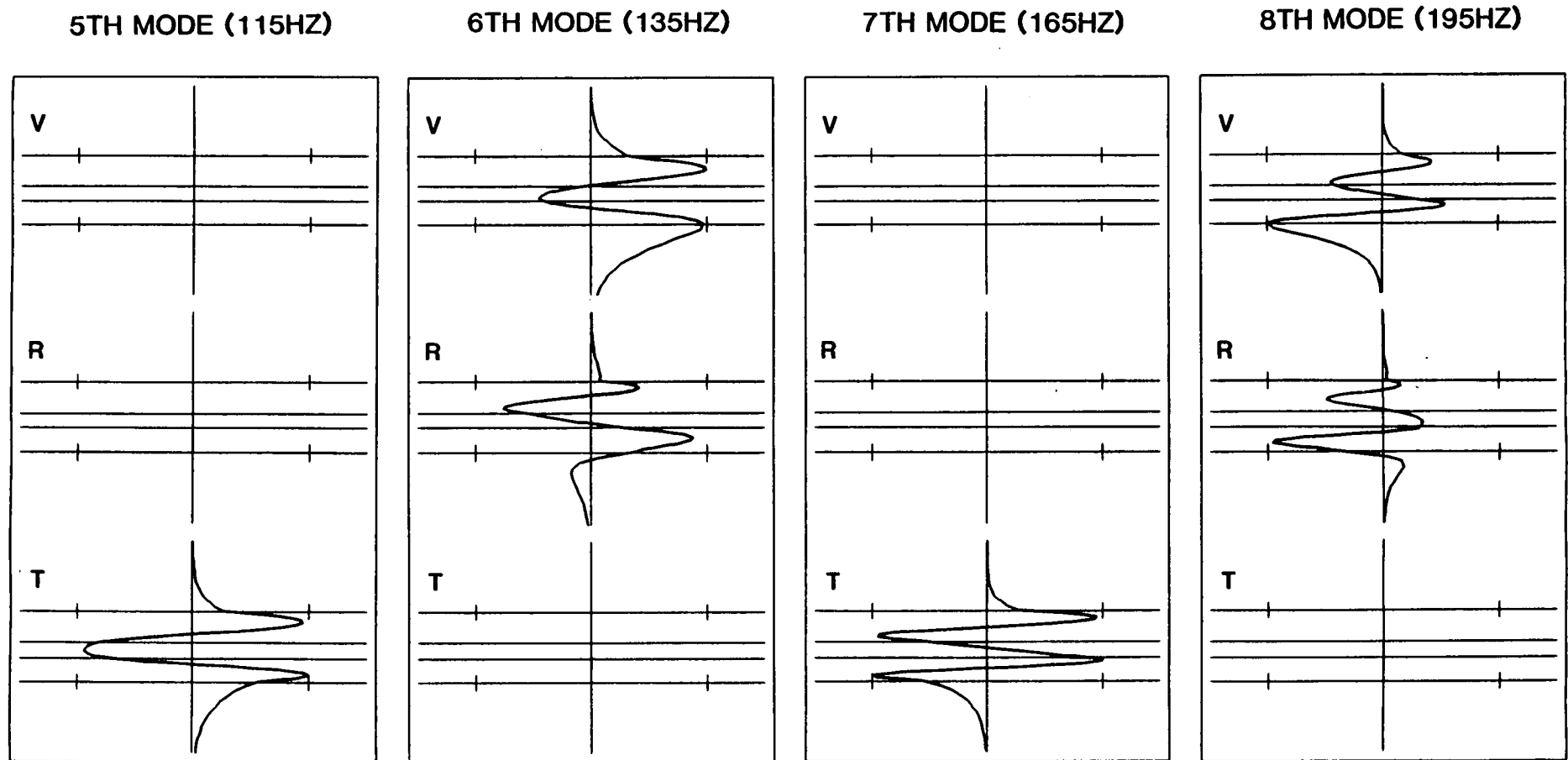
Figure 4.13(a)

Figure 4.13 Amplitude/depth distribution of fifth to eighth
Generalized modes at 115Hz, 135Hz, 165Hz and 195hz frequencies,
respectively, for the waveguide model marked in Figure 4.1 with
(a) vertical fractures with orientation along the direction of
guided-wave propagation, and (b) dipping fractures (dipping 70° to
the SE) with orientation along the direction of guided-wave
propagation. The fractures are water-filled with crack density $CD = 0.12$.

5TH MODE (115HZ)　　6TH MODE (135HZ)　　7TH MODE (165HZ)　　8TH MODE (195HZ)
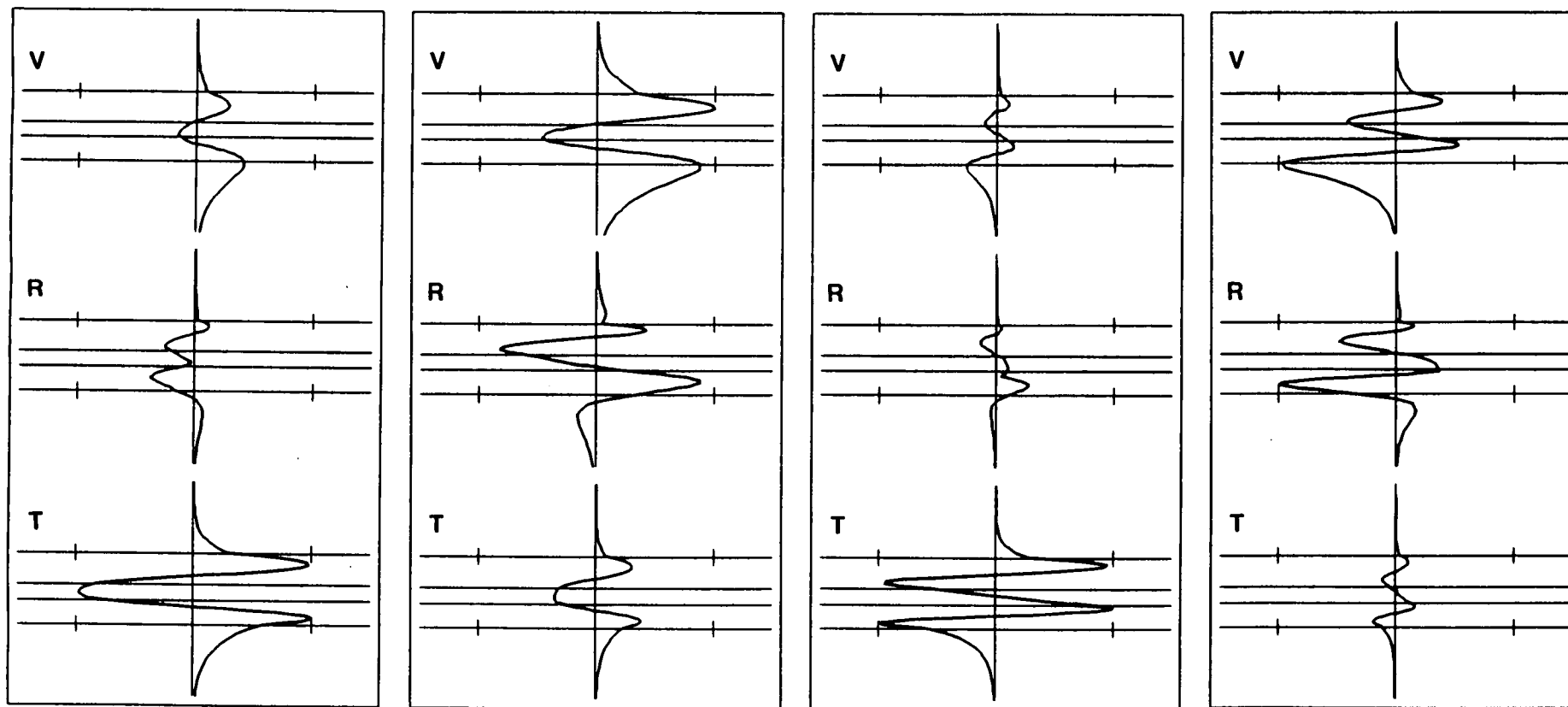
Figure 4.13(b)

symmetrical direction, the particle motions of *Generalized* modes are decoupled into pure Rayleigh and pure Love motions, respectively. Here, the fifth *Generalized* mode is equivalent to the third Love mode, the sixth mode to the third Rayleigh mode, the seventh mode to the fourth Love mode, and so on. It is obvious that near vertical fractures in the rockmass can not explain the strong three-component energy coupling of the seismograms received in borehole GW2 for both in-line and X-line sources.

Figure 4.13 (b) shows the amplitude/depth distributions for the fractures with the same crack striking N75°E as Figure 4.13(a), but dipping 70° to the SE (20° from the vertical). As seen from the amplitude distribution curves, the dipping fractures result in the propagation of typical *Generalized* modes of guided-waves with three-dimensional particle motions. All three components of four modes receive signals with almost equivalent amplitudes, and this supports the interpretation that the dipping fractures can be responsible for the strong energy coupling.

The higher modes of guided-waves have complicated amplitude/depth distribution patterns in multilayered waveguide structures. The positions of sources and geophones are very sensitive to the modes to be excited or received. Because of their possible interference with each other, it is difficult to identify and seperate these different higher modes.

The aligned dipping-fracture model may not be only cause of strong energy cross-coupling in three-compnonents of the observed seismograms. Other causes, such as inhomogeneity in the media and irregularities at the interfaces, more complex fracture systems,

borehole noise, also be possible. The errors in source orientation in crosshole surveys could be another important reason of strong energy coupling in vertical component, although the study of Liu *et al* (1991) and the field observations (Queen *et al* 1990, Rizer 1990) suggest that the non-vertical large fractures near the surface could be the main reason of such amplitude anomaly at the CBTF site.

4.4 SYNTHETIC MODELLING

To testfy the above interpretation of guided-waves and their propagation behaviour in the aligned fracture-induced anisotropic media, we calculate fullwave synthetic seismograms using the ANISEIS modelling package, and try to match synthetic seismograms to observed guided-waves. The anisotropic model parameters are based on the study of Liu *et al* (1991). In the isotropic model with the velocities, attenuation factors and densities of Table 4.1, anisotropy is introduced by simulating parallel fluid-filled fractures for each layer with a crack density CD = 0.12 and fractures striking N75°E and dipping 70° to the SE. Liu *et al* (1991) emphasize that it is necessary to introduce strong attenuation in the model in order to match the relative amplitudes and the dominant frequencies of the different body-wave arrivals. This relatively high-attenuation may be attributed to the shallow depth and highly fractured rocks at the CBTF site.

The source pulse function used in the modelling is: $F(t)$ = $exp(\omega t /d)$ sin (ωt), where $\omega=2\pi f$ is the circular frequency; and d is the damping factor of the source function. We have chosen the peak frequency f = 250Hz and the damping is d = 5.

We have calculated the synthetic seismograms for a common geophone gather from borehole GW2. The geophone and sources positions are the same as Figure 4.4(b). Figure 4.14(a) shows the synthetic seismograms for in-line source, and Figure 4.14(b) for X-line source. Comparing Figure 4.14 with Figure 4.6, we can find that the synthetic seismograms display many of the characteristics of observations, which are consistent with our interpretation for guided-wave propagation in anisotropic structures at the CBTF site. The synthetic seismograms have the following features:

(1) The dominant signals in the seismograms are the guided-waves trapped inside the three low-velocity layers (from source S41 to S61). The waveforms of guided-waves are similar to the observed, and show complicated interferences of different modes. Except for first arrivals, it is almost impossible to search for seperate body-wave arrivals from these dispersive wavetrains. However, the first arrival in the synthetic seismograms from X-line source is 10-20 milliseconds later than in the observed seismograms. It is noted that the observations from both in-line and X-line sources have almost the same first arrival time. This suggests the first arrivals in the observed seismograms from X-line sources may be the *P*-waves excited by some misalignment of X-line sources. It is also possible that there is a residual coupling if the rotation of observed seismograms is not exactly correct.

(2) The strong energy-coupling of three components, especially the large amplitudes on the vertical components, are produced for both in-line and X-line orientated sources. For in-line source, when there is no transverse energy excited, the amplitude in the
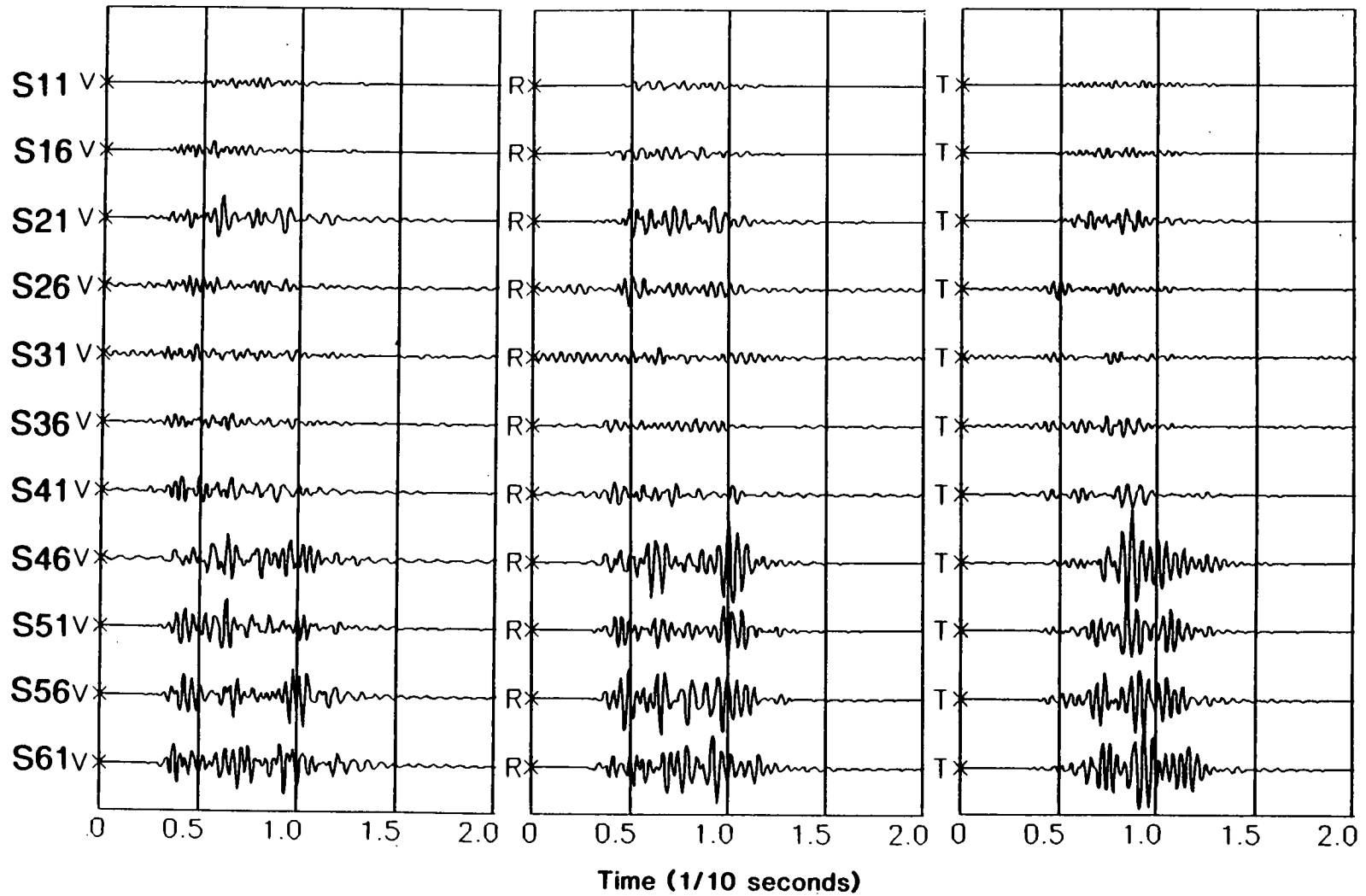
Figure 4.14(a)

Figure 4.14 Synthetic seismograms with the same source and geophone positions (a common geophone gather) in borehole GW2, for (a) in-line source orientation, and (b) X-line source orientation.

GW-2 (TRANSVERSE) SYNTHETIC

Time (1/10 seconds)
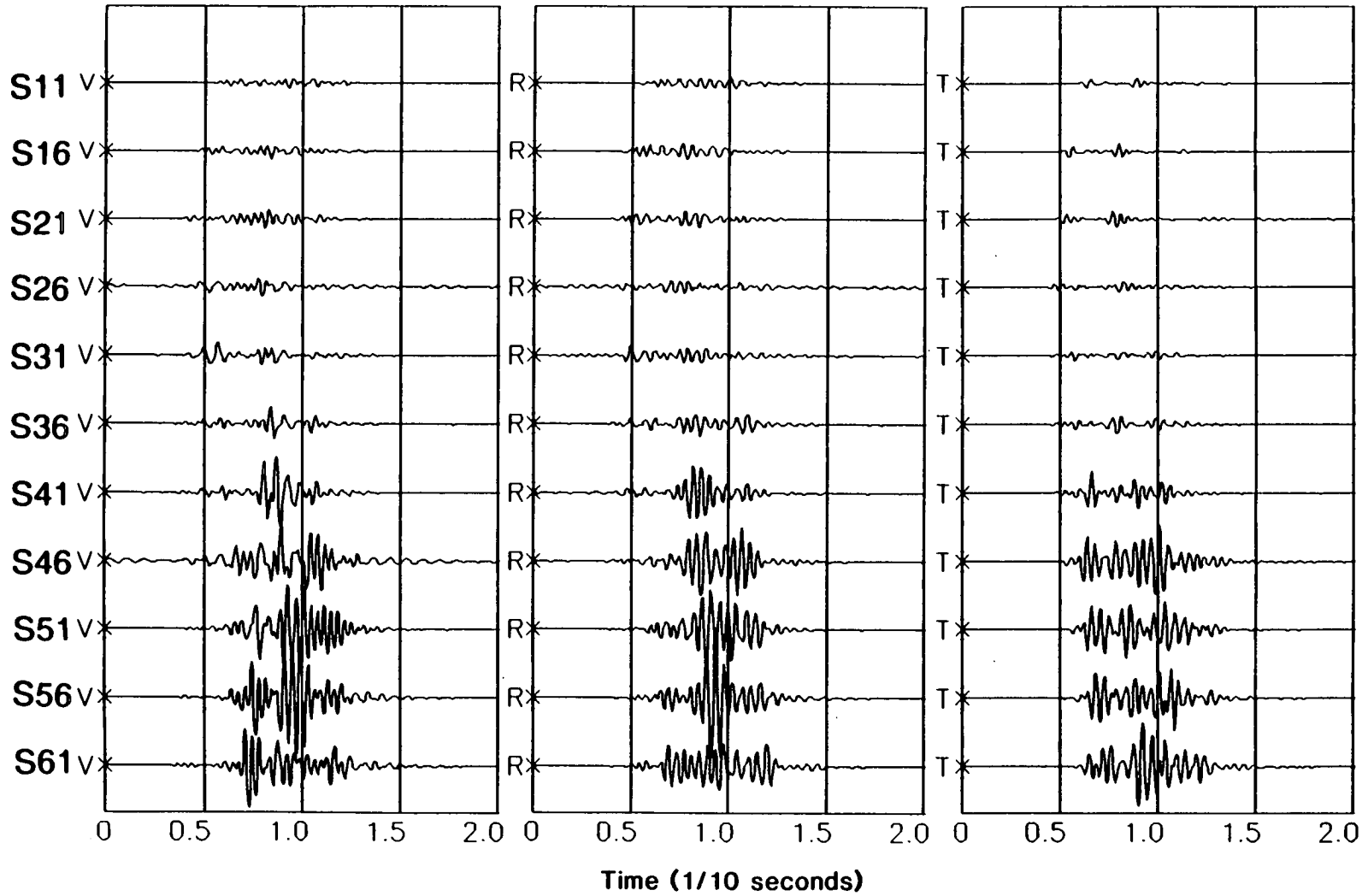
Figure 4.14(b)

transverse component is equivalent to, or even larger than amplitudes in the radial and vertical components. Similarly, for X-line source, the vertical and radial components receive almost the same order of amplitude as the transverse component.

(3) The polarization diagrams (see Figure 4.15) of the selected synthetic seismograms show similar type of elliptical particle motion as the observation of Figure 4.11.

In summary, although the waveforms and polarization diagrams of synthetic seismograms do not match the observations in details, the overall characteristics of the seismograms and polarizations are in agreement with the recorded seismograms.

4.5 DISCUSSION AND CONCLUSSIONS

The main result of this chapter is that guided-waves in crosshole data at the CBTF site have been clearly identified by analysing their amplitude distribution, dispersion, and polarization diagrams. The guided-waves in crosshole data at the CBTF site have the dominant energy. These guided-waves are usually associated with the low-velocity layers which have a large velocity-contrast. The propagation of these guided-waves shows the typical behaviour of a single family of *Generalized* modes with three-dimensional elliptical particle motions, as a result of strong aligned dipping-fracture distribution at the CBTF site.

The waveforms of guided-waves from crosshole surveys at the CBTF site vary significantly with different wells, different depths and

GW-2 (RADIAL) SYNTHETIC

GW-2 (TRANSVERSE) SYNTHETIC

Time (mseconds)
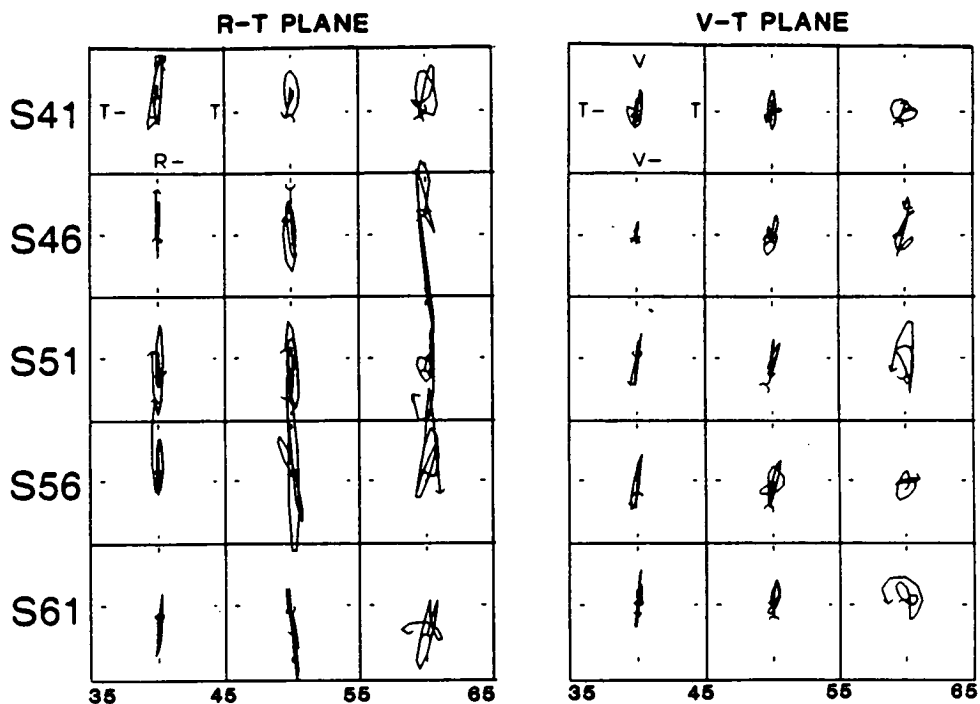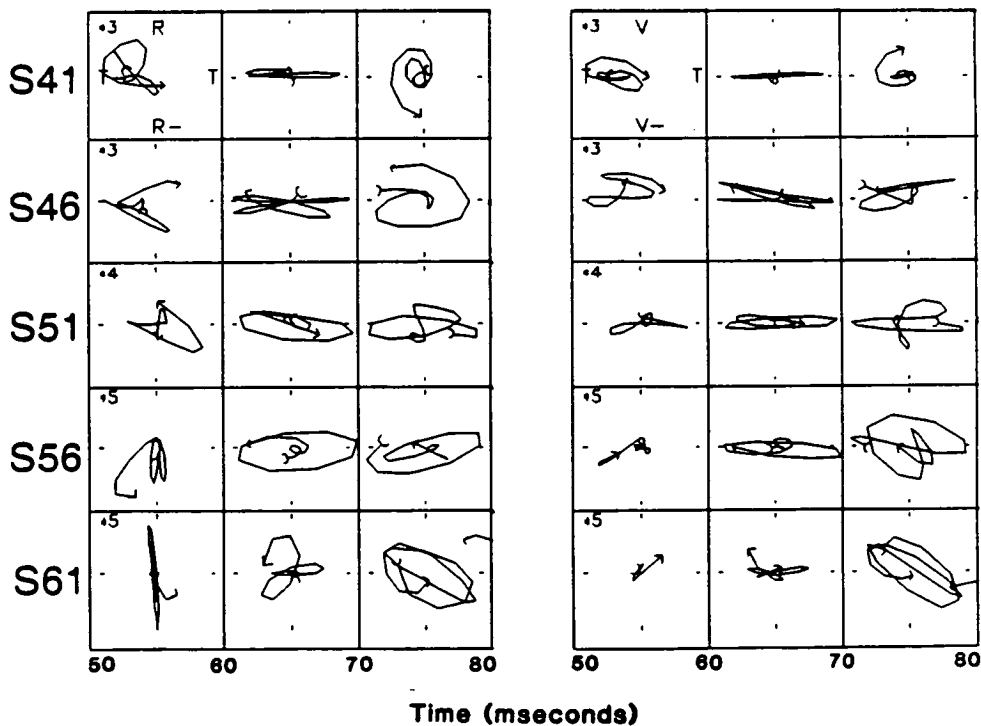
Figure 4.15 Selected polarization diagrams for the synthetic seismograms (S41-S61) in Figure 4.14, with the same notation as Figure 4.12.

different source and geophone orientations. This suggests that guided-waves are very sensitive to the some changes of layer properties and source and geophone configurations.

One remarkable feature of the seismograms at the CBTF site is that in many cases, the dominant energy is on the vertical components for both in-line and X-line horizontal source orientations. This amplitude anomaly may be caused by the presence of large dipping fractures at the CBTF site. It also suggests that Rayleigh-like modes of guided-waves are often excited in the crosshole seismic surveys at the CBTF site. Some large amplitudes on the vertical components can also be caused by minor source and recorded component misalignments or structural irregularities, inappropriate borehole recording conditions, and some other borehole noises resulted from tube-waves.

We have not modelled in detail   the propagation of guided-waves at the CBTF site. Some discrepancies between recorded and synthetic seismograms and polarization diagrams may suggest that the geometry and the fracture systems are more complicated than we have suggested. Any further improvement to the detailed modelling of guided-waves would require some consideration for minor irregularities at the interfaces. Another important effect on seismic wave propagation is the strong attenuation caused by large fractures near surface layers. These important effects have not yet been investigated, which is beyond the scope of this present study.

CHAPTER 5

GUIDED-WAVES IN CROSSHOLE SEISMIC SURVEYS
II. POTENTIAL APPLICATIONS

5.1 INTRODUCTION

Both theoretical study (Chapter 3) and field data analysis (Chapter 4) have shown that, in many circumstances, the dominant signals in crosshole seismic surveys are those modes of guided-waves, rather than body-waves as are sometimes assumed. It is significant to study and exploit their potential applications in hydrocarbon reservoir seismics. The previous study (Chapter 3) has suggested that thin-layered sedimentary reservoirs may act as seismic waveguides in crosshole surveys. In this chapter, we will investigate two potential applications of such guided-waves: reservoir layer(s) continuity tests between boreholes; and monitoring Enhanced Oil Recovery (EOR) operations for thin-layered sedimentary reservoirs by crosshole seismic surveys.

Thickness, area, and continuity are three important parameters defining a hydrocarbon reservoir. These parameters may be obtained by seismic methods (including three-dimensional seismic reflection surveys, acoustic loggings, vertical seismic profile (VSP) surveys, and crosshole surveys). For thin-layered sedimentary reservoirs, however, the body-waves employed in conventional reflection or VSP surveys are unlikely to have high enough resolution to image them.

Guided-waves in crosshole surveys may be particularly useful in determining the thickness, and continuity of thin-layered sedimentary reservoirs, as channel-waves in 1-2 meter thick coal seams are very successful in locating faults with throws of the order of the seam thickness or smaller, even for the wavelengths of body-waves as large as 30 meters (Jackson 1985, Buchannan *et al*. 1983). Krohn (1990) and Worthington (1991) have suggested the use of guided-waves, combining with Stoneley waves in boreholes, for continuity tests for a particular low-velocity layer. Here we will further study this possible application of guided-waves for any plane interface.

It has been estimated that 70-80 percent of mobile oil is left behind after initial extraction (Rutledge 1989). Some forms of enhanced oil recovery are being widely carried out in almost all oilfields in the world. During this operation, it is very necessary that the changes in the reservoir are monitored as production and injection proceed, through repeated seismic surveys. Guided-waves in crosshole surveys could be particular helpful to monitoring EOR operations, because most of energy may be trapped inside reservoir zone, so the guided-waves can display the properties of the zone of interest more strongly and directly than nearly vertically propagating reflection profiles or VSPs (Lou and Crampin 1991a, 1992b,c). We will take a sedimentary gas/oil reservoir as an example, to study the propagation of such guided-waves inside the reservoir zone with different saturations by modelling techniques.

5.2 THE USES OF GUIDED-WAVES FOR CONTINUITY TESTS BETWEEN BOREHOLES

5.2.1 ANY CONTINUOUS LAYER AS A WAVEGUIDE IN CROSSHOLE SURVEYS

Any complicated layering structure can usually be decomposed into combinations of three basic cases: Low-velocity channels, high-velocity channels, and single interfaces between thick layers. Most continuous interfaces, or combinations of interfaces may act as waveguides for some form of guided-waves, if signals at appropriate frequencies, polarizations, and amplitudes can be generated in one well and recorded at appropriate levels in neighbouring wells in crosshole seismic surveys.

(a) Low-velocity channels:

A continous low-velocity layer(s) embedded between two halfspaces is the waveguide model which we have extensively studied in Chapter 3. Theory and field data studies have shown that a low-velocity layer will transmit normal-mode guided-waves (or channel-waves) often with a large proportion of their energy trapped within the layer. Such modes will be dispersive, that is the wave velocity will vary with the frequency of the signal, so that the amplitude along any path to any geophone and the distribution of the energy around the low-velocity layer will also vary with the frequency. Such low-velocity channels form good conduits for guided-waves.

In Chapter 3, we have studied the guided-waves in low-velocity channels with a large velocity-contrast (say, more than 20%). Here we consider a more general low-velocity channel with a small velocity-contrast across the interfaces. Figure 5.1 shows a 4m thick

Figure 5.1 A low-velocity waveguide with 10% velocity-contrast, and source and geophone geometry for synthetic seismogram calculations.

low-velocity channel with a 10% velocity-contrast. Figure 5.2 shows the dispersion curves for the fundamental Rayleigh (*FR*) and Love (*FL*) modes and the second (first higher) Rayleigh (*2R*) and Love (*2L*) modes, where the phase-velocity dispersion is a solid line, and group-velocity is a dashed line. The group-velocity is the velocity that energy propagates from the source, and is the velocity observed in most field studies. Figure 5.3 shows the amplitude variations with depth for various frequencies of the four main modes. At frequencies of about 100Hz and below, the fundamental modes are essentially plane-waves with little concentration of energy within the waveguide and very little frequency dispersion. The fundamental modes of both Rayleigh and Love guided-waves begin to be excited at about 200Hz, and at 400Hz and higher frequencies there is a well dispersed wavetrain with a large proportion of its energy trapped within the low-velocity layer.

Figure 5.4 shows synthetic seismograms for the model with the source/geophone geometry of Figure 5.1. The sources are horizontal forces oriented radially to excite *SV*-waves and transversely to excite *SH*-waves, with dominant frequencies of 200, 300, and 400Hz. At 200Hz, the signal shows very little dispersion, but the dispersed wavetrains of both fundamental modes (*FR* from the *SV*-source and *FL* from the *SH*-source) are relatively well-developed above 200Hz. An interesting feature of signals from the *SV*-source, demonstrated both by the synthetic seismograms in Figure 5.4 and the eigenfunction variation of *FR* with depth in Figure 5.3, is that the radial component of amplitude is small, so that the particle displacement is predominantly vertical. This mode of propagation with motion almost wholly confined to vertical displacements is well known in the vibration of thin plates. Note also that impulsive signals contain a
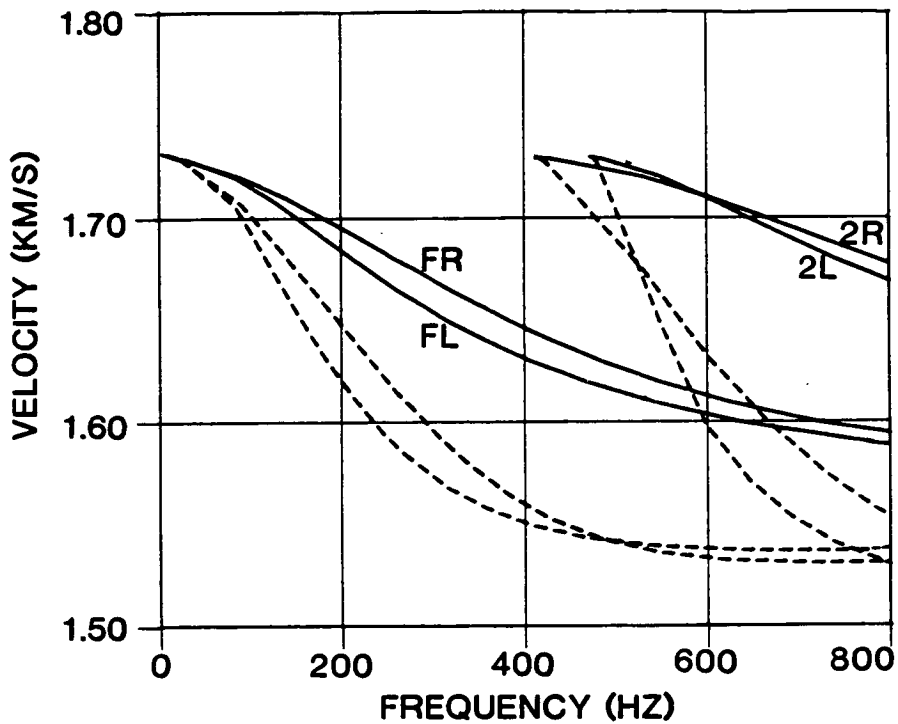
Figure 5.2 Dispersion curves for phase-velocity (solid lines) and group-velocity (dashed lines) of the first four modes of guided-waves for the low-velocity waveguide of Figure 5.1, where *FR* is the Fundamental Rayleigh mode, *FL* the Fundamental Love mode, *2R* the Second Rayleigh mode, and *2L* the Second Love mode.

FUNDAMENTAL RAYLEIGH

VERTICAL

4m

400Hz 200Hz 100Hz

RADIAL

4m

100Hz 400Hz

SECOND RAYLEIGH

VERTICAL

4m

800Hz 800Hz

RADIAL

4m

800Hz 800Hz

FUNDAMENTAL LOVE

TRANSVERSE

4m

400Hz 200Hz 100Hz

SECOND LOVE

TRANSVERSE

4m

800Hz 800Hz
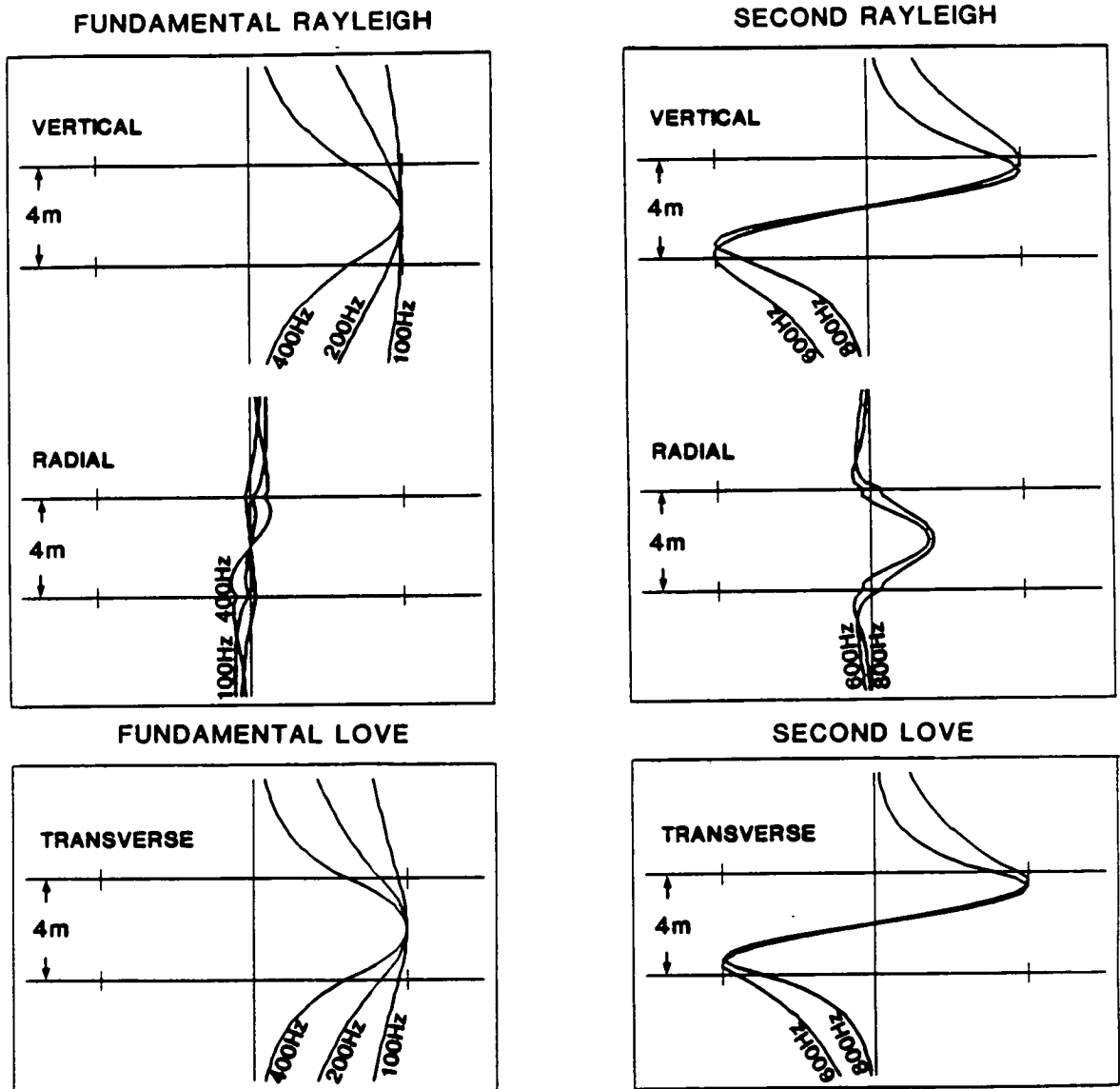
Figure 5.3 Amplitude/depth distributions of guided-waves for several different frequencies for the low-velocity waveguide of Figure 5.1.
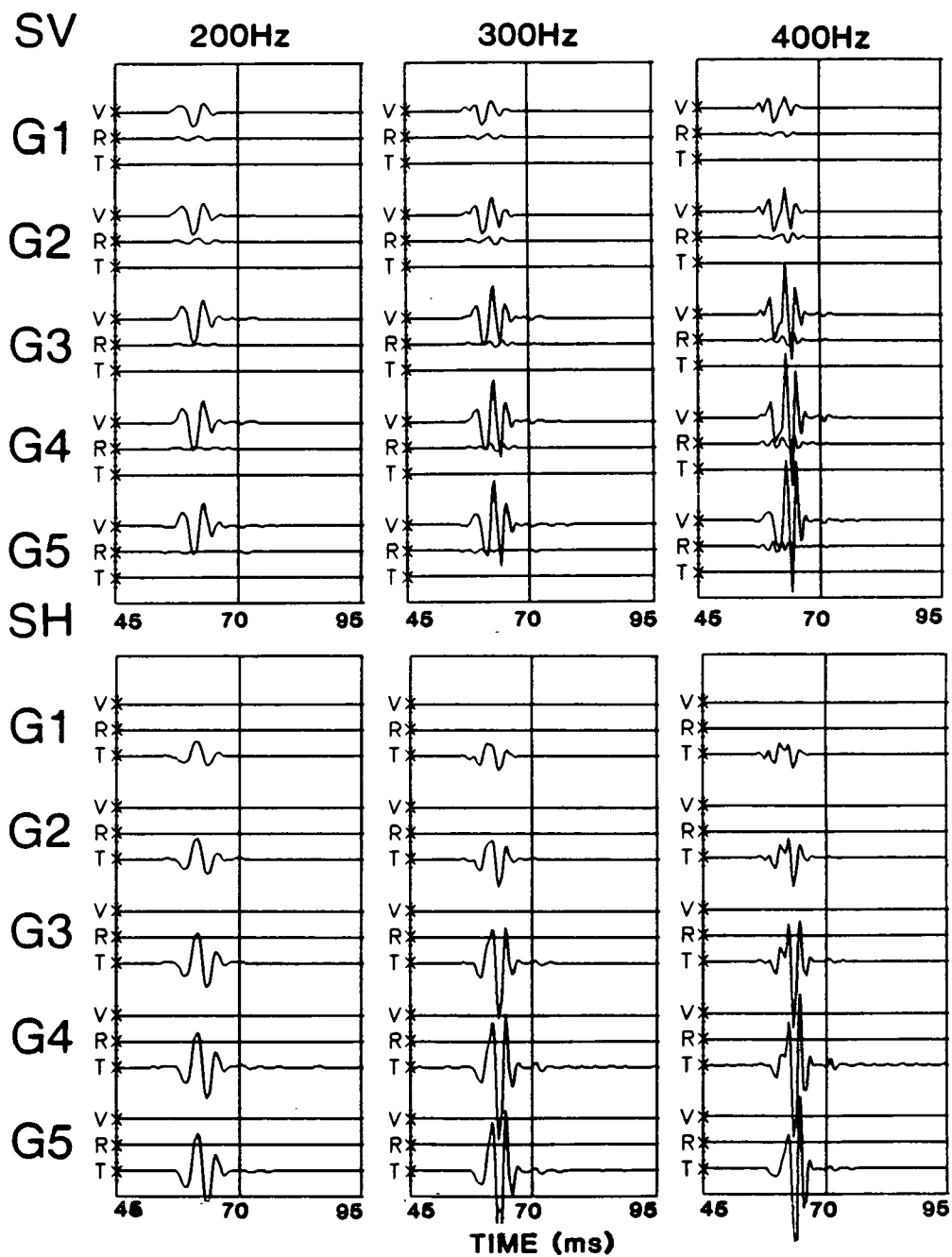
Figure 5.4 Synthetic seismograms of guided-waves with the source/geophone geometry of Figure 5.1 from a vertical point-force exciting *SV*-waves, and a transverse horizontal point-force exciting *SH*-waves, with dominant frequencies of 200, 300, and 400Hz.

wide range of frequencies so that, although the dominant source
frequency is 400Hz in Figure 5.4, for example, the dispersed
wavetrain of *FR* contains frequencies as low as 200Hz, and the radial
components at geophones G3, G4, and G5 contain a low-amplitude signal
of the *2R*-mode at frequencies as high as 600Hz.

The low-velocity channels with larger velocity contrasts mean that
the reverbrations in the channels have substantially lower
frequencies, so that more higher modes can be received in the same
source/frequency band (see Chapter 3).

(b) High-velocity channels:

These will not in general transmit guided-waves in the same way as
low-velocity channels. However, most combinations of layers will
contain combinations of high- and low-velocity sequences that will
transmit dispersive leaky modes (inhomogeneous interface-waves)
which, in some circumstances at least, may still carry energy
substantial distances from the source. At high enough frequencies,
simple high-velocity layers may carry the leaky-mode guided-waves.

Figure 5.6 shows seismograms for the high-velocity channel in
Figure 5.5, with a 10% velocity-contrast, and the same
source/geophone geometry as in Figure 5.1. Sources exciting *SV*- and
SH-motion are shown for dominent frequencies of 200, 1000, and
2000Hz. At lower frequencies (200Hz) the signal is principally a
body-wave arrival travelling at the velocity of the high-velocity
channel. At higher frequencies of 1000 and 2000Hz, where the
wavelengths (1.9m and 0.95m, respectively) are smaller than the

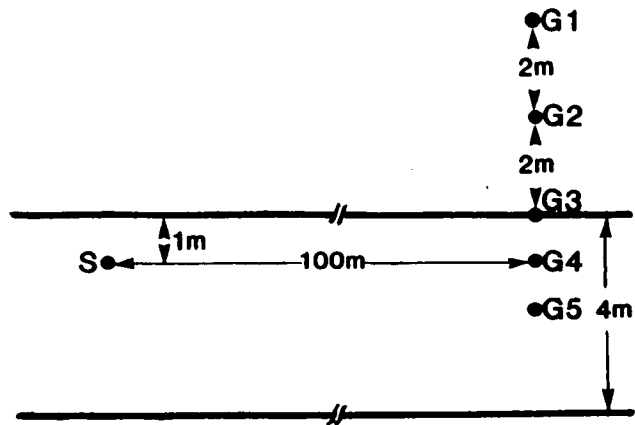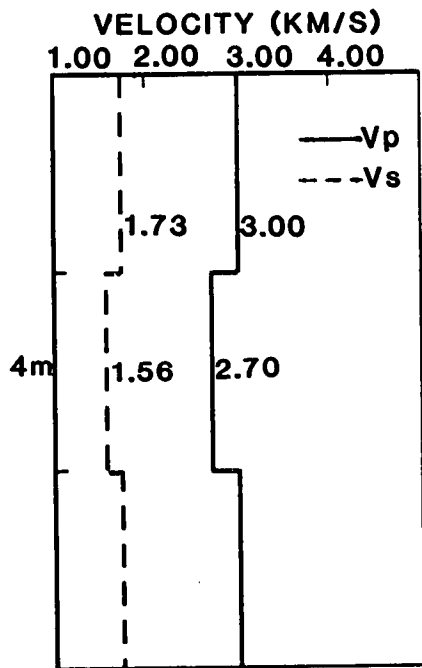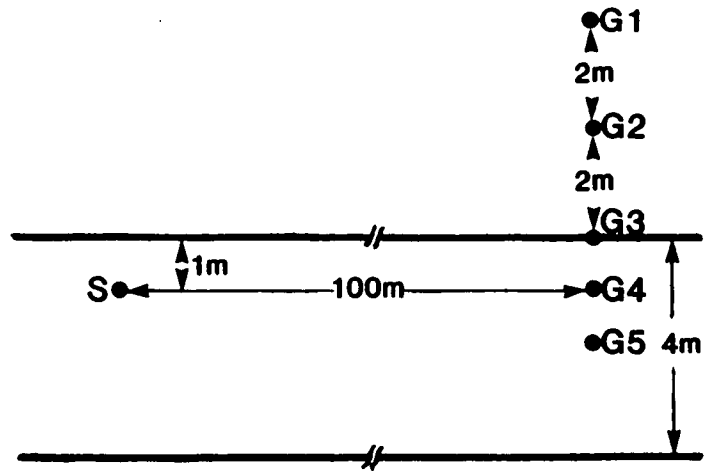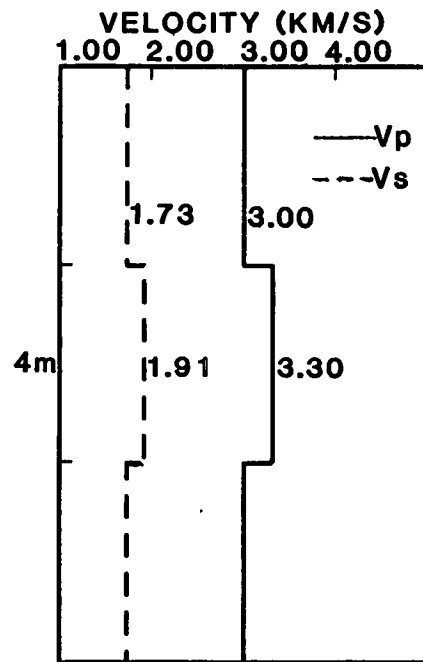**Figure 5.5** A high-velocity waveguide with 10% velocity-contrast, and source and geophone geometry for synthetic seismogram calculations.

Figure 5.6 Synthetic seismograms of guided-waves for the high-velocity waveguide with source/geophone geometry of Figure 5.5. Dominant source frequencies are 200, 1000, and 2000Hz.

thickness of the layer, the main arrival is a reverberation travelling at the velocity of the channel that leaks energy into the surrounding rocks. For reasons that are unclear to us, this signal has low to negligible amplitude for the SV-source at 1000Hz.

For geophones outside the channel there is also a pulse with a one-sided waveform characteristic of head-wave propagation and represents a head-wave travelling at the lower-velocity of the surrounding rocks.

(c) Single interfaces between thick layers

Almost any interface between two thick layers will carry a non-dispersive leaky-mode guided-wave (or inhomogeneous guided-waves, see Chapter 3), where the energy is radiated away from the interface so that the wave attenuates but may still carry energy, in some circumstances, for considerable distances from the source. The non-dispersive nature means that the source pulse will propagate without significant change of waveform. If the receiver is located a significant distance away from the interface, this leaky interface-wave is usually called a head-wave.

As discussed in Chapter 3, if the two layers have a specific and limited range of elastic constants, a single interface between two thick layers may carry a non-dispersive normal-mode Stoneley wave, where the energy is again trapped near the interface and does not radiate into the surrounding structure. This particular combination of properties seldom occurs in practice, except along liquid/solid boundaries, and Stoneley waves do not occur in most crosshole surveys.

Figure 5.7 shows a single interface model between two halfspaces with a 10% velocity difference. The synthetic seismograms for the model are given in Figure 5.8, for both *SV-* and *SH-*source excitations at 200 and 1000Hz. The first arrival on records from geophones G1, G2, and G3 is head-wave propagating in the higher-velocity halfspace and leaking energy into the lower-velocity medium (it has very small amplitude from the S1 source). There is also a pulse travelling in the lower-velocity medium, which for the source S1 in this halfspace is essentially a body-wave, whereas for the source S2 in the higher-velocity medium, the pulse is a head-wave arrival travelling in the lower-velocity medium. The signals from geophones G4 and G5 from the S1 source appear to be body-wave arrivals propagating parallel to the interface. Note that the behaviour of these signals is independent of frequency and sources with high dominant frequencies were used for easy comparison with the head-waves in the high-velocity channel in Figure 5.6.

5.2.2 LAYER CONTINUITY TESTS BETWEEN BOREHOLES BY USING GUIDED-WAVES

We have shown that an appropriate source at an appropriate level in a well will generate signals that carry energy parallel to any simple combination of layers. Recording the signals in other wells would test the continuity of the interfaces between the wells. This simple layering carries a wide variety of different modes of propagation. The layering around reservoirs is seldom so simple, and in a real reservoir the variety of signals may be very complicated. In all cases, if the velocities of the *P-* and *S*-waves and the layer thicknesses can be determined from well-logs, say, then the dispersion, amplitudes, and synthetic seismograms of the guided-waves can be calculated from the velocity structure. Since the presence of
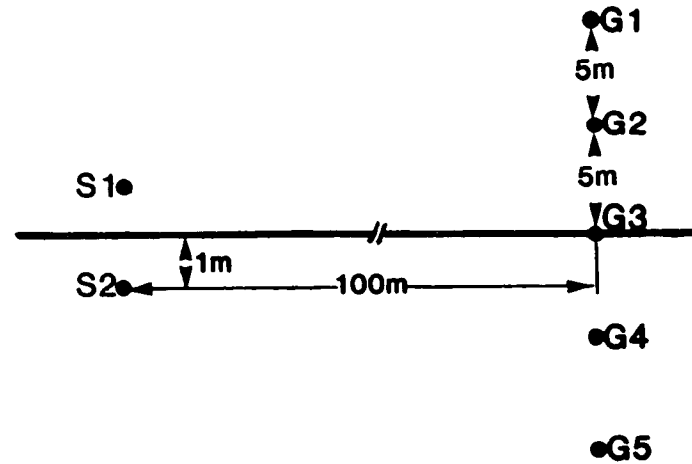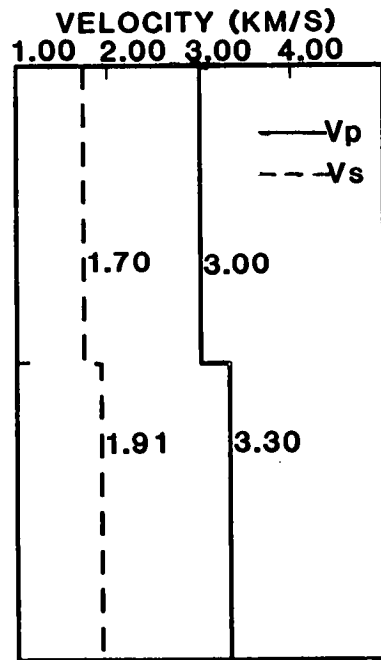
Figure 5.7 A single interface model between two halfspaces with 10% velocity-contrast.

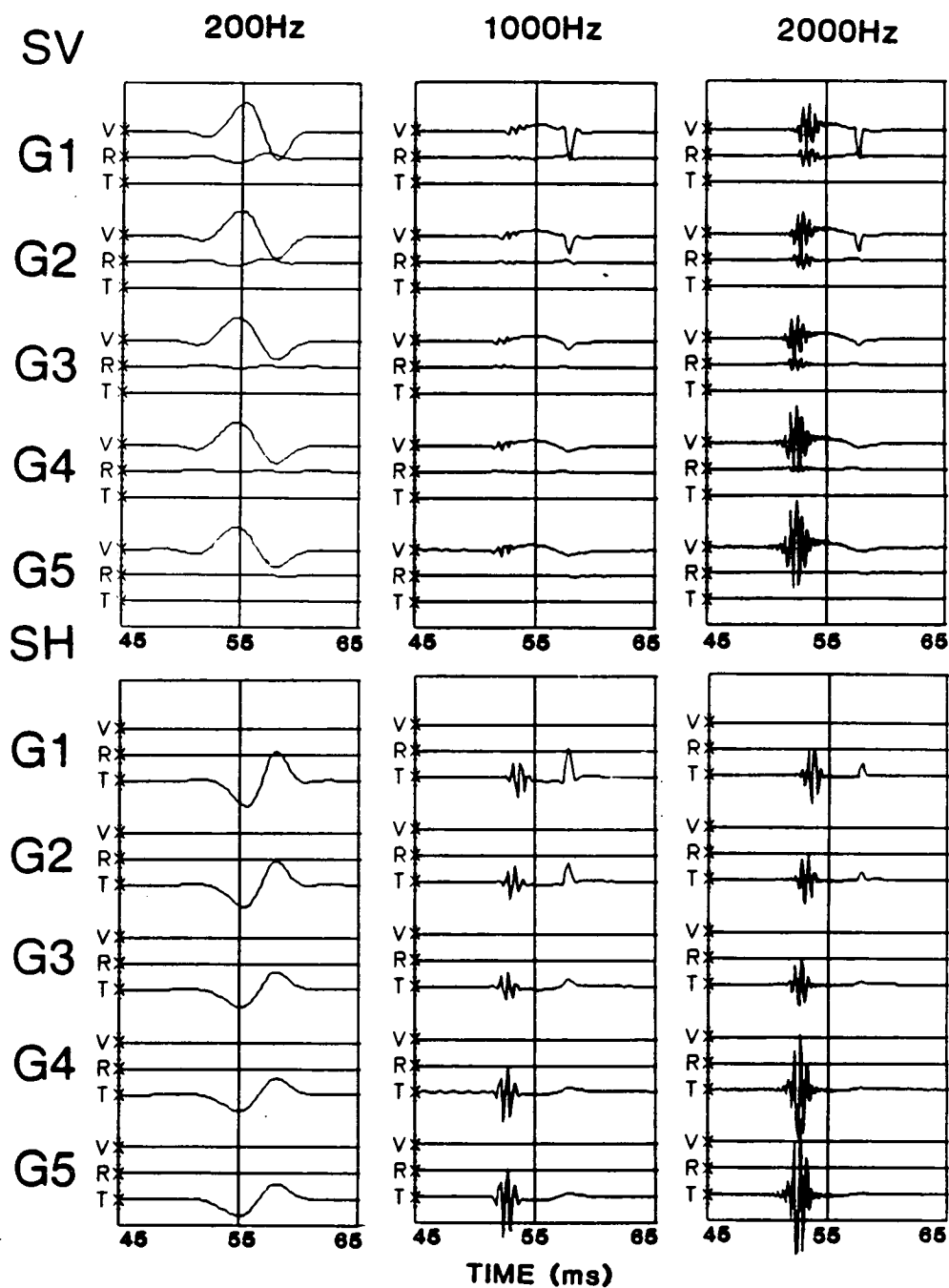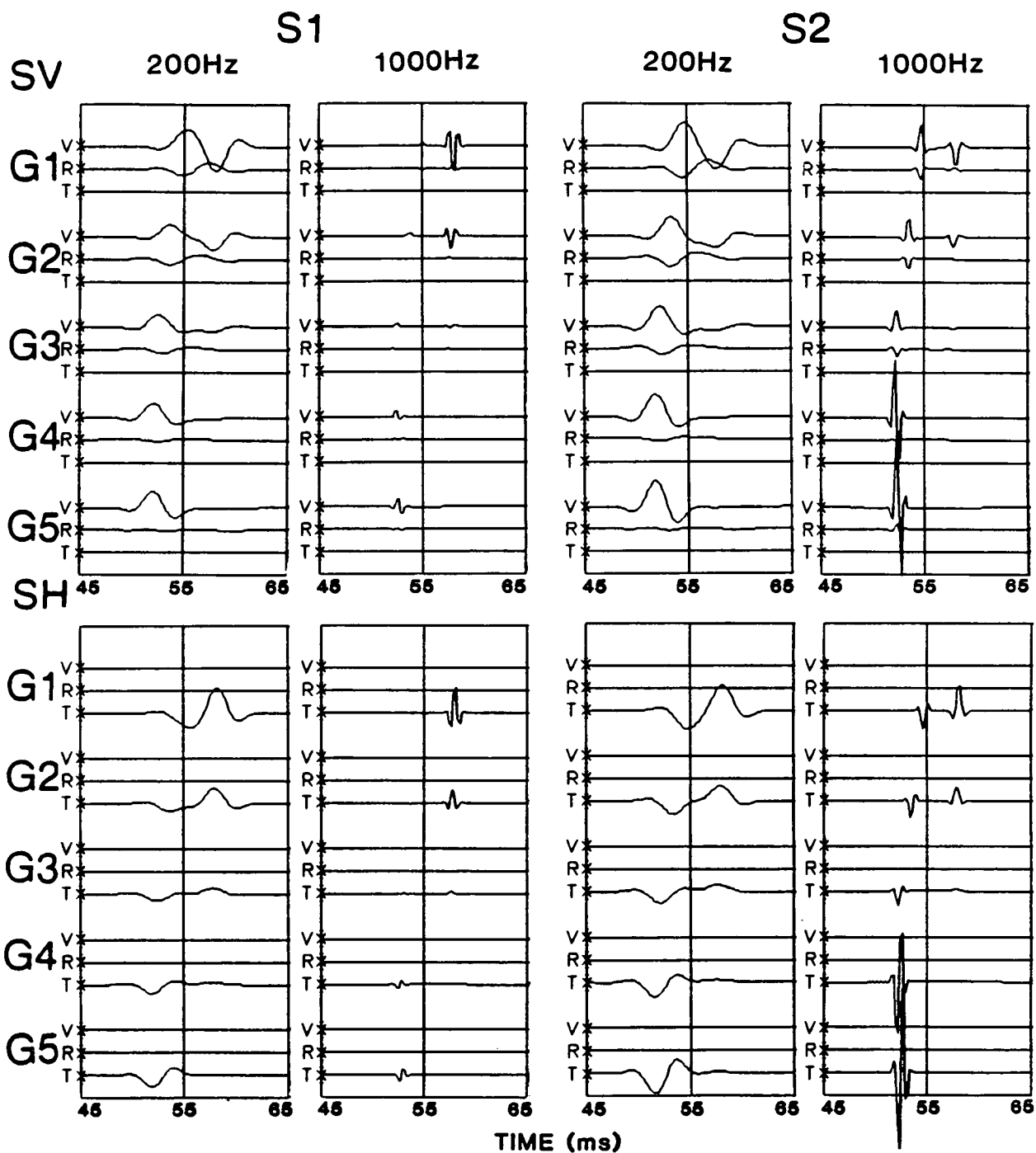**Figure 5.8** Synthetic seismograms of guided-waves for the single interface waveguide with source/geophone geometry of Figure 5.7. Dominant source frequencies are 200 and 1000Hz.

an expected guided-wave with an expected amplitude necessitates the continuity of the waveguide, observations of appropriate guided-waves may be used to test for continuity between wells. Since low-velocity layers are likely to carry the most useful guided-waves, it is fortunate that many reservoirs have lower seismic velocities than the surrounding rocks, and may act as channel-wave guides. Such guided-waves could be easily identified by the behaviour of their dispersion, amplitude distribution, and polarization pattern. Krohn (1990) has developed an approach for detecting the boundaries of a low-velocity layered system with high velocity-contrast. The method requires only computing differences between adjacent seismic traces in a seismogram, and then the difference may clearly outline the boundaries of low-velocity channels.

Guided-waves could be strongly coupled to tube-waves (or Stoneley waves) which propagate along the source and receiver boreholes in some crosshole surveys. The Stoneley wave in a source borehole may be converted into a guided-wave along a particular interface, and then the guided-wave may be converted into Stoneley wave again in a receiver borehole. It suggests that we could combine the guided-waves and the borehole Stoneley waves together to detect the layer continuity between boreholes.

Another factor that may make guided-waves particularly important in hydrocarbon production is the seismic anisotropy of the stress-aligned cracks or preferentially oriented pore-space existing in most reservoirs. The effect of this anisotropy on guided-waves is to couple together the Rayleigh- and Love-type family of modes into a single *Generalized* family with their dispersion and particle

displacements particularly sensitive to the properties of the fluids within the cracks and pores, which we have studied in Chapter 3. The potential of using guided waves to monitor the progress of production processes will be studied in the following section.

5.3 THE USES OF GUIDED-WAVES IN MONITORING EOR OPERATIONS

5.3.1 EOR AND EOR MONITORING

Flow of oil into a production well requires that pressure in the reservoir be higher than bottom-hole pressure in the well. Removal of fluids tends to reduce the reservoir pressure, and oil production rates will be declined. Finally, a limit will be reached, and a great deal of hydrocarbons may be left in place. On the other hand, some significant deposits of hydrocarbons have no adequate energy source in the first place. It is estimated that up to 70-80 percent of mobile oil can be left behind after initial extraction. For these reasons, additional energy has been introduced into the ground through a series of practices which has become known as Enhanced Oil Recovery (EOR).

The commonest and oldest method of EOR is the so called 'water flood', a procedure of pumping water into a pattern of injection wells in order to force oil into a number of producing wells. A great advance in this method involves the initial injection of a slug of fluid which is miscible with oil on the front end and miscible with water in the back end, thus reducing the tendency of water to by pass more viscous oil. Injection of live steam reduces the viscosity of oil and renders it more mobile. The 'fire flood' process makes direct use of heat as a driving force through the injection of air in

such a way that a small part of the hydrocarbons is oxidized, forcing the bulk of the hydrocarbons to flow ahead of the burning front. Other methods, such as injection of carbon dioxide, hydraulic fracturing of low-permeablity reservoirs, could also be employed during EOR operations.

During EOR operations, a great deal should be known about the reservoir and its fluid content. Tabel 5.1 lists the properties of reservoirs that have the most important impact on oil recovery (after Nur 1989). The volume, compressibility, and pressure of injected fluids should be carefully monitored in order to successfully carry out EOR operations. Characterization of oil reservoirs and monitoring for EOR could be obtained by repeated seismic surveys including surface seismic profiles, vertical seismic profiles, and crosshole seismic profiles. However, the resolution power of surface seismic data is limited. Vertical seismic profile data (especially reverse VSP) can provide better resolution than surface data, but the frequency content is still often inadequate for detailed imagining of reservoirs. In the crosshole environment, it is possible to acquire much higher frequency data because of proximity to the target, low noise levels, and because the rock's seismic Q is higher. Also, the acquisition geometry of crosshole usually gives a greater coverage of the target area than VSPs.

Many sedimentary oil reservoirs have approximately plane layers, and it has been shown that these plane-layered reservoirs may act as seismic waveguides in crosshole surveys. The field data study in Chapter 4 has comfirmed that the dominant signals in some crosshole surveys are often guided-waves. We suggest that these guided-waves could have important applications in monitoring EOR operations. An

Table 5.1 Reservoir properties that have the most important impact on oil recovery (after Nur 1989)

1. Mineralogy

2. Rock properties

Porosity
Saturations (oil, water, gas)
Permeability
Rock compressibility

3. Fluid properties

Fluid viscosity
Hydrocarbon chemistry
Wetability
Fluid compressibility
Fluid chemistry

4. Environmental factors

Pore pressure
Stress
Temperature

... and their spatial and temporal variations.

unique advantage of guided-waves is that most of the energy will be
channelled in the zone of interest. In contrast to VSPs or surface
reflection surveys, where only a small percentage of the travel path
samples the zone of interest, guided-waves should respond to the
properties of the zone of interest more strongly and directly if they
can be excited in appropriate signal frequency bands and
polarizations. Such guided-waves may be of special importance for
reservoirs with thin-layers, since other surveying techniques usually
lose much of their resolution in thin layering.

5.3.2 A SEDIMENTARY GAS RESERVOIR MODEL (WHITE'S MODEL)

Here we choose a gas-water sand reservoir encased in shale from the
Gulf Coast as a waveguide model, to examine the potential appliaction
of guided-waves in monitoring EOR operations. Figure 5.9 and Table
5.2 describe the thin-layered sedimentary hydrocarbon reservoir
model. The gas sand is trapped above water by a shale roof and a
shale floor. The liquid could be oil, instead of water, which would
cause further subtle differences, although we have not modelled the
oil/water effects in this model.

The isotropic matrix parameters of the rocks in Table 5.2 are based
on well logging through the reservoir (Figure 5.9(a), White and
Sengbush 1987) and other publications (Domenico 1974, Gardner *et al*.
1974, Dutta and Odé 1983). The thickness of the sandstone has been
chosen as 5 metres, but note that frequencies and thicknesses scale
inversely, so that thicker layers would correspond to smaller
frequencies proportionally. We choose a crack density (CD) of 0.1 to
model the reservoir, and the orientation of cracks can be varied
relative to the wave propagation direction. We will examine the
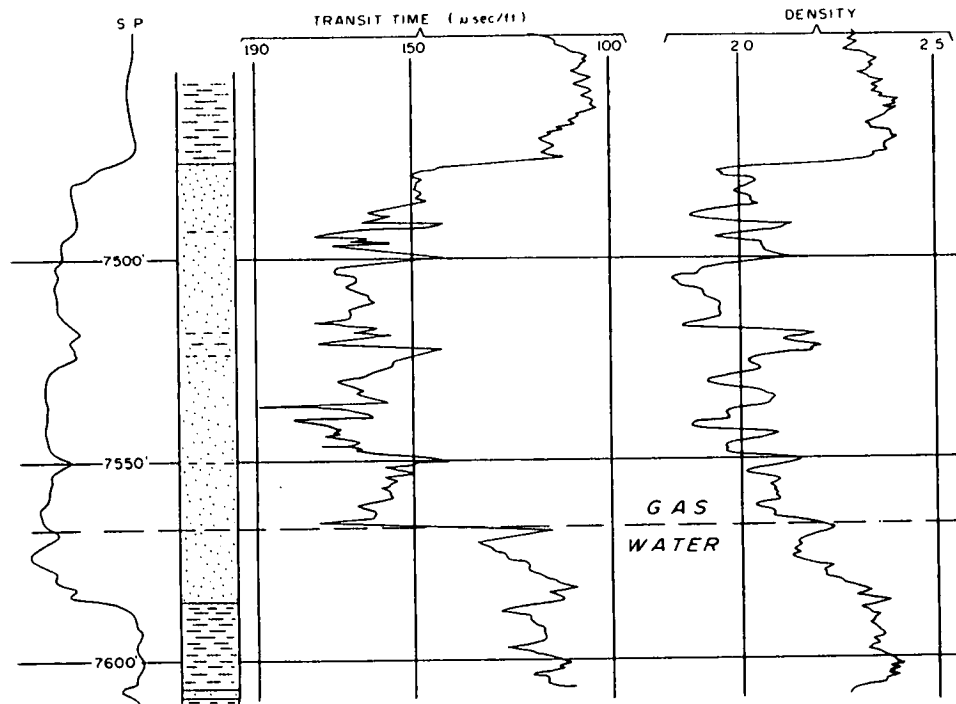
(a)
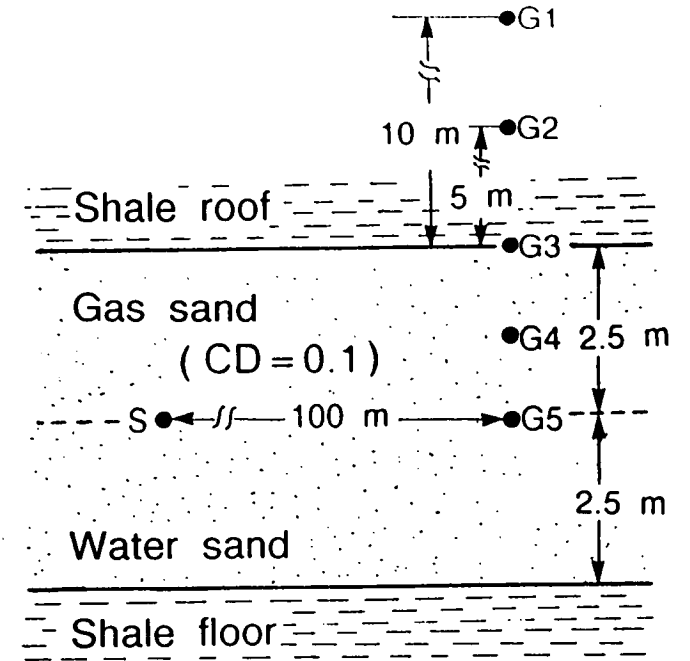
(b)

Figure 5.9 A cracked gas-sand reservoir waveguide model with crack density $CD = 0.1$. (a) P- wave velocity and density well-logs from the reservoir zone (after White and Sengbush 1987); (b) Source and geophone geometry for synthetic seismogram calculations.

Table 5.2 The isotropic matrix parameters
of the rocks in the reservoir model

	Vp (m/s)	Vs (m/s)	ρ (g/cm^3)
Gas sand	1900	1270	2.00
Water sand	2500	1200	2.23
Shale	2770	1600	2.34

effects of different saturations on the propagation of guided-waves.

5.3.3 GUIDED-WAVES WITH DIFFERENT RESERVOIR SATURATIONS

(1) Dispersion curves

Figure 5.10 shows the phase- and group-velocity dispersion curves of the first four *Generalized* modes for the reservoir model in Figure 5.9. Dispersion is shown for three different saturations of the inclusions [complete gas saturation, complete water saturation, and 50% gas 50% water saturation], and five different directions of propagation relative to the crack orientations [parallel to the vertical cracks (0° orientation), and every 22.5° to normal to the vertical cracks (90° orientation).] Arrowheads in Figure 5.10 indicate approximately the pinch positions of phase-velocity dispersion curves where the modes effectively exchange properties, in particular the slope of the dispersion curve and the type of particle displacement (Love-type to Rayliegh-type, and Rayleigh-type to Love-type, for example, see Chapter 3).

The dispersion curves have the following behaviour:

(a) The group-velocity of the first *Generalized* mode [equivalent to the fundamental Love mode] has a minimum at about 200Hz. This is expected to lead to an increase in amplitude of the seismograms known as an Airy phase, and means that a source frequency of about 200Hz is likely to excite strong fundamental mode guided-waves, and there may also be higher mode Airy phases at higher frequencies.

(b) The dispersion of most of the *Generalized* modes is sensitive to

Figure 5.10 Dispersion curves of first four *Generalized* modes of
guided-waves for different crack saturations: solid lines - complete
gas saturation; dashed line - complete water saturation; and
dash-dot line - 50% gas and 50% water saturation. Curves are shown
for different directions of propagation relative to vertical crack
orientation: (a)0°(parallel to crack strike); (b)22.5°; (c)45°;
(d)67.5°; and (e)90°(perpendicular to crack strike). The frequency
and phase-velocities at which different generalized modes pinch
together in off-symmetry directions is indicated by solid arrowheads.
The minima of the group-velocity dispersion of the first *Generalized*
mode are indicated by open arrowheads.
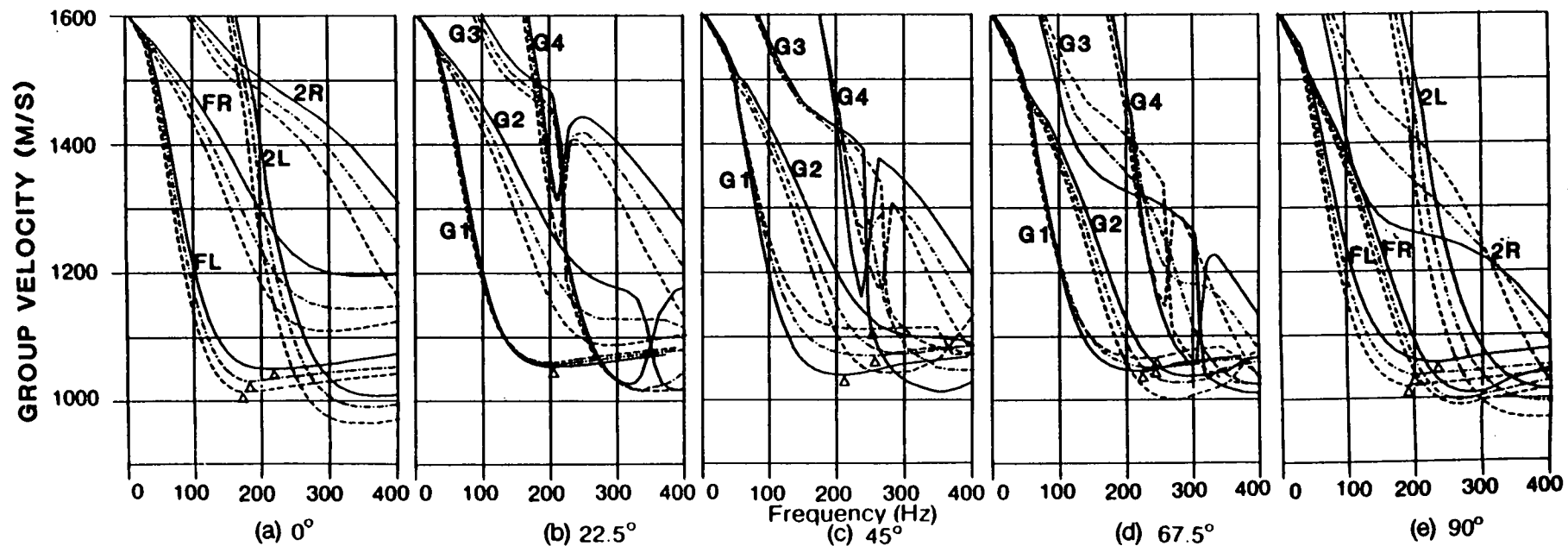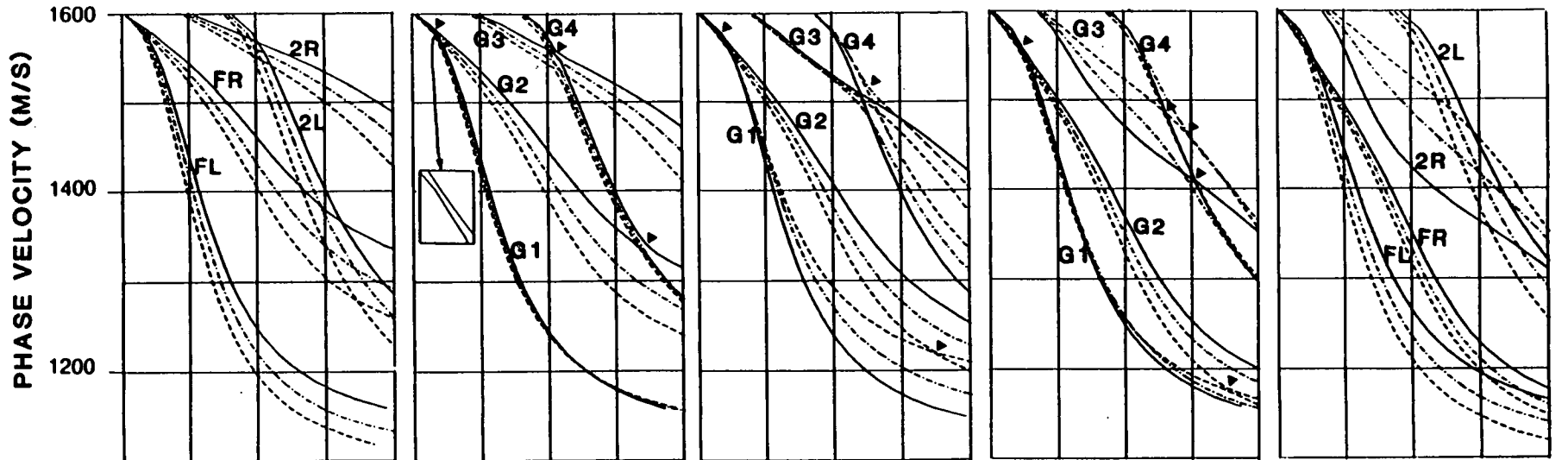
Figure 5.10

the direction of propagation relative to the crack strike. The exception is the first mode in the gas saturated sand, with Love-type characteristics, which shows very little change with direction (the solid curve of the first mode shows very little variation with direction). This is in contrast to the behaviour of the first mode in a water-saturated sand which shows significant differences: at some velocities the frequency changes by at least 30% for different directions of propagation [different crack orientations].

(c) The dispersion of most of the guided-wave modes is sensitive to crack saturations at most directions of propagation, as is shown by the different curves (solid, dot-dash, and dashed lines) at each direction of propagation. (The major exception is the first mode at propagation directions of 22.5° and 67.5°, which shows very little change with saturation.) The largest differences are in the third and fourth modes, but probably the most significant differences are in: the frequencies and velocities of the minimum of the first mode (marked by open arrowheads), which indicates the positions of the increase in amplitude of the Airy phases on seismograms; and the large range of frequencies and velocities of the second (Rayleigh type) mode.

(2) Amplitude/depth distribution

Figure 5.11 shows a three-component amplitude/depth distribution of the first four *Generalized* modes of guided-waves in the cracked model with gas saturation (solid lines), and water saturation (dashed lines), for propagation of a direction 45° relative to crack strike. All four modes are shown at a frequency of 300Hz. At a high enough

FIRST MODE (300Hz) SECOND MODE (300Hz) THIRD MODE (300Hz) FOURTH MODE (300Hz)

VERTICAL

5m

RADIAL

5m

TRANSVERSE

5m

VERTICAL

5m

RADIAL

5m

TRANSVERSE

5m

VERTICAL

5m

RADIAL

5m

TRANSVERSE

5m

VERTICAL

5m

RADIAL

5m

TRANSVERSE

5m
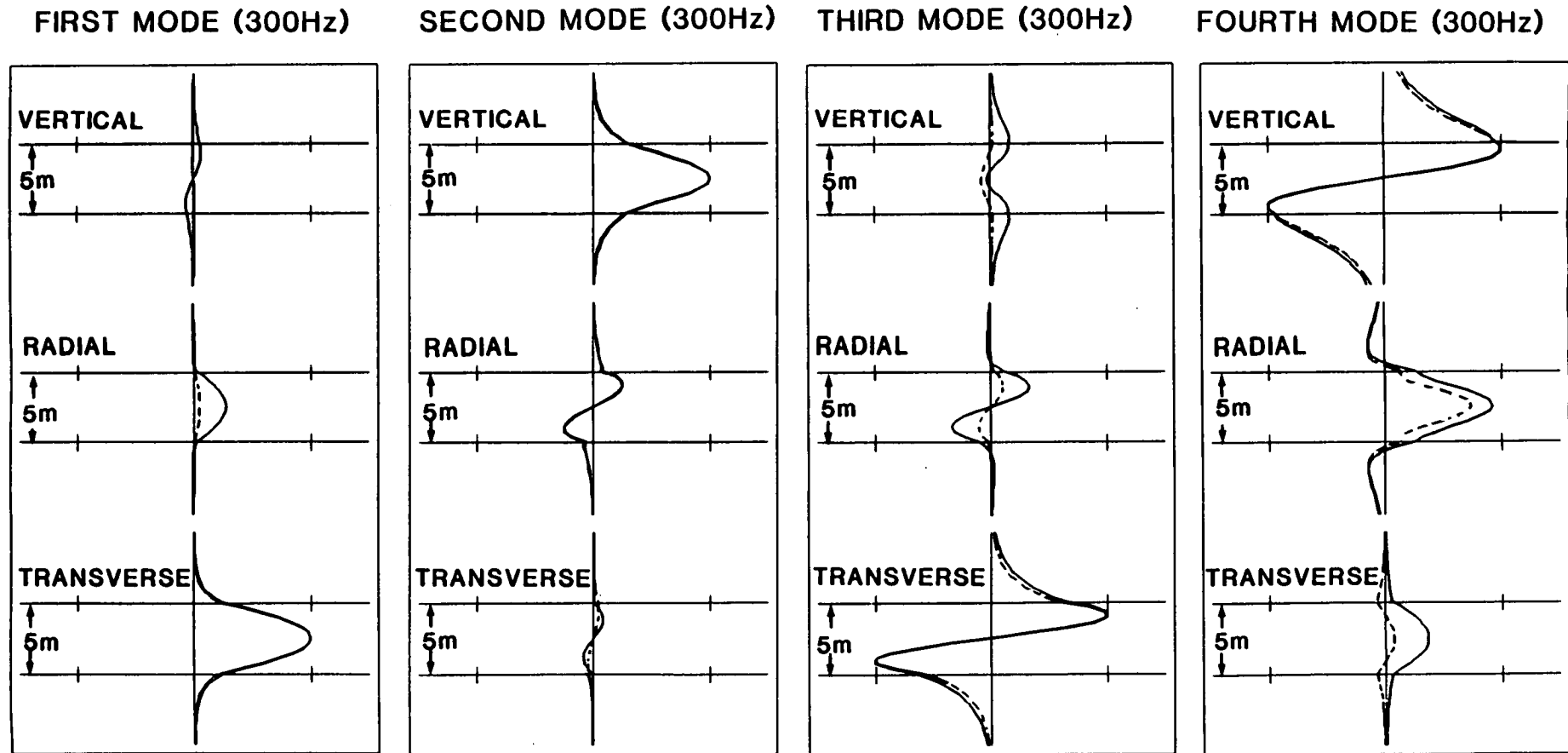
Figure 5.11 Three component amplitude/depth distribution of first four *Generalized* modes of guided-waves in the reservoir model containing parallel vertical cracks with crack density CD = 0.1, and crack strike 45° from the radial direction, where solid lines are water saturated sand, and dashed lines are gas saturated sand.

frequency (say, 300Hz in the Figure 5.11), the most energy of guided-waves will be trapped inside the reservoir layer. It is likely that gas-filled cracks result in greater three-dimensional energy coupling than water-filled cracks.

(3) Synthetic seismograms

Figure 5.12 shows synthetic seismograms for propagation in completely gas-saturated sandstone parallel to the strike of the cracks (0° orientation) for a transverse force source exciting, for this direction of propagation, waves with Love-type motion, and for a vertical force source exciting Rayleigh-type motion. Seismograms are shown for five different dominant signal frequencies.

For this direction of propagation, the vertical-radial and horizontal transverse motion (Rayleigh- and Love-type motion) are decoupled. For the 50Hz source, the arrival is essentialy a body-wave shear-wave, particularly for the vertical force source, which shows almost the same amplitude at all geophones. The arrival from the transverse horizontal force shows the beginnings of some channelling by the gas sand and shows larger amplitude at the geophone (G5) in the centre of the sand.

For higher source frequencies, the seismograms show pronounced channelling with the amplitudes at the geophones outside the gas sand much diminished, for both Love- and Rayleigh-type motion (see also Figure 5.11). There is a marked change in mode excitation for the Love-type seismograms between source frequencies of 200 and 300Hz, with the large-amplitude high-frequency signals for the 300 and 400Hz

Figure 5.12 Synthetic seismograms for a range of characteristic source frequencies for the reservoir model with complete gas satuaration. Seismograms are shown for the five geophone positions in Figure 5.9(b), for a propagation direction parallel to the strike of the vertical cracks. The source is in the centre of the gas-sand, and seismograms are shown for a horizontal transverse source (*SH*) and a vertical force (*SV*).

Source Transverse force

50 Hz 100 Hz 200 Hz 300 Hz 400 Hz

Source Vertical force

Time (1/10*Seconds)
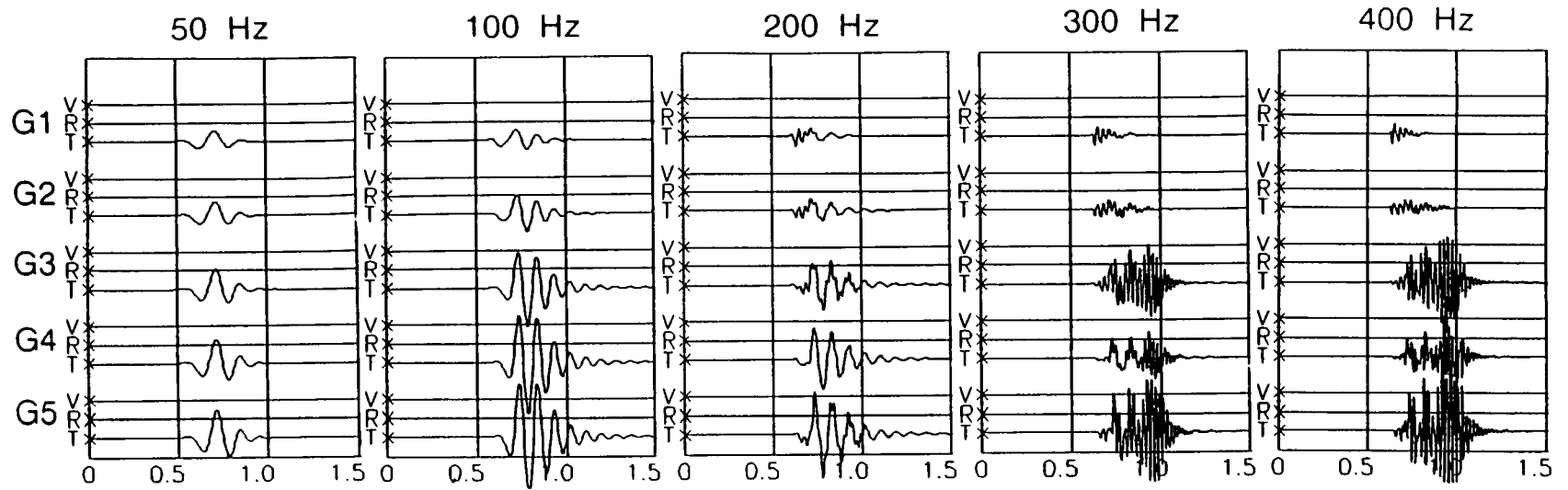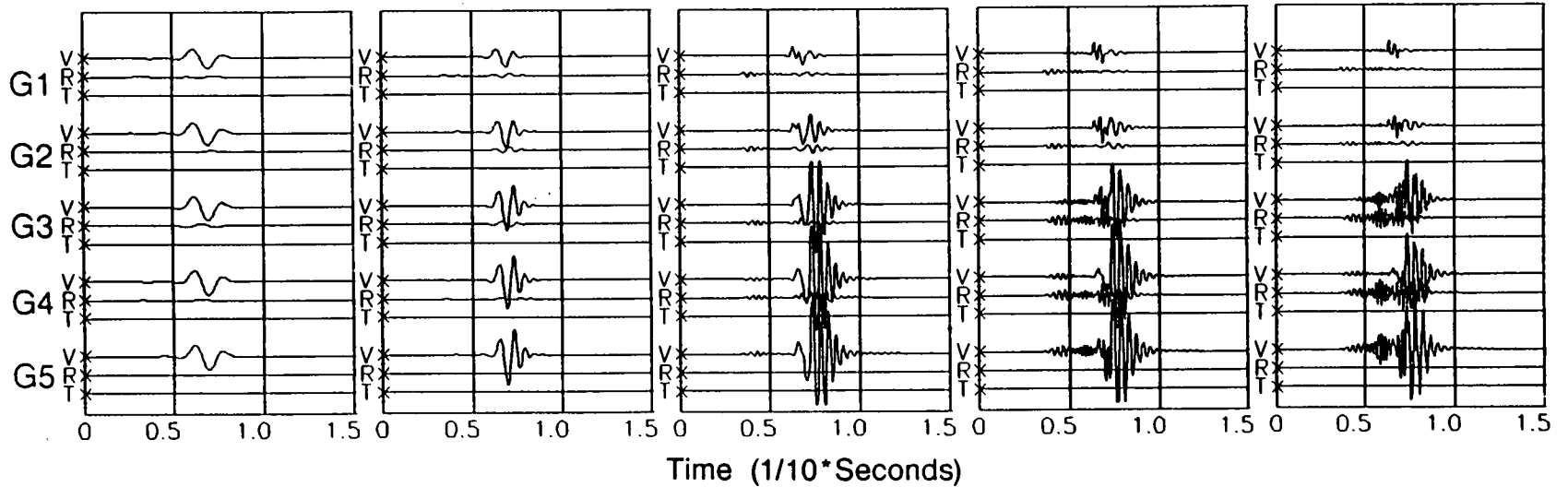
Figure 5.12

sources being the fourth mode, which is the slowest curve in the group-velocity dispersion for this propagation direction in Figure 5.10.

The guided-waves begin to show strong channelling for the vertical force source as a result of the broad minimum of the second (here a Rayleigh-type) mode between 300 and 400Hz. The channelling begins for sources of 200Hz, and persists for 300 and 400Hz. For the 300 and 400Hz sources, the higher-mode Rayleigh-waves effectively arrive earlier than the lower frequency second mode.

Figure 5.13(a) shows synthetic seismograms for the G4 geophone for five different directions of propagation relative to the crack strike through complete water-saturated gas sand, for both transverse force source (400Hz) and vertical force source (300Hz). In off-symmetry directions, the modes do not separate into transverse and sagittal-plane motion, and each mode excites motion in all three dimensions. These polarization abnormalities may give diagnostic information about anisotropy of cracked reservoirs. The three-component seismograms show comparatively subtle differences for different propagation directions. The differences are principally in the three-dimensional particle motion, and are much more clearly displayed in polarization diagrams (See Figure 5.13(b)).

Figure 5.14 compares three-component seismograms for the G4 geophone for propagation through complete gas and complete water saturated sand at three different directions of propagation for a 400Hz transverse and vertical force source. Very significant differences are visible on the seismograms between gas- and water-saturated sand. There are differences in: frequency; velocity;

(a) Source

(b)
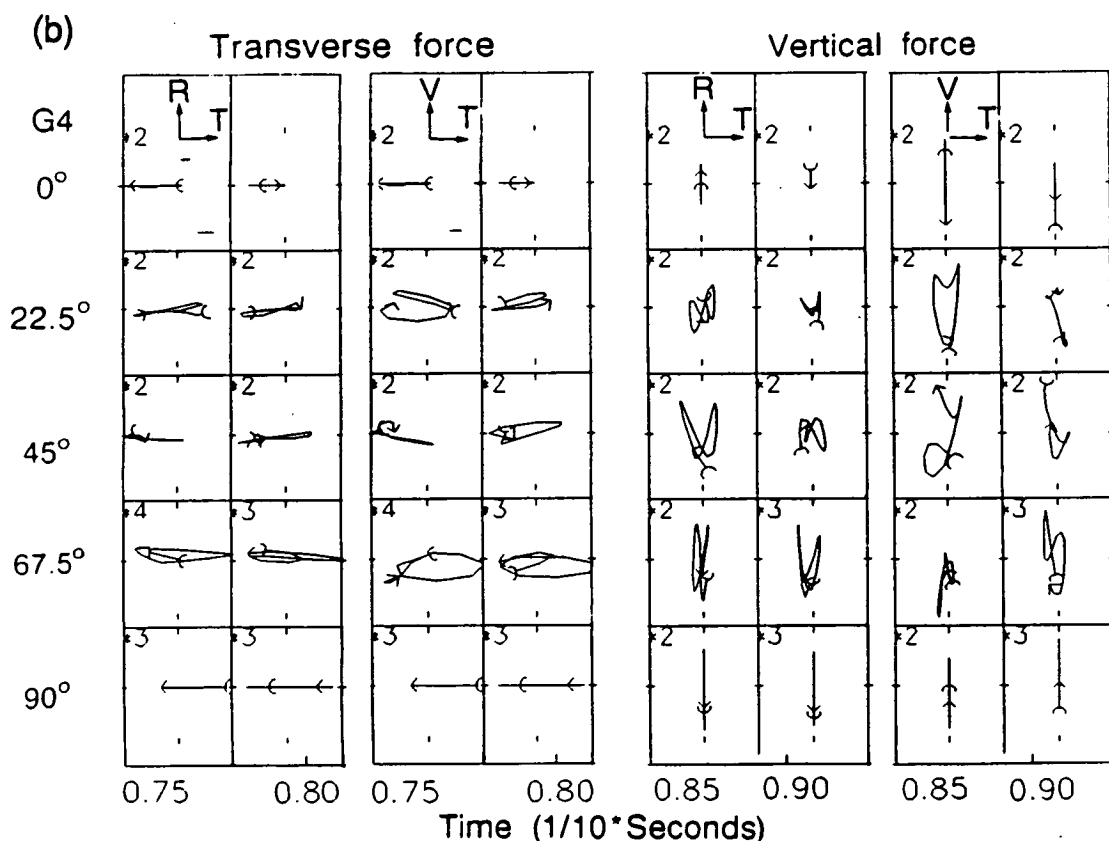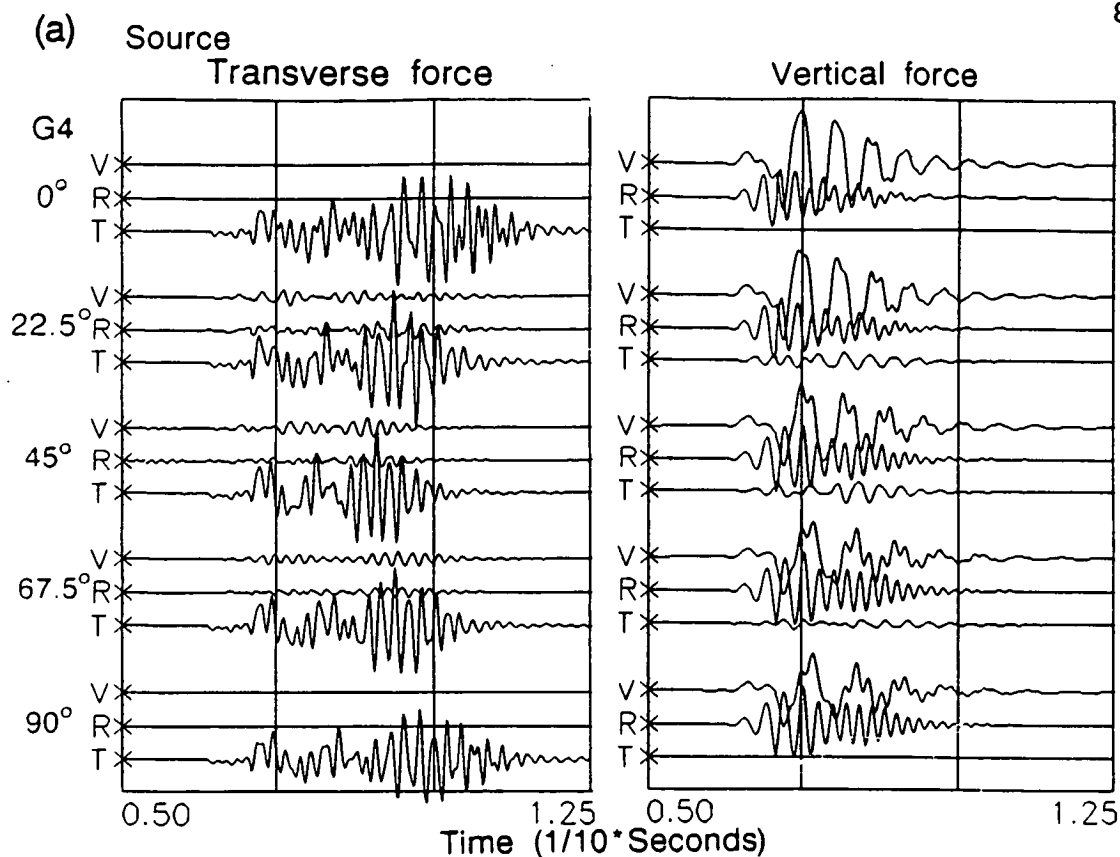
Figure 5.13 (a) Synthetic guided-wave seismograms at geophone G4 for transverse force (400Hz) and vertical force (300Hz) for different directions of propagation through water saturated gas sand. In off-symmetry directions, all modes excite displacements in all three dimensions. (b) Polarization diagrams for the selected seismograms in (a): radial(R)-transverse(T) and vertical(V)-transverse(T) planes.
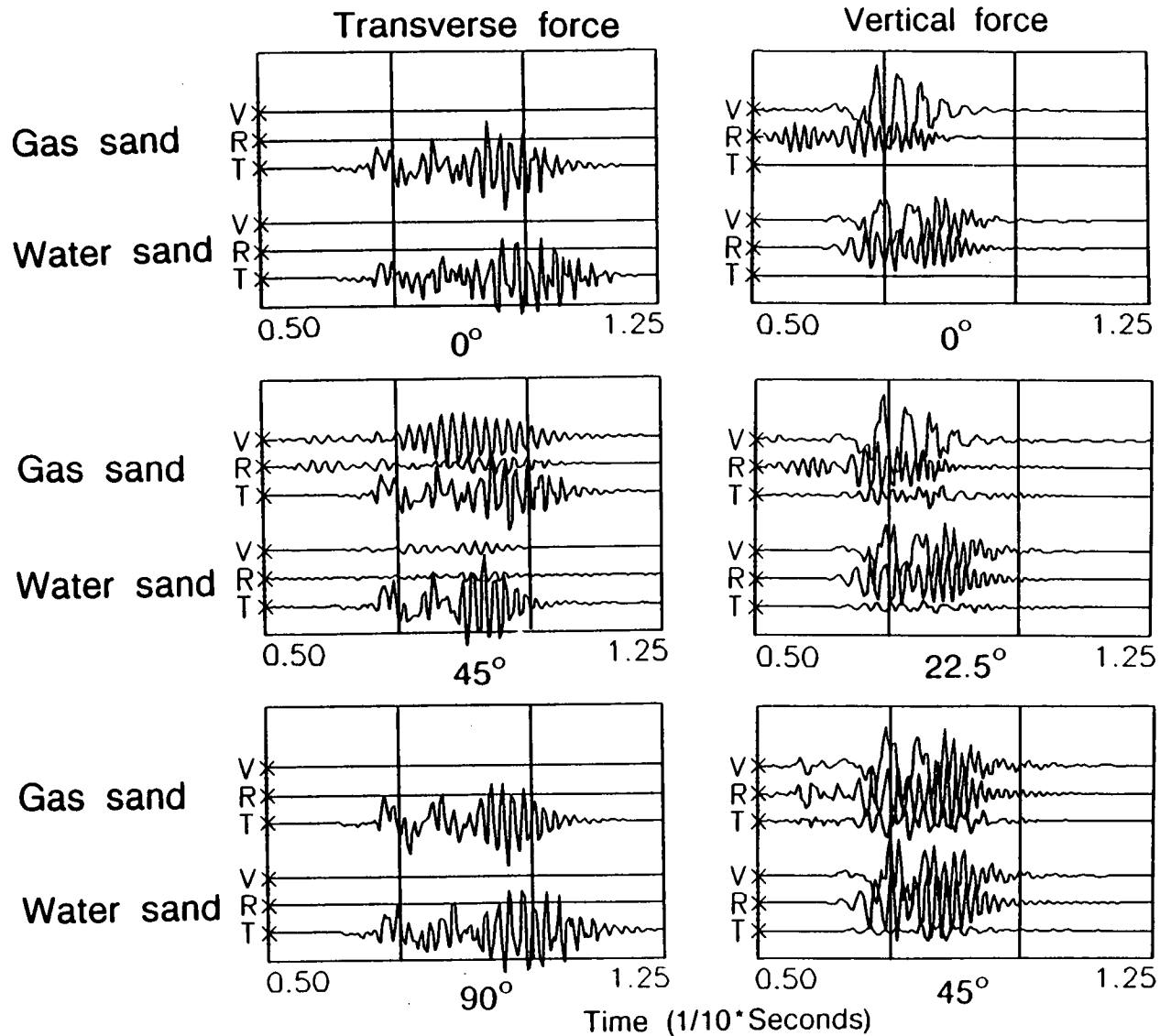
Figure 5.14 Comparison of seismograms in gas sand and water-saturated gas sand at geophone G4 for 400Hz vertical force source and transverse force source for several different directions of propagation.

particle motion; amplitude; and mode excitation. The differences
between levels of saturation will certainly vary for different
velocity and crack structures, but it certainly suggests there is the
potential for monitoring changes in the level of the gas and water
saturation by analyzing guided-waves between appropriate crosshole
situations.

(4) Comparison of theoretical dispersion with synthetic seismograms

The theoretical dispersion curves in Figure 5.10, and the synthetic
seismograms in Figures 5.12, 5.13, 5.14, show that the dispersion of
guided-waves is sensitive to crack parameters, crack saturation, and
direction of propagation relative to the crack strike. The
correspondence between the theoretical dispersion calculations with
the dispersion of the synthetic seismograms is demonstrated in Figure
5.15, where the dispersion in the synthetic seismograms is calculated
by multiple filter technique. The comparison in Figure 5.15 is for
the transverse component seismogram (inset) at the G4 geophone for
propagation parallel to the strike of the cracks for complete gas
saturation. The spectrum (inset) suggests the presence of two modes.
The contoured multiple filter plot also shows two modes, which agree
reasonably well with the corresponding theoretical curves. The large
amplitudes of the seismogram appear to be principally those of the
second Love-type mode, equivalent to the fourth *Generalized* mode. The
low values in the centre of the plot are probably due to the
destructive interference of the two modes at similar frequencies.
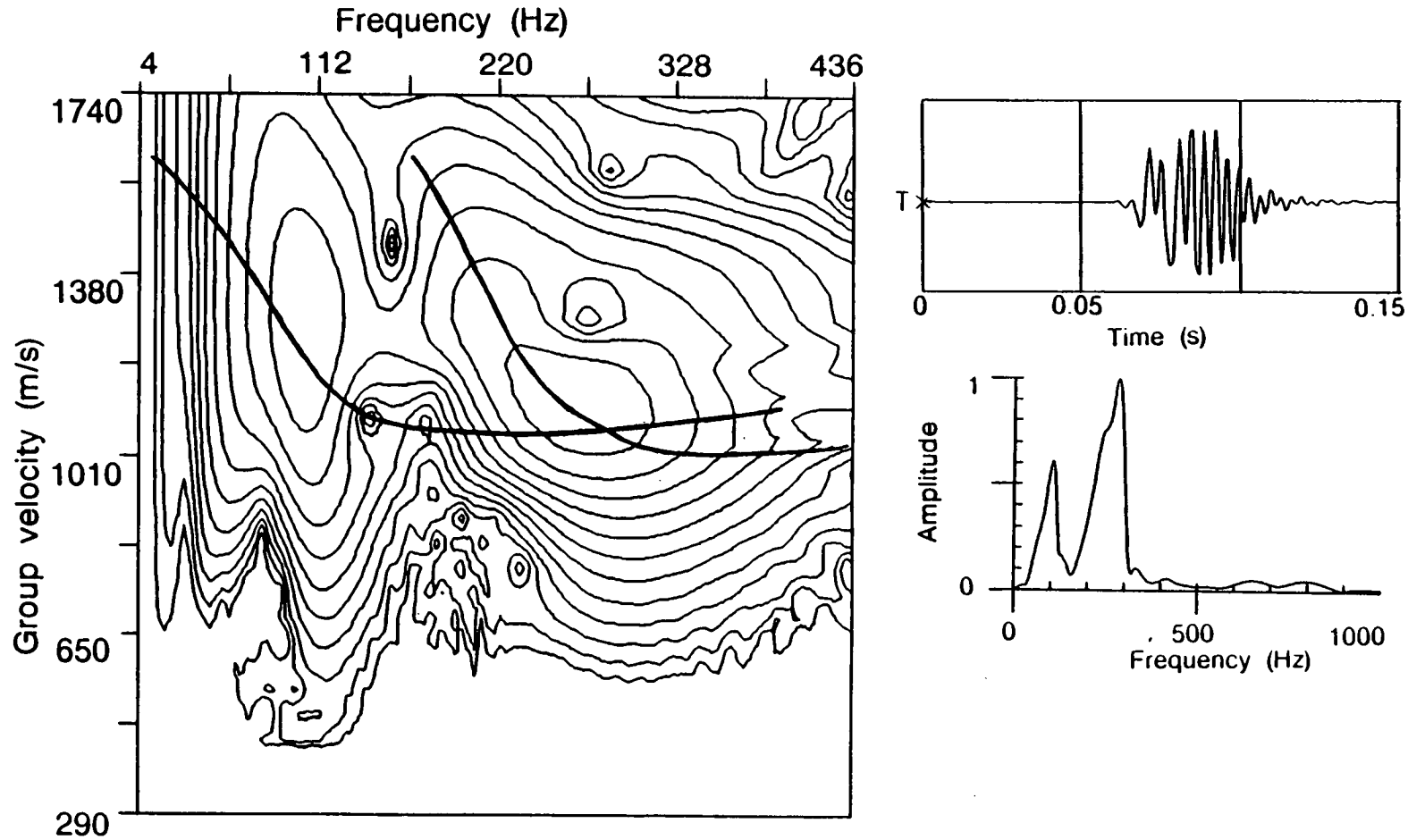
Figure 5.15 Contoured multiple-filter map of the dispersion of the horizontal transverse component at geophone G4 from a 200Hz horizontal transverse force source positioned 1.25m deep, in the direction parallel to the strike of the cracks. Lines are theoretical group-velocity dispersion of the first two Love-type modes. Insets show seismogram and amplitude spectrum.

5.3.4 THE USES OF GUIDED-WAVES IN MONITORING EOR OPERATIONS

We have shown (see also Chapter 3) that guided-waves are very sensitive to the changes of crack parameters including pore-fluid velocities, gas/liquid ratios, and crack orientations. This great sensitivity suggests that guided-waves could have applications to monitoring EOR procedures in thin hydrocarbon reservoirs, where the variations of gas and water saturation (or gas and oil saturation) are crucially important. Here we have examined guided-waves in a particular reservoir model structure. The behaviour of guided-waves is likely to be significantly different for different velocity and cracked structures.

It is suggested that for a given velocity structure (determined from well logging, for example), theoretical dispersion and amplitude/depth calculations will indicate optimum frequencies and depth levels for exciting appropriate guided-modes. The channelling of the energy in the gas sand shows that, if appropriate frequencies at appropriate depth levels can be identified, it is likely that the appropriate (possibly high-frequency) signal can propagate for significant distances with not too much loss of amplitude.

The potential is clear. What is needed is examination of field data from crosshole surveys in sedimentary basins, in situations where there is some change to saturation characteristics.

5.4 DISCUSSION AND CONCLUSIONS

The modelling studies (by calculating dispersion, amplitude/depth distribution, and synthetic seismograms) suggest that almost any

continuous plane layer or combination of layers will support guided-waves, which can propagate to significant distances with relatively large amplitudes, if appropriate source frequency, polarization, and source and geophone positions can be chosen in crosshole surveys. Their propagation are dominated by the continuity and structure of waveguide layers. These guided-waves could be easily identified by their dispersive behaviour, amplitude distribution, and polarization pattern, and it is suggested that guided-waves could provide a useful tool to test continuity of plane layered reservoirs. This test could be very important for the production of hydrocarbons and the estimation of hydrocarbon reserves.

We have demonstrated that the more important application of guided-waves may be their use in monitoring EOR operations. The major effect on the rockmass during EOR or other production processes is to modify the contents or the geometry of the internal structure of aligned inclusions. This can appear by modifying the pore-fluid by changing its velocity or viscosity or by changing the ratio of gas to liquid in the pore space, but crack density and crack shape can also be modified as the pressure changes. Since guided-waves are sensitive to this internal structure, the behaviour of guided-waves recorded during production processes are also expected to change as the internal structure is modified. Although any single observation of guided-waves is likely to be difficult to interpret, observations from repeated source and geophone locations showing changes in temporal behaviour may place tight constraints on possible interpretaions. Consequently, it is suggested that guided-waves may be used to monitor any production process that modifies the geometry of the internal structure of the rockmass.

CHAPTER 6

GUIDED-WAVES IN A CRACK-CONTROLLED CHANNEL
AND A FAULT ZONE

6.1 INTRODUCTION

In the previous chapters, we have studied the seismic waveguides
raised from horizontal layers or interfaces. As an additional
interest, here we shall briefly describe the propagation of seismic
waves in two special waveguides: (a) a waveguide controlled by two
fluid-filled thin-plane fractures; and (b) a fault-zone waveguide.

A crack-controlled waveguide may be formed during hydraulic
fracturing for the extraction of geothermal energy from hot dry rock,
or for enhancing the recovery of hydrocarbon reservoirs. The basic
concept and practice for hydraulic fracturing are described by
Hubbert and Willis (1957), Cremer (1981), Fehler (1981), Aki *et al.*
(1982), Robert and Crampin (1986), and Mahrer and Mauk (1987). In
acoustic emission or seismic surveys, the crack-controlled reservoir
zone may trap some modes of guided-waves. Booth (1982) and Liu
(1989) have given a modelling study to this kind of guided-waves.
Based on their modelling result, we further study the dispersion and
other propagation behaviours of such guided-waves in this chapter.

A highly-fractured fault zone with low velocity, sandwiched by
surrounding rocks, can also be considered a waveguide. The trapped

modes of seismic waves in such anisotropic waveguides have been observed by Li *et al* (1990) in a VSP experiment in Oroville and San Andreas Fault Zones, California. We shall attempt to model the propagation of such trapped modes in the fault zone.

The propagation of such guided-waves will be controlled by the the geometry and internal properties of a crack-controlled channel or an active fault zone. Therefore, the observation and study of such guided-waves may have important applications in geothermal reservoir engineering geophysics and earthquake prediction studies.

6.2 GUIDED-WAVES IN A CRACK-CONTROLLED CHANNEL

6.2.1 MODEL

The geothermal energy exists in great quantities at certain depths of many normal continental areas, and the energy can be extracted if it is possible to establish a circulation of fluid through the hot rocks to the surface. However, the hot rocks at depth are usually impermeable, and do not themself contain any fluid for circulation. It is necessary, by hydraulic fracture treaments, to create an artificial circulation path through the geothermal reservoir, and to use fluid pumped in from above to accomplish the transfer of energy from the hot dry rock to the surface.

Figure 6.1 shows an example of the inferred geometry of the circulation path in a commercial geothermal reservoir. The boreholes EE-1 and GT-2B are connected by a system of natural joints and two large parallel plane fractures orthogonal to the direction of minmum tectonic stress, which were created by two seperate hydraulic
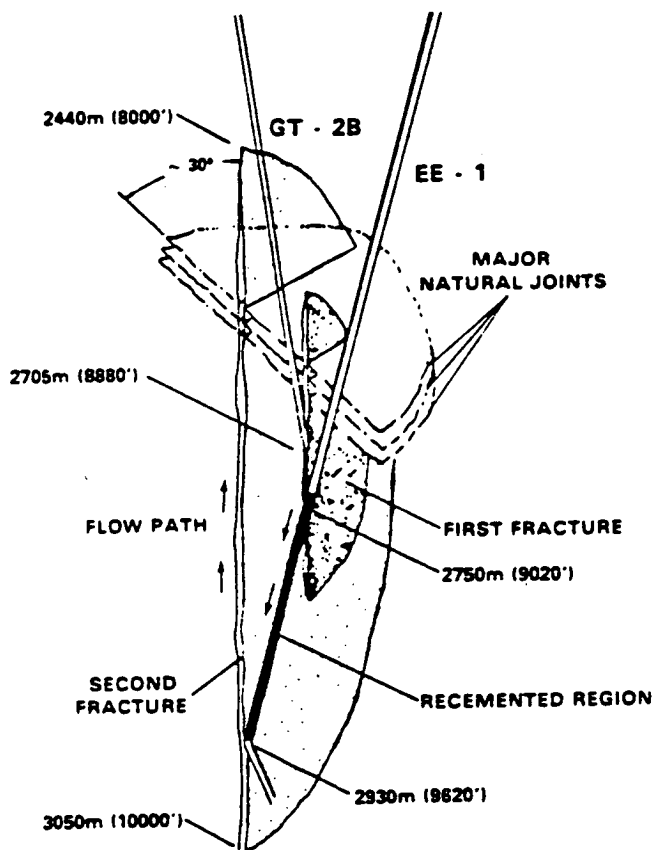
Figure 6.1 The inferred geometry of the circulation path in a geothermal reservoir. The boreholes GT-2B and EE-1 are connected by a system of natural joints and two large parallel fractures. These fractures were created by two seperate hydraulic pressurizations of the borehole EE-1 (after Cremer 1981).

pressurizations of borehole EE-1. The two large plane cracks cut the rocks into a slab with a thickness of about 10 meters. This slab may behave as a typical waveguide in microseismic events or VSP surveys. Figure 6.2 shows the simplified theoretical model of the crack-controlled waveguide. The slab is likely to be cracked as a result of thermal contraction on cooling during pressurization of the circulation. Therefore, the slab channel displays crack-induced anisotropy.

6.2.2 DISPERSION OF *SH* TYPE GUIDED-WAVES

For the crack-controlled channel shown as Figure 6.2, the transverse and tangential displacements and stresses on the crack-slab interfaces are no longer continuous, and the propagator matrix technique in Chapter 2 is not approriate for calculation of dispersion of the guided-waves in the channel. Appendix B presents a procedure to determine the dispersion relation of *SH* type guided-waves, in which the material within the channel is assumed to be isotropic.

Figure 6.3 shows the dispersion curves of the several modes of *SH* type guided-waves in the model of Figure 6.2. In the crack-controlled waveguide, the phase-velocity of guided-waves is higher than the shear-wave velocity V_s in the channel, whereas the group-velocity is always slower than V_s. Each mode of the guided-waves has a cutoff frequency. There are two major dispersion differences between a crack-controlled waveguide and a plane-layered waveguide: firstly, for a symmetrical plane-layered waveguide, the cutoff frequency of fundamental modes of guided-waves is zero, whereas for a symmetrical crack-controlled waveguide, the cutoff
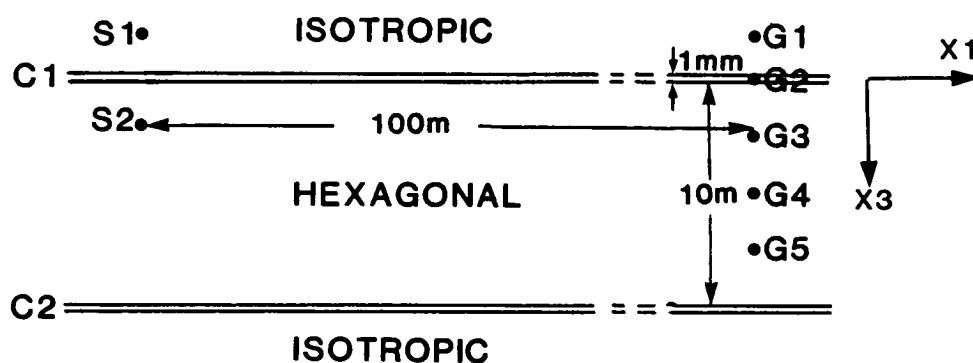
Figure 6.2 The simplified theoretical model structure of crack-controlled waveguide. Two major 1mm thick water-filled cracks C1 and C2 on the either side of a cracked slab which is modelled by a crack-induced anisotropic medium with hexagonal symmetry of 10m thick. The rocks on either side of the channel are assumed to be isotropic. Two sources and five geophones are located in the model for synthetic seismograms calculations: S1 and S2 are positioned on two sides of the crack C1 and with 2.5m away from the crack; five geophons G1 - G5 are placed alone depth direction in 2.5m interval. The elestic constants of materials are described in Table 6.1.
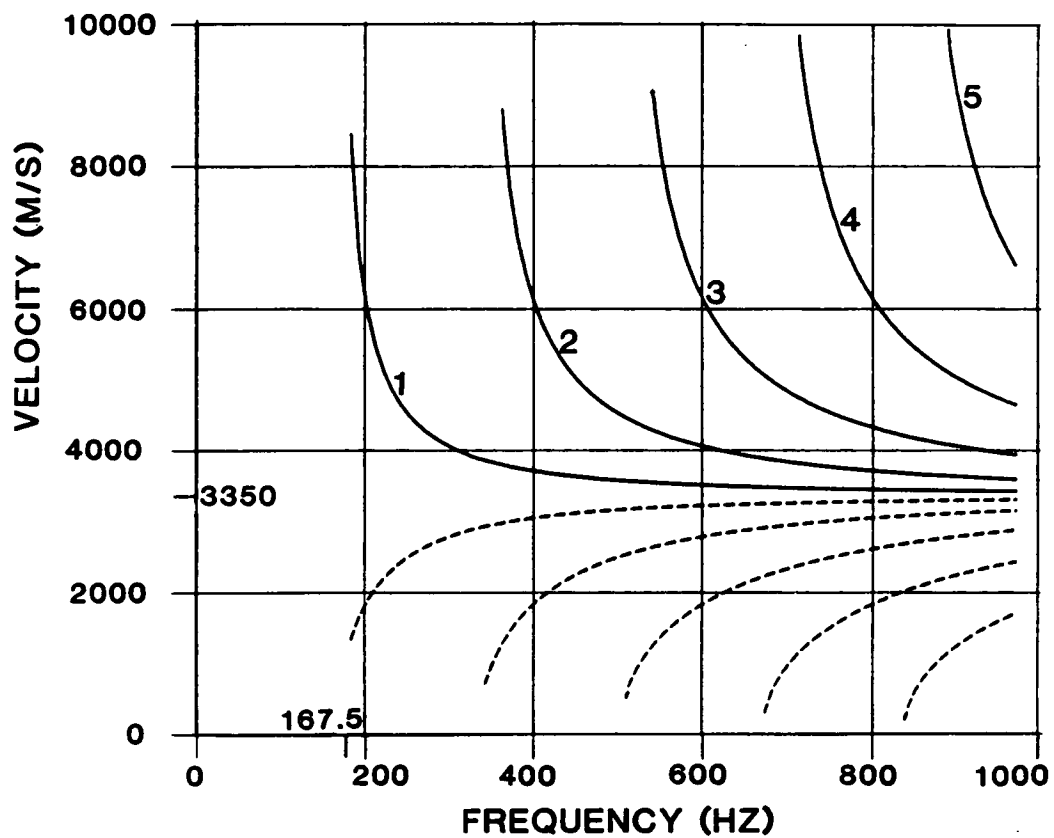
Figure 6.3 Dispersion curves of first several modes of *SH* type guided-waves for the crack-controlled channel model. Solid lines are phase-velocity, and dashed lines are group-velocity.

frequency of the fundamental modes is determined by the ratio of the shear-wave velocity and thickness of the channel; secondly, near the cutoff frequencies, for a plane-layered waveguide both phase- and group-velocity of guided-waves are equal to the shear-wave velocity in surrounding halfspaces, while in a crack-controlled waveguide the phase-velocity of guided-waves can be theoretically infinite with its group-velocity tending to zero. Therefore, the guided-waves in the crack-controlled waveguide usually display abnormal dispersion behaviour.

6.2.3 OBSERVATIONAL EVIDENCES

Figure 6.4 shows five microseismic events which were recorded by downwell three-component geophones during a pressurization of a hydraulic fracturing for the geothermal reservoir project. The precise position of geophone is unknown. It is seen from the seismograms that there is a difference in the frequency content of the shear-wave coda between the vertical and horizontal components. However, the principal characteristic of most seismograms perhaps is the large amplitude, low frequency wavetrain which begins at, or soon after, the onset of the first shear-wave. The particle motion of this wavetrain is polarized principally in the vertical direction, and thus approximately parallel to the planes of the major cracks. It is suggetsed that this characteristic wavetrain could be due to the presence of the waveguide or channel formed by two large parallel water-filled cracks (Booth 1982).
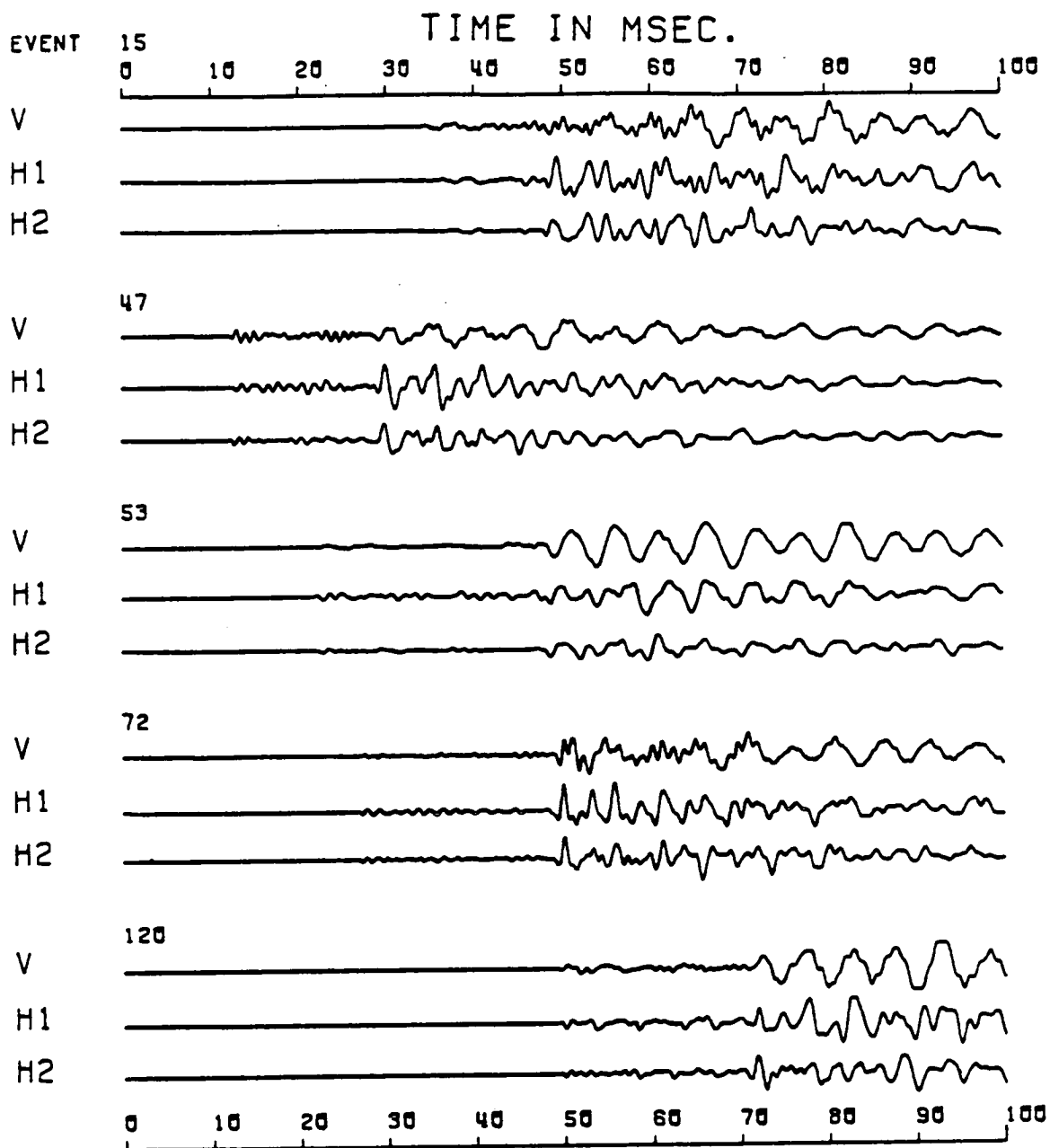
Figure 6.4 A selection of seismograms of microseismic events recorded by a three-component geophone package in GT-2B (at depth of 2695m) during pressurization of EE-1 in the geothermal reservoir of Figure 6.1. The V component is parallel to the axis of borehole GT-2B. The horizontal components *H1* and *H2* are orthogonal to V, but their exact orientation is unknown (after Booth 1982).

6.2.4 SYNTHETIC SEISMOGRAMS

We have calculated the synthetic seismograms with different source
types and frequencies for the model and source/geophone positions of
Figure 6.2. The crack-controlled channel is permeated by the
hexagonal columnar microcracks having a strike parallel to x_3
direction, which may be caused by thermal contraction (Booth 1982).
The elastic constants for the cracked rock are given in Table 6.1.
We assume that the halfspaces are isotropic in the model. For the
shear-wave velocity (V_S = 3.35 km/s) of isotropic matrix of the
channel, the cutoff frequency for the first mode of SH type
guided-waves is approximately 167.5Hz.

Figure 6.6 shows the synthetic seismograms excited by an explosive
source for two different positions: (a) the source outside the
fracture-controlled channel (S1), and (b) the source inside the
channel (S2) (see Figure 6.2). The seismograms are displayed for two
dominant frequencies 100 and 400Hz. For the 100Hz frequency (less
than the cutoff frequency), the sources in both S1 and S2 positions
basically excite body-waves. When source frequency is increased to
400Hz, the source in S2 position excites highly dispersive
guided-waves, containing two possible modes. Such guided-waves have
the dominant energy in the seismograms. The source in S1 position
only excites weak guided-waves. One remarklable feature on the
seismograms of Figure 6.6(b) (S2 source position, 400Hz frequency) is

Table 6.1 Elastic constants (in Pascals X 10^9) of the anisotropic material with hexagonal symmetry which models the cracked slab: a random distribution of coplanar normal saturated cracks in an isotropic matrix with Vp = 5.8, and Vs = 3.35 km/s, and ρ = 2.6 g/cm^3. The crack density is 0.1. The axis of symmetry is parallel to the x_3 axis.

c_{1111} = 86.307 c_{2222} = 86.307 c_{3333} = 77.017

c_{2233} = 25.630 c_{3311} = 25.630 c_{1122} = 27.950

c_{2323} = 23.253 c_{1313} = 23.253 c_{1212} = 29.178
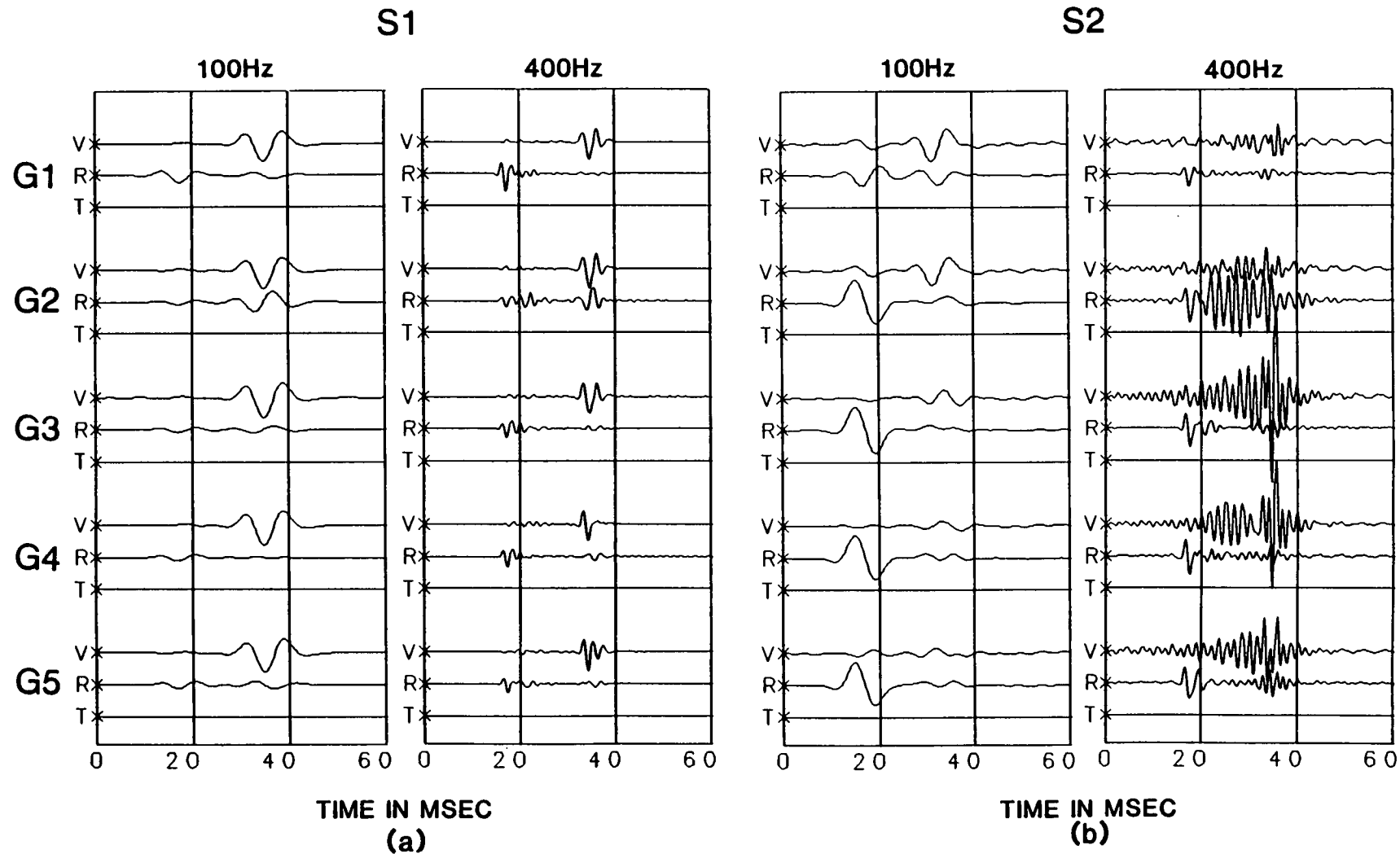
Figure 6.6 Synthetic seismograms for the crack-controlled channel of Figure 6.2 from an explosive point source with two different source positions: **(a)** source outside the channel (S1); and **(b)** source inside the channel (S2).

that vertical components of the three geophones inside the channel receive much stronger energy (2 - 4 times higher amplitudes) than the radial components. This phenomenon is very simliar to the observed records in Figure 6.4. However, the dominant energy of the guided-waves received in the geophone G2 (inside the fracture C1) is in the radial component. This is because only compressive wave motion can propagate in and near the fluid-filled fracture. The first arrivals of seismograms of Figure 6.6 vary with source frequency. This perhaps is due to the interference of direct-waves, reflected-waves, and guided-waves with different frequencies. This feature appears to be characteristic of some of the hydraulic fracturing downwell records (Figure 6.4).

Figure 6.7 shows the synthetic seismograms excited by a shear-wave source with polarization of *SH45°SV* (a shear-wave having equal amplitudes of *SH* and *SV*-waves with 45° polarization angle) in S2 position (within the channel), with two dominant frequencies 100 and 400Hz. The seismograms display different behaviour in comparison with Figure 6.6(b). Most of energy of the seismic waves in Figure 6.7 is trapped inside the channel by two liquid-filled fractures. The channel acts like a resonator to the seismic waves polarized in transverse direction (*SH* component), and no energy in the transverse component will be leaked out from the channel. Therefore, Figure 6.7 shows extrordinarily complicated wavesforms. At high frequency (say, 400Hz in Figure 6.7), the dominant energy of guided-waves is concentrated on the transverse components of the four geophones inside the channel. The seismograms also display strong interferences with different modes for different frequencies along the whole time axis. This phenomenon agrees with the theoretical dispersion curves of Figure 6.3.

S2
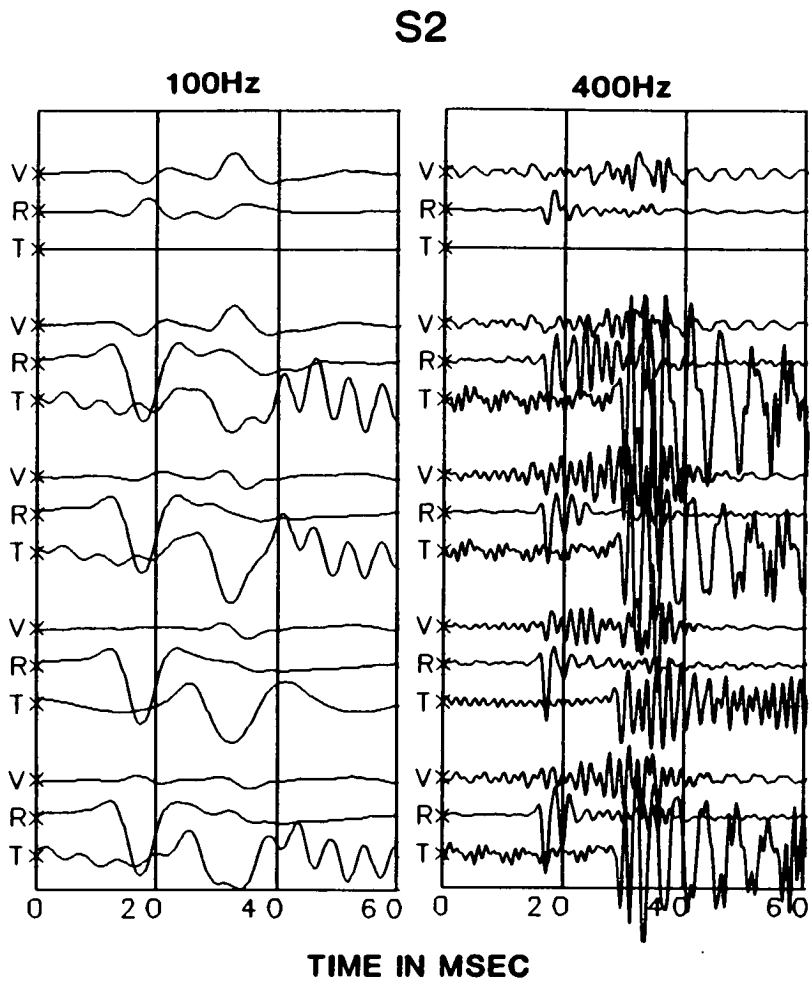
Figure 6.7 Synthetic seismograms for the crack-controlled channel of Figure 6.2 from a shear-wave point source with orientation *SH45°SV* with the source inside the channel (S2).

The behaviour of seismograms of both Figures 6.6 and 6.7 varies significantly with source type, source frequency, and geophone/source position. To obtain strong guided-waves in a crack-controlled channel, it usually requires that both sources and geophones are located inside the channel, with appropriate source types and source frequency.

6.3 GUIDED-WAVES IN A FAULT ZONE

6.3.1 A FAULT-ZONE WAVEGUIDE MODEL

A highly-fractured fault zone usaully has low seismic velocity relative to their surrounding rocks. Therefore, the fault zone together with its hall and foot wall rocks may form a low-velocity waveguide. Stierman and Kovach (1979) studied their logging results obtained from a 600m borehole in the flank of the San Andreas fault at Stone Canyon, California, and comfirmed an existance of such low-velocity zone in the fault zone. Many other studies of fault zones by using seismic methods have also shown such low-velocity fault zone (For example, Healy and Peake 1975, Aki and Lee 1976, Mooney and Luetgert 1982, Feng and Mc Evilly 1983, Cormier and Spudich 1984, Leary and Henyey 1985, and Mereu 1986).

Li *et al* (1990) have observed *SH* and *P-SV* type trapped modes in an active normal fault zone at Oroville, California in borehole VSP experiments. Figure 6.8 shows the layout of the borehole VSP survey at the Oroville normal fault zone, and Figure 6.9 shows the schematic fault-zone model (after Li *et al*. 1990). The model parameters are given in Table 6.2. The model is composed of a highly fractured fault zone (crack density CD = 0.08) with a thickness of 28m, a
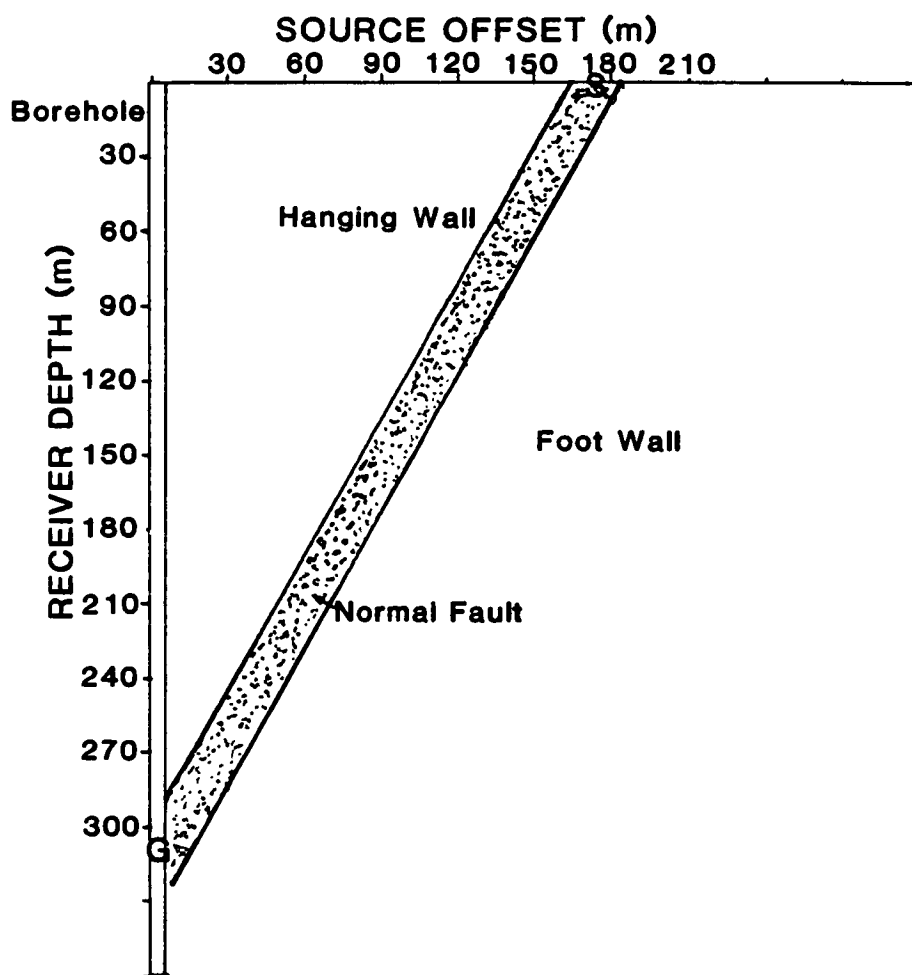
Figure 6.8 The layout of a borehole VSP survey at the normal fault zone, Oroville, California (after Li *et al* 1990).

HANGING WALL

32 m — TRANSITION ZONE

28 m — FAULT

FOOT WALL
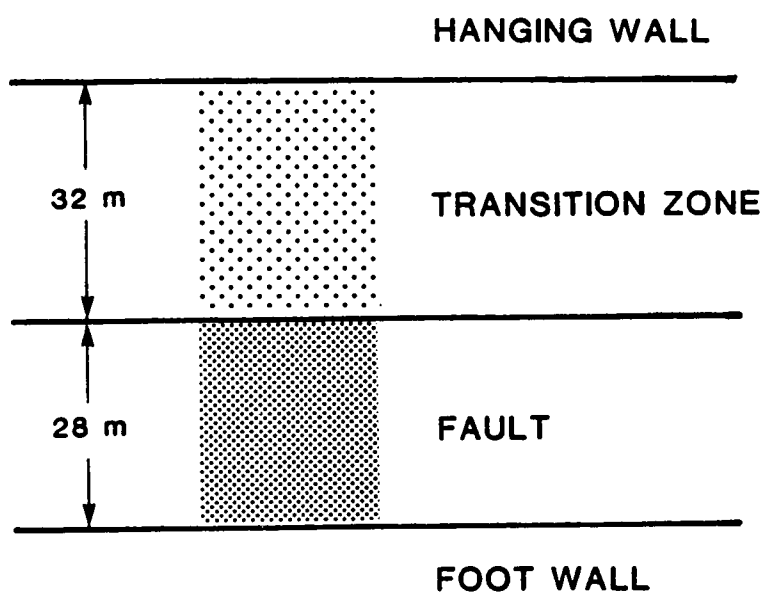
Figure 6.9 The schemetic fault-zone model as a waveguide. The parameters of materials in the model are given in Table 6.2.

Table 6.2 The parameters of uncracked matrix
for the fault-zone waveguide model.

	thickness (m)	Vp (m/s)	Vs (m/s)	ρ (g/cm^3)
Hanging wall	∞	3600	2100	2.50
Transition zone	25	3300	1900	2.50
Fault	18	2900	1700	2.50
Foot wall	∞	3600	2100	2.50

mildly fractured transition zone (CD = 0.04) with thickness 32m overlying the fault-zone and two slightly fractured halfspaces (hanging wall and foot wall). The hanging wall and foot wall are assumed to be isotropic.

Figure 6.10 shows the phase-velocity (solid lines) and group-velocity (dashed lines) dispersion curves for the fundamental and second Rayleigh type, and fundamental and second Love type modes of guided-waves, respectively. The direction of propagation of guided-waves is along the strike of aligned fractures. So the *Generalized* modes of guided-waves in an anisotropic medium are decomposed into pure Rayleigh and pure Love modes. Figure 6.11 shows the amplitude/depth distribution curves at 40Hz frequency. The dispersion and amplitude distribution curves show that the fault zone starts to act as a waveguide when source frequency is about 10Hz, and at 40Hz most energy of fundamental modes of guided-waves will be trapped in the fault zone.

6.3.2 OBSERVATIONAL EVIDENCES

In the VSP survey in the Oroville borehole, a three-component orientated sonde was deployed in the borehole depth interval 90 - 305m in the hanging wall of the fault, and a vertical impact source was applied on the surface along a survey line from the wellhead perpendicular to the fault surface trace (Li *et al*. 1990). Figure 6.12 shows the seismograms recorded by the horizontal geophones oriented parallel to the fault trace (*SH* components) (after Li *et al*. 1990). Figure 6.12(a) is a common receiver gather with a fixed receiver at depth of 296m for several source locations at 150 to 196m. The trapped *SH*-type waves are conspicuously recorded within
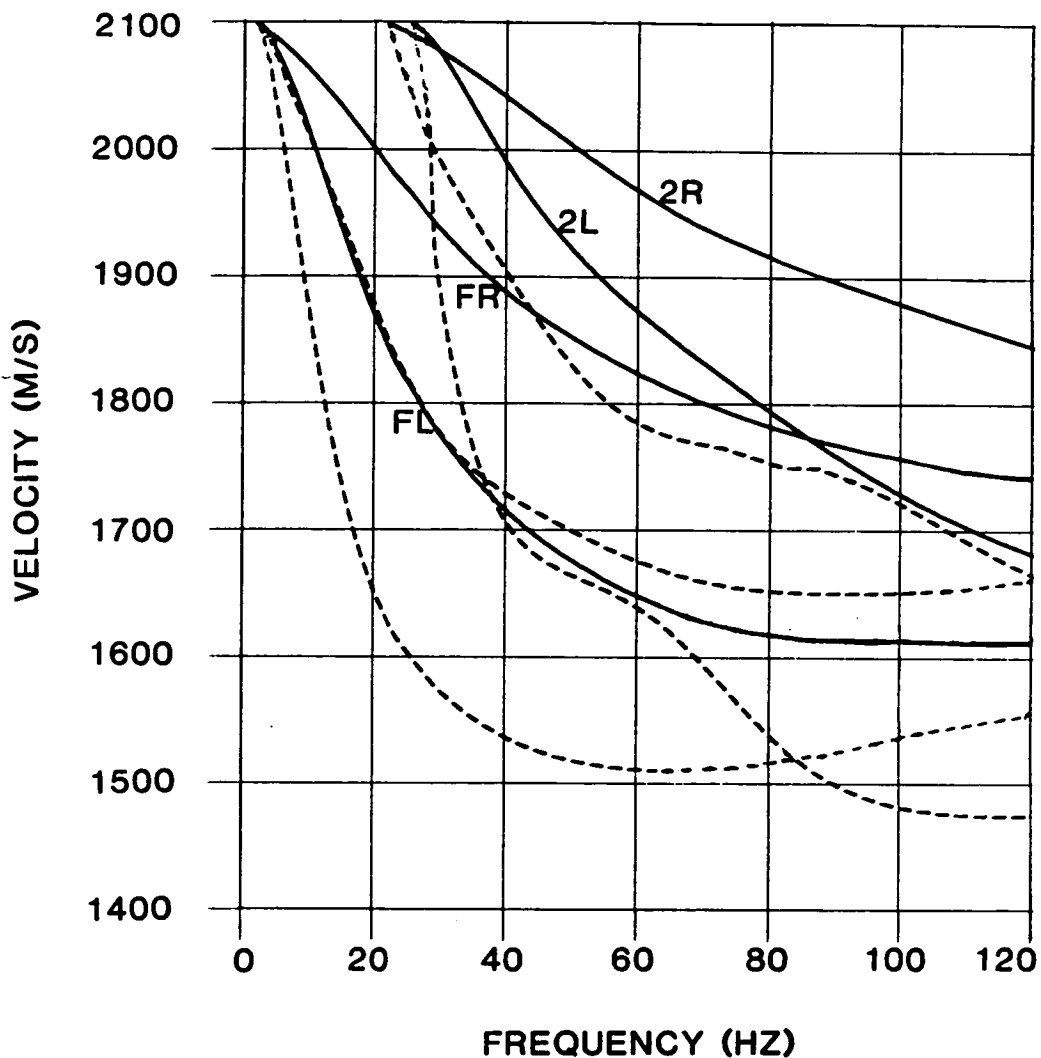
Figure 6.10 The theoretical dispersion curves of guided-waves for the fault-zone waveguide model of Figure 6.9. The solid lines are phase-velocity, and dashed lines are group-velocity: *FR*, and *2R* - Fundamental and Second Rayleigh modes; *FL*, and *2L* - Fundamental and Second Love modes.

FUNDAMENTAL LOVE

SECOND LOVE

TRANSVERSE

32m

28m

TRANSVERSE

32m

28m

FUNDAMENTAL RAYLEIGH

SECOND RAYLEIGH

VERTICAL

32m

28m

RADIAL

32m

28m

VERTICAL

32m

28m

RADIAL

32m

28m
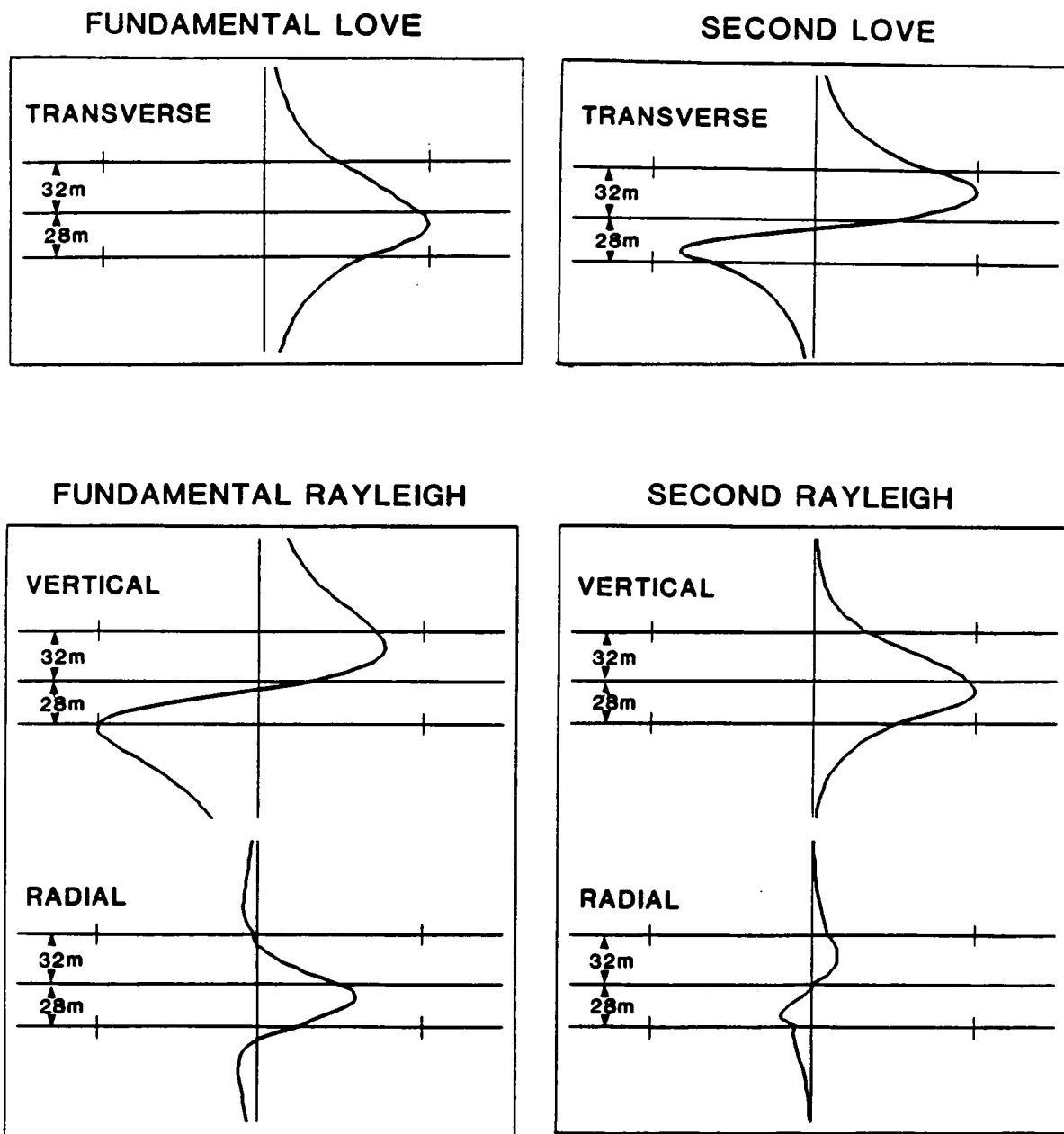
Figure 6.11 The ampliltude/depth distributions of Fundamental and Second modes of both Rayleigh and Love guided-waves for the fault-zone waveguide of Figure 6.9 at 40Hz frequency.

Figure 6.12 The seismograms recorded by *SH* components in the VSP
survey in the Oroville borehole: (a) A common receiver gather with
a fixed receiver at depth of 296m for a range of source offsets from
wellhead across the fault (150 - 196m). SH body-waves and trapped
modes are marked by circular bracket and square bracket,
respectively. The peak-to-peak amplitudes of trapped modes are
donated by solid bars on the right to the seismograms; (b) A common
source gather with the source located at the center of the surface
fault trace with 173m offset from the wellhead, and for five
receiver depths from 270 -305m in the hanging wall of the fault
(after Li *et al* 1990).
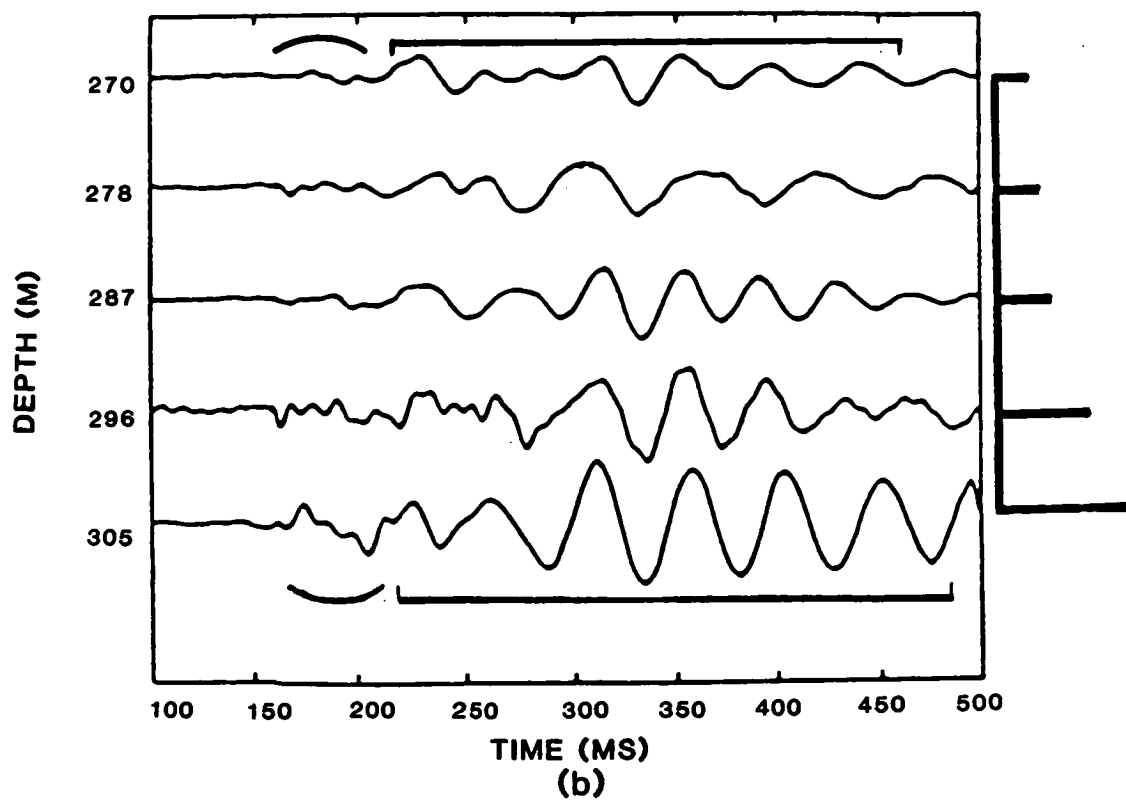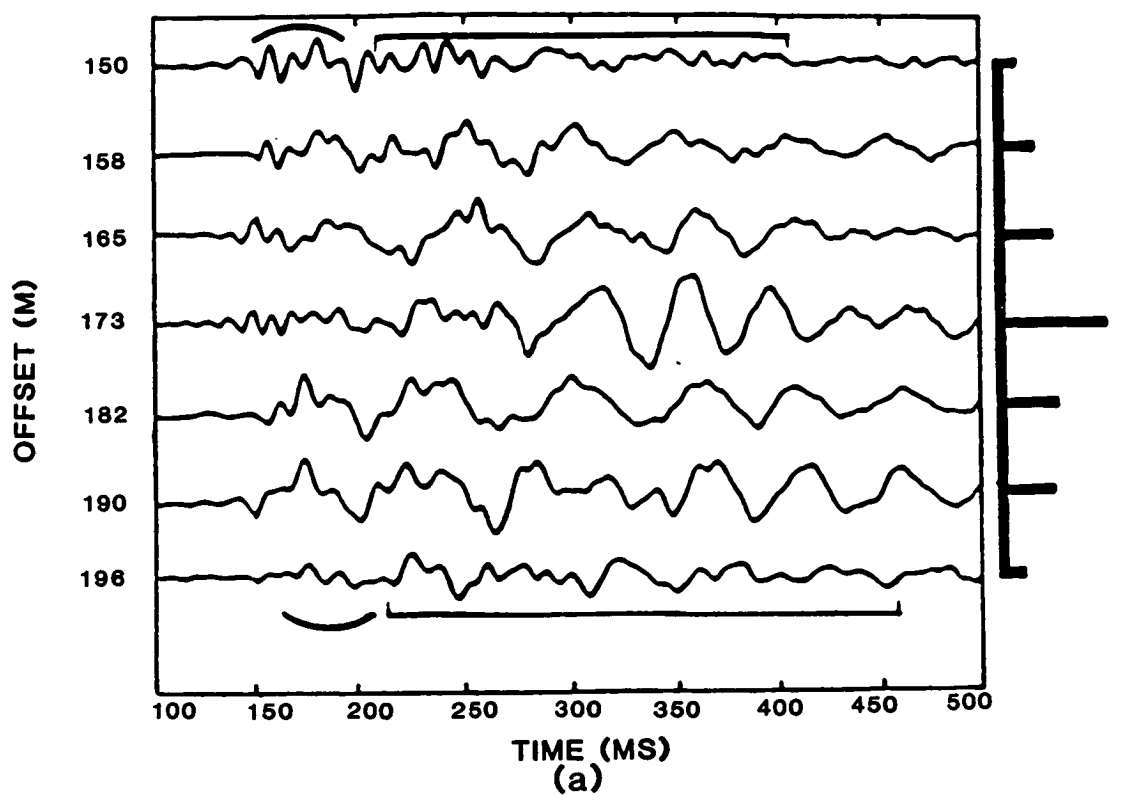
Figure 6.12

the offset range across the surface trace of the fault zone at 158 - 190m, and those periodic trapped wavetrains (in square bracket) appeared following *SH*-waves (in circular bracket) have maximum amplitudes when source position is at the center of the fault surface trace. The peak-to-peak amplitudes of trapped modes are donated by solid bars on the right to the seismograms. Figure 6.12(b) shows *SH*-components of seismograms for a common source (located at the center of the surface fault trace with 173m offset from the wellhead) and for five receiver depths from 270 to 305m in the hanging wall of the fault. Again the maximum amplitude is recorded by the geophone near to the fault and decreased as a function of the distance from the fault zone. The trapped wavetrains of Figure 6.12 show dispersion with frequency increasing from 20 Hz at the begining to 32Hz near the end (Li 1988), which is expected from the theortectical dispersion curves.

6.3.3 SYNTHETIC SEISMOGRAMS

Based on the fault model in Figure 6.8, and model parameters in Table 6.2, we have calculated the *SH*-component synthetic seismograms of *SH* waves with the same source/geophone positions as Figure 6.12(b). The dominant frequency of source is 40Hz, and source pulse function is $F(t) = exp(\omega t/d) \sin (\omega t)$, where $\omega = 2\pi f$, $f = 40Hz$, and $d = 5$. The synthetic seismograms (Figure 4.13) basically match the oberserved records (Figure 4.12(b)) in their arrival times, amplitude distribution, and dispersive behaviour. This is consistent with the model structure and model parameters of the fault zone shown in Figure 6.8.

6.4 CONCLUSIONS

We have modelled the propagation of the guided-waves in two particular waveguides: a crack-controlled channel, and an active fault zone. For the crack-controlled channel (or waveguide), we have presented a formulation to determine the dispersion relation of *SH* type guided-waves (Appendix B). Both the observation and the synthetics in a crack-controlled channel show complicated waveforms, as a result of the interference of different wave types and different modes of guided-waves.

The propagation of guided-waves in a crack-controlled channel is essentially controlled by the geometry and space distribution of fractures, the study of such guided-waves should be helpful for monitoring the hydraulic fracturing operations of a geothermal or hydrocarbon reservoir.

The dispersion and synthetic seismogram calculations comfirm the waveguide model structure and material parameters of an active normal fault-zone at Oroville, California, which was observed by Li *et al*. (1990). The observation and study of such guided-waves may be particular useful for delimitating a fault zone, and monitoring the stress and fracture development inside an active fault-zone.

Our study is very preliminary. Furthur study is required to understand the effects of different fracture system and different crack distribution in the crack-controlled channel or a fault zone on the excitation and propagation of guided-waves.

CHAPTER 7

CONCLUSIONS AND FUTURE WORK

7.1 MAIN RESULTS OF THIS THESIS

We have developed the techniques to calculate dispersion,
three-dimensional amplitude/depth distribution, and synthetic
seismograms of guided-waves in multilayered anisotropic media
(Chapter 2). Using the developed techniques, we have studied the
propagation behaviours of guided-waves in crack-induced anisotropic
waveguides. Our studies have shown that: (a) almost any interface,
or combination of interafces will support some forms of guided-waves,
and thin-layered sedimentary reservoirs may act as waveguides in
crosshole seismic surveys, if signals at appropriate frequencies,
amplitudes, and polarizations can be generated in one well and
recorded at appropriate levels in neighbouring wells; (b) in
crack-induced anisotropic waveguides, the distinct families of
Rayleigh and Love modes of guided-waves in isotropic waveguides
combine into a single family of *Generalized* modes with
three-dimensional elliptical particle motions; and (c) guided-waves
are very sensitive to the internal properties and geometry of
waveguide, and such guided-waves characteristics may vary
substantially with crack or pore orientations, crack densities, crack
or pore saturations, and crack aspect ratios (Chapter 3).

Guided-waves have been clearly identified from crosshole datasets

at the Conoco Borehole Test Facility (CBTF) by analysing their
amplitude distributions, dispersion characteristics, and 3-D
polarization diagrams (Chapter 4). In many circumstances,
guided-waves have dominant energy in crosshole seismic data. The
propagation of guided-waves is dominated by the continuity and
structure of waveguide. The dispersion and waveforms of guided-waves
carry detailed information about the internal structure, particularly
the stress-aligned structure of fluid-filled inclusions in the
immediate neighbourhood of the waveguide. We have demonstrated with
synthetic seismograms that such guided-waves in crosshole surveys
have two important applications: continuity tests of plane-layered
reservoirs; and moinitoring Enhanced Oil Recovery (EOR) operations
for thin-layered sedimentary reservoirs (Chapter 5).

Finally, we have modelled the propagation of guided-waves in two
special waveguides: a crack-controlled channel, which may be formed
in hydraulic fracturing in geothermal reserviors; and an active
fault zone. Study of such guided-waves is useful for understanding
the fracture structure and distribution in geothermal reservoirs, and
for delimitating fault-zones or mointoring the stress and fracture
accumulation and development inside an active fault zone (Chapter 6).

7.2 DISCUSSION, AND SUGGESTIONS FOR FUTURE WORK

7.2.1 INTERPRETATIVE TECHNIQUES OF GUIDED-WAVES

We have demonstrated the potential value of guided-waves in
characterizing sedimentary reservoirs and monitoring EOR operations
by crosshole surveys. However, the necessary interpretative
techniques for guided-waves in anisotropic structures should be

developed.

One possible interpretative technique is anisotropic dispersion
inversion of guided-waves (see Chapter 3). Mitchell (1984) has
discussed the anisotropic dispersion inversion for surface-waves.
The dispersion inversion procedures for guided-waves or surface-waves
have appeared in the literature, but they are not strictly valid in
anisotropic media, where guided-waves or surface-waves do not, in
general, seperate into two independent families of Rayleigh and Love
modes but instead form a family of *Generalized* modes having
three-dimensional particle motions. Formal dispersion inversion of
guided-waves for anisotropic structures would be difficult, because
of the large number of elastic constants to be estimated, and the
comprehensive computation. However, we can place some constraints on
possible interpretations for the guided-waves recorded during
reservoir production processes, where observations from repeated
source and geophone locations may only show some changes in temporal
behaviour. From the observation data, we can extract group-velocity
dispersion by using multiple filter technique (see Appendix A).
Given an anisotropic reservoir waveguide model, we can calculate the
theoretical group-velocity dispersion curves for different crack
parameters (crack strike, crack saturation, crack content, etc), if
the thickness, and isotropic matrix parameters of the waveguide had
been determined by well logs. By minimizing the least square error
between observed and theoretical group-velocity dispersion series, we
can obtain the reasonable crack parameters to characterize the
reservoirs.

The Edinburgh Anisotropy Project (EAP) of the British Geological
Survey has developed several techniques for anisotropic parameters

inversion from shear-waves by using dataset (MacBeth 1991a, b). It mignt be possible to adapt these techniques to guided-waves interpretations. In particular, the polarization inversion of guided-waves may be more attractive, since polarization motion of guided-wave provides some diagnostic information on anisotropic properties of waveguides.

7.2.2 ATTENUATION

We have not yet considered the effects of attenuation on propagation of guided-waves in the thesis. Seismic attenuation is a fundamental phenomenon in seismic wave propagation. Many mechanisms for seismic attenuation have been presented so far, but one common feature is that almost all of them assign the major cause of attenuation to the presence of cracks, fractures, or pores in rocks. Attenuation may be caused by scattering at the faces of cracks or pores, bubble movements in partially saturated cracks, liquid squirting in fully saturated cracks, and friction in thin cracks and along grain boundaries (Toksöz and Johnston 1981). Most systems of cracks in the crust display some alignments, and such aligned cracks will result in velocity anisotropy and attenuation anisotropy. Crampin and Lovell (1991) suggested that there is a reciprocal relationship between velocity anisotropy and attenuation anisotropy: In directions where the velocity is relatively high, the attenuation is relative low, and in directions where the velocity is low the attenuation is high. Differential seismic wave attenuation may also give information about crack alignments, crack contents, viscosity of crack fluid, and degree saturation of cracks in rocks.

Attenuation will also have significant effects on propagation of

guided-waves. Buchannan (1978) has studied the attenuation of Love channel-waves in isotropic coal-seam by using complex Lamé constant. The Quality factor Q of coal-seam may vary between 20 and 60. The attenuation of channel-waves usually holds a linear relation with frequency in most coal-seams (Buchanan *et al.* 1983). There may be a similar relation in other waveguides. The introduction of attenuation will inevitably lead to dispersion in seismic waveforms. The dispersion due to attenuation, and due to layered structures or interfaces which we have studied in this thesis, is likely to be coupled together. Their relationship needs to be studied. We may replace the elastic tensors in the wave equations of Chapter 2 with complex constants, to study the effects of attenuation caused by aligned cracks on propagation of guided-waves. However, the validity of calculating the dispersion of guided-waves for the materials having complex elastic constants needs to be tested in the future.

Introducing attenuation will improve the dispersion inversion of guided-waves, and waveforms match of synthetics to observations (Chapter 4). The study of attenuation can also help us to decide the maximum distance that guided-waves could propagate for a given layered structure in crosshole surveys. The attenuation of guided-waves may also carry important information of cracks and crack contents inside waveguides. If we have high quality measurements, the attenuation inversion of guided-waves may also be possible.

7.2.3 LATERALLY INHOMOGENEOUS WAVEGUIDES

The existing techniques in Chapter 2 are not directly applicable to structures where the properties or conditions of rocks are changing in horizontal directions. Laterally inhomogeneous waveguide

structures can often be found in many crosshole seismic surveys, for example, faults or vertical discountinuities, the movement of injected gas and chemical or heat flood front during EOR operations. The study of propagation of guided-waves in such laterally inhomogeneous waveguide structures is particularly important to exploit applications of guided-waves in monitoring EOR operations. Guided-waves are in many aspects similar to surface-waves, which have been extensively studied by seismologists. It may be possible to adapt techniques developed for surface-waves in laterally varying inhomogeneous rocks to studying guided-waves in crosshole surveys (Crampin, personal communications).

There are two types of laterally inhomogeneous structures which have been successfully treated in surface-wave propagation studies (Keilis-Borok 1989). The first type of structure is where there are smooth changes of properties in a horizontal direction. This allows us to model the wavefields with the ray-mode approach which describes the propagation of each mode by asymptotic two-dimensional ray theory. This technique neglects such effects as possible mode-to-mode conversions or scattering of the surface-wave energy. The second type of structure is when there is an abrupt vertical or near vertical discontinuities between the source and receiver. There are two approaches to study the surface-waves in this kind of structures: The Born scattering technique (Snieder 1988, Snieder and Romanowicz 1988, Romanowicz and Snieder 1988), and the approximate methods developed by Levshin (1984, 1985) for calculating reflection and transmission coefficients of surface-waves in isotropic structures. Application of these various techniques to modelling guided-waves requires adapting existing algorithms for surface-waves due to the change in boundary conditions.

There are other more sophisticated methods to directly study the propagation of guided-waves in laterally varying media. Kennett (1984) used the coupled-mode technique to calculate the modulus of the modal reflection and tramsmisssion coefficients for diffrent modes and frequencies in heterogeneous zone of a waveguide. Its and Yarovoy (1986) used Green's function and a superpositions of plane homogeneous and inhomgeneous body-waves to calculate transmission and reflection coefficients of Love guided-waves for a waveguide containing a vertical fault. However, their techniques have not yet applied to anisotropic structures.

Other numerical methods like finite difference, and finite element techniques may be required to calculate synthetic seismograms of guided-waves which allow smooth lateral and radial variation of properties to be inclued.

7.2.4 FIELD DATA EXAMINATION

In Chapter 4, we have studied the propagation of guided-waves in a shallow crosshole field survey. What we need now is the examination of more field data from crosshole surveys in sedimentary reservoir areas, especially during EOR operation where there are some changes in saturation and thermal fire or steam front in the reservoirs. Crosshole seismic surveys have already been carried out by many oil companies for P-wave tomography. Such crosshole surveys may be appropriate datesets for guided-wave analysis. We suggest the guided-wave analysis may be an alternative to P-wave tomography, and may provide more detailed information about the internal structure of reservoirs than P-wave tomography can provide.

APPENDIX A

MULTIPLE FILTER TECHNIQUE

The algorithm of multiple-filter analysis was originally developed by Dziewonski *et al* (1969). The analysis procedure can be divided into two steps: first, each seismic trace, $s(t)$, is time windowed, and the arrival time is transformed into group velocity-frequency domain by Fourier transform; second, to seperate arrival times of different frequencies, the trace is filtered using a filter function represented by

$$F_n(\omega) = \exp\{-\alpha[(\omega - \omega_n)/\omega]\}.$$

where ω is the angular frequency, ω_n is the center frequency, and

$$\alpha = \beta/B^2$$

where

$$\beta = \ln[F_n(\omega)/F_n(\omega_{nl})] = \ln[F_n(\omega_n)/F_n(\omega_{nu})],$$

B is the half-bandwidth, and $\omega_{nl} = (1-B)\omega_n$ and $\omega_{nu} = (1+B)\omega_n$ are the lowerband and upperband limits, respectively. This Guassian filter function is practically equivalent to the optimum filter function, a truncated prolate spheroidal wave function of zero order (Slepian, Pollack and Landau 1961). The filtered trace is converted to the time domain $g(t)$, by inversed Fourier transform. The analytic signal associated with the real signal $g(t)$ is

$$g(t) - iq(t),$$

where q(t) is the Hilbert transform of g(t), that is

$$q(t) = -1/\pi \int_{-\infty}^{\infty} [g(\xi)/(t-\xi)] \, d\xi$$

Thus, the instantaneous spectral amplitude A(t) and phase $\phi(t)$ are defined by

$$A(t) = [\, g^2(t) + q^2(t) \,]^{\frac{1}{2}},$$

and

$$\phi(t) = \tan^{-1} [q(t)/g(t)], \text{ respectively.}$$

The instantaneous spectral amplitudes are normalized with respect to the maximum value, and the results can be ploted as a contour diagram in the frequency and group velocity domain. The ridge crest, or crests, of the contour represents the group-velocity dispersion relationships of the seismic trace s(t).

APPENDIX B

DISPERSION RELATION OF SH TYPE GUIDED-WAVES
IN A CRACK-CONTROLLED CHANNEL

For the crack-controlled channel model as Figure 6.2, the transverse and tangential displacements and stresses on crack-slab interfaces are no longer continuous, the propagator matrix technique in Chapter 2 is not appropriate for calucalation of dispersion of guided-waves in the channel. Here we present a procedure to determine the dispersion relation of *SH* type guided-waves in the crack-controlled channel. We assume the material inside the channel is isotropic.

In the coordinate system shown as Figure B.1, we suppose an incident *SH* plane-wave as

$$U_I = A \cos (\omega t - K_1 x_1 - K_3 x_3)$$

where U_I is the displacement of the incident wave; A is amplitude; K_1 and K_3 are the wave numbers along x_1 and x_3 directions, respectively.

On the plane $x_3 = 0$, the incident wave is totally reflected, and the reflected wave may be written as

$$U_R = - A \cos (\omega t - K_1' x_1 - K_3' x_3)$$
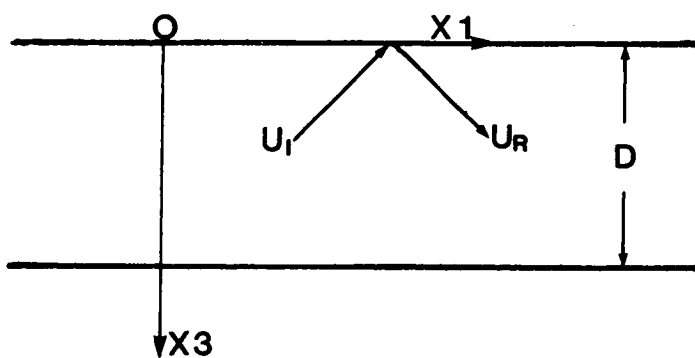
Figure B.1 Co-ordinate system for *SH* type guided-wave dispersion calculation in the crack-controlled channel model of Figure 6.2.

where K_1' and K_3' are wave numbers of the reflected wave.

The resulting wave motion of U_I and U_R is

$$U = 2A \sin \{\omega t - [(K_1 + K_1')/2]x_1 - [(K_3 + K_3')/2]x_3\}$$

$$\sin \{\omega t - [(K_1 - K_1')/2]x_1 - [(K_3 - K_3')/2]x_3\}$$

The U has to vanish everywhere on the plane $x_3 = 0$, and this gives $K_1' = K_1$. To keep the relation

$$K = [K_1^2 + K_3^2]^{\frac{1}{2}} = K' = [K_1^{2\prime} + K_3^{2\prime}]^{\frac{1}{2}} = \omega/v$$

we have $K_3' = \pm K_3$. For a non-vanishing value of U, only is $K_3' = -K_3$ possible.

Therefore

$$U = 2A \sin [\omega t - K_1 x_1] \sin K_3 x_3$$

Similarly, for U to vanish also on the plane $x_3 = D$, it is required that

$$K_3 = n \pi/D \qquad n = 1, 2, 3, \ldots$$

The final expression for U is

$$U = 2A \sin [\omega t - K_1 x_1] \sin n \pi x_1/D$$

which represents a wave propagating along the x_1 axis between the

boundary planes $x_3 = 0$ and $x_3 = D$. Its phase-velocity $c = \omega/K_l$ is higher than $v = \omega/K$ -velocity of the incident wave. To every value of the integer n, there corresponds a mode. The nth mode has $(n-1)$ equidistant nodal planes, parallel and between the two interface planes.

The phase-velocicty dispersion relation (c, f) of *SH* type guided-waves in the channel is given by

$$c = 2D \; vf / [(2D \; f)^2 + (nv)^2]^{\frac{1}{2}}.$$

The smallest possible value π/D of K corresponds to the minimum frequency $f_c = v/2D$, which is called the cut-off frequency. This means guided-waves can only propagate with frequencies above the cut-off frequency f_c in the crack-controlled channel. For the waves with frequencies less than f_c, the wave number K_3 is imaginary and the wave is absorbed on entering the guide.

By differentiating the phase-velocity with frequencies, we will obtain the group-velocity dispersion of the *SH* type guided-waves, that is

$$c_g = \partial\omega/\partial K_l = D \; vK_l \, [(D \; K_l)^2 + (n\pi)^2]^{\frac{1}{2}}.$$

Therefore, the product of phase-velocity and group-velocity

$$cc_g = v$$

is a constant.

REFERENCES

Aki, K. and Lee, W.H.K., 1976. Determination of three-dimensional velocity anomalies under a seismic array using first P arrival times from local earthquakes, 1. A homogeneous initial model. *J. Geophys. Res.*, 23, 4381-4399.

Aki, K. and Richards, P.G., 1980. *Quantitative Seismology, Theory and Method*, Freeman, San Francisco

Aki, K., Fehler, M., Aamodt, R.L., Albright, J.N., Potter, R.M., Pearson, V.M. and Tester, J.W., 1982. Interpretation of seismic data from hydraulic fracturing experiments at the Fenton Hill, New Mexico hot dry rock geothermal site, *J. Geophys. Res.*, 87, 936-944.

Alford, R. M., 1986. Shear wave data in the presence of azimuthal anisotropy: Dilley, Texas, *Expanded Abstracts, 56th Ann. Int. SEG Meeting, 1986, Houston*, 476-479.

Avé Lallemant, H.G. and Carter, N.L., 1970. Syntectonic recrystallization of olivine and modes of flow in the upper mantle, *Bull. Geol. Soc. Am*, 81, 2203-2220.

Babuska, V., 1984. *P*-wave velocity anisotropy in crystalline rocks, *Geophys. J. R. astr. Soc.*, 76, 113-119.

Banik, N.C., 1984. Velocity anisotropy of shales and depth estimation in the North Sea Basin, *Geophysics*, 49, 1411-1419.

Booth, D.C., 1982. *The anisotropic reflectivity technique*, PhD Thesis, University of Edinburgh.

Booth, D.C. and Crampin, S., 1983a. The anisotropic reflectivity technique: theory, *Geophys. J. R. astr. Soc.*, 72, 755-766.

Booth, D.C. and Crampin, S., 1983b. The anisotropic reflectivity technique: anomalous arrivals from an anisotropic upper-mantle, *Geophys. J. R. astr. Soc.*, 72, 767-782.

Booth, D.C., Crampin, S., Evans, R. and Roberts, G., 1985. Shear-wave polrarizations near the North Anatolian Fault- I. Evidence for anisotropy-induced shear-wave splitting, *Geophys. J. R. astr. Soc.*, 83, 61-73.

Booth, D.C., Crampin, S., Lovell, J.H. and Chiu, J.M., 1990. Temporal changes in shear-wave splitting during an earthquake swarm in Arkansas, *J. Geophys. Res.*, 95, 11 151-11 164.

Brodov, L. U., Tikhonov, A. A., Chesnokov, E. M., Tertychnyi, V. V. and Zatsepin, S. V., 1991. Estimating physical parameters of crack-porous reservoirs by inverting shear-wave splitting, *Geophys. J. Int.*, 107, 429-432.

Buchanan, D.J., 1978. The propagation of attenuated SH channel waves, *Geophys. Prosp.*, 17, 17-28.

Buchanan, D.J., 1983. *Developments in Geophysical Exploration Methods*, Vol 5., Applied Science Publishers, 1-34.

Buchanan, D.J., 1987. Dispersion calculations for *SH* and *P-SV* waves in multilayered coal seams, *Geophys. Prosp.*, 35, 62-70.

Buchanan, D.J., Davis, R., Jackson, P.J. and Taylor, P.M., 1981. Fault location by channel wave seismology in United Kingdom coal seams, *Geophysics*, 46, 994-1002.

Buchanan, D.J., Jackson, P.J. and Davis, R., 1983. Attenuation and anisotropy of channel waves in coal seams, *Geophysics*, 48, 133-147

Buchbinder, G.G.R., 1985. Shear-wave splitting and anisotropy in Charlevoix seismic zone, Quebec, *Geophys. Res. Lett.*, 12, 425-428.

Budiansky, B. and O' Connell, R.J., 1976. Elastic moduli of a cracked solid, *Int. J. solid Struct.*, 12, 81-97.

Bush, I., 1990. *Modelling shear-wave anisotropy in the Paris Basin*, PhD Thesis, University of Edinburgh.

Bush, I. and Crampin, S., 1991. Paris Basin VSPs: case history establishing combinations of fine-layer (or lithologic) anisotropy and crack anisotropy from modelling shear wavefileds near point singularities, *Geophys. J. Int.*, 107, 433-447.

Cerveny, V. and Psencik, I., 1972. Rays and travel-time curves in inhomogeneous anisotropic media, *Geophysics*, 38, 565-567.

Chapman, C.H. and Shearer, P.M., 1989. Ray tracing in azimuthally anisotropic media - II: Quasi-shear wave coupling, *Geophys. J.* 96, 65-83.

Christensen, N.I. and Salisbury, M.H., 1979. Seismic anisotropy in the oceanic upper mantle: evidence from the Bay of Islands ophiolite complex, *J. Geophys. Res.*, 84, 4601-4610.

Cliet, C., Brodov, L., Tikhonov, A., Martin, D. and Michon, D., 1991. Anisotropy survey for reservoir description, *Geophys. J. Int.*, 107, 417-427.

Comier, V.F. and Spudich, P., 1984. Amplification of ground motion and waveform complexity in fault zones: Examples from the San Andreas and Calaveras faults, *Geophys. J. Roy. astr. Soc.*, 79, 135-152.

Crampin, S., 1970. The dispersion of surface wave in multilayered anisotropic media, *Geophys. J. R. astr. Soc.*, 21, 387-402.

Crampin, S., 1975. Distinctive particle motion of surface waves as a diagnostic of anisotropic layering, *Geophys. J. Roy. astr. Soc.*, 40, 177-186.

Crampin, S., 1977. A review of the effects of anisotropic layering on the propagation of seismic waves, *Geophys. J. R. astr. Soc.*, 49, 177-186.

Crampin, S., 1978. Seismic wave propagation through a cracked solid: polarization as a possible dilatancy diagnostic, *Geophys. J. R. astr. Soc.*, 53, 467-496.

Crampin, S., 1981. A review of wave motion in anisotropic and crack elastic- media, *Wave Motion*, 3, 343-391.

Crampin, S., 1984a. Anisotropy in exploration seismics, *First Break*, 2, 19-21.

Crampin, S., 1984b. Effective elastic-constants for wave propagation in cracked solids, *Geophys. J. R. astr. Soc.*, 76, 135-145.

Crampin, S., 1985. Evidence for aligned cracks in the Earth's crust, *First Break*, 3, 12-15.

Crampin, S., 1986. Anisotropy and transverse isotropy, *Geophys. Prosp.*, 34, 94-99.

Crampin, S., 1987. Geological and industrial implications of extensive-dilatancy anisotropy, *Nature*, 328, 491-496.

Crampin, S., 1989. Suggestions for a consistent terminology for seismic anisotropy, *Geophys. Prosp.*, 37, 753-770.

Crampin, S., 1990. The potential of shear-wave VSPs for monitoring recovery: a letter to management, *The Leading Edge*, 9, 3, 50-52.

Crampin, S., 1991. Effects of point singularities on shear-wave propagation in sedimentary basins, *Geophys. J. Int.*, 107, 531-543.

Crampin, S. and Booth, D.C., 1989. Shear-wave splitting showing hydraulic dilatation of pre-existing joints in granite, *Sci. Drilling*, 1, 21-26.

Crampin, S. and King, D.W., 1977. Evidence for anisotropy in the upper mantle beneath Eurasia from the polaraization of higher mode seismic surface waves, *Geophys. J. R. astr. Soc.*, 49, 59-85.

Crampin, S. and Taylor, D.B., 1971. The propagation of surface waves in anisotropic media, *Geophys. J. R. astr. Soc.*, 25, 71-87.

Crampin, S. and Lovell. J.H., 1991. A decade of shear-wave splitting in the Earth's crust: what does it mean? what use can we make of it? and what should we do next? *Geophys. J. Int.*, 107, 387-407.

Crampin, S., Booth, D.C., Evans, R., Peacock, S. and Fletcher, J.B., 1990. Changes in shear wave splitting at Anza near the time of the North Palm Springs Earthquake, *J. geophys. Res.*, 95, 11 197-11 212.

Crampin, S., Booth, D. C., Krasnova, M. A., Chesnokov, E. M., Maximov, A. B. and Tarasov, N. T., 1986b. Shear-wave ploralizations in the Peter and the First Range indicating crack-induced anisotropy in a thrust-fault regime, *Geophys. J. R. astr. Soc.*, 84, 401-412.

Crampin, S., Bush, I., Naville, C. and Taylor, D. B., 1986a.
Estimating the internal structure of reservoirs with shear-wave
VSPs, *The Leading Edge*, 5, 11, 35-39.

Crampin, S., Chesnokov, E.M. and Hipkin, R.A., 1984a. Seismic
anisotropy - the state of the art, II, *Geophys. J. R. astr. Soc.*,
76, 1-16.

Crampin, S., Evans, R. and Atkinson, B.K., 1984b. Earthquake
prediction: a new physical basis, *Geophys. J. Int.*, 76, 147-156.

Crampin, S., Evans, R. and Üçer, B., 1985. Analysis of records of
local earthquakes: the Turkish Dilatancy Projects (TDP1 and TDP2),
Geophys. J. R. astr. Soc., 83, 31-45.

Crampin, S., Evans, R., Üçer, B., Doyle, M., Davis, J.P., Yegorkina,
G.V. and Miller, A., 1980. Observations of dilatancy-induced
polarization anomalies and earthquake prediction, *Nature*, 286,
874-877.

Cremer, G.M.(editor), 1981. Hot dry rock geothermal energy
development program: annual report: fiscal year 1980, *University
of California, Los Alamos National Laboratory, (LA-8855-HDR.
UC-66a)*.

Dahlen, F.A., 1972. Elastic velocity anisotropy in the presence
of an anisotropic initial stress, *Bull. seism Soc. Am.*, 62,
1183-1193.

Davis, E.E. and Clowes, R.M., 1986. High velocities and seismic
anisotropy in Pleistocene turbidetes off Western Canada, *Geophys.
J. R. astr. Soc.*, 84, 381-399.

Davis, T. L. and Lewis, C., 1990. Reservoir characterization by 3-D,
3-C seismic imaging, Silo Field, Wyoming, *The Leading Edge*, 9, 11,
22-25.

Dieulesain, E. and Royer, D., 1980. *Elastic waves in solids.* in
French, by Masson & Cie, Editeurs, Paris, translated by Wiley,
New York.

Domenico, S.N., 1974. Effect of water saturation on seismic
reflectivity of sand reservoirs encased in shale, *Geophysics*, 39,
759-769

Douma, J., 1988. The effect of the aspcet ratio on crack-induced
anisotropy, *Geophy. Prosp.*, 36, 614-632.

Duff, G.F.D., 1960. The Cauchy problem for elastic wave propagation
in anisotropic media, *Phil. Trans. R. Soc.*, A, 252, 249-273.

Dutta, N.C. ann Odé, H., 1983. Seismic reflections from a gas-water
contact, *Geophysics*, 48, 148-162

Dziewonski, A., Bloch, S. and Landisman, M., 1969. A technique for
the analysis of transient seismic signals, *Bull.seism Soc.Am*, 59,
427-444.

Eshelby, J. D., 1957. The detemination of the elastic field of an ellipsoidal inclusion, and related problems: *Proc. Roy. Soc. London, Ser. A,* **241,** 376-396.

Evans, R., Beamish, D., Crampin, S. and Üçer, S.B., 1987. The Turkish Dilatancy Project (TDP3): multidisciplinary studies of a potential earthquake source region, *Geophys. J. R. astr. Soc.* , **91,** 265-286.

Evison, F.F., 1955. A coal seam as a guide for seismic energy, *Nature,* **176,** 1224-1225.

Feng, R. and McEvilly, T.V., 1983. Interpretation of seismic reflection profiling data for the structure of the San Andreas Fault Zone, *Bull. seism Soc. Am* , **73,** 1701-1702.

Fehler, M., 1981. Changes in *P* wave velocity during operation of a hot dry rock geothermal system, *J. Geophys. Res.,* **86,** 2925-2928.

Fehler, M., 1982, Interaction of seismic waves with a viscous liquid layer, *Bull. seism Soc. Am* , **72,** 55-72.

Ferrazzini, V. and Aki, K., 1987. Slow waves trapped in a fluid-filled infinite cracks: implication for vocanic tremor, *J. Geophys. Res.* , **92,** 9215-9223.

Forsyth, D.W., 1975. The early structural evolution and anisotropy of the oceanic upper mantle, *Geophys. J. R. astr. Soc.* , **43,** 103-162.

Francis, T.J.G., 1969. Generation of seismic anisotropy in the upper mantle along the mid-ocean ridges, *Nature,* 221, 162-165.

Franssens, G.R., Lagasse, P.E. and Mason, I.M., 1985. Study of the leaking modes of in-seam exploration seismology by means of synthetic seismograms, *Geophysics,* **50,** 414-424.

Fuchs, K., 1983. Recently formed elastic anisotropy and petrological models fro the continental subcrustal lithosphere in southern Germany, *Phys. Earth Planet.Int.,* **31,** 93-118.

Gajewski, D. and Psencik, I., 1987. Computation of high-frequency sesimic wavefileds in 3-D laterally inhomgeneous anisotropic media, *Geophys. J. Roy. astr. Soc.* , **91,** 383-411.

Garbin, H.D. and Knopoff, L., 1973. The compressional modulus of a material permeated by a random distribution of free circular cracks, *Q appl. Math.* , **3,** 453-464.

Garbin, H.D. and Knopoff, L., 1975a. The shear modulus of a material permeated by a random distribution of free circular cracks, *Q appl. Math.* , **33,** 296-300.

Garbin, H.D. and Knopoff, L., 1975b. Elastic moduli of a medium with liquid-filled cracks, *Q appl. Math.* , **33,** 301-303.

Gardner, G.H.F., Gardner, L.W. and Gregory, A.R., 1974. Formation velocity and density- The diagnostic basics for stratigraphic traps, *Geophysics,* **39,** 770-780

Greenhalgh, S.A., Burns, D. and Mason, I., 1986, A cross-hole and face-to-borehole in-seam seismic experiment at the Invincible Colliery, Australia, *Geophys. Prosp.*, 34, 30-55.

Hashin, Z., 1962. The elastic moduli of heterogeneous materials, *J. Appli. Mech.*, 29E, 143-150.

Haskell, N.A., 1953. The dispersion of surface waves in multilayered media, *Bull. Seism Amer.*, 43, 17-34.

Healy, J.H. and Peake, L.G., 1975. Seismic velocity atructure along a section of the San Andreas fault near Bear Valley, California, *Bull. seism Soc. Am*, 65, 1177--1197.

Helbig, K., 1984. Anisotropy and dispersion in periodically layered media, *Geophysics*, 49, 177-211.

Hess, H., 1964, Seismic anisotropy of the uppermost mantle under oceans, *Nature*, 203, 629-631.

Hubbert, M.K. and Willis, D.G., 1957, Mechanics of hydraulic fracturing, *Trans. AIME*, 210, 153-170.

Hudson, J.A., 1980. Overall properties of a cracked solid. *Math. Proc. Camb. phil, Soc.*, 88, 371-384.

Hudson, J.A., 1981. Wave speeds and attenuation of elastic waves in material containing cracks. *Geophys. J. Roy. astr. Soc.*, 64, 133-150.

Hudson, J.A., 1986. A higher order approximation to the wave propagation constants for a cracked solid. *Geophys. J. R. astr. Soc.*, 87, 265-274.

Hudson, J.A., 1988. Seismic wave propagation through material containing partially saturated cracks, *Geophys. J.*, 92, 33-37

Hudson, J.A., 1990. Overall elastic properties of isotropic materials with arbitrary distribution of circular cracks, *Geophys. J. Int.*, 102, 465-469.

Jackson, P.J., 1985. Horizontal seismics in coal seams: its use by the UK coal industry, *First Break*, 3, 15-24

Johnson, T.C., Hamilton, E.C. and Berger, W.H., 1977. Physical properties of calcareous sediments: control by dissolution at depth, *Marine Geol.*, 24, 259-277.

Johnston, D.H., 1986. VSP detection of fracture-induced velocity anisotropy, *Expanded Abstracts, 56th Ann. Int. SEG Meeting, 1986, Houston*, 464-466.

Kaarsberg, E.A., 1960. Elasticity studies of isotropic and anisotropic rock samples, *Trans. Soc. Mn. Engrs.*, 241, 470-475.

Kaneshima, S., 1990. Origin of crustal anisotropy: shear wave splitting studies in Japan, *J. geophys. Res.*, 95, 11 121-11 133.

Kaneshima, S., Ando, M. and Crampin, S., 1987. Shear-wave splitting above small earthquakes in the Kinki District of Japan, *Phys. Earth. planet. Inter.*, **45**, 45-58.

Keilis-Borok, V.I., editor, 1989. *Seismic surface waves in laterally varying inhomogeneous Earth.* Kluwer Acad. Publ., Dordrecht, Boston, London.

Keith, C.M. and Crampin, S. 1977a. Seismic body waves in anisotropic refraction at a plane interface, *Geophys. J. R. astr. Soc.*, **49**, 181-208.

Keith, C.M. and Crampin, S. 1977b. Seismic body waves in anisotropic media: propagation through a layer, *Geophys. J. R. astr. Soc.*, **49**, 209-223.

Keith, C.M. and Crampin, S. 1977c. Seismic body waves in anisotropic media: synthetic seismograms, *Geophys. J. R. astr. Soc.*, **49**, 225-243.

Kirkwood, S.C. and Crampin, S., 1981. Surface-wave propagation in an ocean basin with an anisotropic upper-mantle: observations of polarization anomalies, *Geophys. J. R. astr. Soc.*, **64**, 487-497.

Korringa, J., 1973. Theory of elastic constants of heterogeneous media, *J. Math. Phys.*, **14**, 509-513.

Krajewski, P., Dresen, L., Schott, W. and Rüter, H., 1987. Studies of road way modes in a coal seam by dispersion and polarization analysis: a case history, *Geophys. Prosp.*, **35**, 767-786.

Kraut, E.A., 1963. Recent advances in the theory of anisotropic elastic wave propagation, *Rev. Geophys.*, **1**, 401-448.

Krey, T.C., 1963. Channel wave as a tool of applied geophysics in coal mining, *Geophysics*, **28**, 701-714.

Krey, T.C., Arnetzl, H. and Knecht, M., 1982, Theoretical and practical aspects of absorption in the application of in-seam seismic coal exploration, *Geophysics*, **47**, 1645-1656.

Krohn, C.E., 1990. Cross-well continuity logging using seismic guided waves. *60th Annual International SEG Meeting, 1990, San Francisco, Expanded Abstracts*, **1**, 43-46.

Kuster, G.T. and Toksöz, M.N., 1974. Velocity and attenuation of seismic waves in two-phase media, Part I - Theoretical formulations, *Geophysics*, **39**, 587-606.

Leary, P.C. and Henyey, T.L., 1985. Anisotropy and fractured zones about a geothermal well from *P*-wave velocity profiles, *Geophysics*, **50**, 25-36.

Levshin, A.L., 1984. Effects of lateral inhomogeneity on surface wave measurements, (In Russian with English abstract.) *Vychisl. Seismol.*, **16**, 118-127.

Levshin, A.L., 1985. Effects of lateral inhomogeneity on surface wave amplitude measurements, *Annls Geophys.*, B, **3**, 511-518.

Levin, F.K., 1979. Seismic velocity in transversely isotropic media, *Geophysics*, 43, 528-537.

Lewis, C., 1989. *Three-dimensional multicomponent imaging of reservoir heterogeneity, Silo Field, Wyoming*, PhD dissertation, Colorado School of Mines.

Li, Y.G., 1988. *Seismic wave propagation in anisotropic media with applications to defining fractures in the earth*, PhD Thesis, University of Southern California.

Li, Y.G., Leary, P., Aki, K., and Malin, P., 1990. Seismic trapped modes in the Oroville and San Andrears fault zones, *Science*, 249, 763-766.

Lighthill, M.J., 1960. Anisotropic wave motions, *Phil. Trans. R. Soc. Lond.*, 252, 397-470.

Lines, L.R., Kelly, K.R. and Queen, J., 1991. Channel waves in cross-borehole data, *61th Annual International SEG Meeting, 1991, Houston, Expanded Abstracts*, 2, 850-854.

Liu, E., 1989. *Shear-wave splitting in cross-hole seismology and channel waves in anisotropic waveguides*, PhD Thesis, University of Edinburgh.

Liu, E. and Crampin, S., 1990. The effects of the internal shear wave window: comparison with anisotropy induced splitting, *J. Geophys. Res.*, 95, 11275-11283

Liu, E., Crampin, S. and Queen, J.H., 1991. Fracture detection using crosshole surveys and reverse seismic profiles at the Conoco Borehole Test Facility, Oklahoma, *Geophy. J. Int.*, 107, 449-463.

Liu, E., Crampin, S. and Roth, B., 1992. Modelling channel waves with synthetic seismograms in an anisotropic in-seam seismic survey, *Geophys. Prosp.*, in press.

Lou, M. and Crampin, S., 1991a. Dispersion of guided waves in thin anisotropic waveguides, *Geophy. J. Int.*, 107, 545-555.

Lou, M. and Crampin, S., 1991b. Seismic guided waves propagation in cracked thin-layer sedimentary reservoirs and its potential application in EOR monitoring by crosshole survey, *61th Annual International SEG Meeting, 1991, Houston, Expanded Abstracts*, 2, 846-849.

Lou, M. and Crampin, S., 1992a. The use of guided-waves for continuity tests between boreholes, *The Leading Edge*, submitted.

Lou, M. and Crampin, S., 1992b. Modelling guided-waves in crosshole surveys in cracked and uncracked rock, *Geophys. Prosp.*, submitted.

Lou, M. and Crampin, S., 1992c. The use of guided-waves for monitoring Enhanced Oil Recovery, *The Leading Edge*, in preparation.

Love, A.E.H., 1892. *A treatise on the mathematical theory of elasticity*, Cambridge Univ. Press.

Love, A.E.H., 1944. *A treatise on the mathematical theory of elasticity*, 4th ed. Dover, New York.

Lynn, H. B. and Thomsen, L. A., 1986. Reflection shear wave data along the principal axes of azimuthal anisotropy, *Expanded Abstracts, 56th Ann. Int. SEG Meeting, 1986, Houston*, 473-476.

Mahrer, K.D. and Mauk, F.J., 1987. Seismic wave motion for a new model of hydraulic fracture with an induced low-velocity zone, *J. Geophys. Res.*, **92**, 9293-9309.

Mason, I.M., Buchanna, D.J. and Boore, A.K., 1980. Channel wave mapping of coal seams in the United Kingdom, *Geophysics*, **45**, 1131-1143.

Mason, I.M., Greenhalgh, S.A. and Hatherly, P., 1985. A channel wave transmission study in the Newcastle coal measures, Australia, *Geoexploration*, **23**, 395-413.

Martin, M. A. and Davis, T. L., 1987. Shear-wave birefringence: a new tool for evaluating fractured reservoirs, *The Leading Edge*, **6**, 10, 22-28.

Mecbeth, C., 1991a. Inverting shera-wave polarizations for anisotropy using three-component offset VSPs: synthetic seismograms, *Geophys. J. Int.*, **107**, 571-583

Mecbeth, C., 1991b. Inversion for subsurface anisotropy using estimates of shear-wave splitting, *Geophys. J. Int.*, **107**, 585-595.

Mitchell, B.J., 1984. On the inversion of Love- and Rayleigh-wave dispersion and implications for Earth structure and anisotropy, *Geophys. J. R. astr. Soc.*, **76**, 233-241.

Mooney, W.D. and Luetgert, J.H., 1982. A seismic refraction study of the Santa Clara Valley and southern Santa Cruz Mountains, West-central California. *Bull. seism Soc. Am*, **72**, 901-909.

Muller, M. C., 1991. Prediction of lateal variability in fracture intensity using multicomponent shear wave surface seismic as a precursor to horizontal drilling, *Geophys. J. Int.*, **107**, 409-415.

Musgrave, M.J.P., 1954. The propagation of elastic waves in crystal and other anisotropic media, *Proc. R. Soc., London, A*, **226**, 339-355.

Nikitin, L.V. and Chesnokov, E. M., 1984. Wave propagation in elastic media with stress-induced structure and anisotropy, *Geophys. J. R. astr. Soc.*, **76**, 129-133.

Nishizawa, O., 1982. Seismic velocity anisotropy in a medium containing oriented cracks - transversely isotropic case, *J. Phys. Earth.*, **30**, 331-347.

Nur, A., 1989, Four- dimensional seismology and (true) direct detection of hydrocarbons: the petrophysical basis, *The Leading Edge*, **8** (9), 30-36.

O'Connell, R.J. and Budiansky, B., 1974. Seismic velocities in dry and saturated cracked solids, *J. Geophys. Res.*, **79**, 5412-5426.

O'Connell, R.J. and Budiansky, B., 1977. Viscoelastic properties of fluid-saturated cracked solids, *J. Geophys. Res.*, **82**, 5719-5735.

Peacock, S., Crampin, S., Booth, D.C. and Fletcher, J.B., 1988. Shear-wave splitting in the Anza seismic gap, Sourthern California: temporal variations as possible precursors, *J. Geophys. Res.*, **93**, 3339-3356.

Peselinick, L. and Nicolas, A., 1978. Seismic anisotropy in an opholite peridotite: application to oceanic upper mantle, *J. Geophys. Res.*, **83**, 1227-1235.

Petrashen, G.I. and Kashtan, B.M., 1984. Theory of body-wave propagation in inhomogeneous anisotropic media, *Geophys. J. Roy. astr. Soc.*, **76**, 29-39.

Pilant, W.L., 1972. Complex roots of the Stoneley wave equation. *Bull. seism Soc. Am*, **62**, 285-299.

Pyrak-Nolet, L.J. and Cook, G.W., 1987, Elastic interface waves along a fracture, *Geophys. Res. Lett.*, **14**, 1107-1110.

Queen, J.H. and Rizer, W.D., 1990. An integrated study of seismic anisotropy and the natural fracture system at the Conoco Borehole Test Facility, Kay County, Oklahoma, *J. geophys. Res.*, **95**, 11 255-11 273.

Räder, D., Schott, W., Dresen, L. and Rüter, H., 1985. Calculation of dispersion curves and amplitude-depth distributions of Love channel waves in horizontally layered media, *Geophys. Prosp.*, **33**, 800-816.

Rayleigh, Lord, 1887. On waves propagated along the plane surface of an elastic solid. *Proc. Lond. math. Soc.*, **17**, 4-11.

Regueiro, J.S., 1990. Seam waves: What are they? *The Leading Edge*, **9**, 4, 19-23.

Richter, C.F., 1941. *Elementary Seismology*, Freeman, San Francisco.

Rizer, W.D., 1990. Seismic detection of natural fractures in the near surface - Part I: Site geology of the Conoco Borehole Test Facility, *4th Int. Workshop on Seismic Anisotropy, July 2-6, 1990, Edinburgh, Abstracts*, British Geological Survey.

Robertson, J.D. and Corrigan, D., 1983. Radiation patterns of a shear-wave vibrator in near-surface shale, *Geophysics*. **48**, 19-26.

Robert, G. and Crampin, S., 1986. Shear-wave polarization in a Hot Dry Rock geothermal reservoir: anisotropic effects of fractures, *Int. J. Rock Mech. Mn. Sci. & Geomech. Abstr.*, **23**, 291-302.

Romanowicz, B. and Snieder, R., 1988. A new formalism for the effect of lateral heterogeneity on normal modes and surface waves - II. General anisotropic perturbations, *Geophys. J. R. astr. Soc.*, 93, 91-99.

Rutledge, T.T., 1989. Interwell seismic surveying workshop: An overview, *The Leading Edge*, 8, 6, 38-40.

Silver, P.G. and Chan, W.W., 1988. Implications for continental structure and evolution from seismic anisotropy, *Nature*, 335, 34-39.

Slepian, D., Pollack, H.O. and Landau, H.J., 1961. Prolate spheroidal wave functions, Fourier analysis and uncertainty, *Bell Telphone System Tech. Publ.*, *Monograph* 3746.

Snieder, R., 1988. Large-scale waveform inversion of surface waves for lateral heterogeneity: 1. Theory and numerical examples, *J. geophys. Res.*, *B*, 93, 12055-12065.

Snieder, R. and Romanowicz, B., 1988. A new formalism for the effect of lateral heterogeneity on normal modes and surface waves - I. isotropic perturbations, perturbations of interfaces and gravitational perturbations, *Geophys. J. R. astr. Soc.*, 92, 207-222.

Squires, S. G., Kim, C. D. and Kim, D. Y., 1989. Interpretation of total wave-field data over Lost Hills field, Kern Country, California, *Geophysics*, 54, 1420-1429.

Stierman, D.J. and Kovach, R.L., 1979. An *in situ* velocity study: The Stone Cajon well, *J. Geophys. Res.* 84, 672-678.

Stoneley, R., 1924. Elastic waves at the surface of separation of two solids, *Proc. R. Soc.* A, 106. 416-428.

Strick, E. and Ginzbarg, A.S., 1956. Stoneley-wave velocity for a liquid-solid interface, *Bull. seism Soc. Am*, 46, 281-292.

Tang, X.M. and Cheng, C.H., 1988. Wave propagation in a fluid-filled fracture - an experimental study, *Geophys. Res. Lett.*, 15, 1463-1466.

Tang, X.M., Cheng, C.H. and Toksöz, M.N., 1991. Stoneley-wave propagation in a fluid-filled borehole with a vertical fracture, *Geophysics*, 56, 447-460.

Taylor, D.B., 1990. *Aniseis Manual: Version 4.5*, Applied Geophysical Software, Houston.

Taylor, D.B. and Crampin, S., 1978. Seismic surface waves in anisotropic media: propagation in a homogeneous piezo-electric halfspace, *Proc.R. Soc.*, *A.*, 364, 161-179.

Toksöz, M.N. and Johnston, D.H., 1981. *Seismic wave attenuation, geophysical reprint series*, *NO.* 2, Society of Exploration Geophysicists.

Walsh, J.B., 1965. The effect of cracks on the compressibility of rock, J. Geophys. Res., 70, 381-389.

White, J.E., Martineau-Nicoletis, L. and Monash, C., 1983. Measured anisotropy in Pierre shale, *Geophys. Prosp.*, 31, 709-725.

White, J.E. and Sengbush, R.L., 1987, *Production seismology*, Geophysical Press, London. 41-49

Wild., P. and Crampin, S., 1991. The range of effects of azimuthal isotropy and EDA anisotropy in sedimentary basins, *Geophys. J. Int.*, 107, 513-529.

Willis, H.A., Rethford, G.L. and Bielandski, E., 1986. Azimuthal anisotropy: occurence and effect on shear-wave data quality, *56th Annual International SEG Meeting, 1986, Houston, Expanded Abstracts*, 479-481.

Worthington, M.H., 1991. Cross-well continuity logging using Stoneley waves at the Whitchester borehole test site, *53rd Annual International EAEG Meeting, 1991, Florence, Technical Programme and Abstracts of Papers*, 180-181.

Wu, T.T., 1966. The effect of inclusion shape on the elastic moduli of a two-phase material, *Int. J. Sol. Struct.*, 2, 1-8.

Dispersion of guided waves in thin anisotropic waveguides

Min Lou[1,2] and Stuart Crampin[1]

[1] *British Geological Survey, Murchison House, West Mains Road, Edinburgh* EH9 3LA, *UK*
[2] *Department of Geology and Geophysics, University of Edinburgh, James Clerk Maxwell Building, Edinburgh* EH9 3JZ, *UK*

SUMMARY

This paper shows that: if appropriate source mechanisms and frequency bands can be selected, thin layers in sedimentary reservoirs may act as seismic waveguides, and guided waves may be useful for reservoir characterization in cross-hole surveys; and that the dispersion of such guided waves is sensitive to crack saturations and crack orientations, and could contain important information about the level of saturation in specific thin layers in enhanced oil recovery operations. In the first part of the paper, we extend a technique, previously used for calculating the dispersion of surface waves in a plane-layered anisotropic half-space, to calculating the dispersion of guided waves in the interior of a multilayered anisotropic solid. In the second part, we demonstrate the effects of anisotropy by calculating synthetic guided waves in a thin gas-sand layer displaying crack-induced anisotropy.

Key words: anisotropic layers, channel waves, dispersion, guided waves, monitoring enhanced oil recovery.

THEORY: CALCULATION OF DISPERSION OF GUIDED WAVES IN ANISOTROPIC LAYERS

1 INTRODUCTION

The dispersion of guided waves (channel waves, or interface waves) in multilayered *isotropic* solids has been calculated by Räder *et al.* (1985) and Buchanan (1987). However, it has been recognized that stress-aligned fluid-filled cracks, microcracks and preferentially oriented pore-space exist in most rocks in the uppermost 10 to 20 km of the crust, where it is known as *extensive-dilatancy anisotropy* or *EDA* (Crampin 1987). In particular, coal seams, where channel waves have been widely used, are often visibly anisotropic with a well-defined direction of planar cracks or 'cleats' with consistent orientations over substantial areas (Jackson 1985). The crack-induced anisotropy significantly modifies the dispersion of guided waves in such anisotropic media.

We present a procedure for determining the dispersion of guided waves in multilayered anisotropic structures. The procedure is an extension of the techniques of Crampin (1970) and Crampin & Taylor (1971) for calculating the dispersion of surface waves in a half-space of thin anisotropic layers. We consider a model made of n parallel anisotropic layers embedded between two half-spaces (Fig. 1). The half-spaces are assumed to be isotropic. This simplifies mathematical treatment without loss of generality, since anisotropic half-spaces may be treated by increasing the thickness of the first and nth layers to a large enough value.

We choose the coordinate system shown in Fig. 1. The interference of the body waves, which are multiply reflected within the internal layers, form guided waves propagating in the x_1 direction with phase velocity c. The conditions for forming the propagator matrix formulations are the continuity of three displacement components (u_1, u_2, u_3) and the three stresses ($\sigma_{13}, \sigma_{23}, \sigma_{33}$) of a plane body wave at an interface, where there are no sources at infinity in the half-spaces.

2 WAVE EQUATION AND BOUNDARY CONDITIONS IN ANISOTROPIC LAYERS

This section is adapted from Taylor & Crampin (1978). We choose the following notation: x_1, x_2, x_3 = orthogonal coordinates; u_1, u_2, u_3 = components of displacement; $\sigma_{13}, \sigma_{23}, \sigma_{33}$ = vertical, and horizontal radial and transverse components; d_i = thickness of ith layer; and ρ = density.
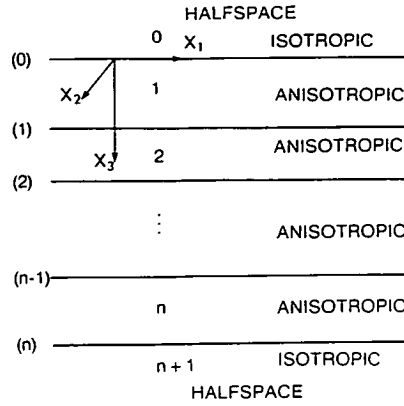
Figure 1. Geometry for guided wave dispersion calculations.

In each anisotropic layer, the equations of motion of elastic waves may be written

$$\rho \ddot{u}_i = C_{ijkm} u_{k,jm} \qquad (i, j, k, m = 1, 2, 3), \tag{1}$$

where C_{ijkm} are the elastic tensors with the following symmetries:

$$C_{ijkm} = C_{kmij} = C_{mkij} \qquad (i, j, k, m = 1, 2, 3). \tag{2}$$

We suppose the periodic solution of a plane wave with displacements

$$u_j = a_j \exp[i\omega(t - q_k x_k)] \qquad (j, k = 1, 2, 3), \tag{3}$$

where a_j is the amplitude coefficient of the jth displacement; and q_k is the kth component of the slowness vector. In the sagittal plane (x_1, x_3), there is no variation of motion normal to the plane, so we assume $q_2 = 0$ and write $q_1 = 1/c$, where c is phase velocity along the x_1 direction.

Substitution of (3) into (1) gives three simultaneous equations in a_k:

$$F_{ik} a_k = 0, \tag{4}$$

where $F_{ik} = -\rho \delta_{ik} + C_{ijkm} q_j q_m$, for $i, j, k, m = 1, 2, 3$. The condition for a non-trivial solution of (4) is

$$\det(\mathbf{F}) = 0, \tag{5}$$

yielding a polynomial of degree six in q.

Following Taylor & Crampin (1978), equation (4) can be written in the matrix form:

$$\mathbf{Fa} = (\mathbf{R}p^2 + \mathbf{S}p + \mathbf{T} - \rho c^2 \mathbf{I})\mathbf{a} = \mathbf{0}, \tag{6}$$

where $\mathbf{a}$ is the vector of amplitude coefficients; $q_1 = 1/c$; $q_2 = 0$; $q_3 = p/c$; $\mathbf{I}$ is the unit matrix; $\mathbf{R} = \{C_{i3j3}\}$; $\mathbf{S} = \mathbf{V} + \mathbf{V}^T$; $\mathbf{V} = \{C_{i3j1}\}$; and $\mathbf{T} = \{C_{i1j1}\}$ for $(i, j = 1, 2, 3)$.

Furthermore, since the matrix $\mathbf{R}$ is non-singular, the equation (6) can be written in the form:

$$\left[\begin{pmatrix} -\mathbf{R}^{-1}\mathbf{S} & -\mathbf{R}^{-1}\mathbf{T}' \\ \mathbf{I} & 0 \end{pmatrix} - p \begin{pmatrix} \mathbf{I} & 0 \\ 0 & \mathbf{I} \end{pmatrix} \right] \begin{pmatrix} p\mathbf{a} \\ \mathbf{a} \end{pmatrix} = \mathbf{0}, \tag{7}$$

where $\mathbf{T}' = \mathbf{T} - \mathbf{I}\rho c^2$.

This is a 6×6 linear eigenvalue problem for p, and forms the basis of numerical computation in the procedure. Each eigenvalue p contributes to the displacements, and the solution $\mathbf{u}$ may be constructed by

$$\mathbf{u} = \mathbf{ABfe}(x_1, t); \tag{8}$$

where $\mathbf{u} = (u_1, u_2, u_3)^T$; $\mathbf{A} = (\mathbf{a}_1, \mathbf{a}_2, \mathbf{a}_3, \mathbf{a}_4, \mathbf{a}_5, \mathbf{a}_6)$; $\mathbf{B} = \mathrm{diag}(b_1, b_2, b_3, b_4, b_5, b_6)$; $b_i = \exp[-i\omega p_i x_3 / c]$; $\mathbf{f}$ is a vector of excitation factor; and $\mathbf{e}(x_1, t) = \exp[i\omega(t - x_1/c)]$.

The relation between displacements and stresses is given by

$$\sigma_{jk} = C_{jkmn} u_{m,n} \qquad (j, k = 1, 2, 3). \tag{9}$$

Combining (8) and (9), we have

$$\begin{pmatrix} \mathbf{u} \\ \mathbf{\tau} \end{pmatrix} = \begin{pmatrix} 0 & \mathbf{I} \\ \mathbf{R} & \mathbf{V} \end{pmatrix} \begin{pmatrix} \mathbf{AP} \\ \mathbf{A} \end{pmatrix} \mathbf{Bfe}(x_1, t), \tag{10}$$

where $\mathbf{u}^T = (u_1, u_2, u_3)$; $\boldsymbol{\tau}^T = (ic/\omega)(\sigma_{13}, \sigma_{23}, \sigma_{33})$; and $\mathbf{P} = \text{diag}(p_1, p_2, p_3, p_4, p_5, p_6)$.

Let

$$\begin{pmatrix} \mathbf{0} & \mathbf{I} \\ \mathbf{R} & \mathbf{V} \end{pmatrix} \begin{pmatrix} \mathbf{AP} \\ \mathbf{A} \end{pmatrix} = \mathbf{E};$$

then

$$(\mathbf{u} \quad \boldsymbol{\tau})^T = \mathbf{EBf} e(x_1, t). \tag{11}$$

The boundary conditions at an interface between two layers are the continuity of the three displacements and three stresses. Applying (11) to all the interfaces of the model, we have the matrix recurrence relation:

$$[u_1, u_2, u_3, (ic/\omega)\sigma_{13}, (ic/\omega)\sigma_{23}, (ic/\omega)\sigma_{33}]_0^T = \mathbf{G}[u_1, u_2, u_3, (ic/\omega)\sigma_{13}, (ic/\omega)\sigma_{23}, (ic/\omega)\sigma_{33}]_n^T, \tag{12}$$

where $\mathbf{G} = \mathbf{E}_1 \text{ diag}[\exp(i\omega q_3^{(1)}d_1)]\mathbf{E}_1^{-1} \cdot \mathbf{E}_2 \text{ diag}[\exp(i\omega q_3^{(2)}d_2)]\mathbf{E}_2^{-1} \cdots \mathbf{E}_n$; and subscripts 0 and n refer to the top and bottom interfaces, respectively.

3 DISPLACEMENTS AND STRESSES AT TOP AND BOTTOM (ISOTROPIC) HALF-SPACES

In the isotropic half-spaces, *P–SV* components and *SH* component are decoupled and may be treated independently.

3.1 *P–SV* components

The displacements may be constructed by combining the dilatational and the rotational wave solutions:

$$u_1 = U_p + U_s \quad \text{and} \quad u_3 = W_p + W_s \tag{13}$$

where subscripts p and s refer to dilatational and rotational components; U_p and W_p satisfy the dilatational wave equation; and U_s and W_s satisfy the rotational wave equation.

The dilatational motion is irrotational, and the rotational motion is divergence-less, that is

$$\nabla \times \begin{pmatrix} U_p \\ 0 \\ W_p \end{pmatrix} = \mathbf{0} \quad \text{and} \quad \nabla \cdot \begin{pmatrix} U_s \\ 0 \\ W_s \end{pmatrix} = 0. \tag{14}$$

The U_p, U_s, W_p, W_s have the following general periodic solutions:

$$\begin{aligned} U_p &= [A' \exp(-ik\gamma_\alpha x_3) + A'' \exp(ik\gamma_\alpha x_3)]e(x_1, t), & U_s &= [B' \exp(-ik\gamma_\beta x_3) + B'' \exp(ik\gamma_\beta x_3)]e(x_1, t), \\ W_p &= [C' \exp(-ik\gamma_\alpha x_3) + C'' \exp(ik\gamma_\alpha x_3)]e(x_1, t), & W_s &= [D' \exp(-ik\gamma_\beta x_3) + D'' \exp(ik\gamma_\beta x_3)]e(x_1, t), \end{aligned} \tag{15}$$

where $\{A', B', C', D'\}$ and $\{A'', B'', C'', D''\}$ are constants referring to downward and upward travelling plane waves, respectively, where

$$\gamma_\alpha = \begin{cases} [(c/\alpha)^2 - 1]^{1/2} & c > \alpha, \\ -i[1 - (c/\alpha)^2]^{1/2} & c < \alpha, \end{cases} \quad \gamma_\beta = \begin{cases} [(c/\beta)^2 - 1]^{1/2} & c > \beta, \\ -i[1 - (c/\beta)^2]^{1/2} & c < \beta, \end{cases}$$

$\alpha = [(\lambda + 2\mu)/\rho] = $ velocity of propagation of dilatational waves in an isotropic half-space; $\beta = (\mu/\rho) = $ velocity of propagation of rotational waves in an isotropic half-space; and $\lambda, \mu = $ Lamé elastic constants in isotropic half-space.

The curl and divergence condition (14) give

$$C' = \gamma_\alpha A', \qquad C'' = -\gamma_\alpha A'', \qquad D' = -B'/\gamma_\beta, \qquad D'' = B''/\gamma_\beta. \tag{16}$$

The normal and tangential stress components are

$$\sigma_{33} = \rho\alpha^2 \partial u_3/\partial x_3 + \lambda \partial u_1/\partial x_1, \qquad \sigma_{13} = \mu(\partial u_1/\partial x_3 + \partial u_3/\partial x_1). \tag{17}$$

So, we have the general displacements and stresses expressions for *P–SV* components:

$$\begin{aligned} u_1 &= [A' \exp(-ik\gamma_\alpha x_3) + A'' \exp(ik\gamma_\alpha x_3) + B' \exp(-ik\gamma_\beta x_3) + B'' \exp(ik\gamma_\beta x_3)]e(x_1, t), \\ u_3 &= [\gamma_\alpha A' \exp(-ik\gamma_\alpha x_3) - \gamma_\alpha A'' \exp(ik\gamma_\alpha x_3) - B'/\gamma_\beta \exp(-ik\gamma_\beta x_3) + B''/\gamma_\beta \exp(ik\gamma_\beta x_3)]e(x_1, t), \\ \sigma_{33} &= \{-ik(\rho\alpha^2\gamma_\alpha^2 + \lambda)[A' \exp(-ik\gamma_\alpha x_3) + A'' \exp(ik\gamma_\alpha x_3)] + ik(\rho\alpha^2 - \lambda)[B' \exp(-ik\gamma_\beta x_3) + B'' \exp(ik\gamma_\beta x_3)]\}e(x_1, t), \\ \sigma_{13} &= \{-ik2\mu\gamma_\alpha[A' \exp(-ik\gamma_\alpha x_3) - A'' \exp(ik\gamma_\alpha x_3)] - ik\mu(\gamma_\beta - 1/\gamma_\beta)[B' \exp(-ik\gamma_\beta x_3) - B'' \exp(ik\gamma_\beta x_3)]\}e(x_1, t). \end{aligned} \tag{18}$$

3.2 *SH* component

Similarly, the *SH* displacement and transverse stress in isotropic half-spaces can be expressed by

$$u_2 = [T' \exp(-ik\gamma_\beta x_3) + T'' \exp(ik\gamma_\beta x_3)]e(x_1, t),$$

$$\sigma_{23} = \mu \partial u_2 / \partial x_3 = -ik\mu\gamma_\beta [T' \exp(-ik\gamma_\beta x_3) - T'' \exp(ik\gamma_\beta x_3)]e(x_1, t),$$

(19)

where T' and T'' are constants referring to downward and upward travelling plane waves, respectively.

3.3 Displacements and stresses at top (0) and bottom (n) interfaces

Setting $x_3 = 0$ in (18) and (19) and omitting the term $e(x_1, t)$, we obtain the displacements and stresses at top interface (0) and bottom interface (n):

$$[u_1, u_2, u_3, (ic/\omega)\sigma_{13}, (ic/\omega)\sigma_{23}, (ic/\omega)\sigma_{33}]_0^T = \mathbb{E}_0(A', T', B', A'', T'', B'')_0^T,$$

(20)

where

$$\mathbb{E}_0 = \begin{pmatrix} 1 & 0 & 1 & 1 & 0 & 1 \\ 0 & 1 & 0 & 0 & 1 & 0 \\ \gamma_\alpha & 0 & -1/\gamma_\beta & -\gamma_\alpha & 0 & 1/\gamma_\beta \\ 2\mu\gamma_\alpha & 0 & \mu(\gamma_\beta - 1/\gamma_\beta) & -2\mu\gamma_\alpha & 0 & \mu(1/\gamma_\beta - \gamma_\beta) \\ 0 & \mu\gamma_\beta & 0 & 0 & -\mu\gamma_\beta & 0 \\ \lambda + \rho\alpha^2\gamma_\alpha^2 & 0 & \lambda - \rho\alpha^2 & \lambda + \rho\alpha^2\gamma_\alpha^2 & 0 & \lambda - \rho\alpha^2 \end{pmatrix}_0.$$

In general, we have

$$[u_1, u_2, u_3, (ic/\omega)\sigma_{13}, (ic/\omega)\sigma_{23}, (ic/\omega)\sigma_{33}]_n^T = \mathbb{E}_{n+1}(A', T', B', A'', T'', B'')_{n+1}^T,$$

(21)

where the subscript '0' refers to parameters in layer 0; and $\mathbb{E}_{n+1}$ has the same form as $\mathbb{E}_0$, except that the subscript '0' is replaced by '$n + 1$'.

4   DISPERSION EQUATION

Substituting (20) and (21) into (12), and noting that there are no sources at infinity in the half-spaces, that is, the downward components in the top half-space:

$$A_0' = T_0' = B_0' = 0,$$

and upward components in the bottom half-space:

$$A_{n+1}'' = T_{n+1}'' = B_{n+1}'' = 0.$$

Thus, we have

$$(0, 0, 0, A'', T'', B'')_0^T = \mathbb{E}_0^{-1}\mathbb{G}\mathbb{E}_{n+1}(A', T', B', 0, 0, 0)_{n+1}^T.$$

(22)

The condition for non-trivial values of A_{n+1}', T_{n+1}' and B_{n+1}' is the vanishing of the following sub-determinant, and we have the dispersion equation:

$$\det(\mathbb{H}_{ij}) = 0 \qquad (i, j = 1, 2, 3),$$

(23)

where $\mathbb{H} = \mathbb{E}_0^{-1}\mathbb{G}\mathbb{E}_{n+1}$. Solving (23) by numerical methods, we obtain the relationship for the phase velocity dispersion of guided waves.

In anisotropic media, the propagation of energy of guided waves is not usually parallel to the propagation vector (except in particular symmetry directions), and the group velocity cannot be obtained by a simple differentiation of the phase velocity as in the isotropic case. To evaluate the group velocity in an anisotropic structure, we need to differentiate the phase velocity in three directions. In this paper, we present only the projection of the group velocity in the direction of propagation by differentiation of the phase velocity. This is a good first-order approximation, except in strong anisotropy greater than 10 per cent, say. (In any case, there is no simple technique for calculating the group velocity of surface or guided waves in particular azimuthal directions.)

GUIDED WAVES IN A THIN LAYERED ANISOTROPIC RESERVOIR

5 MODEL STUDIES

Guided waves (channel waves) have been widely used in in-seam seismology (Krey 1963; Buchanan, Jackson & Davis 1983; Liu, Crampin & Roth 1991a), since coal-seams usually provide a low-velocity waveguide within nearly parallel plane interfaces. In oil production and enhanced oil recovery (EOR) geophysics, because of low-velocity high-attenuation surface layers, large distances from the target zones, and noisy surface environments, the resolution power of surface seismic data is severely limited, and cross-hole seismic surveying appears increasingly attractive. Many oil reservoirs have approximately plane layers, and it is interesting to investigate the possibilities of recording and identifying guided waves in cross-hole surveys, where waves are guided by the impedance contrasts across plane layers in sedimentary basins. A unique advantage of such guided waves is that, if appropriate waves can be excited, most of the energy will be channelled in the zone of interest. In contrast to VSPs or surface reflection surveys, where only a small percentage of the travel path samples the zone of interest, guided waves should respond to the properties of the zone of interest more strongly and directly if they can be excited in appropriate signal frequency bands and polarizations. Such guided waves may be of special importance for reservoirs with thin layers, since other surveying techniques usually lose much of their resolution in thin layering.

Here, we investigate guided waves in a thin sandstone layer pervaded by stress-aligned cracks, microcracks, and oriented pores (EDA cracks) containing different proportions of gas and water. An important feature of guided waves is the frequency–velocity dispersion. Given particular velocity contrasts, a preliminary dispersion study should be able to identify the frequencies and source parameters that would excite appropriate guided waves between boreholes in a particular zone of interest.

We calculate a series of dispersion curves and synthetic seismograms, and examine the effects on dispersion of the different parameters (directions of propagation, gas/water saturations, etc.). The theoretical dispersion curves are compared with the results calculated from synthetic seismograms by multifilter techniques. This could provide forward modelling techniques for inverting the dispersion of guided waves in anisotropic layers, once sufficient experience of the behaviour of guided waves in anisotropic layers has been gained.

6 MODEL OF A THIN LAYER GAS–SAND RESERVOIR

The model described in Fig. 2 is an example of a thin sedimentary hydrocarbon reservoir. The gas sand is trapped above water by a shale roof and a shale floor. The liquid could be oil, instead of water, which would cause further subtle differences, although we have not modelled the oil/water effects in this present example.
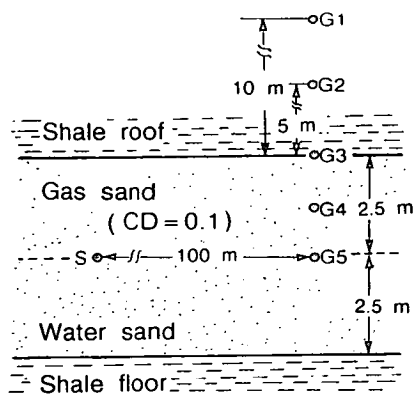
(CD = Crack density)

The material parameters

	Vp (m/s)	Vs (m/s)	ρ (kg/m³)
Gas sand	1900	1270	2000
Water sand	2500	1200	2230
Shale	2770	1600	2340

Figure 2. Model of a cracked gas-sand reservoir with 50 per cent gas and 50 per cent water saturation for dispersion calculations. The crack (EDA crack) density is 0.1, and the isotropic matrix parameters are indicated. The source and geophone positions are shown for the synthetic seismograms calculations.

The isotropic matrix parameters of the rocks in Fig. 2 are based on some publications (Domenico 1974; Gardner, Gardner & Gregory 1974; Dutta & Odé 1983; White & Sengbush 1987). The thickness of the sandstone has been chosen as 5 m, but note that frequencies and thicknesses scale inversely, so that thicker layers would correspond to smaller frequencies proportionally. We choose a crack density (CD) of 0.1 to model the reservoir, and the orientation of cracks can be varied relative to the wave propagation direction.

7 DISPERSION CURVES

Figure 3 shows the phase and group velocity dispersion curves of the first four generalized modes for the reservoir model in Fig. 2. Dispersion is shown for three different saturations of the inclusions (complete gas saturation, complete water saturation, and 50 per cent gas 50 per cent water saturation), and five different directions of propagation relative to the crack orientations [parallel to the vertical cracks (0° orientation), and every 22.5° to normal to the vertical cracks (90° orientation)].

[Note that, except for propagation in directions of sagittal symmetry, generalized modes in anisotropic structures have 3-D particle displacements (polarizations) intermediate between Rayleigh and Love motion. When there is sagittal symmetry as in the directions in Figs 3(a) and (e), the motion is either in the sagittal plane (*P* and *SV* motion), or transverse to the sagittal plane (*SH* motion). These modes are indicated in Figs 3(a) and (e) by *R* and *L*, for Rayleigh-type and Love-type motion, respectively.

Note also that the phase velocities of generalized modes in off-symmetry directions may pinch together (Crampin & Taylor 1971). At such pinches, the equivalent group-velocity curves cross each other (intersect). In equivalent isotropic structures, the pinches are places where the (essentially independent) Rayleigh and Love phase-velocity curves intersect. At such pinches, indicated approximately by arrowheads in Fig. 3, the modes effectively exchange properties, exchanging particularly the slope of the dispersion curve and the type of particle displacement (Love-type to Rayleigh-type, and Rayleigh-type to Love-type, for
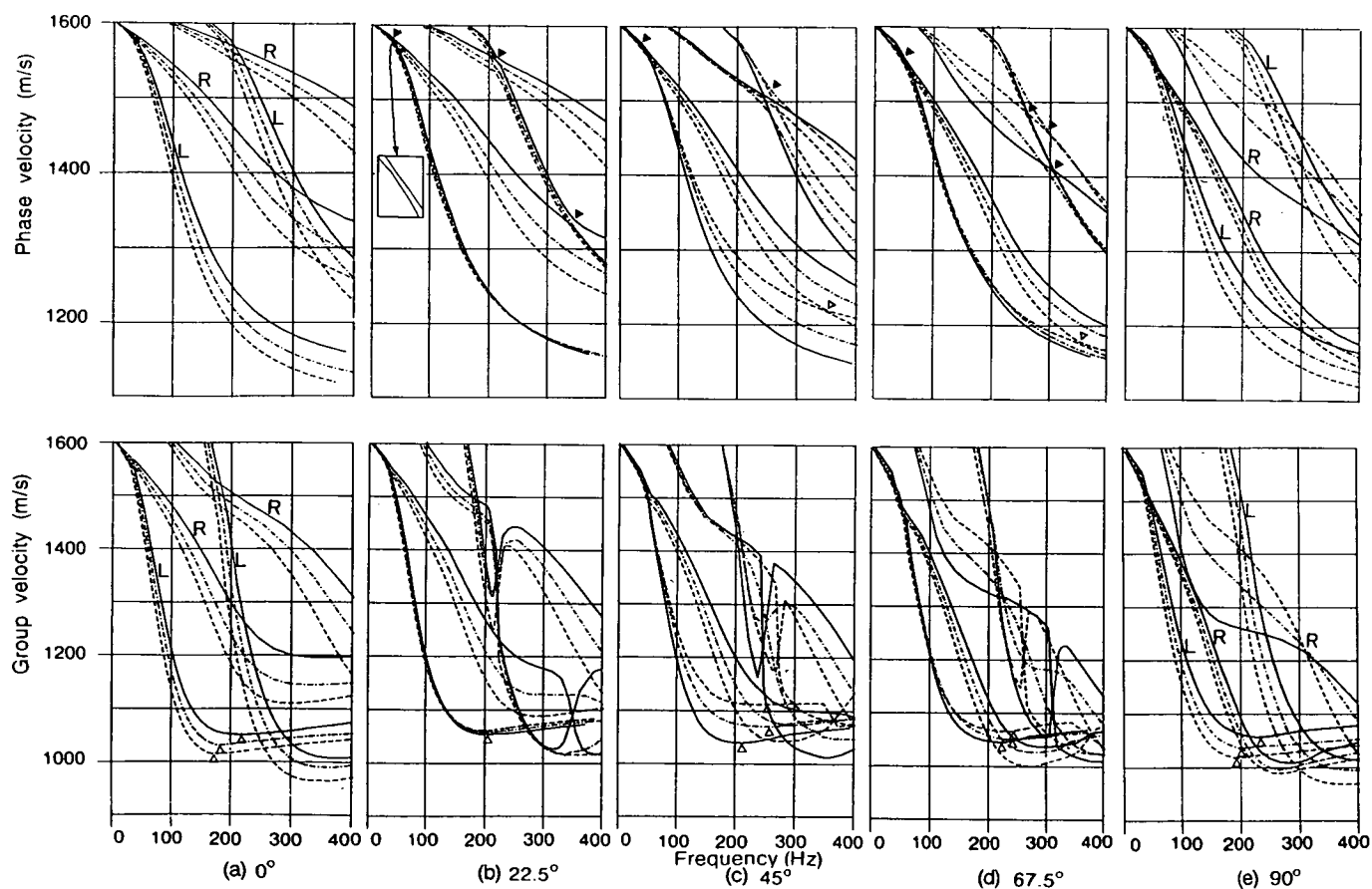

Figure 3. Dispersion curves of first four generalized-mode guided waves for different crack saturations: solid line—complete gas saturation; dashed line—complete water saturation; and dash–dot line—50 per cent gas and 50 per cent water saturation (as in Fig. 2). Curves are shown for different directions of propagation relative to vertical crack orientation: (a) 0° (parallel to crack strike); (b) 22.5°; (c) 45°; (d) 67.5°; and (e) 90° (perpendicular to crack strike). The frequency and phase velocities at which different generalized modes pinch together in off-symmetry directions is indicated by solid arrowheads. The minima of the group-velocity dispersion of the first generalized mode are indicated by open arrowheads.

example). Such pinches in the phase-velocity dispersion, cause wide ranging changes of dispersion in group-velocity dispersion curves, in Fig. 3. Pinches are discussed in Crampin (1981).]

The dispersion curves have the following behaviour.

(1) The group velocity of the first generalized mode (equivalent to the fundamental Love mode) has a minimum at about 200 Hz. This is expected to lead to an increase in amplitude to the seismograms known as an Airy phase (Räder *et al.* 1985), and means that a source frequency of about 200 Hz is likely to excite strong fundamental mode guided waves, and there may also be higher mode Airy phases at higher frequencies. (Note that the reason why the first mode is equivalent to the fundamental Love wave, and not the Rayleigh wave, as would usually be the case, is that there is a pinch intersection at orientations of 0° and 90°, in the phase velocity at about 50 Hz. This allows the Love-type characteristics to be interchanged from the second mode to the first mode.)

(2) The dispersion of most of the generalized modes is sensitive to the direction of propagation relative to the crack strike. The exception is the first mode in the gas-saturated sand, with Love-type characteristics, which shows very little change with direction (the solid curve of the first mode shows very little variation with direction). This is in contrast to the behaviour of the first mode in a water-saturated sand which shows significant differences: at some velocities the frequency changes by at least 30 per cent for different directions of propagation (different crack orientations).

(3) The dispersion of most of the guided wave modes is sensitive to crack saturations at most directions of propagation, as is shown by the different curves (solid, dot–dash, and dashed lines) at each direction of propagation. (The major exception is the first mode at propagation directions of 22.5° and 67.5°, which shows very little change with saturation.) The largest differences are in the third and fourth modes, but probably the most significant differences are in (a) the frequencies and velocities of the minimum of the first mode (marked by open arrowheads), which indicates the positions of the increase in amplitude of the Airy phases on seismograms; and (b) the large range of frequencies and velocities of the second (Rayleigh) mode, indicating that equivalents of the Rayleigh modes are more sensitive than Love-type modes to variations of gas–water saturation.

8 SYNTHETIC SEISMOGRAMS

We use the ANISEIS package to calculate synthetic seismograms for the source and geophone positions in Fig. 2, for a range of source excitations, source frequencies, and crack and saturation parameters. Fig. 4 shows synthetic seismograms for propagation in completely gas-saturated sandstone parallel to the strike of the cracks (0° orientation) for a transverse force source exciting, for this direction of propagation, waves with Love-type motion, and for a vertical force source exciting Rayleigh-type motion. Seismograms are shown for five different dominant signal frequencies.

For this direction of propagation, the vertical-radial and horizontal-transverse motion (Rayleigh- and Love-type motion) are decoupled. For the 50 Hz source, the arrival is essentially a body-wave shear wave, particularly for the vertical force source, which shows almost the same amplitude at all geophones. The arrival from the horizontal transverse force shows the beginnings of some channelling by the gas sand and shows larger amplitude at the geophone (G5) in the centre of the sand.
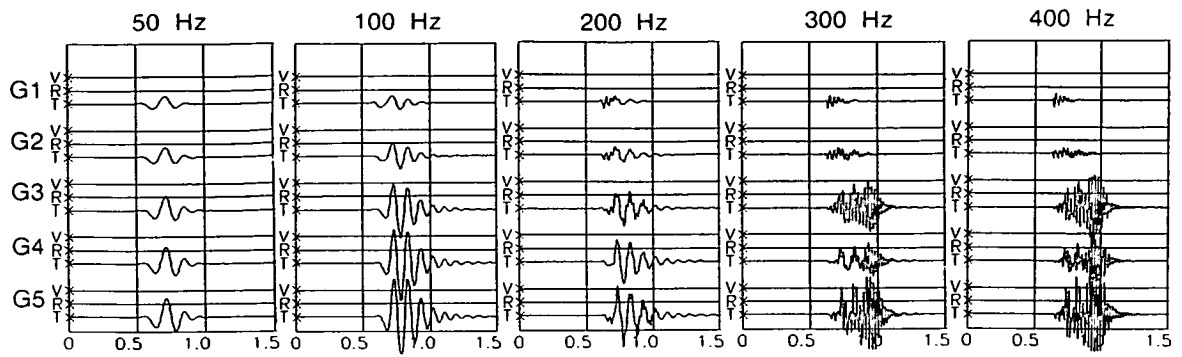
For higher source frequencies, the seismograms show pronounced channelling with the amplitudes at the geophones outside the gas sand much diminished, for both Love- and Rayleigh-type motion. There is a marked change in mode excitation for the Love-type seismograms (upper diagrams) between source frequencies of 200 and 300 Hz, with the large-amplitude high-frequency signals for the 300 and 400 Hz sources being the fourth mode, which is the slowest curve in the group-velocity diagram for this propagation direction in Fig. 3.

The guided waves begin to show strong channelling for the vertical force source as a result of the broad minimum of the second (here a Rayleigh-type) mode between 300 and 400 Hz. The channelling begins for sources of 200 Hz, and persists for 300 and 400 Hz. For the 300 and 400 Hz sources, the higher mode Rayleigh waves effectively arrive earlier than the lower frequency second mode.

Figure 5(a) shows synthetic seismograms for the G4 geophone for five different directions of propagation relative to the crack strike through completely water-saturated gas sand, for both transverse force source (400 Hz) and vertical force source (300 Hz). In off-symmetry directions, the modes do not separate into transverse and sagittal-plane motion, and each mode excites motion in all three dimensions. These polarization abnormalities may give diagnostic information about anisotropy of cracked reservoirs and deserves further investigation. The three-component seismograms show comparatively subtle differences for different propagation directions. The differences are principally in the 3-D particle motion, and are much more clearly displayed in polarization diagrams (see Fig. 5b).

Figure 6 compares three-component seismograms for the G4 geophone for propagation through completely gas- and completely water-saturated sand at several (selected) different directions of propagation for a 400 Hz transverse and vertical force source. Very significant differences are visible on the seismograms between gas- and water-saturated sand. There are differences in: frequency; velocity; particle motion; amplitude; and mode excitation. The differences between levels of saturation will certainly vary for different velocity and crack structures, but it certainly suggests there is the potential for

Source Transverse force
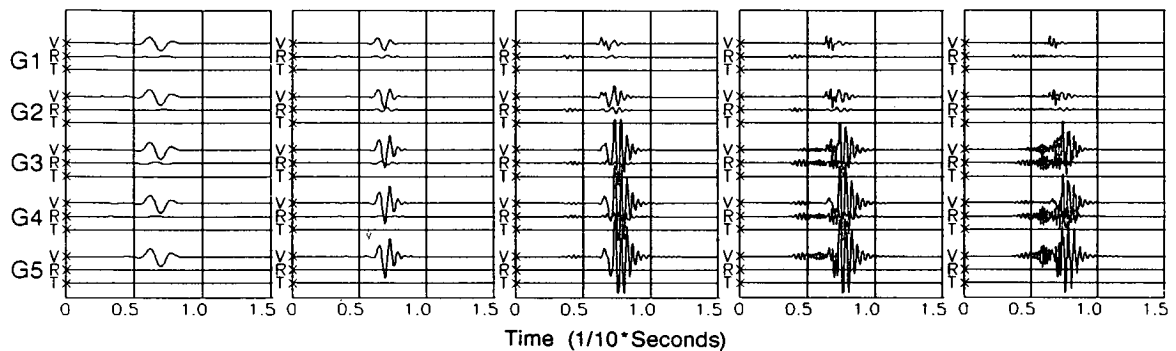

Source Vertical force

Time (1/10*Seconds)

Figure 4. Synthetic three-component seismograms for a range of characteristic source frequencies (indicated above seismograms) for the gas-sand model in Fig. 2 with complete gas saturation. Seismograms are shown for the five geophone positions in Fig. 2, for a propagation direction parallel to the strike of the vertical cracks. The source is in the centre of the gas-sand, and seismograms are shown for a horizontal transverse source (upper diagrams) and a vertical force (lower diagrams).

monitoring changes in the level of the gas and water saturation by analysing guided waves between appropriate cross-well situations.

9 COMPARISON OF THEORETICAL DISPERSION WITH SYNTHETIC SEISMOGRAMS

The theoretical dispersion curves in Fig. 3, and the synthetic seismograms in Figs 4, 5, and 6, show that the dispersion of guided waves is sensitive to crack parameters, crack saturation, and direction of propagation relative to the strike of the cracks. The correspondence between the theoretical dispersion calculations with the dispersion of the synthetic seismograms, calculated with ANISEIS, is demonstrated in Fig. 7, where the dispersion in the synthetic seismograms is calculated by the multiple filtering technique (see below) of Dziewonski, Bloch & Landisman (1969). The comparison in Fig. 7 is for the transverse component seismogram (inset) at the G4 geophone for propagation parallel to the strike of the cracks for complete gas saturation. The spectrum (inset) suggests the presence of two modes. The contoured multiple filter plot also shows two modes, which agree reasonably well with the corresponding theoretical curves. The large amplitudes of the seismogram appear to be principally those of the second Love-type mode, equivalent to the fourth generalized mode. The low values in the centre of the plot are probably due to the destructive interference of the two modes at similar frequencies.

In the multiple filter technique, each seismic trace is time windowed and the arrival time transformed into group velocity–frequency domain, and the trace passed through a bank of overlapping filters to separate arrival times of different frequencies. The filtered in-phase and quadrature spectra, for each frequency point, are then transformed back into the time domain and combined to form a smooth envelope of instantaneous amplitude. The complete set of amplitudes for all signal frequencies therefore describe the signal in both the velocity and frequency domains. The amplitudes are normalized with respect to the maximum value, and the results are displayed as a contour diagram in the velocity–frequency domain. The group velocity dispersion can be found by following the ridge, or ridges, representing the signal across the diagram.
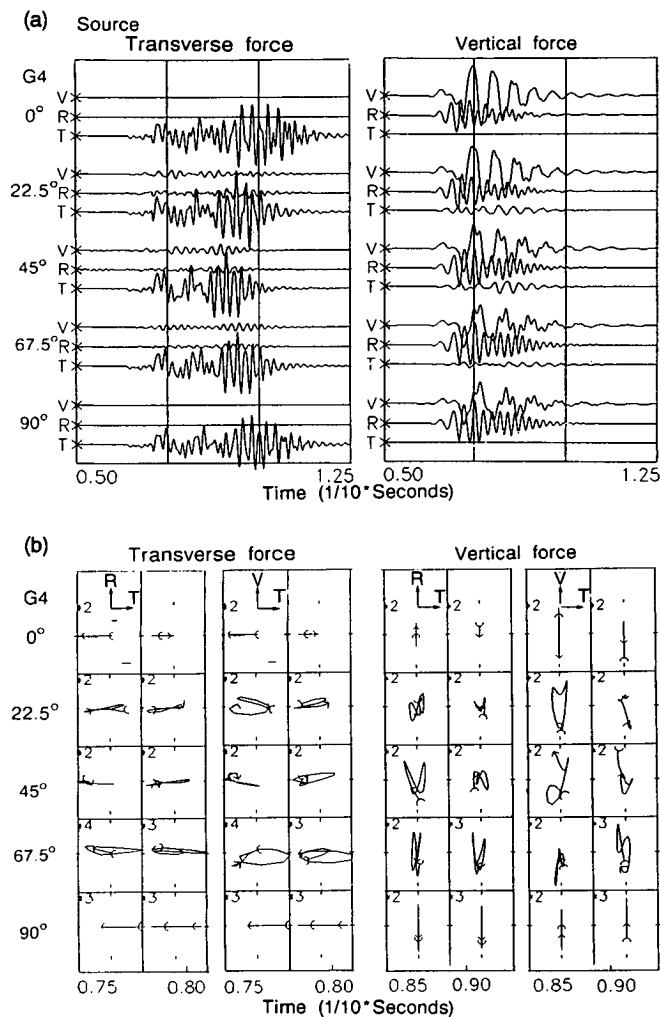
Figure 5. (a) Synthetic guided wave seismograms at geophone G4 for transverse force (400 Hz) and vertical force (300 Hz) for different directions of propagation through water saturated gas sand. In off-symmetry directions, all modes excite displacements in all three dimensions. (b) Polarization diagrams for the selected seismograms in (a): radial(R)-transverse(T) and vertical(V)-transverse(T) planes.
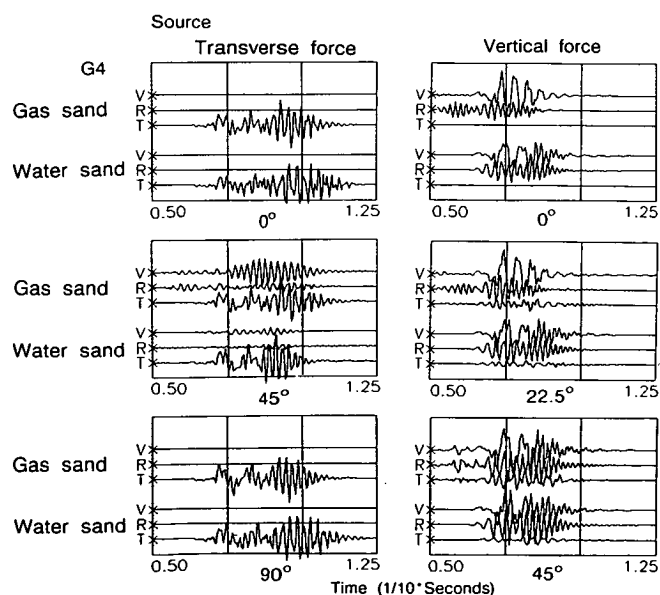

Figure 6. Comparison of seismograms in gas sand and water-saturated gas sand at geophone G4 for 400 Hz vertical force source and transverse force source for several different directions of propagation.
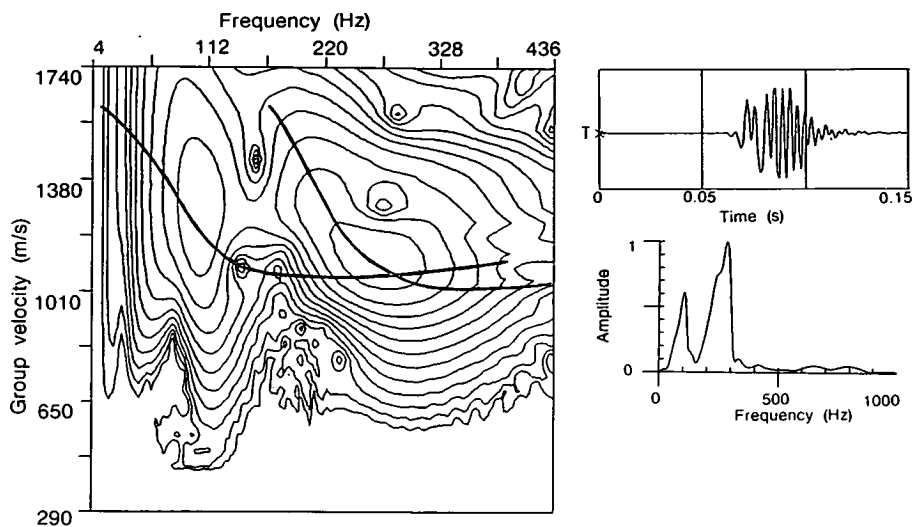
Figure 7. Contoured multiple-filter map of the dispersion of the horizontal transverse component at geophone G4 from a 200 Hz horizontal transverse force source positioned 1.25 m deep, in the direction parallel to the strike of the cracks. Lines are theoretical group-velocity dispersion of the first two Love-types modes. Insets show seismogram and amplitude spectrum.

10   CONCLUSIONS

This is probably the first examination of guided waves parallel to thin cracked layers. We have demonstrated techniques for calculated theoretical dispersion curves and synthetic seismograms of guided waves (channel waves or interface waves) along internal interfaces in layered structures containing aligned cracks. It should be noted that in cross-hole seismic surveys, the dominant amplitudes may well be those of guided wave modes, not body waves (Liu, Crampin & Queen 1991b). Such guided waves are very sensitive to crack parameters, crack orientations and directions of propagation, degree of saturation, and type and frequency of source excitation.

This great sensitivity suggests that the study of guided waves may have applications to monitoring enhanced oil recovery procedures (EOR) in thin hydrocarbon reservoirs (see also Crampin 1990), where the variations of gas and water saturation (or air and oil saturation) are crucially important. This paper examines guided waves in a particular model structure. The behaviour of guided waves is likely to be significantly different for different velocity and cracked structures.

It is suggested that for a given velocity structure (determined from well logs, for example), theoretical dispersion calculations will indicate optimum frequencies and depth levels for exciting appropriate guided modes. The channelling of the energy in the gas sand, indicated by the synthetic seismograms in Figs 4, 5, and 6, shows that, if appropriate frequencies at appropriate depth levels can be identified, it is likely that the appropriate (possibly high-frequency) signal can propagate for significant distances with not too much loss of amplitude.

The potential is clear. What is needed is examination of field data from cross-hole surveys in sedimentary basins, in situations were there is some change to saturation characteristics.

ACKNOWLEDGMENTS

REFERENCES

Buchanan, D. J., 1987. Dispersion calculation for *SH* and *P–SV* waves in multilayered coal seams, *Geophys. Prosp.*, **35**, 62–70.
Buchanan, D. J., Jackson, P. J. & Davis, R., 1983. Attenuation and anisotropy of channel waves in coal seams, *Geophysics*, **48**, 133–147.
Crampin, S., 1970. The dispersion of surface wave in multilayered anisotropic media, *Geophys. J. R. astr. Soc.*, **21**, 387–402.
Crampin, S., 1981. A review of wave motion in anisotropic and crack elastic-media, *Wave Motion*, **3**, 343–391.
Crampin, S., 1987. Geological and industrial implications of extensive-dilatancy anisotropy, *Nature*, **328**, 491–496.

Crampin, S., 1990. The potential of shear-wave VSPs for monitoring recovery: a letter to management, *The Leading Edge*, **9**, 3, 50–52.

Crampin, S. & Taylor, D. B., 1971. The propagation of surface waves in anisotropic media, *Geophys. J. R. astr. Soc.*, **25**, 71–87.

Domenico, S. N., 1974. Effect of water saturation on seismic reflectivity of sand reservoirs encased in shale, *Geophysics*, **39**, 759–769.

Dutta, N. C. & Odé, H., 1983. Seismic reflections from a gas-water contact, *Geophysics*, **48**, 148–162.

Dziewonski, A., Bloch, S. & Landisman, M., 1969. A technique for the analysis of transient seismic signals, *Bull. seism. Soc. Am.*, **59**, 427–444.

Gardner, G. H. F., Gardner, L. W. & Gregory, A. R., 1974. Formation velocity and density—The diagnostic basics for stratigraphic traps, *Geophysics*, **39**, 770–780.

Jackson, P. J., 1985. Horizontal seismics in coal seams: its use by the UK coal industry, *First Break*, **3**, 15–24.

Krey, T. C., 1963. Channel waves as a tool of applied geophysics in coal mining, *Geophysics*, **28**, 701–714.

Liu, E., Crampin, S. & Roth, B., 1991a. Modelling channel waves with synthetic seismograms in an anisotropic in-seam seismic survey, *Geophys. Prosp.*, in press.

Liu, E., Crampin, S. & Queen, J., 1991b. Fracture detection using crosshole surveys and reverse vertical seismic profiles at the Conoco Borehole Test Facility, Oklahoma, *Geophys. J. Int.*, this issue.

Räder, D., Schott, W., Dresen, L. & Rüter, H., 1985. Calculation of dispersion curves and amplitude–depth distributions of Love channel waves in horizontally layered media, *Geophys. Prosp.*, **33**, 800–816.

Taylor, D. B. & Crampin, S., 1978. Seismic surface waves in anisotropic media: propagation in a homogeneous piezo-electric halfspace, *Proc. R. Soc. Lond.*, A, **364**, 161–179.

White, J. E. & Sengbush, R. L., 1987, *Production Seismology*, pp. 41–49, Geophysical Press, London.